TAMPEREEN TEKNILLINEN YLIOPISTO
TAMPERE UNIVERSITY OF TECHNOLOGY

Tiia-Maaria Caroline Ketola

Binding Affinity and Mechanism of Polymer–DNA Polyplexes for Gene Delivery

Julkaisu 1187 • Publication 1187

Tampere 2014

Tampereen teknillinen yliopisto. Julkaisu 1187
Tampere University of Technology. Publication 1187

Tiia-Maaria Caroline Ketola

Binding Affinity and Mechanism of Polymer–DNA Polyplexes for Gene Delivery

Thesis for the degree of Doctor of Science in Technology to be presented with due permission for public examination and criticism in Festia Building, Auditorium Pieni Sali 1, at Tampere University of Technology, on the 31st of January 2014, at 12 noon.

Tampereen teknillinen yliopisto - Tampere University of Technology
Tampere 2014

ISBN 978-952-15-3216-0 (printed)
ISBN 978-952-15-3223-8 (PDF)
ISSN 1459-2045

Abstract

The mechanism of polyethylenimine−DNA, poly(L-lysine)−DNA, peptide–DNA, and PBAE–DNA complex formation was studied by a time-resolved spectroscopic method. The data were analysed by a cooperative model for multivalent ligand binding to multisubunit substrate. The formation of polyplexes with polyethylenimines, poly(L-lysine) and peptide $(KK)_2KGGC$ is observed to be positively cooperative and negatively cooperative with PBAEs. Polymers with positive cooperativity reach about 100% saturation in binding DNA, whereas for polymers with negative cooperativity, the saturation level remains at about 80–90%. The type of amine groups (primary, secondary and tertiary) of the polymers has an effect on the binding constants and the degree of cooperativity.

The effects of pH, type of amine groups and polymer structure on the mechanism of the polyplex formation were studied with polyethylenimines (PEI) and poly(L-lysine) (PLL). At pH 5.2 and 7.4 for PEIs and PLL, the formation of the polyplex core was observed to be complete at N/P = 2, at which point nearly all DNA phosphate groups were bound by polymer amine groups. At higher N/P ratios, excess polymer binds to the core polyplex, forming a shell over the core. At pH 9.2, the core is formed at higher N/P ratios than at lower pH levels except for PLL, which behaves similarly at all pH levels. The overall cooperative binding constants are higher at pH 5.2 than at 9.2 due to the higher degree of amine group protonation at lower pH levels.

The ionic strength and pH affect the binding mechanism with peptide $(KK)_2KGGC$ polyplexes, but changing the buffer does not. Molecular weight shows a clear effect on the mechanism and efficiency of the polyplex formation: for the high-molecular weight polymers (BPEI and PLL), the saturation level is reached at lower N/P ratios than for low-molecular weight polymers (SPEI and peptide). In the absence of excess PEI, the transgene expression levels are lower than in the presence of it. However, the fluorescence properties of the polyplexes in the absence and the presence of excess PEI are similar. Hence, the original structure of the polyplex core is retained during the shell formation.

The molecular structures of the poly(*β*-amino ester)s (PBAEs) can be modified in a controlled way with the accuracy of single carbon unit. The effect of very small changes in the polymer structure on the formation of the polyplexes was studied by changing the length of the backbone and the side chain, by adding end caps to the polymers and by changing the molecular weight of the polymers.

For PBAEs without end caps, the highest saturation levels and overall binding constants were observed for the linear backbones and side chains when the number of carbons was four or five, respectively. The end-capping of PBAEs increases the amine density and the efficiency of polyplex formation, which is observed as higher saturation levels for the end-capped PBAEs. The presence of an OH-group in the end cap induces a change in the binding mechanism. The length of the backbone and the side chain of PBAEs were observed to be important via amine density, hydrophobicity and steric hindrance to the complex formation. High-molecular weight PBAEs formed polyplexes more effectively than smaller ones.

Preface

The research work presented in this thesis was carried out at the Department of Chemistry and Bioengineering at Tampere University of Technology from 2009–2013. The Academy of Finland is gratefully acknowledged for its funding.

I thank my supervisors, Prof. Helge Lemmetyinen, both for the opportunity to do my PhD work in his group and for the instrumentations to use in my research, Prof. Marjo Yliperttula, for the very interesting subject and her valuable advice from the biological side and Dr Elina Vuorimaa-Laukkanen, who deserves my deepest gratitude for her instruction in both the practical and the theoretical issues and her guidance throughout the PhD work. I also offer her special thanks for introducing me to a new and exciting way to study the subject of my research. Her help has always been available when I have needed it and with her large expertise of the area, especially written expertise, my Thesis came true.

I am grateful to all the co-authors of my publications and especially to Mr Corey Bishop for his very fruitful cooperation and discussions yielding new ideas for my work, Mrs Martina Hanzlíková for the compounds and the good looking-figures, Ms Manuela Raviña for her teaching on the Zetasizer and Prof. Arto Urtti for notable tips concerning the articles. Everyone at the chemistry lab deserves acknowledgement for creating a nice working atmosphere and for help in all types of technical and practical problems, especially Dr Vladimir Chukharev, Prof. Nikolai Tkachenko and Mrs Anne-Maarit Tikkanen. I would like to thank my officemates at different time points, Ms Kati Stranius, for her excellent companionship, and Mrs Hanna Hakola, for the good moments. I am grateful to my colleague Dr Rajeev Dubey for the funny coffee breaks and MSc Marja Asp-Lehtinen for the refreshing corridor talks. I would like to thank Mrs Ekaterina Lisitsyna for her fruitful collaboration, and I look forward to continuing it.

Finally, I thank my daughter, Ada-Emilie, for her smiles and hugs, just being with me and giving me something to think about other than my work. My parents, Marketta and Olavi, deserve special compliments for their support and attentiveness to my daughter anytime I needed their help. I would also like to thank my brother, Jani, and my sister, Hanna-Riikka, for their support and being on my side. To my dearest friends, Toni, Jonna, Marjaana, Noora and Tiina, thank you for your support, discussions, laughs and nice moments with you, and special thanks to my English teacher, Toni, for his time-consuming work with me.

Each of you has been a piece of the jigsaw puzzle of my thesis. Thanks to everyone for giving me the strength to complete my thesis.

Tampere, October 2013

Tiia-Maaria C. Ketola

Table of Contents

List of Figures

List of Tables and Schemes

Tables

Schemes

List of Publications

The thesis is based on the work contained in the following publications, which are hereafter referred to by their Roman numerals:

I Independent versus Cooperative Binding in Polyethylenimine–DNA and Poly(L-lysine)–DNA Polyplexes

Tiia-Maaria Ketola, Martina Hanzlíková, Linda Leppänen, Manuela Raviña, Corey J. Bishop, Jordan J. Green, Arto Urtti, Helge Lemmetyinen, Marjo Yliperttula and Elina Vuorimaa-Laukkanen, *J. Phys. Chem. B* **2013**, *117*, 10405–10413.

II Role of Polyplex Intermediate Species on Gene Transfer Efficiency: Polyethylenimine–DNA Complexes and Time-Resolved Fluorescence Spectroscopy

Tiia-Maaria Ketola, Martina Hanzlíková, Arto Urtti, Helge Lemmetyinen, Marjo Yliperttula and Elina Vuorimaa, *J. Phys. Chem. B* **2011**, *115*, 1895–1902.

III Poly(*β*-amino ester)–DNA Complexes: Time-Resolved Fluorescence and Cellular Transfection Studies

Elina Vuorimaa, Tiia-Maaria Ketola, Jordan J. Green, Martina Hanzlíková, Helge Lemmetyinen, Robert Langer, Daniel G. Anderson, Arto Urtti and Marjo Yliperttula, *J. Control. Release* **2011**, *154*, 171–176.

IV The Effect and Role of Carbon Atoms in Poly(β-amino ester)s for DNA Binding and Gene Delivery

Corey J. Bishop, Tiia-Maaria Ketola, Stephany Y. Tzeng, Joel C. Sunshine, Arto Urtti, Helge Lemmetyinen, Elina Vuorimaa-Laukkanen, Marjo Yliperttula and Jordan J. Green, *J. Am. Chem. Soc.* **2013**, *135*, 6951–6957.

Author's contribution

Tiia-Maaria Ketola either planned or carried out almost all the fluorescence and particle size measurements and data analysis. She wrote publications I–II and participated in writing publications III and IV.

Abbreviations and Symbols

A	Spectral area
A_1	Spectral area of the short-living component
A_2	Spectral area of the long-living component
$A_{1,NoQYcor}$	Raw spectral area without correction of relative quantum yield (ϕ_{rel})
ABS_i	Absorbance at 483 nm
AD	Amine density = average number of amine-groups in a polymer molecule (N_N) per the average molecular weight of the polymer (M_w)
$a_i(\lambda)$	Local amplitude (pre-exponential factor)
$a_{i,max}$	Maximum amplitudes at each N/P ratio
$a_{1,max}$	Maximum amplitudes of short-living component at each N/P ratio
$a_{2,max}$	Maximum amplitudes of long-living component at each N/P ratio
α	Experimental Hill coefficient
Am/Ac	Amine:acrylate ratio
B	Proportion of DNA bound by the polymer
BB	Backbone, diacrylate monomer of PBAE
BPEI	Branched polyethylenimine, 25 kDa
DAS	Decay-associated spectra
DLS	Dynamic light scattering
DNA	Deoxyribonucleic acid, double-stranded, plasmid DNA, about 5000 bp or 7164 bp
EC	End cap, end group amine monomer of PBAE
ETI	Ethidium bromide
FWHM	Full width at half maximum
I	Intensity
IF_i	Area of the fluorescence spectra with excitation wavelength of 483 nm
K_{co}	Average cooperative binding constant per amine
$(K_{co})^{\alpha}$	Overall cooperative binding constant, K_{tot}

K_I	Independent binding constant per amine
K_{tot}	Overall cooperative binding constant, $(K_{co})^{\alpha}$
ϕ_{rel}	Relative quantum yield
ϕ_{ETI}	Quantum yield of free ETI
ϕ_{ED}	Quantum yield of ETI–DNA
χ^2	Mean-square deviation
x_{ETI}	*B*, the proportion of DNA bound by the polymer
LPEI	Linear polyethylenimine, 22 kDa
λ	Wavelength
λ_{exc}	Excitation wavelength
M_w	Average molecular weight of the polymer (g/mol = Da)
M–H	50 mM Mes–50 mM Hepes–75 mM NaCl buffer
N	Number of phosphate groups on the DNA molecule
N_C	Number of carbons in polymer backbone or side chain
N_N	Number of amine groups in polymer molecule
NaAc	25 mM sodium acetate buffer
N/P ratio	Molar ratio of polymer nitrogens (N) to DNA phosphates (P)
[P]	Concentration of free amine groups (mol N groups dm^{-3})
PBAEs	Poly(β-amino ester)s
PEI	Polyethylenimine
pK_a	Logarithmic acid dissociation constant
PLL	Poly(L-lysine), 200 kDa
R_{max}	Maximum amplitude ratio at w/w = 100
R_{min}	Minimum amplitude ratio at w/w = 1
RNA	Ribonucleic acid
SC	Side chain, amine monomer of PBAE

siRNA	Small interfering RNA, short interfering RNA or silencing RNA, a class of double-stranded RNA molecules (20–25 bp)
sNaAc	25 mM sodium acetate–87 mM NaCl buffer
SPEI	Branched polyethylenimine, 0.8 kDa
TCSPC	Time-correlated single photon counting
τ	Lifetime
τ_1	Short-living lifetime
τ_2	Long-living lifetime
vector	DNA carrier in gene transfer
w/w	PBAEs polymer weight to DNA weight ratio
ZP	Zeta potential, V

1 Introduction

Cancers and inheritable diseases result from inactive genes[1, 2]. Gene therapy is a technique for correcting defective genes that are responsible for disease development. Gene delivery is the process of introducing foreign DNA into host cells. Thus, gene delivery is one of the necessary steps for gene therapy. The intracellular delivery of gene medicines is of utmost importance because transgenes must be transferred in active form into the nucleus, and efficient gene knockdown by siRNA, ribozymes and antisense oligonucleotides takes place only upon the cytoplasmic delivery of these gene medicines.[3–8] However, DNA and oligonucleotides have poor permeability in the cell membranes due to their large size, hydrophilicity and negative charges. In addition, DNA is biodegradable: outside the nucleus, where enzymes are not able to repair it, it degrades in a few minutes. Thus, to deliver DNA to its target, it has to be protected, and its endocytosis into cells must be made possible. The viruses are able to transfer their genetic cargo to the host cells. Although most current gene therapy research relies on viral vectors, safety problems (including deaths in clinical trials) have slowed down the progress of this approach.[5] Non-viral (chemical) vectors, based on nano-sized particles, are potential alternatives to the viral vectors.[6] They possess advantages that are difficult to achieve with viral vectors: versatility, lack of immunogenicity, easy large-scale production, unrestricted DNA size and the opportunity to incorporate several different DNA species into the same particle.[7, 9] However, the chemical vectors (e.g., cationic dendrimers, polymers, peptides and lipids) show poor efficacy in intracellular gene transfer.[10–12] Biodegradable non-viral carriers contain, e.g., ester bonds that include oxygen in their backbone. Thus, they degrade easily, being less toxic, but at the same time, oxygen decreases the efficiency of the vector.[13]

The mechanisms of formation and uptake of the nanoparticles and the release of DNA inside the cell are still unknown. Many different types of non-viral vectors have been synthesised and studied with time- and material-consuming *in vitro* transfection experiments[4, 14–16]. Through these studies, it is possible to find out which carriers can transfect the carried genes and how efficient the transfection is compared with known references. Very little information on the reasons why one carrier works and another does not is obtained. Other methods, such as fluorescence spectroscopy, surface plasmon resonance, quartz crystal microbalance and different microscopy techniques should be utilised to yield information on what will happen to the carrier–DNA complex during the complex formation in a test tube, *in vitro* interaction with the cell surface, endosomal uptake of the complex in to the cell, the escape from the endosome inside the cell and the release of the DNA to the nucleus of the cell (**Scheme 1**). Advanced polymer synthesis combined with time-resolved spectroscopic methods can reveal, e.g., how the molecular structure of the carrier influences its efficiency. The effect of the molecular size or the functional groups of the carrier and the effect of the environment on the binding and releasing of DNA can be studied quantitatively. Correlating such data with the *in vitro* and *in vivo* transfection studies will yield valuable information for developing better chemical vectors for gene delivery.

Scheme 1 Nanoparticle formulation and extracellular and intracellular barriers for successful gene delivery.

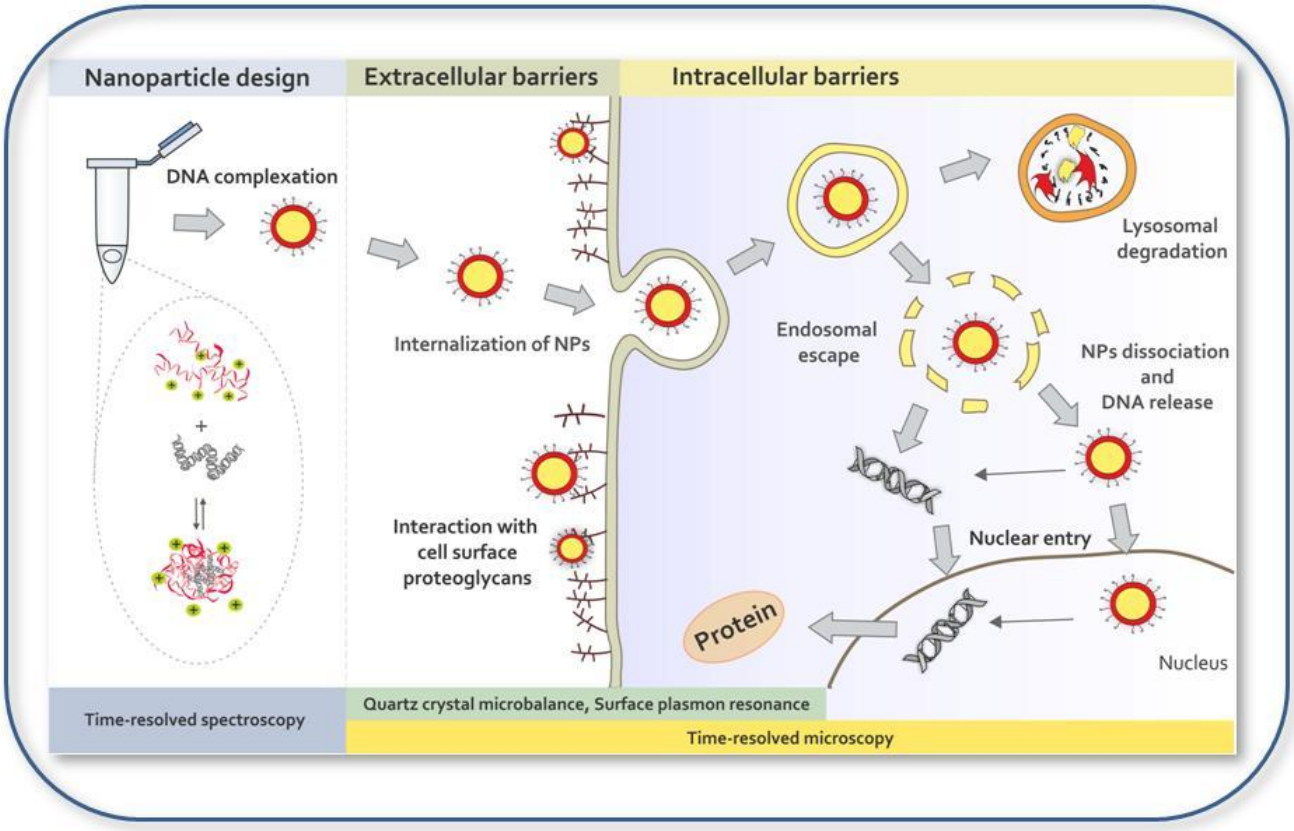

1.1 Aims and Outline of the Thesis

This thesis aims to contribute to understanding the complex formation between chemical vectors and DNA, i.e., the very first step in the gene delivery process. A method based on time-resolved fluorescence measurements recently developed in the research group[17] was utilised and improved further. With this technique, it is possible to obtain quantitative information on the mechanism and the binding affinities of the polyplex formation and thus reveal differences between the polyplexes prepared with different polymers.

There are many types of polymers used for non-viral gene delivery, such as polyethylenimine (PEI)[18], chitosan[19], cyclodextrins[20], polypeptides (i.e., poly(L-lysine) (PLL) and peptides)[21], and others.[7] PLL is one of the earliest investigated gene carriers because of its excellent DNA condensation ability and efficient protection of DNA from nuclease digestion. However, it transfects poorly both *in vitro* and *in vivo*.[4] PEI, on the other hand, is one of the most potent synthetic gene carriers and the most widely studied[22–26]. PEI delivers DNA successfully both *in vitro* and *in vivo*[27]. These two common model polymers, i.e., PEI[I, II] and PLL[I], were used for testing and developing the time-resolved fluorescence method. The effects of pH, type of amine groups, polymer structure, molecular weight, ionic strength, buffer, incubation time and free polymer on the mechanism and efficiency of the polyplex formation were studied. One class of polymers of interest for gene delivery are the poly(β-amino ester)s (PBAEs), which have low cytotoxicity due to their degradability. This reduced cytotoxicity can be 100-fold compared to commonly used non-degradable, cationic polymers such as PEI.[27] The best PBAEs have high gene

delivery efficacy and low cytotoxicity both *in vitro* and *in vivo*[9]. A selection of poly(*β*-amino ester)s[III, IV] with very different molecular structures compared to the model polymers were used to test the applicability of the method in analysing the formation of DNA polyplexes generally. Furthermore, the molecular structures of the poly(*β*-amino ester)s used in this thesis can be modified in a controlled way with the accuracy of single carbon unit. Thus, the effect of very small changes in the polymer structure on the formation of the polyplexes could be studied.

2 Background

Typical non-viral DNA delivery systems involve polycationic species, such us cationic polymers, peptides, cationic liposomes or micelles, that complex and condense plasmid DNA in solution, forming nanoparticles of 40–500 nm in diameter[14, 18, 28, 29]. Nanoparticle-mediated gene transfection involves several phases: DNA complexation, binding to the cell surface, endocytic uptake, endosomal escape to the cytosol, nuclear entry, transcription and translation (**Scheme 1**). The DNA carriers/vectors have several tasks in the gene delivery process: the vector should pack and protect DNA from various sources of degradation, such as nucleases. It should facilitate good circulation through tissue barriers right down to the target cell membrane. The vector should help to fix the DNA in the cell since, as a polyanion, DNA has no spontaneous ability to adhere to the polyanionic plasma membrane in cells. It should also help the DNA to cross the endosomal membrane and to promote intracellular circulation and penetration of the nucleus. Finally, DNA must be released from the nanoparticles before transcription.[30] Each of these steps can be potentially influenced by the vector used for DNA delivery systems[31].

In the next section, the properties affecting the gene delivery efficiency of the chemical vectors used in this thesis are discussed from the literature point of view. The binding models describing the independent and cooperative binding are introduced. Finally, the method based on time-resolved fluorescence spectroscopy used for determining the binding affinities and constants is described.

2.1 Formation and Properties of Polymer–DNA Complexes

The cationic vectors used in gene delivery studies contain primary (NH_2), secondary (NH) and/or tertiary (N) amine groups that can be protonated. Polyethylenimine (PEI) is a cationic polymer exhibiting the highest positive charge density when fully protonated in aqueous solution.[15, 18, 32, 33] Branched and linear polyethylenimines (**Figure 2.1**) are considered promising candidates as non-viral vectors for plasmid[18, 34, 35] and oligonucleotide delivery[36, 37] both *in vitro* and *in vivo*. They provide an attractive alternative to cationic lipid formulations because they combine remarkable transfection efficiencies with high complex stability[38] and allow transfection in the presence of serum[39]. Different kinds of polyethylenimines (PEIs) were characterized by Harpe et al.[40] to gain insight into their structural and functional properties. Analysis of the obtained data revealed differences in the extent of branching based on the ratio of primary (1°), secondary (2°) and tertiary (3°) amino groups. An amino group ratio of 1°:2°:3° = 1:2:1 was obtained for the synthesized PEI, whereas commercially available PEI generally showed a higher degree of branching and thus an amino group ratio of 1:1:1, respectively.[40] While some authors argue that lower molecular weight PEIs are more effective transfection reagents[35, 41], others report failing transfection for very low molecular weights in the range of 600–1800 Da and increasing efficiency with increasing molecular weights of PEI[42]. The purity, toxicity and biocompatibility of PEI is a matter of concern; e.g., high molecular weight polyethylenimine (800 kDa) is a non-biodegradable polymer and cannot be renally excreted and presents, therefore, problems for *in vivo* applications.[40] The optimal PEI architecture for gene delivery is not known, but the 25 kDa branched PEI and 22 kDa LPEI used in the present study are considered good model polymers of efficient vectors.[14]

Poly(L-lysine) (PLL) (**Figure 2.1**) is one of the earliest investigated gene carriers because of its excellent DNA condensation ability and efficient protection of DNA from nuclease digestion. Because of its peptide structure, PLL is biodegradable, which is an advantage for *in vivo* use[14, 43]. However, low-molecular weight (less than 3 kDa) PLLs do not form stable polyplexes[44], and high-molecular weight PLL ($M_w \geq 25$ kDa) is quite cytotoxic and transfects poorly both *in vitro* and *in vivo*.[4, 45] With 211 kDa PLL the polyplexes display up to 20-fold higher levels in the blood compared to 20 kDa PLL[43]. Thus, 200 kDa PLL used in this study is a perfect choice as a negative model vector.

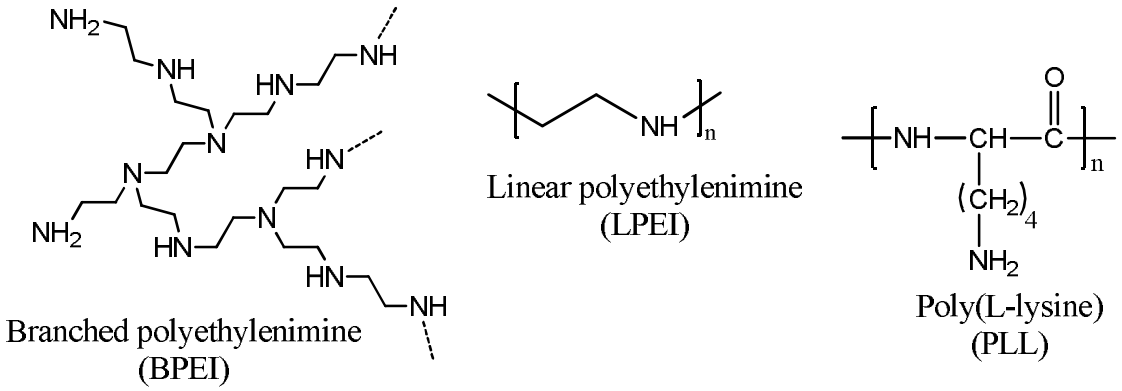

Figure 2.1 Structures of BPEI, LPEI and PLL.

Poly(β-amino ester)s (PBAEs)[9, 46–48] are promising agents for non-viral gene delivery due to their large potential for structural diversity, ability to condense DNA into small and stable nanoparticles, ability to buffer the endosome and facilitate endosomal escape. Furthermore, they are biodegradable via hydrolytic cleavage of ester groups, have low cytotoxicity compared with some other cationic polymers and relatively high transfection efficacy *in vitro* and *in vivo*. A library of 2350 structurally unique, degradable PBAEs have been synthesized[49], 46 of these new polymers can transfect with a higher efficiency than PEI[4]. In addition to the overall chemical structure and molecular weight of the polymers, attaching amine-containing groups to the acrylate-end groups leads to a significant increase in the transfection efficiency[4, 50].

The vectors interact with the negatively charged DNA through electrostatic interactions leading to polyplexes[43]. At physiological pH (≈ 7.4), the phosphates ($pK_a \approx 1$) of the DNA are always negative, so the number of negative charges is known[3]. Only the charged amines are active and participate in the complex formation with the negative phosphates of the DNA. However, the degree of protonation varies with the nature of the amine groups, i.e., primary, secondary or tertiary, and the pH of the medium.[3] Furthermore, the degree of protonation is affected by environmental constraints induced by the polymer, considerably reducing the pK_a of the amine groups. Hence, the overall charge of the polymer may be distinctly smaller than the number of amine groups.[3, 30, 51]

The pK_a values depend on the number of methylene units between two amines[52] (amine density), the temperature and the molecular weight of the polymers. Protonation states between neighbouring amines in PEI will be reduced when the methylene units between two amines increases[52]; hence, the high-amine density polymers, such as PEIs, have lower pK_a values than low-amine density polymers, such as PLLs. The effect of temperature has not been studied in this context and is not addressed here since the studies are conducted at a constant temperature. The effect of molecular

weight has been studied more elaborately[40]. For PEIs, the pK_a values decrease with increasing molecular weight. However, the buffer capacity at physiological pH levels does not vary in a systematic manner for PEIs of different molecular weights, suggesting that factors other than protonation are involved.[40] The complexation and condensation of oligonucleotides and DNA are influenced by the level of protonation and the flexibility of the polymer chains[40]. Hennink *et al.*[51, 53] studied the effect of the pK_a of the cationic groups on their transfection efficacy using various cationic vinyl polymers. The pK_a values varied from 7.5 to 8.8, and the lower the pK_a value is, the higher the amount of gene expression is. The pK_a values for PLL vary between 9 and 11[54–57], and for LPEI, the pK_a = 7.4–8.5[52, 58]. The average pK_a for BPEI is equal to that of LPEI, i.e., 7.4–8.5[52, 58, 59]. However, BPEI contains primary (100% protonated at pH << 9), secondary (50% protonated at pH 7.4) and tertiary amine groups (pK_a = 6–7, less than 50% protonated at pH 7.4)[60, 61]. The uptake of PLL complexes into cells is as efficient as for PEI complexes, but the transfection efficiencies of PLL remain several orders of magnitude lower than PEIs independent of the cell line used. A potential reason for this is the lack of amino groups with a pK_a between 5 and 7, thus allowing no endosomolysis[8, 14]. At physiological pH, a large fraction of the amines of PEIs is not protonated and can function in endosomes as a proton sponge, with endosomolytic properties[3].

For cationic polymers with a high buffering capability over a wide pH range, the endosomal escape to the cytosol has been observed to take place via the 'proton sponge' phenomenon.[33, 62–64] These polymers usually contain secondary and/or tertiary amine groups with pK_a close to endosomal/lysosomal pH. Since the *in vivo* transfection studies are made at pH 7.4, not all the amine groups of the polymer with the 'proton sponge' ability are protonated. During the maturation of endosomes, the membrane-bound ATPase proton pumps actively translocate protons from the cytosol into the endosomes, leading to the acidification of endosomal compartments and the activation of hydrolytic enzymes. At this stage, unprotonated amine groups of the polymer will become protonated and resist the acidification of endosomes (**Figure 2.2**). As a result, more protons will be continuously pumped into the endosomes with the attempt to lower the pH. The proton pumping action is followed by the passive entry of chloride ions, increasing ionic concentration and leading to water influx. Eventually, the osmotic pressure causes swelling and rupture of endosomes, releasing their contents to the cytosol.

For transfection experiments, the optimal N/P ratio of the PEI–DNA complexes is usually 3–15 depending on the vector used[65, 66], while the polycation–DNA binding becomes saturated at an N/P ratio about 2–3.5[31, 33, 66, 67]. Boeckle et al.[31] demonstrated that the removal of free PEI from the complexes eliminated their gene transfection ability. Thus, efficient polymer-mediated gene delivery in the cells requires the presence of excess polymer in the solution[59, 65, 66]. During the formation of the polyplexes, the negative phosphate groups (P) of DNA are bound by the positive amine groups (N) of the polymer. At a certain N/P ratio, unique to each type of polymer, nearly all the DNA's P groups are bound by the polymer N groups and the polyplex becomes electrically neutral; i.e., its zeta potential (ZP) is close to zero. These complexes form the *core of the polyplexes*. The excess polymer, added to this system to increase the N/P ratio to the values giving efficient gene delivery, forms a positively charged *shell* around the *core polyplex* increasing its ZP.

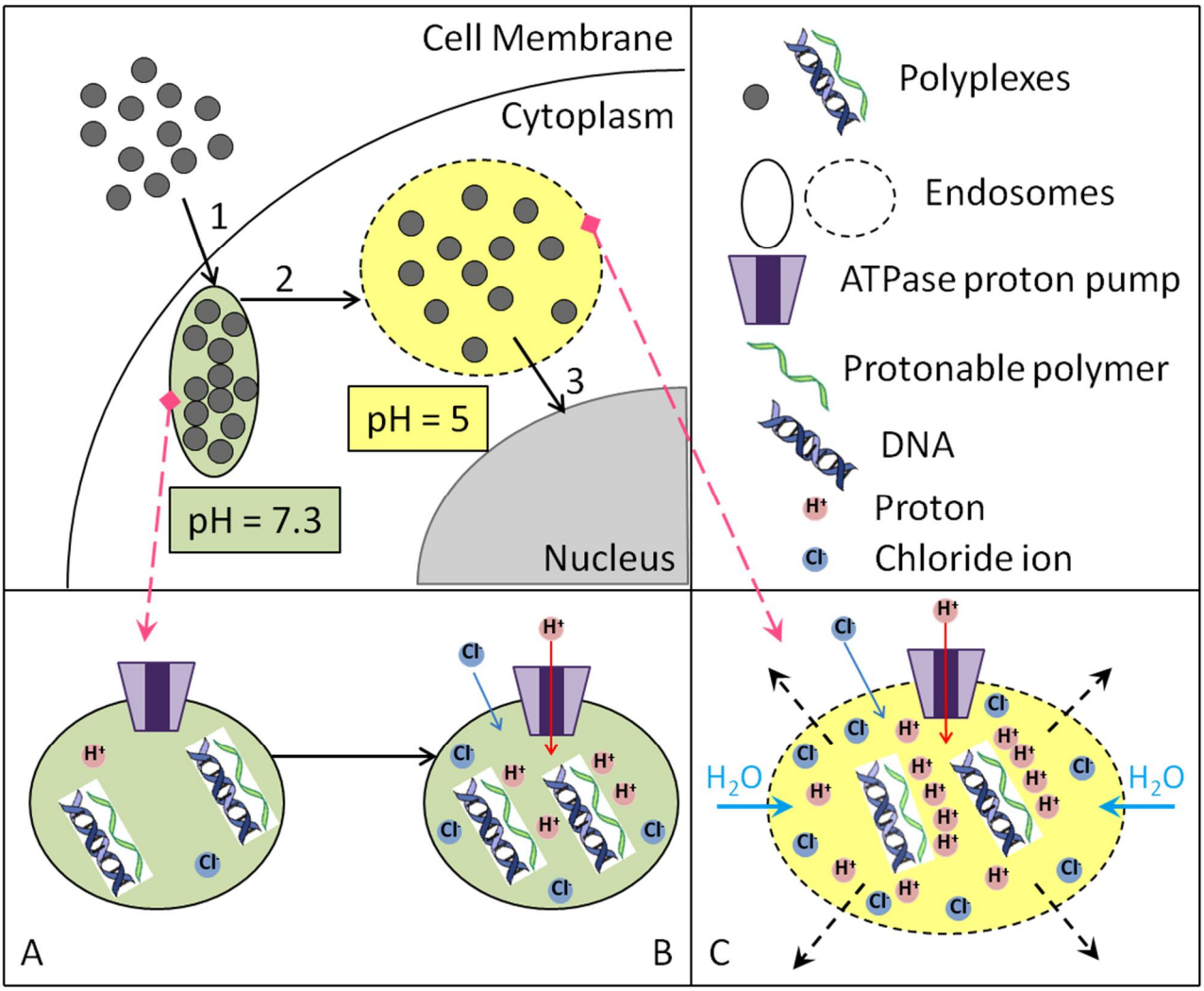

Figure 2.2 The 'proton sponge' hypotheses (pH-buffering effect). (1 & A) Polyplexes enter cell via endocytosis and are trapped in endosomes. (2 & B) Acidic endosome buffering leads to increased osmotic pressure and (3 & C) finally to lysis. (B) The membrane-bound ATPase proton pumps actively translocate protons into endosomes. Polymers become protonated and resist the acidification of endosomes. Hence, more protons will be pumped into the endosomes continuously to lower the pH. (C) The proton pumping action is followed by passive chloride ion entry, increasing ionic concentration and, hence, water influx. High osmotic pressure causes the swelling and rupture of endosomes, releasing their contents to cytosol. Figure modified from Ref. 33 and 64.

In addition to ZP measurements, the formation of the core–shell polyplex can be studied by measuring the particle sizes of the polyplexes at different N/P ratios. At N/P ratios, where the polyplex ZP ≈ 0 mV, the polyplexes aggregate significantly, and the size of the observed particles increases to > 1000 nm[15, 67]. With the presence of excess polymer, the ionic repulsion between the positive polyplexes keeps their sizes considerably smaller. For example, 25–26 kDa PLL–DNA complexes with N/P ratios greater than 1.0 form either 25–50 nm toroids[15, 44] or 40–80 nm rods[44] and complexes of PEI–DNA (using 25 kDa PEI) at an N/P ratio of 9.2 are homogenous 40–60 nm toroids[15]. These results were obtained from dry samples with electron microscopy. When measured with dynamic light scattering from wet samples, the size of PEI–DNA complexes ranged from 90 to 130 nm (at N/P > 8.0)[15, 68], and the size of PLL–DNA complexes was 50 nm (at N/P > 1.4)[44].

For non-viral vectors, in addition to the molecular weight of the vector and the N/P ratio used, the size of the polyplexes also depends on the salt concentration of the buffer solution. For instance,

when PEI is added to a plasmid solution (**Figure 2.3**), it very quickly associates with several plasmid segments. There then follows a rapid condensation of several plasmids in a complex that becomes positive when excess PEI is used. When this PEI–DNA condensation is carried out in the absence of salts, these complexes, positively charged at the surface, are particles measuring between 50 and 70 nm in diameter. Ionic repulsion then ensures their stability in solution. However, these same particles aggregate very quickly when their ionic surface is screened by other ions at physiological concentrations, e.g., 150 mM NaCl. It has thus been demonstrated that aggregates 500–1000 nm in diameter are obtained after a 10 min incubation in 150 mM of NaCl (at a N/P ratio of 5 for PEI) (**Figure 2.3**).[3]

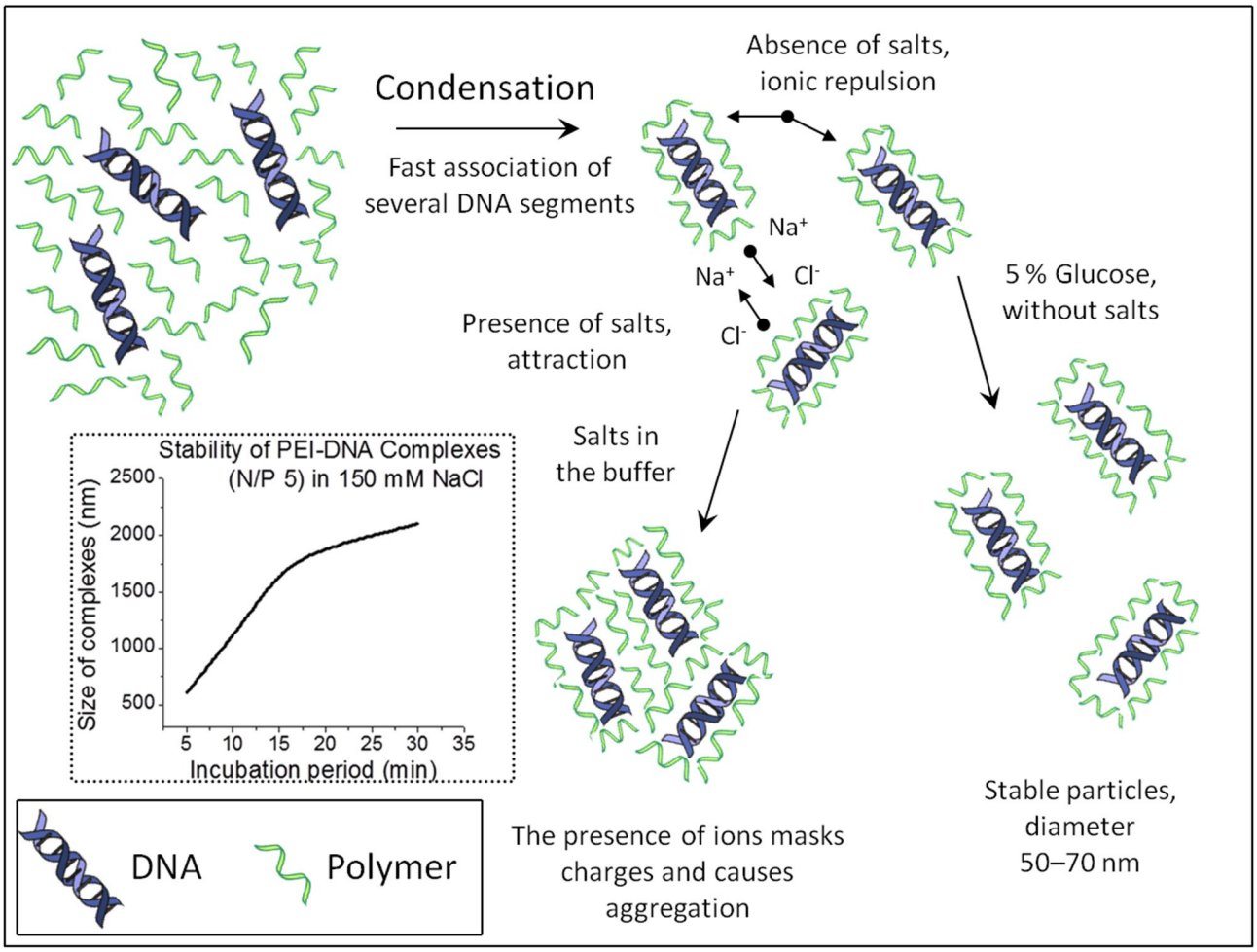

Figure 2.3 The stability of PEI–DNA polyplexes formed in the presence of excess cationic charge depends on the ionic strength of the reaction medium. Figure modified from Ref. 3.

Since positively charged complexes interact with the cell surface by an electrostatic interaction with anionic substances on the cell surface, such as sialic acid and proteoglycan, the zeta potential of polyplexes is important. Polyplexes composed of polycations with molecular weights of several thousand exhibit significantly higher zeta potentials than smaller polycations, irrespective of the polycation used. Internalisation events also seem to be affected by polyplex particle size and zeta potential. Generally, aggregation of the complexes makes their internalisation difficult because of their large size. Aggregation of the polyplexes in serum-containing medium or in blood is also a problem. However, the correlation between the transfection efficiency and particle size of the

polyplexes remains unclear[15, 30], not the least because of the good transfection results obtained with highly aggregated LPEI[I, 23, 58, 69, 70]. For gene expression in the lungs (*in vivo)*, the best results are obtained with small particle size of LPEI (22 kDa) and large particle size of BPEI (800 kDa and 25 kDa)[70]. The *in vitro* large particle size of PEIs (LPEI and BPEIs) gives better transfection efficiencies[70, 71].

Dai et al. have shown that the cellular uptake rate of BPEI–DNA polyplexes at N/P ratio 3 increased significantly when adding excess PEI up to N/P = 10. Free 25 kDa BPEI was especially effective in enhancing polyplex internalization. Addition of free 2.5 kDa LPEI has a comparable promoting effect as 25 kDa LPEI and 25 kDa BPEI, with respect to transfection efficiency, when the final N/P ratio is 10 or 15. More efficient non-viral gene transfection systems could therefore be constructed by using high-molecular weight (M_w) PEIs for polyplex formation in combination with free PEIs with low M_w, as low M_w PEIs are associated with a lower cytotoxicity.[66]

Hanzlikova *et al.*[65] studied the role of free BPEI by removing the free BPEI from the polyplexes and/or the glycosoaminoglycans (GAGs) from the cell surface (**Figure 2.4A–D**). The transfection efficiency decreased in the following order: no free BPEI, no GAGs (**Fig. 2.4D**) > free BPEI, no GAGs (**Fig. 2.4C**) > free BPEI + GAGs (**Fig. 2.4A**) > GAGs, no free PEI (**Fig. 2.4B**)[65]. It appears that the inhibition of polyplex transfection by cell-surface GAGs is one of the critical factors in PEI-mediated transfection[31, 72]. This inhibition can be overcome by free PEI: the free PEI masks the GAGs in the cell surface by binding to them, and thus the endocytosis of the core polyplex becomes easier. Hence, the role of free PEI is linked to the GAG concentration of the target cell type. Whether the free PEI also has some other function in the transfection process was studied by adding free PEI at different times after the experiments with purified polyplexes were started. Since the addition of free PEI 4 h after the purified polyplexes led to the strongest enhancement of gene expression, it is likely that free PEI also contributes to the endosomal release or some other process thereafter.[31] First, the purified polyplexes are internalised into endosomes. The free PEI added afterward is also internalised into endosomes, and these vesicles containing PEI alone merge with the polyplex containing-vesicles. The free PEI can now aid in the releasing of the polyplexes from the endosomes by the proton sponge effect. The positive effect of adding free PEI to purified polyplexes indicates that a certain minimum amount of excess PEI (final N/P ratio > 6) is necessary to achieve the proton sponge effect[33, 71]. This can also be accomplished by using either high N/P ratios[73] or large aggregated polyplexes. The role of PEI was confirmed by a recent study[62] showing that both free PEI and PEI polyplexes contribute to the proton sponge mechanism of PEI: both lead to the accumulation of chloride in vesicles and the buffering of vesicular pH. Free PEI can also have an impact on gene delivery when added to polyplexes with poor endosomal escape, e.g., PLL–DNA polyplexes[33]: the reporter gene expression of PLL–DNA polyplexes was reported to increase 10-fold in the presence of free PEI.[31]

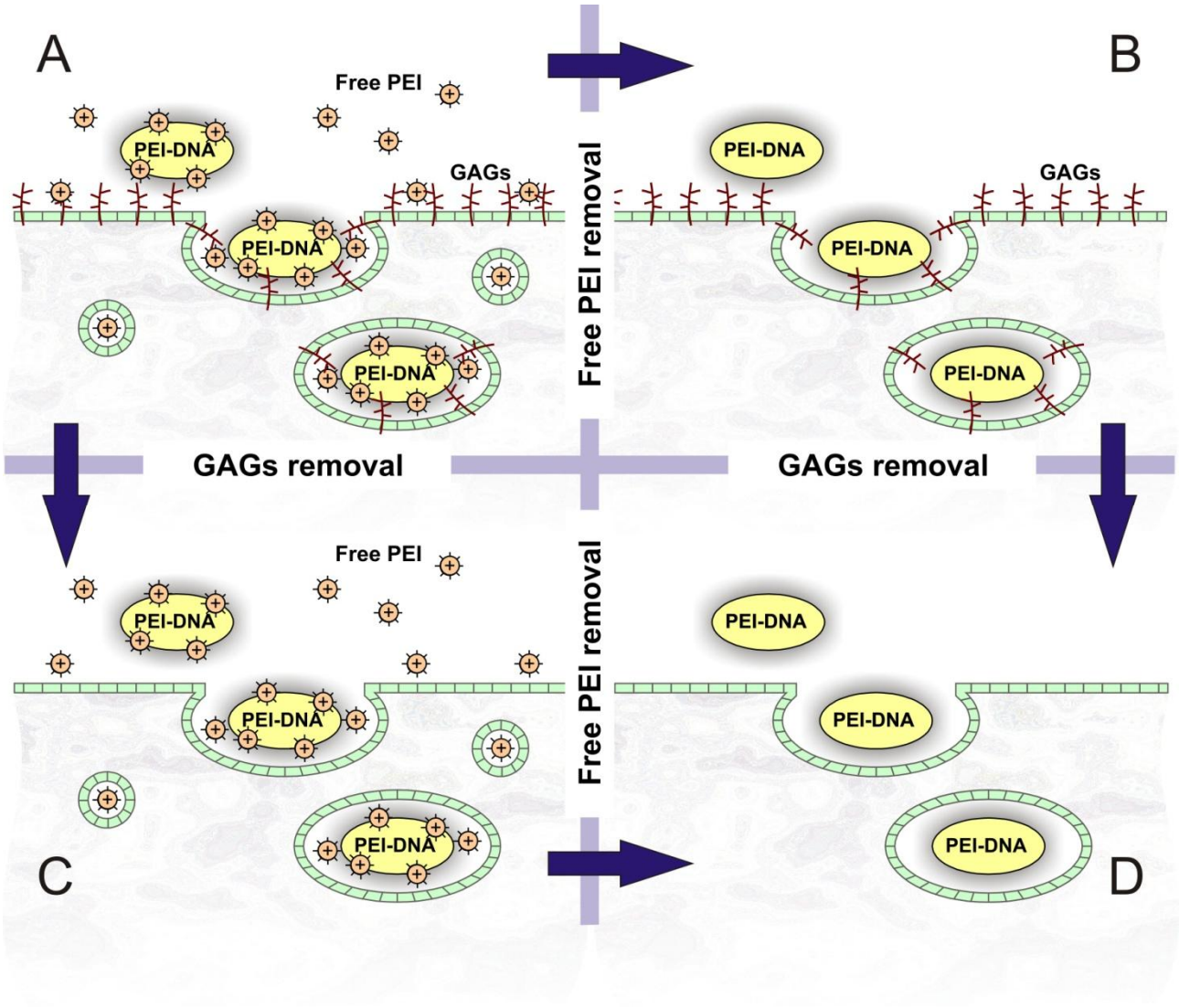

Figure 2.4 Concept of transfection experiments illustrating four different alternatives: (A) wild-type cells and polyplexes with free PEI; (B) wild-type cell and polyplexes without free PEI; (C) GAG-deficient cells and polyplexes with free PEI; (D) GAG-deficient cells and polyplexes without free PEI. The highest transfection efficiencies are observed for cases D and C. Figure from Ref. 65.

2.2 Binding Equilibria of Polymer–DNA Complexes

Equilibrium processes in which non-covalent interactions take place occur widely in chemical and biochemical systems. The determination of the equilibrium constant of a reaction is an important step in describing and understanding these systems. In this thesis, the substrate, i.e., DNA, is the component whose binding is experimentally observed and the ligand, i.e., a cationic polymer, is the component whose concentration is varied. The stoichiometric ratios are expressed in the order of ligand–substrate. Since the binding actually takes place between the polymer amine groups and DNA phosphate groups, we have a case where a multivalent ligand binds to a multi-subunit substrate. Two models, the independent binding model, which is mostly used for polymer–DNA systems in the literature, and the cooperative binding model applied in I and IV, can be used to determine the binding constants and the binding mechanism.

2.2.1 Independent Binding Model

In the independent binding model, the binding of a ligand (P, polymer N group) to a site on a macromolecule (DNA phosphate group) has no impact on simultaneous or subsequent binding to other unoccupied sites, and the reaction can be written as

$$P + DNA \rightleftharpoons P{:}DNA \,. \qquad (2.2.1.\mathbf{1})$$

Thus, the proportion of DNA bound by the polymer, *B*, can be correlated to the binding constant of the polyplex formation (K_I) by

$$B = \frac{[P{:}DNA]}{[DNA]+[P{:}DNA]} = \frac{K_I[DNA][P]}{[DNA]+K_I[DNA][P]} = \frac{K_I[P]}{1+K_I[P]} \,. \qquad (2.2.1.\mathbf{2})$$

Taking the reciprocal of the resulting equation, we obtain:

$$\frac{1}{B} = 1 + \frac{1}{K_I[P]} \,, \qquad (2.2.1.\mathbf{3})$$

where K_I is the independent binding constant of the overall equilibrium and *[P]* is the concentration of free amine groups (mol N groups dm^{-3}). According to equation 2.2.1.**3** plotting the ratio $1/B$ as a function of the $1/[P]$ should yield a linear dependence with the binding constant equal to the inverse of the slope.

2.2.2 Cooperative Binding Model

In cooperative binding model, the binding of a ligand to a site on a target molecule can influence the binding of other ligands to other unoccupied sites on the same target. For positive cooperativity, the binding of the first ligand makes it easier for the next one to be bound. In negative cooperativity, each succeeding ligand is bound less strongly than the previous one.[74, 75] The Hill plot model for multivalent ligand binding to multi-subunit substrate[76–79], such as a cationic polymer binding to DNA, can be described by the following binding equilibria:

	Binding constant of each reaction	
$P + DNA \rightleftharpoons P{:}DNA$	K_1	(2.2.2.**1**)
$P + P{:}DNA \rightleftharpoons P_2{:}DNA$	K_2	(2.2.2.**2**)
⋮		
$P + P_{N-1}{:}DNA \rightleftharpoons P_N{:}DNA$	K_N	(2.2.2.**3**)
———		
$N\,P + DNA \rightleftharpoons P_N{:}DNA$	K_{tot}	(2.2.2.**4**)

Here, P is one binding group of the ligand; i.e., an active amine group of the polymer and DNA is one phosphate group of the DNA molecule. The binding constant for the overall reaction 2.2.2.**4** is

$$K_{tot} = K_1 \times K_2 \times \ldots \times K_N = \frac{[\mathrm{P_N{:}DNA}]}{[P]^N[DNA]} .$$ (2.2.2.**5**)

If all phosphate groups of DNA are either unoccupied or all are occupied and no other situation is possible, the system is fully cooperative and *N* corresponds to the number of phosphate groups on the DNA molecule. In practice, the degree of cooperativity is less extreme and *N* is replaced with an experimental Hill coefficient α :

$$K_{tot} = \frac{[\mathrm{P_N{:}DNA}]}{[P]^{\alpha}[DNA]} .$$ (2.2.2.**6**)

The Hill coefficient α varies from the independent value α = 1 to α > 1 for positive cooperativity and $\alpha < 1$ for negative cooperativity. If the binding is cooperative, the binding constants K_1, K_2, …, K_N will be unequal and only the average cooperative binding constant for the binding of one functional amine group according to the reaction $\mathrm{P} + \mathrm{P_{x-1}{:}DNA} \rightleftharpoons \mathrm{P_x{:}DNA}$ (x = 1, 2, ….., N), K_{co}, can be obtained as $K_{tot} = (K_{co})^{\alpha}$.

The proportion of DNA bound by the polymer, *B*, is

$$B = \frac{[\mathrm{P_N{:}DNA}]}{[DNA]+[\mathrm{P_N{:}DNA}]}$$ (2.2.2.**7**)

and the proportion of free DNA is

$$1 - B = \frac{[DNA]}{[DNA]+[\mathrm{P_N{:}DNA}]} .$$ (2.2.2.**8**)

Taking a ratio of eq. 2.2.2.**7** and 2.2.2.**8** leads to

$$\frac{B}{1-B} = \frac{[\mathrm{P_N{:}DNA}]}{[DNA]} .$$ (2.2.2.**9**)

Combining eq. 2.2.2.**9** with eq. 2.2.2.**6**:

$$\frac{B}{1-B} = (K_{co})^{\alpha}[P]^{\alpha} .$$ (2.2.2.**10**)

Taking the logarithm of both sides of eq. 2.2.2.**10**, the Hill equation for multivalent ligand binding to a multi-subunit substrate is obtained:

$$\ln\left(\frac{B}{1-B}\right) = \alpha \ln[P] + \ln(K_{co})^{\alpha} .$$ (2.2.2.**11**)

According to this equation, plotting $\ln\left(\frac{B}{1-B}\right)$ as a function of ln *[P]* should yield a straight line with a slope α and an intercept ln K_{tot}. In practice, a Hill plot does not always appear as a single straight line but can be a composite of two or three lines with different slopes[80] or exhibit a curvilinear behaviour[81, 82].

2.2.3 Binding Isotherms

A graphical display of the binding isotherm can be a powerful means of assisting qualitative interpretations and obtaining quantitative estimates of the binding equilibrium. To demonstrate these plotting forms, we use simulated data, which are calculated by

$$B = \frac{[P]^{\alpha}(K_{co})^{\alpha}}{1+[P]^{\alpha}(K_{co})^{\alpha}} . \qquad (2.2.3.\mathbf{1})$$

The cooperative binding isotherm eq. 2.2.3.**1** returns to the independent binding isotherm eq. 2.2.1.**2** when the Hill coefficient α = 1; hence, cooperative binding model can be used as a generic binding model. The characteristic binding isotherms for independent, positive and negative cooperativity systems for three different K_{co} values calculated with eq. 2.2.3.**1** are shown in **Figure 2.5**.

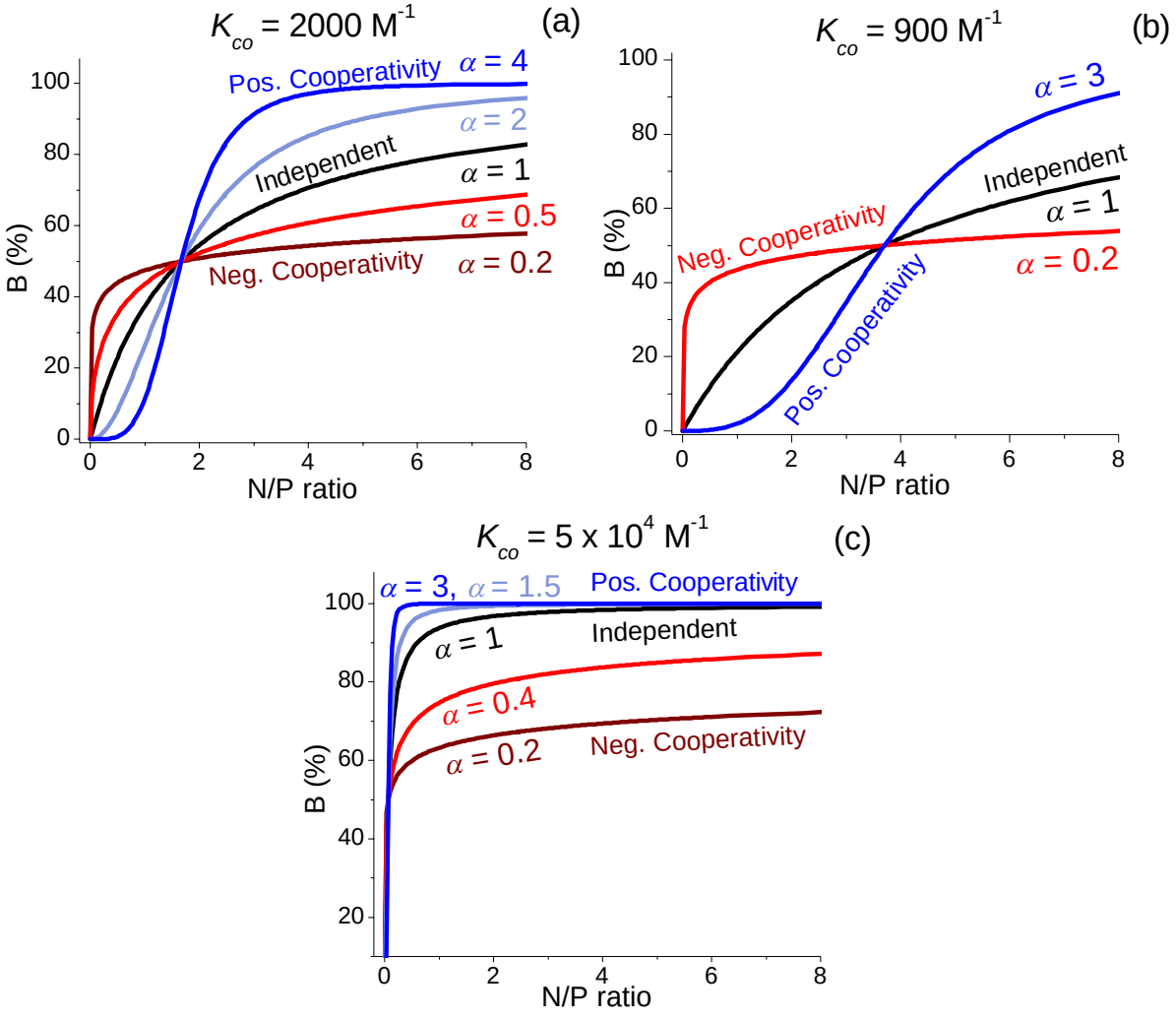

Figure 2.5 Binding isotherms calculated with eq. 2.2.3.**1** for different degrees of cooperativity, α and binding constants per amine, K_{co} (a) 2000 M^{-1} (b) 900 M^{-1} and (c) 5 × 10^{4} M^{-1}.

The effect of the degree of cooperativity can be clearly observed in **Figure 2.5a**. For positive cooperativity at α values from 2 to 4, a characteristic sigmoidal shape of the binding isotherm is observed. The saturation level of nearly 100% of the substrate bound by the ligand is obtained already at N/P = 4 in the case of α = 4. For α = 1, i.e., the independent binding system, a smooth

saturation curve is obtained, with *B* still increasing at N/P = 8. For negative cooperativity at α values from 0.2 to 0.5, the increase in *B* is very steep at small N/P ratios, and the saturation level is reached at smaller N/P ratios than for the independent system with $\alpha = 1$. In addition, the saturation level does not reach 100% at reasonable N/P ratios. By comparing **Figures 2.5a–c** with each other, the effect of the K_{co} value can be observed. The smaller the K_{co} value, the higher N/P ratio is needed for reaching the saturation level of the system. An isosbestic point is observed in the curves at *B* = 50% and an N/P ratio that corresponds to $[P] = 1/K_{co}$.

Figure 2.6 presents a plot of B as a function of the N/P ratio calculated with the typical values for the polymer–DNA complexes used in this thesis. For systems with positive cooperativity, the overall binding constants ($K_{tot} = (K_{co})^{\alpha}$) had very large values on the order of 10^7–10^{14}[I], whereas for the systems with negative cooperativity, K_{tot} values of 8–60[IV] were obtained. The average binding constants (K_{co}) behaved oppositely: for positive cooperativity, the values were smaller, about 4000–7000 M^{-1}[I], than for negative cooperativity, which gave values of 10^3–10^5 M^{-1}[IV]. This feature is logical because, for systems exhibiting positive cooperativity, the individual binding constant increases with each bound ligand, i.e., $K_1 < K_2 < K_{3...}$ until the saturation limit is reached, resulting in $K_{tot} >> K_{co}$. For systems exhibiting negative cooperativity the opposite takes place: the individual binding constant decreases with each bound ligand, i.e., $K_1 > K_2 > K_{3...}$, until the saturation limit is reached, resulting in $K_{tot} << K_{co}$. For the present systems with multivalent ligands binding to multisubunit substrate, this effect is particularly strong. For positive cooperativity systems, when one amine of the chain of amines is bound, it will be very easy for the next amines in the same polymer chain to bind since they are already physically near the phosphates of the DNA. Thus, a small binding constant per amine is obtained. For negative cooperativity systems, the first amine bound will cover a large area of the surface of the DNA, preventing the next amine of the same polymer chain from binding despite being physically close. Thus, although a large binding constant per amine is obtained, some of the phosphate groups of the DNA remain sterically unreachable and the overall binding constant remains small.

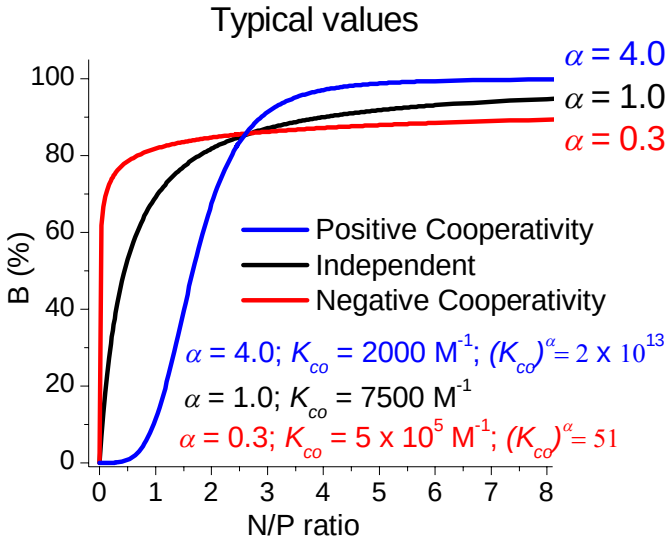

Figure 2.6 Binding isotherms calculated with the typical values for the polymer–DNA complexes used in this thesis.

2.2.4 Time-Resolved Fluorescence for Binding Affinity

In the present thesis, the formation of polymer–DNA complexes is studied by time-resolved fluorescence spectroscopy. Thus, we need a fluorescent probe whose fluorescence properties change clearly during the complex formation and that has a high fluorescence quantum yield, at least either in the presence of the complex or in the absence of it. Ethidium bromide (**Figure 2.7**), a positively charged fluorescence probe, fulfils these requirements.[83–91]

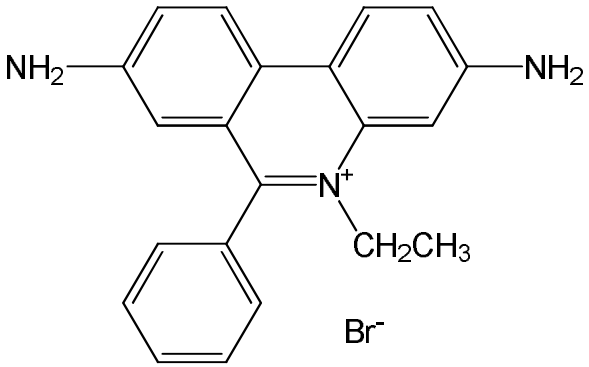

Ethidium bromide (ETI)

IUPAC name	3,8-Diamino-5-ethyl-6-phenylphenanthridinium bromide
Molecular formula	$C_{21}H_{20}BrN_3$
Molar mass (M_w)	394.294 g/mol
Solubility in H_2O	≈ 40 g/l
Melting point	260–262 °C
Appearance	Purple-red solid
Absorption maxima	400–500 nm
Molar absorption coefficient at 480 nm	5450–5600 $M^{-1}cm^{-1}$
pK_{a1}, pK_{a2}	2.0, 0.8

Figure 2.7 Structure and properties of ethidium bromide (ETI).

While ETI is free in the solution, its fluorescence at 640 nm (**Figure 2.8a**) is relatively weak and has a fluorescence lifetime of about 1.8 ns (**Figure 2.8b**). In the presence of DNA, ETI intercalates between two adenine–thymine base pairs. Simultaneously, its fluorescence maximum shifts to 610 nm (**Figure 2.8a**), the quantum yield increases about 7–8 times and its fluorescence lifetime increases to about 24 ns (**Figure 2.8b**). In our experiments, we used an ETI–DNA–nucleotide ratio of 1:15 to ensure that all ETI is bound by DNA. Thus, in the beginning, only ETI–DNA complexes are present in the solution.

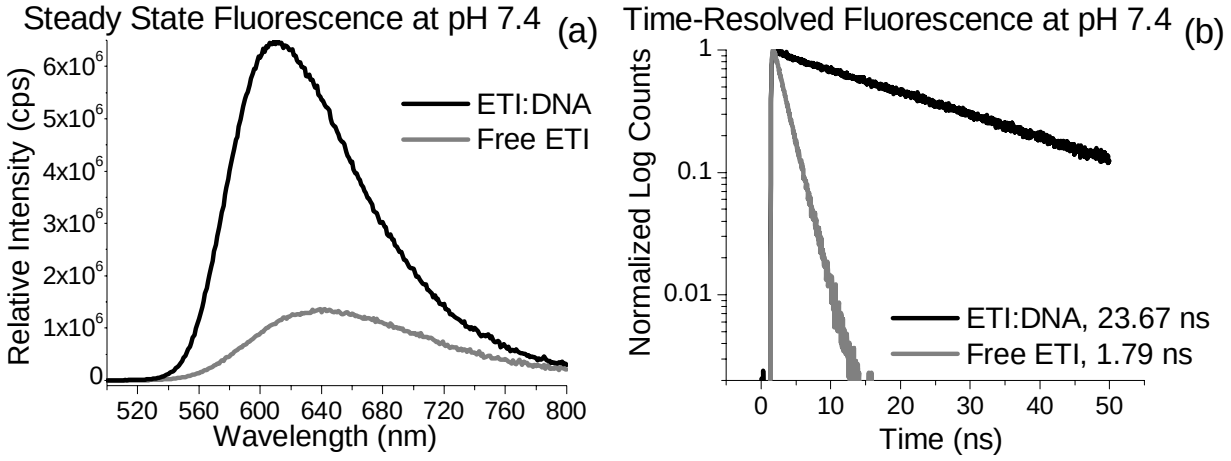

Figure 2.8 Steady-state fluorescence spectra and fluorescence decay curves at 610 nm for ETI–DNA complex and free ETI in Mes–Hepes–NaCl buffer (M–H) at pH 7.4. In all cases the excitation wavelength was 483 nm.

In the presence of a cationic polymer, the DNA is condensed and there is no more space for ETI to stay intercalated into the DNA (**Scheme 2**). In addition, the environment of ETI becomes more

positive, which causes repulsion. Thus, ETI is freed back to the solution and its fluorescence lifetime changes from 24 ns in DNA to 1.8 ns in solution. With increasing amounts of cationic polymer in the solution, i.e., with an increasing N/P ratio, more ETI is freed from the DNA to the bulk solution. Steady-state fluorescence measurements utilising the fluorescence of ETI have been widely used to characterise DNA binding by cationic polymers and lipids[15, 44, 92–94]. Due to the overlapping and broad spectra of free ETI and ETI bound by DNA, this method can only be applied for the qualitative estimation of polyplex formation. With time-resolved fluorescence measurements, it is possible to determine quantitatively the proportions of free ETI and ETI bound by the DNA and thus determine the binding constants and possible multiple states of binding. Furthermore, the time-resolved measurements are not hampered by scattering due to the presence of DNA nanoparticles.

Scheme 2 Complex formation between carrier and DNA in the presence of ETI.

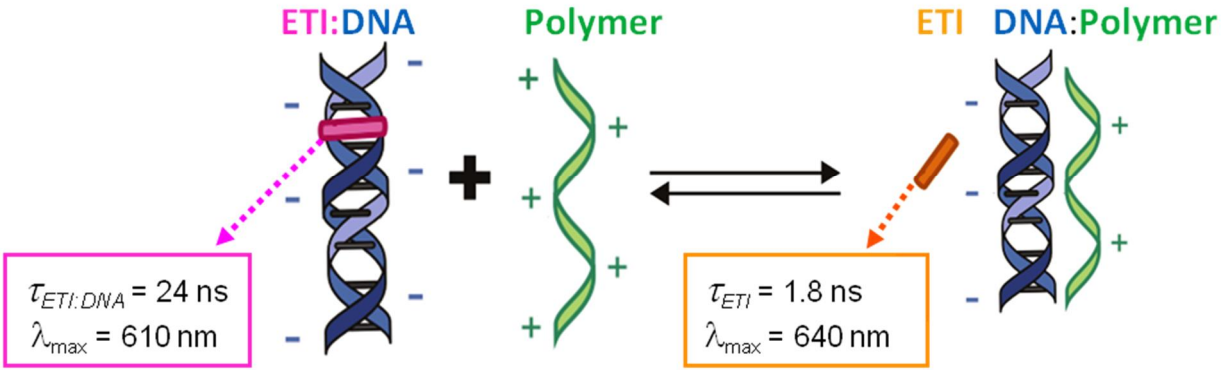

At the equilibrium presented in **Scheme 2**, there are four components present in the system: ETI–DNA complex, free carrier (e.g., polymer), free ETI and carrier–DNA complex. Among these, ETI–DNA complex and free ETI are fluorescent. A two-exponential fluorescence decay curve is observed with two distinct fluorescence lifetimes corresponding to the ETI–DNA complex and free ETI. Since the amount of free ETI is directly proportional to the amount of formed polyplexes, the binding equilibrium can be followed by monitoring the proportion of free ETI in the system. This kind of behaviour can be resolved with the following equation:

$$I(t,\lambda) = a_1(\lambda)e^{-t/\tau_1} + a_2(\lambda)e^{-t/\tau_2} \,. \qquad (2.2.4.\mathbf{1})$$

Here τ_i is the global lifetime and $a_i(\lambda)$ is the local amplitude (pre-exponential factor) at a particular wavelength. The amplitudes $a_i(\lambda)$ represent the relative amount of each fluorescing species at a particular wavelength. The decay curves are measured at different wavelengths and simultaneously fitted to this equation. When the amplitudes obtained from the fits are plotted as a function of wavelength for both components, the decay-associated spectra (DAS) are obtained[II, III]. In the case of a mixture of different non-interacting fluorescing species, these spectra correspond to the individual spectra of the species. Since the fluorescence quantum yield of ETI decreases when it is freed from DNA to the bulk solution, the relative quantum yield of ETI free in the solution versus ETI bound by the DNA, ϕ_{rel}, was determined from steady-state absorption and fluorescence measurements according to

$$\phi_{rel} = \frac{\phi_{ETI}}{\phi_{ED}} = \frac{IF_{ETI}}{IF_{ED}} \times \frac{ABS_{ED}}{ABS_{ETI}} .$$ (2.2.4.**2**)

In eq. 2.2.4.**2** ϕ_{ETI} is the quantum yield of free ETI, ϕ_{ED} is the quantum yield of ETI–DNA complex, IF_i is area of the fluorescence spectra with an excitation wavelength of 483 nm and ABS_i is the absorbance at 483 nm. The quantum yield-corrected spectral area of the short-living component can be calculated by

$$A_1 = \frac{A_{1,NoQYcor}}{\phi_{rel}} ,$$ (2.2.4.**3**)

where $A_{1,NoQYcor}$ is the raw spectral area without the correction of the relative quantum yield (ϕ_{rel}). The proportion of the short-living decay component, *B*, corresponding to ETI free in the solution, was calculated from the spectral areas of the components, $A_i = \int a_i(\lambda)d\lambda$, as follows:

$$x_{ETI} = \frac{A_1}{A_1+A_2} \times 100\% ,$$ (2.2.4.**4**)

where A_1 is the spectral area of the short-living component (free ETI) and A_2 is the spectral area of the long-living component (ETI–DNA complex). Since the amount of free ETI is directly proportional to the amount of P:DNA complex (**Scheme 2**), $x_{ETI} = B$ in eq. 2.2.1.**2** and 2.2.2.**7,** and the extent of the polyplex formation can be monitored by the relative amount of free ETI fluorescence on the system at each N/P ratio. Thus, for the independent binding model, we get

$$\frac{A_2}{A_1} = \frac{1}{K_I[P]} ,$$ (2.2.4.**5**)

and for the cooperative binding model, we get

$$\ln\left(\frac{A_1}{A_2}\right) = \alpha\ln[P] + \ln(K_{co})^{\alpha} ,$$ (2.2.4.**6**)

which were used to determine the degree of cooperativities and binding constants for the present systems[I–IV].

3 Materials and Methods

This chapter presents the experimental aspects of the work, including the polymers, instruments and sample preparation used in the studies. A full description of the experimental techniques is supplied in publications I–IV.

The plasmid pCMVß (7164 bp) encoding for the beta-galactosidase enzyme as a reporter gene was purified using a QIAfilter Plasmid Giga Kit (QIAGEN) according to the manufacturer's instructions at the University of Helsinki and was used as received in publications I–III. In publication IV, a plasmid-enhanced green fluorescent protein (pEGFP-N1) DNA (≈ 5000 bp) (Clontech), amplified and purified by Aldevron (Fargo, ND), was used.

The behaviour of different cationic polymers was compared in this study. However, the overall charge of the polymer may be distinctly smaller than the nitrogen number and varies with the pH of the medium.[3] In addition, the molecular weights of the studied carriers and the amine densities (average number of amine groups in the polymer molecule, N_N, per the average molecular weight of the polymer, M_w) vary between carriers. Thus, the amine to phosphate (N/P) ratio was used to define the amount of vectors in the formed polyplexes. This makes it possible to compare the behaviour of the carriers of different amine densities with each other and the behaviour of the polymers at different pH levels.

3.1 Polyethylenimines (PEIs) and Polypeptides

The polyethylenimines and polypeptides used in this study were commercially available and used without further purification. The properties of these carriers and the sample properties are listed in **Table 3.1**. For PLL, the backbone secondary amines are part of the peptide bonds. Thus, for PLL, only the primary amines at the end of the side chains take part in binding DNA, and only they were taken into account when calculating the N/P ratio. The polyplex formation with branched peptide $(KK)_2KGGC$ was initially measured in IV as a reference for the binding constants of PBAEs. $(KK)_2KGGC$ was chosen since the N/P ratio used in transfection studies is 32[95], which is close to the N/Ps used for the PBAEs. $(KK)_2KGGC$ was also used to study the effect of buffer and salt on the polyplex formation. The molecular structure of peptide $(KK)_2KGGC$ is shown in **Figure 3.1**. As a peptide, only the primary amines at the lysine side chains and the N-terminal amines of $(KK)_2KGGC$ can take part in binding DNA. When calculating the N/P ratios, the N-terminal amines were included as having a half-unit positive charge, so each peptide has 5 active amine groups[95]. The properties of peptide and the sample properties are listed in **Table 3.1**.

Table 3.1 For PEIs and polypeptides, the weight average molecular weights (M_w), amine densities (*AD*), number of amines per polymer (N_N) and measured N/P ranges (N/P Range) at each pH and buffer. M–H = Mes–Hepes–NaCl buffer, NaAc = sodium acetate buffer, absence of NaCl, sNaAc = sodium acetate buffer, presence of NaCl.

Polymer	M_w (kDa)	*AD* $((Da)^{-1})$	N_N	N/P Range	at pH	in Buffer	Complexing Amines	in Paper
BPEI	25	$(43)^{-1}$	581.4	0.2–8	7.4, 5.2, 9.2	M–H	NH_2, NH, N	I, II
SPEI	0.70	$(43)^{-1}$	16.3	0.2–25	9.2	M–H	NH_2, NH, N	II
LPEI	22	$(43)^{-1}$	511.6	0.2–8	7.4, 5.2, 9.2	M–H	NH	I, II
PLL	200	$(128)^{-1}$	1562.5	0.2–8	7.4, 5.2, 9.2	M–H	NH_2	I
Peptide	0.88	$(175)^{-1}$	5.0	0.2–26	7.4, 5.2	M–H, NaAc, sNaAc	NH_2	IV

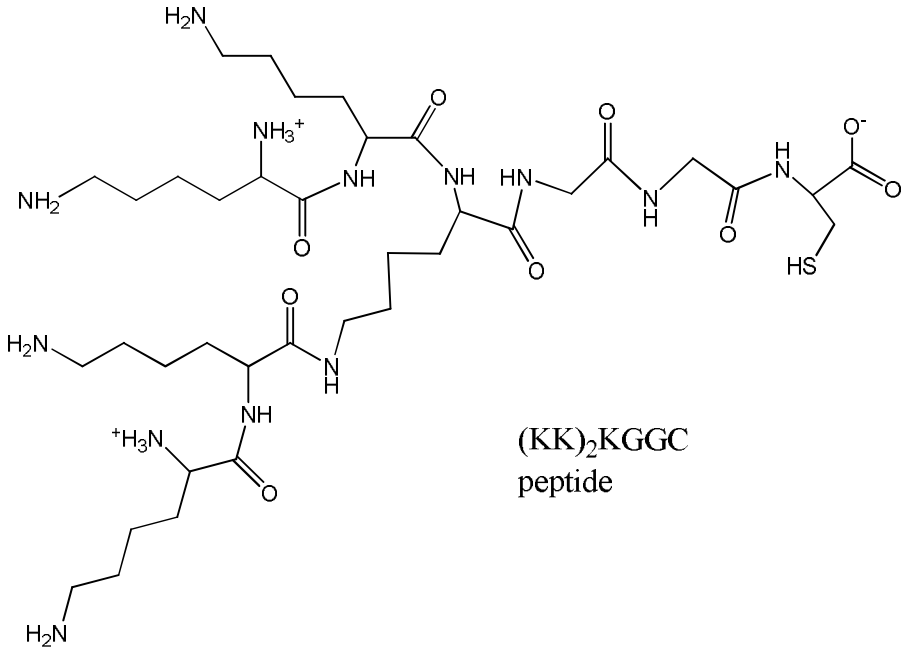

Figure 3.1 Molecular structure of peptide $(KK)_2KGGC$.

3.2 Poly(β-amino ester)s (PBAEs)

The poly(β-amino esters) studied in this thesis were synthesised at the Johns Hopkins University School of Medicine. The monomers are shown in **Figure 3.2**, and a simplified presentation of the synthesis is shown in **Scheme 3**. The studied PBAEs can be divided into two series according to whether they have end-cap groups[IV] or not[III]. During the course of this thesis, the abbreviations used for the different polymer structures changed. In paper III, the backbone monomers were marked with letters and the side chain monomers with numbers, whereas in paper IV, all monomers were coded with a letter, B for backbone, S for side chain and E for end cap, combined with a running number. In coding the polymers, the letters were left out and the numbers were listed in the order BSE. For example, the polymer consisting of the monomers B4 and S4 is denoted as C28 in paper III and as 44 (leaving out the letters) in paper IV. If the monomers are used in both papers, both abbreviations are listed in **Figure 3.2**.

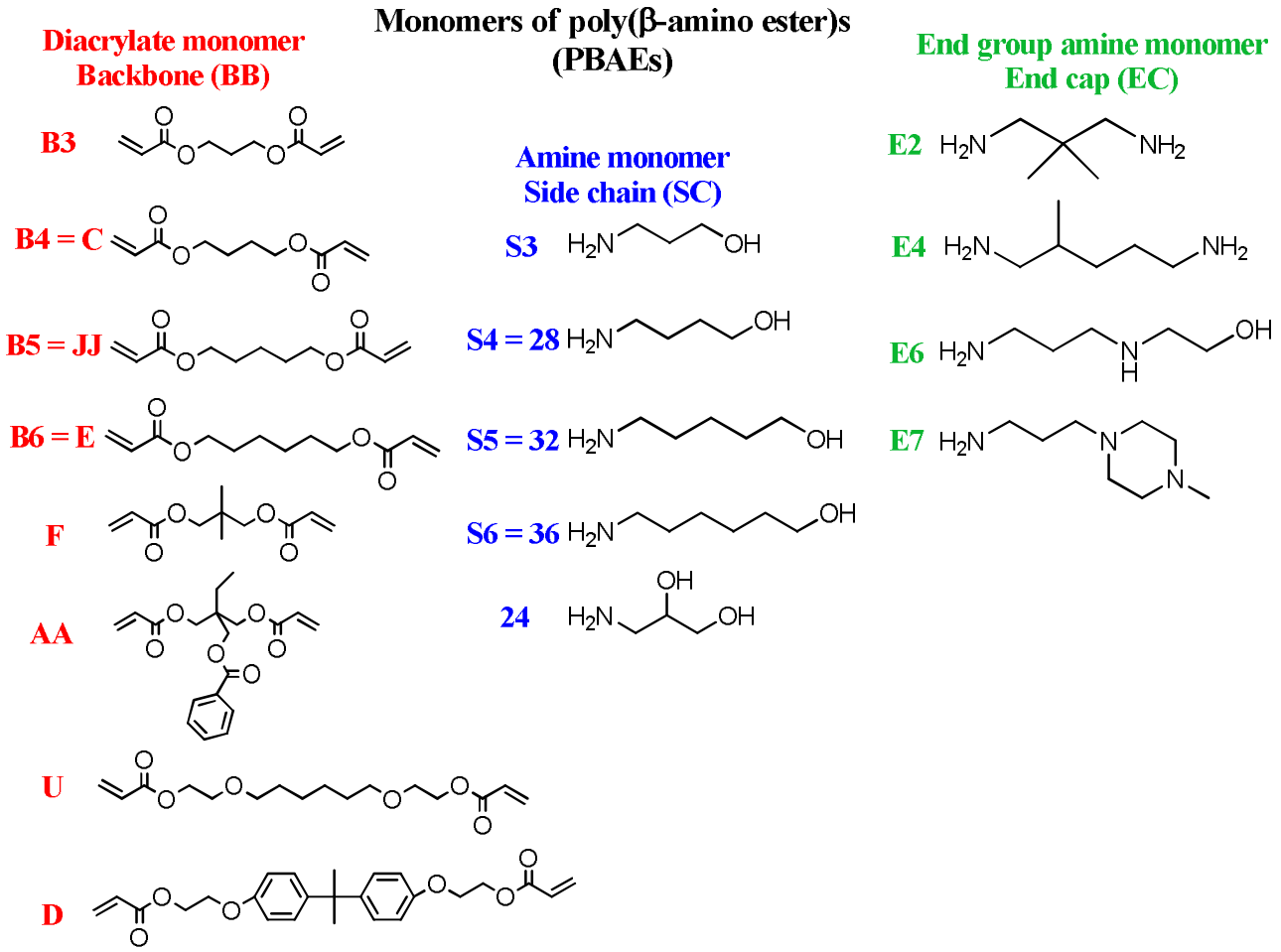

Figure 3.2 Molecular structures of the monomers of PBAEs.

Scheme 3 Synthesis of PBAEs with and without an end cap amine monomer.

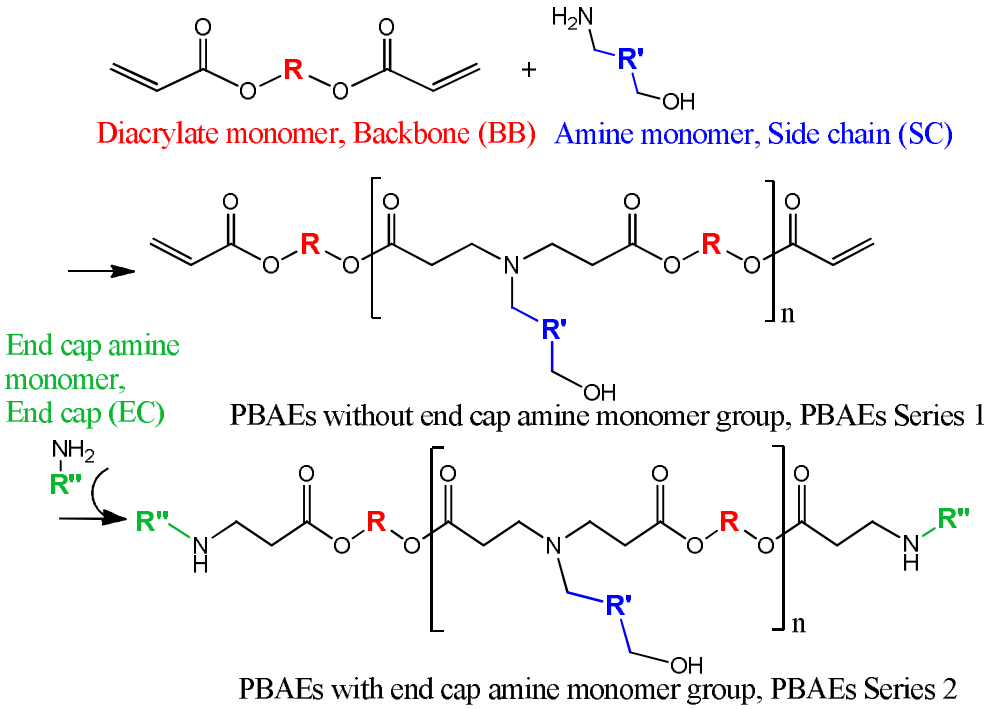

3.2.1 PBAEs without End Cap (PBAEs Series 1)

In paper III, ten PBAEs with no end-cap groups but varying backbone and side chain monomers and molecular weights were studied in Mes–Hepes–NaCl buffer at pH 7.4. The properties of these PBAEs are listed in **Table 3.2**. These PBAEs have only tertiary amine groups and much lower amine densities than the PEIs and PLL. Thus, much higher N/P ratios, up to 113, had to be used for efficient polyplex formation.

Table 3.2 Properties of PBAEs without end cap: weight average molecular weights (M_w), amine:acrylate ratios (Am/Ac), amine densities (*AD*), number of amines per polymer (N_N) and measured N/P ranges (N/P Range) of each polymer.

BB[a]	SC[b]	Polymer	M_w (kDa)	Am/Ac	*AD* ((Da)$^{-1}$)	N_N	N/P Range[c]
C = B4	**36 = S6**	C36 = 46	21.2	1.2	$(315)^{-1}$	67.3	1.0–103.2
F	**28 = S4**	F28	16.1	1.025	$(301)^{-1}$	53.5	1.1–108.0
AA	**28**	AA28	20.9	1.1	$(435)^{-1}$	48.0	0.8–74.7
AA	**24**	AA24	8.1	1.3	$(437)^{-1}$	18.4	0.7–62.5
D	**24**	D24	9.5	1.05	$(515)^{-1}$	18.5	0.6–63.1
C	**32 = S5**	C32	18.1	1.2	$(301)^{-1}$	60.1	1.1–108.0
U	**28**	U28	15.6	1.1	$(403)^{-1}$	38.7	0.8–80.7
E = B6	**28**	E28 = 64	14.3	1.1	$(315)^{-1}$	45.4	1.0–103.2
C	**28**	C28 = 44	27.9	1.05	$(287)^{-1}$	97.2	1.1–113.2
JJ = B5	**28**	JJ28 = 54	16.8	1.1	$(301)^{-1}$	55.8	1.1–108.0

[a]BB = backbone, diacrylate monomer, [b]SC = side chain, amine monomer, [c]These N/P ranges correspond to w/w from 1 to 100, except for AA24, for which the w/w range was 1–84

3.2.2 PBAEs with End Cap (PBAEs Series 2)

In paper IV, the PBAEs were improved by adding end-cap groups containing different types of amine groups. Furthermore, the polymers were fractionated, narrowing the molecular weight distribution and thus improving the homogeneity of the polymers. The structures of these 13 PBAEs were carefully designed to study the effect of four structural variables: (1) the molecular weight, (2) the number of carbon groups in the diacrylate monomers that forms the polymer backbone, (3) the number of carbon groups in the amine monomers that form the polymer side chains and (4) the structure of the end cap. These PBAEs were studied in NaAc buffer at pH 5.2, and the polyplexes were formed with plasmid-enhanced green fluorescent protein (pEGFP-N1) DNA (about 5000 bp). The properties of PBAEs with end caps are listed in **Table 3.3**.

Table 3.3 Properties of PBAEs of series 2: weight average molecular weights (M_w), amine densities (*AD*), number of amines per polymer (N_N), measured N/P ranges (N/P Range) and types and amounts of amines in the end cap of each polymer molecule.

Varying	BB[a]	SC[b]	EC[c]	Polymer	M_w (kDa)	*AD* ((Da)$^{-1}$)	N_N	N/P Range	Amines in End Cap
Molecular Weight	**B4**	**S4**	**E7**	447L[d]	10.3	$(252.9)^{-1}$	40.9	3–40	2(NH + 2N)
				447M[e]	14.7	$(262.2)^{-1}$	56.0	1–40	2(NH + 2N)
				447H[f]	91.6	$(283.0)^{-1}$	323.5	1–40	2(NH + 2N)
Backbone (BB)	**B3**	**S4**	**E6**	346	11.2	$(253.8)^{-1}$	44.0	0.4–40	2(2NH + OH)
	B4			446	11.8	$(266.8)^{-1}$	44.4	0.2–40	2(2NH + OH)
	B5			546	9.1	$(272.4)^{-1}$	33.4	0.9–37.7	2(2NH + OH)
	B6			646	10.5	$(287.5)^{-1}$	36.7	1–39.2	2(2NH + OH)
Side Chain (SC)	**B4**	**S3**	**E7**	437	10.3	$(242.1)^{-1}$	42.5	1–41.8	2(NH + 2N)
		S4		447M[e]	14.7	$(262.2)^{-1}$	56.0	1–40	2(NH + 2N)
		S5		457	13.1	$(270.6)^{-1}$	48.5	1–40	2(NH + 2N)
		S6		467	13.2	$(281.8)^{-1}$	46.9	1–20	2(NH + 2N)
End Cap (EC)	**B4**	**S4**	**-**	44	11.6	$(287.4)^{-1}$	40.3	5–20	-
			E2	442	10.4	$(263.5)^{-1}$	39.6	1–38.1	2(NH + NH_2)
			E4	444	10.3	$(263.9)^{-1}$	39.0	1–14.3	2(NH + NH_2)
			E6	446	11.8	$(266.8)^{-1}$	44.4	0.2–40	2(2NH + OH)
			E7	447L[d]	10.3	$(252.9)^{-1}$	40.9	3–40	2(NH + 2N)

[a]BB = backbone, diacrylate monomer, [b]SC = side chain, amine monomer, [c]EC = end cap, end group amine monomer. [d]L = low M_w, time of fractionation: 27–29 min, [e]M = medium M_w, time of fractionation: 24–26 min, [f]H = high M_w, time of fractionation: 2–23 min

3.3 Sample Preparation

All solutions were prepared either in Mes–Hepes–NaCl buffer (M–H) (at pH 7.4, 5.2 and 9.2) or in 25 mM sodium acetate buffer without salt (NaAc) and with 87 mM NaCl (sNaAc) at pH 5.1–5.2. The final DNA concentration was adjusted to 300 μM per nucleotide, and the molar ETI/nucleotide ratio was 1:15. The complexes were prepared by either a stepwise or a direct method. In the stepwise method, independent of the final N/P ratio between the cationic polymer and DNA, an initial solution with an N/P ratio of 0.2–0.6 was prepared by the vigorous mixing of equal volumes of ETI–DNA solution and cationic carrier solution. The complexation was followed by measuring the fluorescence spectrum of this initial solution. After the measurement, the final N/P ratio was adjusted by the addition of the appropriate amount of carrier solution. In the direct method, the final N/P ratio was reached with a single addition of the carrier to the ETI−DNA solution at the volume ratio of 1:1. The measured N/P-ranges were from 0.2 to 113 depending on which carrier was studied.

3.4 Time-Related Fluorescence, Time-Correlated Single-Photon Counting (TCSPC)

A general scheme of the **t**ime-**c**orrelated **s**ingle-**p**hoton **c**ounting (TCSPC) method is presented in **Figure 3.3**. The main components used in the instrument are pulsed laser diodes (LDH series, PicoQuant GmbH), a microchannel plate photomultiplier tube (PM) (R3809U-50, Hamamatsu) and a TCSPC module (PicoHarp 300, PicoQuant GmbH) that combines together constant fraction discriminators, a time-to-amplitude converter (TAC) and a multichannel analyser (MCA).

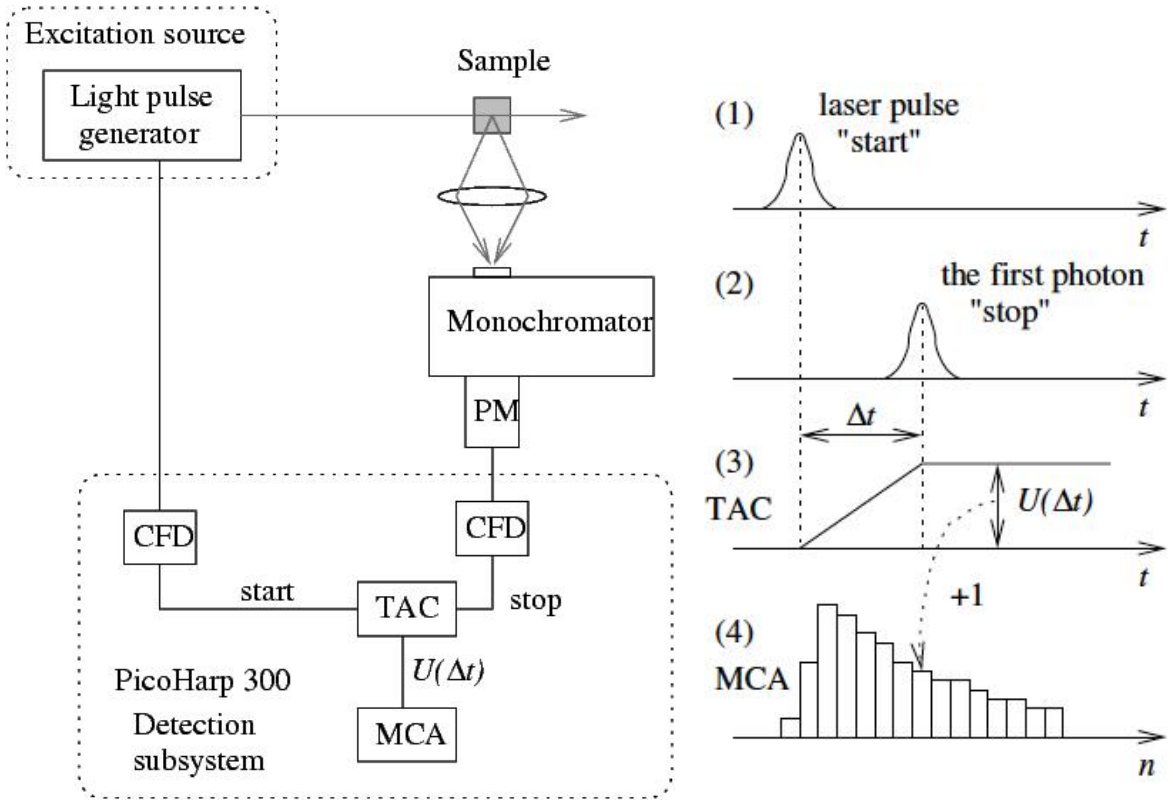

Figure 3.3 Time-correlated single-photon counting instrument. Emission detection consists of a monochromator and microchannel plate photomultiplier tube (PM) detector operating in photon counting mode. The PicoHarp 300 module includes a constant fraction discriminator (CFD), a time-to-amplitude converter (TAC) and multichannel analysers (MCA). Figure from Ref. 96.

The sample is excited by a laser pulse (1), and the same laser pulse is used as a trigger pulse for the TAC (time-to-amplitude converter). The triggering pulse starts the generation of a linearly rising voltage in the TAC (3), and the pulse from emitted photon stops the rising potential in the TAC (2). The emitted photons are detected with a PM (photomultiplier tube) in photon counting mode and thus produces an electrical pulse after each detected photon. Because the rise of TAC output voltage is linear in time, a certain output voltage corresponds to a certain delay time, Δt, between the excitation pulse and the emitted photon (3). The output voltage of TAC, $U(\Delta t)$, as a function of the delay time is processed by the MCA (multichannel analyser), where each channel is associated with some voltage interval and therefore to some delay time interval. Each output voltage value adds one to the value stored in the corresponding channel (4). E.g., the time step of the instrument can be set to 32 ps, and then each channel stores the counts at this resolution. The measurement results, after repeated excitation pulses, in a decay curve with the number of counts as a function of the delay time. The time resolution of the instrument can be obtained by measuring the instrument response function (that is, the decay profile of the scattering of the excitation pulse), and for the setup used, it was ≈ 128 ps (full width at half-maximum, FWHM = 0.128 ns at the excitation wavelength, λ_{exc} = 483 nm). To obtain the decay-associated spectra, the fluorescence decays were collected using a constant accumulation time with wavelengths of 560–670 nm with steps of 10 nm.

The fluorescence decays were deconvoluted and analysed using the iterative least-squares method by simultaneously fitting to the sum of exponents in equation 2.2.4.**1**. The quality of the fit was judged in terms of the weighted mean-square deviation χ^2 for the individual curves and for the

global fit (for acceptable fit, $\chi^2 < 1.1$) and by visual inspection of the weighted residuals and their autocorrelation function.

3.5 Hydrodynamic Particle Size, Malvern Zetasizer Dynamic Light Scattering (DLS)

The mean hydrodynamic diameters of the polyplexes prepared from BPEI, LPEI and PLL[I] were measured by the dynamic light scattering (DLS) technique using a Malvern Zetasizer **a**uto **p**late **s**ampler (APS) (medium refractive index of water, 1.33; scattering angle of 90 degrees in triplicate for each sample). A general scheme of the DLS (also known as **PCS**, **p**hoton **c**orrelation **s**pectroscopy) system is shown in **Figure 3.4**.

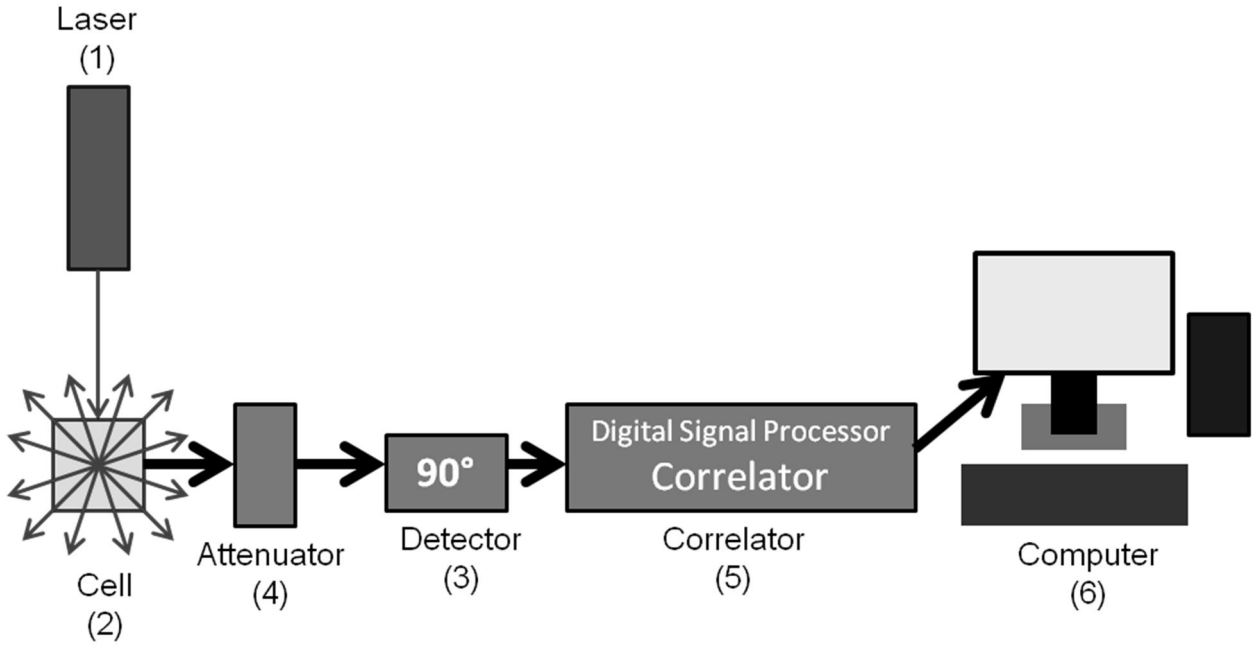

Figure 3.4 Dynamic light scattering (DLS)

A laser (1) is used to illuminate the sample particles within a cell (2). Most of the laser beam passes straight through the sample, but some of it is scattered by the particles within the sample. A detector (3) set at a 90° angle with the incident laser beam is used to measure the intensity of the scattered light. The intensity of the scattered light must be within a specific range for the detector to measure it successfully. An 'attenuator' (4) is used to adjust the signal intensity to a proper level either by adjusting the laser intensity or by decreasing the amount of scattered light allowed to pass through to the detector. The appropriate attenuator position is automatically determined by the Zetasizer during the measurement sequence. The particles are constantly moving due to Brownian motion caused by random collision with the molecules of the liquid that surrounds the particle. An important feature of Brownian motion for DLS is that small particles move quickly and large particles move more slowly. The relationship between the size of a particle and its speed due to Brownian motion is defined in the Stokes-Einstein equation. The Zetasizer APS system measures the rate of the intensity fluctuation and then uses this to calculate the size of the particles. The scattering intensity signal from the detector is passed to a digital signal processing board, called a

correlator (5). The correlator compares the scattering intensity at successive time intervals to derive the rate at which the intensity varies. This correlator information is then passed to a computer (6), where the specialist Zetasizer software will analyse the data and derive size information.[97]

4 Results and Discussion

This chapter summarises the most important results and findings of the studies presented in detail in publications I–IV. First, the polyplex formation with polyethylenimines and polypeptides is discussed[I, II]. In the second part, the effect of minor changes in the molecular structure of the PBAEs on the formation of polyplexes is discussed[III, IV]. In the course of these studies, it became evident that the formation of the polyplexes is more accurately described by the cooperative binding model than the independent binding model used in publications II and III. Thus, the data from these publications was partly reanalysed with the cooperative model and is presented in that form in this chapter. The behaviour of polypeptide $(KK)_2KGGC$, only briefly introduced in paper IV, is introduced more thoroughly by including some unpublished data.

4.1 Polyethylenimine–DNA and Polypeptide–DNA Polyplexes[I, II, IV]

The formation of polyethylenimine–DNA[I, II] and polypeptide–DNA[I, IV] complexes was studied by varying the structure[I, II] and the molecular weight[II] of the polymers. The significance of the pH[I] on the complex formation was studied and analysed using the cooperative[I, IV] binding model. In addition, the effect of incubation time (stability)[II], the buffer used and the presence or absence of salt was studied. The role of the extra polymer[II] was investigated and correlated with transfection data[II]. The high-molecular weight polymers (BPEI, LPEI and PLL) were studied at an N/P range from 0.2 to 8, whereas for the low-molecular weight polymers, higher N/P ratios up to N/P 26 for the peptide and N/P 25 for SPEI were also measured. We would also like to correct misinformation given in the experimental section of paper II: the samples were prepared in a Mes–Hepes–NaCl solution of pH 9.2, not pH 7.4, as mentioned in the paper.

4.1.1 Polyplex Formation of BPEI, LPEI and PLL at pH 7.4[I]

The degree of polyplex formation can be monitored by the binding isotherm, i.e., by plotting *B* (eq. 2.2.4.**4**) as a function of the N/P ratio (**Figure 4.1**)[I, II]. For BPEI, LPEI and PLL, *B* reaches its saturation level of close to 100% at N/P $\approx$ 2[I]. This indicates that nearly all ETI is free in the solution at N/P $\geq$ 2. The behaviour of all polymers is similar, but small differences between polymers are observed at small N/P ($\leq$ 2) ratios.

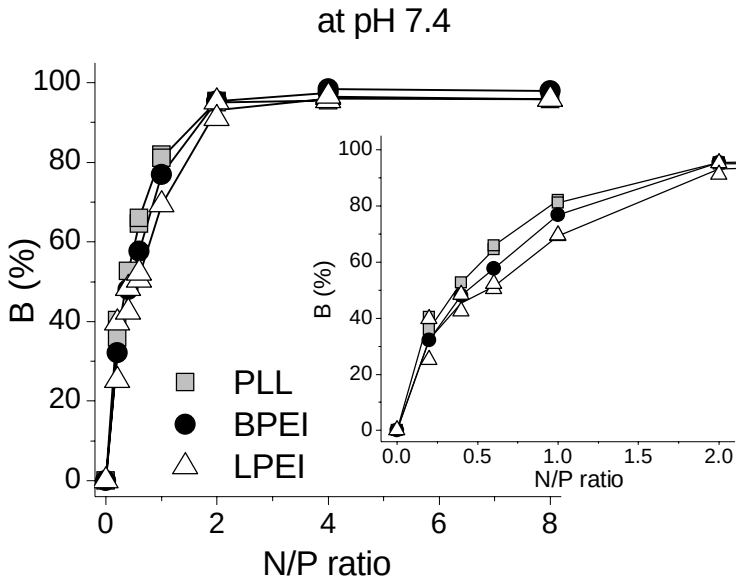

Figure 4.1 Binding isotherms for BPEI, LPEI and PLL at pH 7.4.

The particle size (the mean hydrodynamic diameter) as a function of the N/P ratio was studied in paper I. At low and high N/P ratios, the particle sizes were lower than 500 nm (I, **Figure 3**). At N/P = 2 the particle size increased to values over 2000 nm, with the simultaneous increase in the polydispersity index (PDI) of the samples reflecting a wider particle size distribution (I, **Figure 3**). According to the zeta potential measurements[15, 58, 67, 94, 98], the change from negative to positive potential takes place close to an N/P ratio of 2. Thus, the large particle sizes are probably due to aggregation of the polyplexes when they are at nearly a charge-neutral state[92, 99]. At this point, all the DNA phosphate groups are bound by amine groups of the polymer and the polyplex core has been formed. This N/P ratio also coincides with the saturation point observed in the binding isotherms. At higher N/P ratios, excess polymer binds to the nanoparticle core, forming a protective shell around it, and the particle size decreases[58, 100].

The fluorescence lifetimes change with increasing N/P ratios (I, **Figure S1**). For PLL, the changes are relatively small for both components and take place only at N/P < 2 (I, **Figure S1a** and **b**). For PEIs at N/P < 2, the changes in the lifetimes are larger (see a more detailed discussion in paper I). The fluorescence lifetime of ETI decreases in the presence of positive charges[83]. Thus, it is possible that, at low N/P ratios, when the polyplex is still negatively charged, the ETI freed in the solution during polyplex formation does not all escape to the bulk solution, but part of it stays close to the DNA. At N/P ≥ 2, the polyplexes are positively charged, ETI escapes to the bulk solution and its lifetime is equal to that of free ETI in the absence of DNA.

In the cooperative binding model, the Hill plots (eq. 2.2.4.**6**) are composites of three lines (at pH 7.4) with different slopes (inserts in **Figure 4.2**). At low polymer concentrations (N/P ≤ 0.6), the α values are 0.76–1.01 (**Table 4.1**). This implies that interaction between the polymers and the DNA represents independent binding without cooperativity or, in the case of LPEI, slightly negative cooperativity. At very high polymer concentrations (N/P ≥ 2), the binding isotherm has reached its maximum and polyplex core formation is complete. The α values obtained at intermediate N/Ps (**Table 4.1**) indicate positive cooperativity of binding.

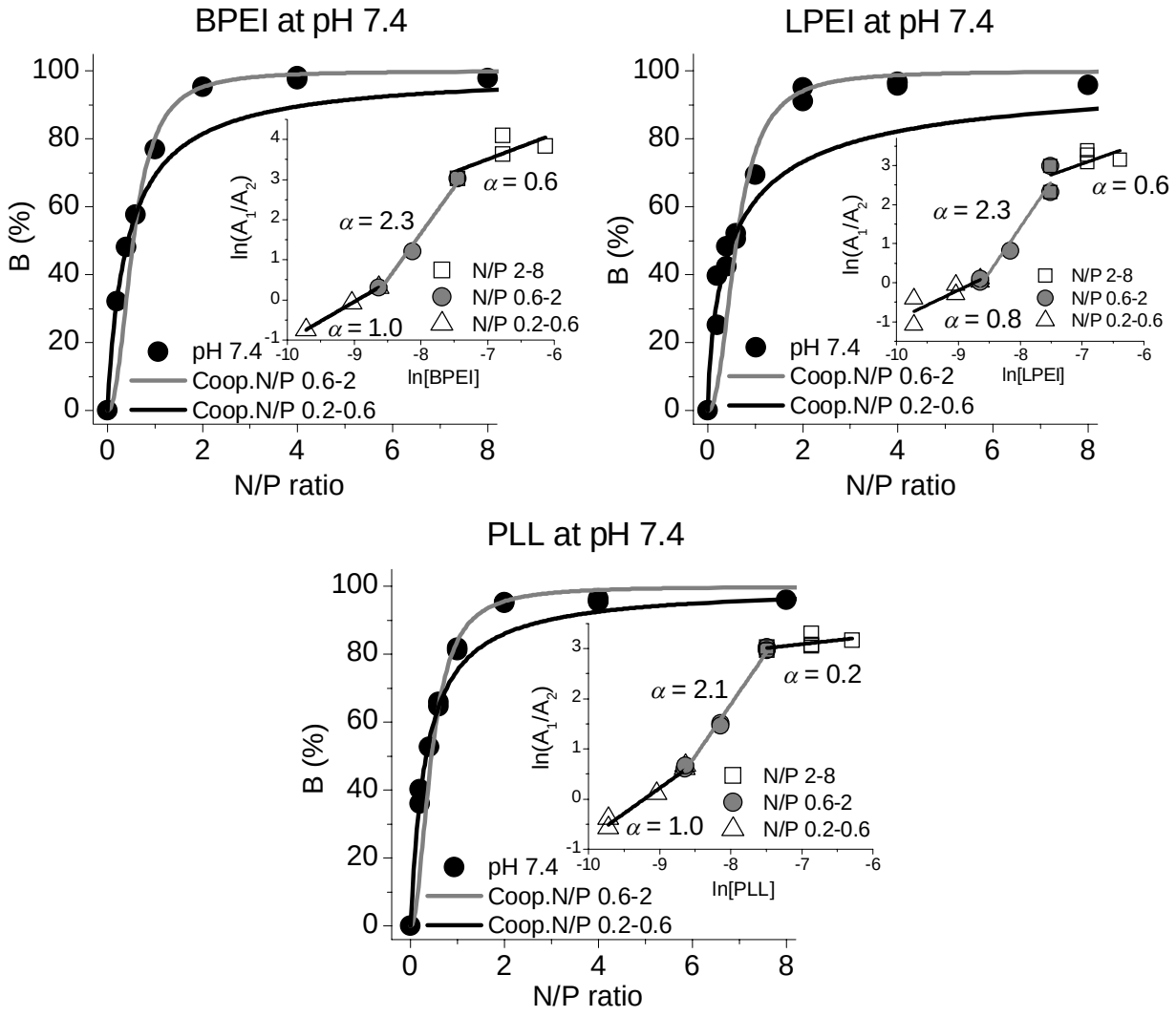

Figure 4.2 Binding isotherms for BPEI, LPEI and PLL at pH 7.4: (●) measured points and (——) calculated by the cooperative binding model (eq. 2.2.3.**1**). Inserts: Hill plots for BPEI, LPEI and PLL at pH 7.4.

Table 4.1 Hill's cooperativity coefficients, α, overall cooperative binding constants, $(K_{co})^{\alpha}$, and average cooperative binding constants per amine, K_{co}, for PEIs, PLL and $(KK)_2KGGC$ at different pHs in Mes–Hepes–NaCl buffer.[I, IV]

Polymer	pH	N/P Range	α	$(K_{co})^{\alpha}$	K_{co} (M^{-1})
SPEI	*9.2*	*2.0–8.0*	*1.36*	*(5.13 ± 0.52) × 10^4*	*(2.96 ± 0.07) × 10^3*
		0.2–2.0	*0.60*	*(1.74 ± 0.07) × 10^2*	*(5.14 ± 0.01) × 10^3*
BPEI	**5.2**	**0.4–2.0**	**3.78**	**(1.0 ± 0.1) × 10^{14}**	**(5.1 ± 0.1) × 10^3**
	7.4	0.6–2.0	2.31	(5.4 ± 0.6) × 10^8	(6.1 ± 0.2) × 10^3
		0.2–0.6	0.97	(5.7 ± 0.2) × 10^3	(7.7 ± 0.2) × 10^3
	9.2	*0.2–7.3*	*1.37*	*(1.03 ± 0.07) × 10^5*	*(4.55 ± 0.05) × 10^3*
LPEI	**5.2**	**0.4–2.0**	**3.16**	**(3.0 ± 0.3) × 10^{11}**	**(4.3 ± 0.2) × 10^3**
	7.4	0.6–2.0	2.32	(4.8 ± 0.5) × 10^8	(5.5 ± 0.2) × 10^3
		0.2–0.6	0.76	(7.5 ± 2.4) × 10^2	(6.3 ± 1.4) × 10^3
	9.2	*0.2–8.0*	*1.60*	*(9.17 ± 0.8) × 10^5*	*(5.46 ± 0.1) × 10^3*
PLL	**5.2**	**0.4–2.0**	**2.63**	**(6.8 ± 0.7) × 10^9**	**(5.5 ± 0.2) × 10^3**
	7.4	0.6–2.0	2.06	(9.7 ± 0.4) × 10^7	(7.4 ± 1.5) × 10^3
		0.2–0.6	1.01	(1.1 ± 0.1) × 10^4	(1.01 ± 0.09) × 10^4
	9.2	*0.6–2.0*	*2.37*	*(6.3 ± 0.8) × 10^8*	*(5.2 ± 0.3) × 10^3*
		0.2–0.6	*0.93*	*(3.7 ± 0.2) × 10^3*	*(6.6 ± 0.3) × 10^3*
$(KK)_2KGGC$	**5.2**	**2.0–8.0**	**3.43**	**(8.0 ± 1.6) × 10^{11}**	**(3.0 ± 0.9) × 10^3**
		0.4–2.0	**1.41**	**(2.4 ± 0.2) × 10^5**	**(6.6 ± 0.1) × 10^3**
	7.4	2.5–16.0	2.32	(1.1 ± 0.2) × 10^8	(2.9 ± 0.3) × 10^3
		0.2–2.5	0.97	(6.8 ± 0.7) × 10^3	(9.3 ± 0.1) × 10^3
	5.2[a]	**0.4–2.0**	**2.31**	**(8.3 ± 1.0) × 10^8**	**(7.3 ± 0.3) × 10^3**
		2.0–16.0	**0.95**	**(5.5 ± 1.1) × 10^4**	**(9.2 ± 1.8) × 10^4**
	5.2[a, b]	**8.0–26.0**	**2.81**	**(2.43 ± 0.38) × 10^8**	**(9.60 ± 1.57) × 10^2**
		0.4–8.0	**1.26**	**(2.74 ± 0.17) × 10^4**	**(3.24 ± 0.03) × 10^3**
	5.2[a, c]	**1.5–3.1**	**2.81**	**(1.28 ± 0.20) × 10^9**	**(1.75 ± 0.18) × 10^3**
		3.1–15.4	**0.50**	**(1.28 ± 0.15) × 10^2**	**(1.56 ± 0.01) × 10^4**

[a]in NaAc buffer without salt, [b]with salt in sNaAc buffer, [c]polyplexes were prepared by the direct method with DNA ≈ 5000 pb[IV]

The α values and binding constants of BPEI and LPEI are very close to each other. For PLL, the α value and the overall cooperative binding constant, $(K_{co})^{\alpha}$, are lower than for PEIs, but the average binding constant per amine, K_{co}, is higher than for PEIs (**Table 4.1**). In **Figure 4.2**, the binding isotherms calculated from the parameters listed in **Table 4.1** are shown together with the measured points for LPEI, BPEI and PLL at pH 7.4. The two-stage cooperative model fits to the measured points that follow the independent or slightly negative cooperative model up to N/P ≈ 0.6. At higher N/Ps (≥ 2), the positive cooperative model realises the measured points.

The effect of molecular structure on the polyplex formation includes the effects of: a) branching or side chains, b) the types of amines (primary, secondary or tertiary) and their ratios and c) the distribution of the amine groups, i.e., amine density. Comparing the structures of BPEI and LPEI, the amine densities of these polymers are equal, but the type of the amine groups differs: there are only secondary amine groups in linear PEI but primary, secondary and tertiary amine groups in BPEI. At pH 7.4, the effect is minor due to the pK_a values and the ratios of the different amine groups in BPEI. Thus, at pH 7.4, the major difference between these polymers is the branched *versus* the linear structure of the polymer backbone. The effect of this structural difference on the binding isotherm is small (**Figure 4.1**), and degree of cooperativity and the obtained binding constants are also very close to each other. At low N/P ratios (≤ 0.6), the degree of cooperativity of LPEI is somewhat negative, leading to a smaller overall binding constant. Thus, it seems that a linear structure with all the amine groups in the backbone of the polymer causes steric hindrance at small N/Ps. Another difference between BPEI and LPEI is the aggregation of LPEI polyplexes at high N/P ratios, which can also be due to the branched *versus* the linear molecular structure (I, **Figure 3**).

Comparing the structures of BPEI and PLL, they differ in all three respects. The amine groups of the PLL backbone are involved in peptide bonds and thus do not take part in binding DNA. Thus, only the primary amines at the end of lysine side chains bind DNA and must be taken into consideration here. Thus, the density of active amine groups is much lower for PLL than for BPEI. However, the primary amine groups of PLL are all protonated at pH 7.4, whereas the degree of protonation of BPEI's variable amine groups is closer to 50%. Again, only small differences in the binding isotherms (**Figure 4.1**) of BPEI and PLL are observed and only at small N/P ratios. The degree of cooperativity at N/Ps ≤ 0.6 is 1 for both polymers, but the overall binding constant is clearly higher for PLL. This effect is attributed to differences in the types of active amines in these polymers. At N/Ps ≥ 0.6, the degree of cooperativity is lower for PLL, leading to a smaller overall binding constant. This can be explained by the larger distance between the active amine groups in PLL compared with PEIs. Since the active amine groups of PLL are at the ends of the flexible side chains, the difference in the average distance between the amine groups is actually not very large. However, the large hydrocarbon skeleton of PLL can cause steric hindrance and thus reduce the degree of cooperativity. The average binding constants per amine are always higher for PLL than for PEIs. Thus, the primary amine groups of PLL seem to bind DNA more strongly than the secondary amine groups of LPEI and the combined affinity between the primary, secondary and tertiary amine groups of BPEI. This is in line with the observations indicating that the PEI–DNA complexes are more easily disrupted than PLL–DNA complexes in the presence of competing polyanions[101, 102].

4.1.2 Effect of pH on BPEI, LPEI and PLL Polyplexes[I, II]

The effect of pH on complex formation was studied with high-molecular weight polymers (LPEI, BPEI and PLL) at pH 5.2, 7.4 and 9.2[I, II].

For BPEI, LPEI and PLL, the pH has a clear effect on the binding isotherms (**Figure 4.3**) at small N/P ratios. The sigmoidal shape of the binding isotherms observed at pH 5.2 is absent at higher pHs. For PEIs, the saturation levels of ≈ 100% are reached at N/P = 2 at low pHs (7.4 and 5.2), but at pH 9.2, the saturation level of ≈ 90% is reached at N/P = 4 for BPEI and N/P = 3 for LPEI. For PLL, the binding isotherms at pH 7.4 and 9.2 are nearly identical.

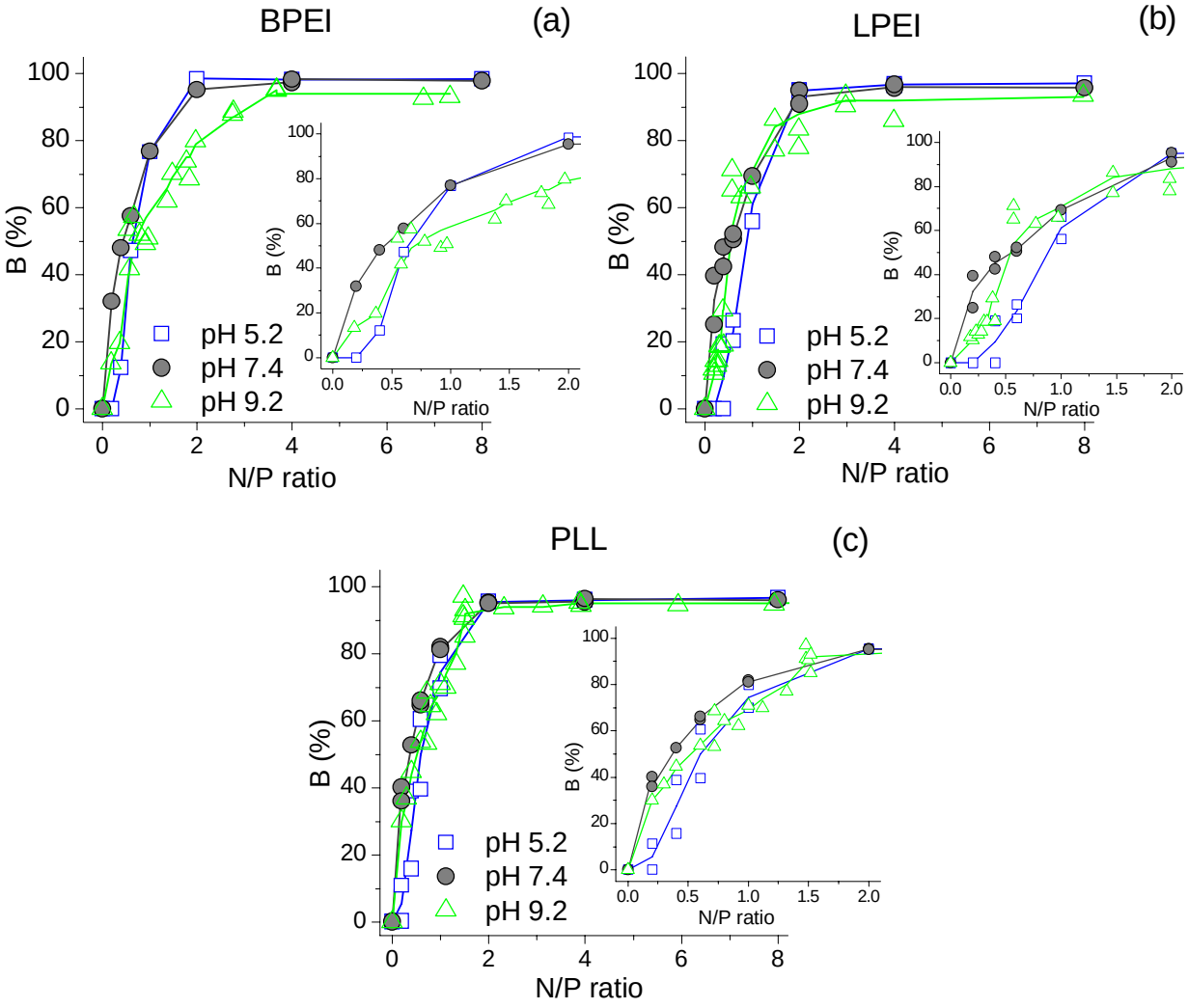

Figure 4.3 Binding isotherms in Mes–Hepes–NaCl buffer at pH 5.2, 7.4 and 9.2 for BPEI (a), LPEI (b) and PLL (c).

These differences between PLL and PEIs are due to the amine groups and, hence, the pK_a values of the polymers. At pH 9.2, the degree of protonation of PEIs is << 50% because of the secondary and tertiary amine groups. The primary amines of PLL are ≥ 50% protonated across the whole pH range from 9.2 to 5.2, so PLL can form polyplexes efficiently at each pH, always reaching its saturation level at close to N/P = 2.

pH does not have an effect on the fluorescence lifetimes of PLL (**Figure 4.4c**). For PEIs, the decrease in the lifetime of the longer-living component is somewhat smaller at pH 5.2 than at higher pH levels. For BPEI, the lifetime of the short-living component at N/P ≤ 2 has clearly higher values at pH 9.2 than at lower pH values (**Figure 4.4a**). A similar phenomenon but weaker and persisting at higher N/Ps is also observed for LPEI (**Figure 4.4b**). This is again an indication that, at low N/P ratios, the ETI freed in the solution during polyplex formation does not all escape to the bulk solution, but part of it stays close to the DNA. Since the pH is basic, the effect on the fluorescence lifetime of ETI is the opposite of that at neutral and acidic pH.

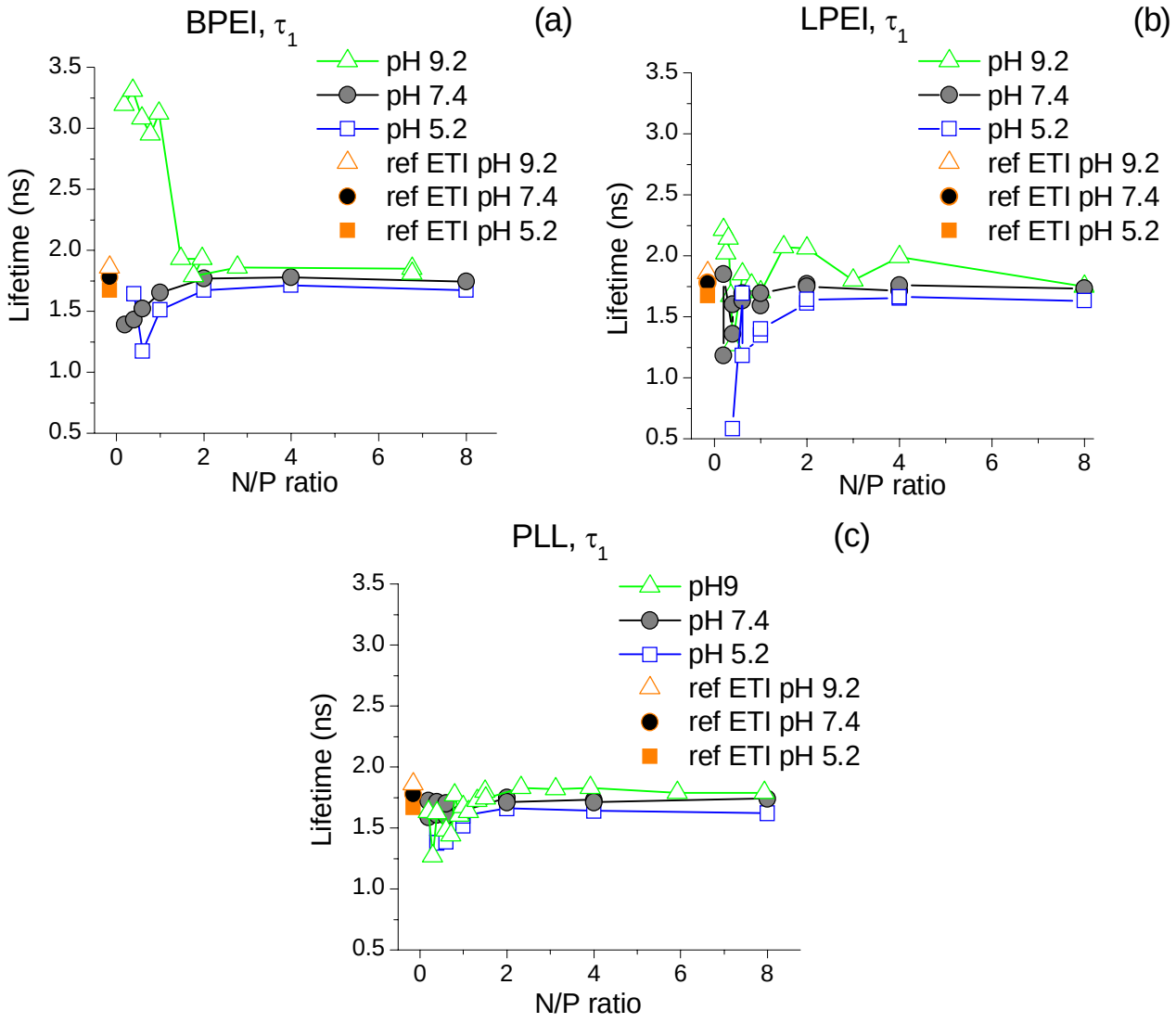

Figure 4.4 Fluorescence lifetimes of the short-living decay components for BPEI (a), LPEI (b) and PLL (c) at different pH values. ref ETI = free ETI in buffer at pH 9.2 (△), 7.4 (○) and 5.2 (□).

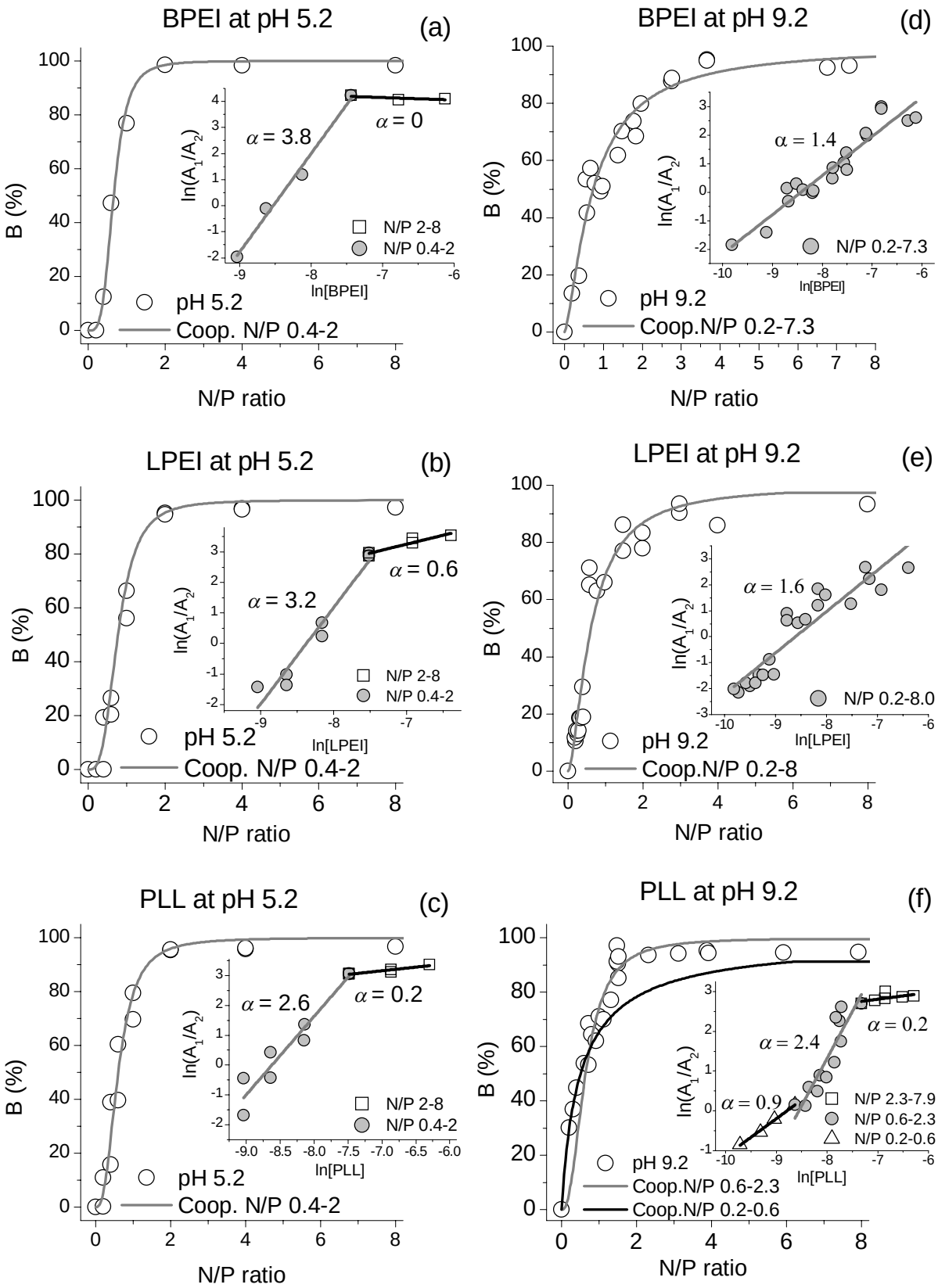

Figure 4.5 Binding isotherms for BPEI (a, d), LPEI (b, e) and PLL (c, f) at pH 5.2 (a–c) and at pH 9.2 (d–f): (○) measured points and (——) calculated by the cooperative binding model (eq. 2.2.3.**1**). Inserts: Hill plots for BPEI, LPEI and PLL at pH 5.2 and 9.2.

The Hill plots (eq. 2.2.4.**6**) for BPEI, LPEI and PLL at pH 5.2 are composites of two lines with different slopes (inserts in **Figure 4.5a–c**). Positive cooperativity (α = 2.63–3.78) is observed already at the lowest N/P ratio. At high polymer concentrations (N/P ≥ 2), the formation of the polyplex core is complete and nearly all ETI has been freed to the bulk solution. At pH 7.4, the independent or slightly negative cooperativity at low N/Ps changes to positive cooperativity at N/P = 0.6 and continuing until N/P = 2. The behaviour of PLL at pH 9.2 (**Figure 4.5f**) resembles that at pH 7.4: at low N/Ps the binding shows negative cooperativity (α = 0.9), at intermediate N/Ps, positive cooperativity is observed (α = 2.4) and at N/P ≈ 2, the formation of the polyplex core is complete and α < 1. For BPEI and LPEI, the Hill plot at pH 9.2 (**Figure 4.5d** and **e**) can be described by one single straight line with α values of 1.4 and 1.6, respectively.

Thus, it seems that pH has a clear influence on the mechanism of polyplex formation. The degree of cooperativity is the highest at pH 5.2 and the lowest at 9.2 (except PLL, which had the lowest cooperativity at pH 7.4). In addition, the overall cooperative binding constant $(K_{co})^{\alpha}$ increases with decreasing pH (**Table 4.1**). For PEIs, the amount of protonated amine groups increases as the pH decreases, so both the degree of cooperativity and the overall binding constant correlate with the number of active amine groups present in the system. For PLL, all the active amine groups are protonated at the pH range studied, and the effect of pH is smaller than for PEIs. However, both α and $(K_{co})^{\alpha}$ also increase with decreasing pH for PLL. This could be due to increased activity of the amine groups at lower pH levels.

4.1.3 Effect of pH, Buffer and Ionic Strength on $(KK)_2KGGC$ Polyplexes[IV]

The polyplex formation with branched peptide $(KK)_2KGGC$ was originally measured in paper IV as a reference for the binding constants of PBAEs. Thus, the polyplexes were prepared in NaAc buffer at pH 5.2 with no additional salt present. This inspired us to study the effect of the buffer and ionic strength of the solution on the formation of the polyplexes (**Figure 4.6**). The Hill plots of $(KK)_2KGGC$ in Mes–Hepes–NaCl buffer at pHs 7.4 and 5.2 are composites of two linear regions (inserts in **Figure 4.6a** and **b**). At low N/P ratios, the degree of cooperativity at pH 7.4 indicates independent binding, whereas at pH 5.2, the degree of cooperativity is clearly positive (**Table 4.1**). At N/P > 2, the degree of cooperativity is close to that obtained for LPEI and BPEI and thus higher than for PLL. Changing the buffer to sNaAc at pH 5.2 and keeping the ionic strength nearly constant did not change the behaviour of $(KK)_2KGGC$ (**Figure 4.6c**). However, if the extra salt is left out, i.e., at about 10 times smaller ionic strength, the binding mechanism of $(KK)_2KGGC$ changes (**Figure 4.6c–e**). The Hill plot is still a composite of two lines, but now positive cooperativity is observed at small N/Ps, and the mechanism changes to independent binding at N/P = 2 (**Figure 4.6d**).

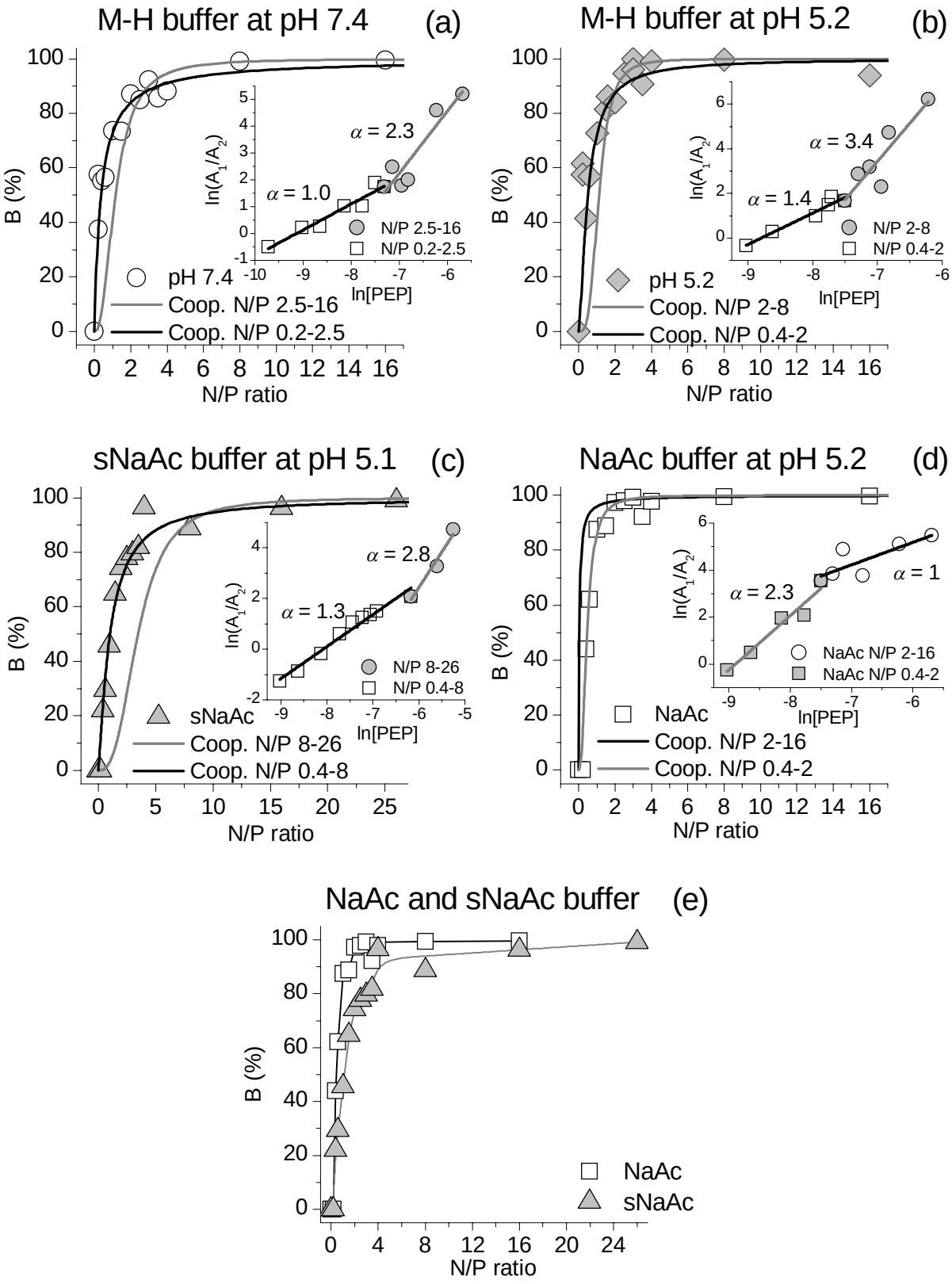

Figure 4.6 Binding isotherms for $(KK)_2KGGC$ at pH 7.4 (a), at pH 5.2 (b), at sNaAc with salt at pH 5.1 (c), at NaAc without salt at pH 5.2 (d) and at NaAc with and without salt (e): (○), (□) and (Δ) measured points and (—) calculated by the cooperative binding model (eq. 2.2.3.**1**). Inserts: Hill plots for Mes–Hepes–NaCl buffer (M–H) at pH 7.4 (a) and 5.2 (b) and with (c) and without (d) salt for NaAc buffer.

4.1.4 Effect of Molecular Weight[I, II]

The effect of the molecular weight of the polymer on the polyplex formation was studied by comparing the behaviour of 0.8 kDa (SPEI) and 25 kDa (BPEI) branched PEI at pH 9.2 with each other. In addition, the behaviour of PLL was compared to that of $(KK)_2KGGC$ at pH 7.4.

The molecular weight has an effect on the N/P ratio at which the saturation level of the binding isotherm is reached: while BPEI reaches its saturation level at N/P = 4, SPEI reaches it at N/P = 8 (**Figure 4.7a**). The same is observed when PLL (N/P = 2) is compared with $(KK)_2KGGC$ (N/P = 8) (**Figure 4.7b**). This indicates that, for polymers with relatively high-molecular weight, the complex formation is efficient already at low N/P ratios, whereas for low-molecular weight polymers, higher N/P ratios are required for efficient binding of DNA.

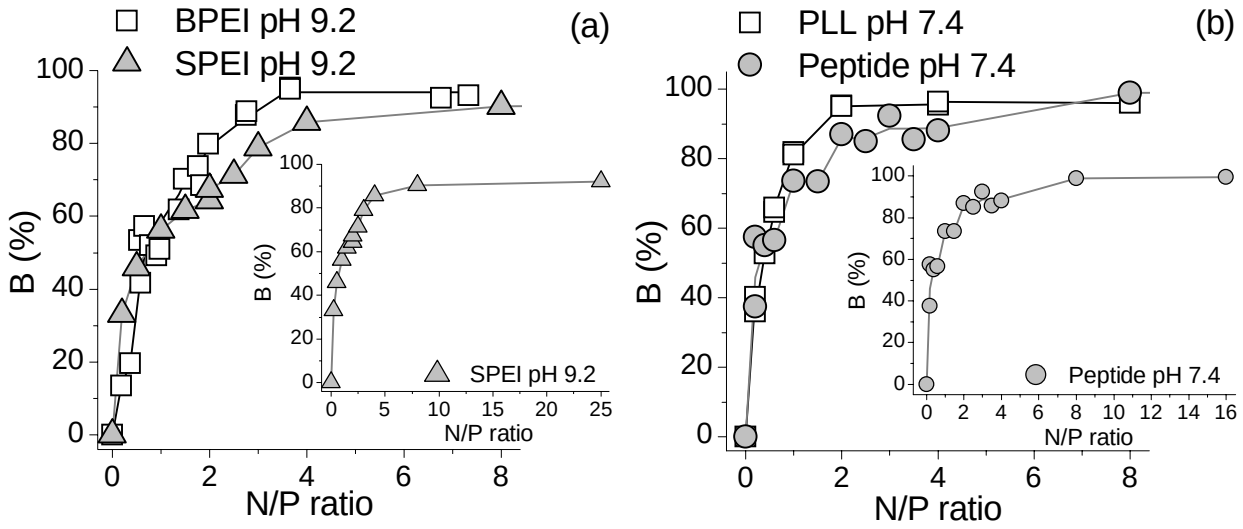

Figure 4.7 Binding isotherms for branched high- (BPEI) and low- (SPEI) molecular weight PEIs at pH 9.2 (a) and for high- (PLL) and low- (peptide $(KK)_2KGGC$) molecular weight polypeptides at pH 7.4 (b) (all in Mes–Hepes–NaCl buffer).

For SPEI, the Hill plot at pH 9.2 (eq. 2.2.4.**6**) is a composite of three lines with different slopes (insert in **Figure 4.8**), like that of PLL but different from that of BPEI. The positive cooperativity of SPEI was observed at intermediate N/Ps (α = 1.4), at low N/Ps (α = 0.6) and at high N/Ps (α = 0.3) negative cooperativity was observed. For SPEI, the three-stage cooperative binding model fits the measured points, as it does for high-molecular weight PLL (**Figure 4.5f**). The degree of cooperativity was similar for SPEI and BPEI (α = 1.4) (**Table 4.1**), but the overall binding constant, $(K_{co})^{\alpha}$, was higher for BPEI than for SPEI. Hence, it seems that BPEI has more active protonated amines than SPEI because of the higher molecular weight[40].

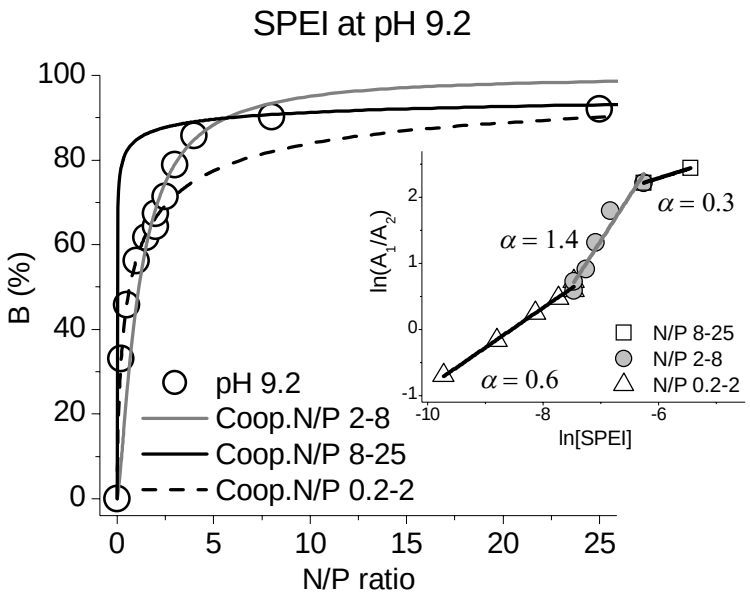

Figure 4.8 Binding isotherms for SPEI at pH 9.2 in Mes–Hepes–NaCl buffer: (○) measured points and (—, – –) calculated by the cooperative binding model (eq. 2.2.3.**1**). Insert: Hill plot for SPEI.

The Hill plots of PLL (insert in **Figure 4.2**) and $(KK)_2KGGC$ (insert in **Figure 4.6a**) at pH 7.4 are very similar, yielding nearly equal cooperativities and binding constants (**Table 4.1**). At pH 5.2 in Mes–Hepes–NaCl buffer, $(KK)_2KGGC$ has two regions of positive cooperativity (insert in **Figure 4.6b**), whereas PLL has only one region spanning from the lowest N/P to N/P = 2 (insert in **Figure 4.5c**).

4.1.5 Effect of the Incubation Time after Complex Formation[II]

The stability of the formed polyplexes was studied with BPEI by measuring the fluorescence decays at different times after the preparation. The lifetime of the short-living component stayed constant but the lifetime and proportion of the long-living component decreased with time at least up to 6 h (I: **Figure S5** and **S6**). In the A_2 values listed in paper I, **Table S6**, the relative fluorescence quantum yield of ETI free in the solution versus ETI bound by the DNA, ϕ_{rel}, has not been taken into account since the corrected values are all so close to 100% that the trend is difficult to see. The particle sizes of LPEI and BPEI polyplexes have been observed to grow as a function of time in salt-containing buffers.[29, 67, 70, 71, 103] This aggregation of the polyplexes can induce the release of more ETI into the bulk solution and reduce the fluorescence lifetime of the remaining ETI trapped in the aggregates.

The polyplex preparation method has an effect on the age of the measured polyplexes. With the direct method, the polyplexes are measured after similar incubation times (about 10–20 min). For the polyplexes prepared by the stepwise method, the age of the polyplexes increases with increasing N/P ratios. For 25 kDa BPEI the preparation method does not have an effect on the properties of the polyplex, but for the 0.9 kDa $(KK)_2KGGC$, the effect is clear (**Figure 4.9a**). It seems that the complexes need more time to reach equilibrium.

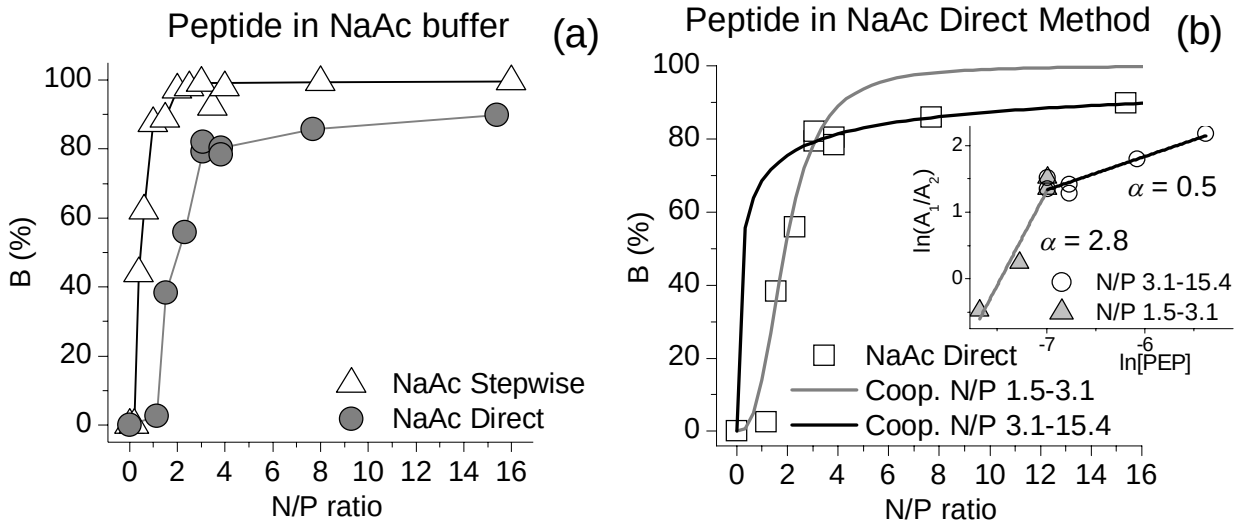

Figure 4.9 Binding isotherms for peptide in NaAc buffer at pH 5.2 prepared by the stepwise (Δ) and direct (○) methods (a) and binding isotherms for peptides prepared by the direct method: (□) measured points and (—) calculated by the cooperative binding model (eq. 2.2.3.**1**). Insert: Hill plot for peptides prepared by the direct method (b).

4.1.6 Effect of the Free PEI[II]

According to the binding isotherms, the DNA is nearly totally bound by BPEI at N/P = 2. However, the best results in the transfection studies are obtained at N/P ratios between 6 and 8. To study the role of the excess BPEI on the complex properties, the extra BPEI was removed from polyplexes at N/P = 6 by size exclusion chromatography[I]. Unfortunately, the remaining ETI was also lost in this procedure. Thus, ETI was added to the sample after the purification. The initial sample N/P ratio decreased close to 3 during purification. The purified samples were spiked with BPEI to restore the original N/P ratio of 6.0. The properties of the nanoparticles did not change during purification and spiking, and they retain the structure formed at the original N/P ratio. However, the transfection studies with three different cell lines (I, **Figure 7**) showed that the removal of excess BPEI from the polyplexes resulted in an approximately 80–90% decrease in transgene expression. The expression levels were restored to the original level by spiking the purified complexes with BPEI. Thus, the excess BPEI must facilitate transfection at the cellular level and not via indirect effects on the BPEI–DNA complexes.

4.1.7 Summary of Polyethylenimine–DNA and Polypeptide–DNA Polyplexes[I, II]

For BPEI, LPEI and PLL, the largest particle sizes, coinciding with the change from negatively charged polyplexes to positively charged polyplexes, are observed at N/P = 2. At this N/P ratio, the binding isotherm reaches its saturation level of about 100% and the formation of the polyplex core is complete. At higher N/P ratios (N/P > 2), excess polymer is bound to the polyplex, the size of the polyplex decreases again and a shell of excess polymer forms around the core polyplex.[I]

The pH value has a clear influence on the mechanism of polyplex formation for PEIs, PLL and $(KK)_2KGGC$. The overall cooperative binding constants are higher at pH 5.2 than at high pH levels, reflecting the higher degree of amine group protonation at lower pH.[I, II]

The presence of NaCl affects the binding mechanism of peptide $(KK)_2KGGC$, but two different types of buffers with similar ionic strength does not change the behaviour of the peptide.

The molecular weight of the polymer is observed to have a clear effect on the complex formation[I, II]. High-molecular weight polymers (BPEI and PLL) form polyplexes more effectively since the saturation level of the binding isotherm is reached at lower N/P ratios than for low-molecular weight polymers (SPEI and peptide).

The incubation time after complex formation is crucial for the small-molecular weight peptide $(KK)_2KGGC$ since the formation of complexes require more time to reach equilibrium than for the high-molecular weight polymers.[I] The absence of free PEI shows lower transgene expression levels, although the fluorescence properties in the absence and the presence of free PEI are similar, and hence the original structure of the polyplex core is retained.

The molecular structure and types of amine groups have an effect on the polyplex formation. Both the amine density and overall cooperative binding constants are higher for BPEI (which contains NH_2, NH and N amine groups) and LPEI (which contains only NH amine groups) than for PLL (which contains only NH_2 amine groups). However, the average binding constants per amine are higher for PLL.[I, II]

4.2 Poly(β-amino ester)–DNA Polyplexes[III, IV]

The complex formation of poly(β-amino ester) (PBAE)–DNA polyplexes was first studied with PBAEs containing only tertiary amines, i.e., PBAEs without end-cap groups[III]. The structures of the monomers of the backbone and the side chain were varied. The second series of PBAEs with end-cap groups adding primary and/or secondary and/or tertiary amines to the polymer was size-fractionated. Thus, the molecular weight distribution in these PBAEs was narrower than in the first series of PBAEs without end caps[IV]. The PBAE–DNA binding was studied systematically by varying polymer molecular weight, adding single carbon units to the backbone and side chain of the monomers that compose the polymers and varying the type of polymer end-cap group.[IV] The binding equilibrium results were analysed using the cooperative binding method. For the PBAEs without end caps (series 1), the weight ratio, w/w, instead of the N/P ratio was used to follow the previously published articles on these polymers. However, the w/w does not take into account the differences in the amine density of the PBAEs. Thus, the used w/w range, from 1 to 100, corresponds to an N/P range from 0.6 to 113 depending on the amine density of the PBAEs.

4.2.1 PBAEs without End Caps[III]

Ten PBAEs (**Figure 3.2** and **Table 3.2**) with different transfection efficacies were chosen from a large library of PBAEs[9]. The molecular structure of the PBAEs was varied by changing the side chain and the backbone monomers.

The binding isotherms presented in paper III, **Figure 2** were constructed from the raw data without taking into account the quantum yield correction factor (eq. 2.2.4.**2**). The corrected binding isotherms for the PBAEs without end caps are presented in **Figure 4.10**. None of the polymers

reached close to 100% saturation levels as PEIs and PLL did, but remained at 73–91%. The differences in the binding isotherms between this set of polymers are small, although F28 and C36 are somewhat less efficient than the other polymers.

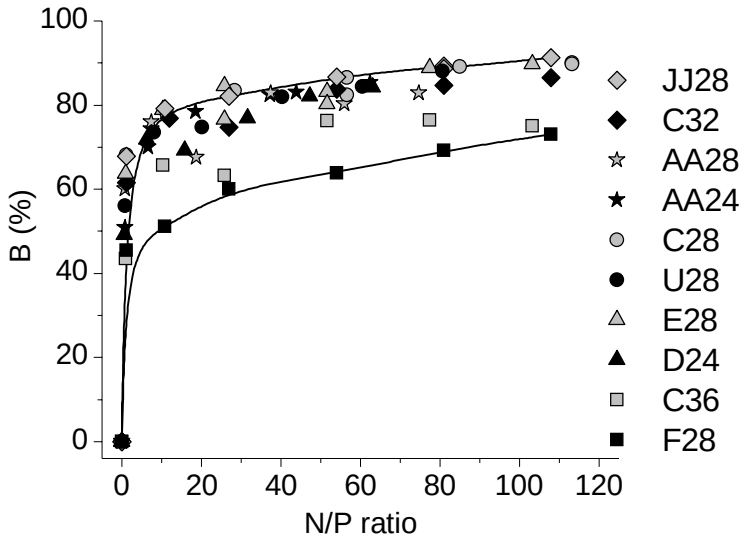

Figure 4.10 Binding isotherms for the ten PBAEs without end caps in Mes–Hepes–NaCl buffer at pH 7.4.

For most of these PBAEs, the Hill plots are composites of two lines with different slopes (**Figure 4.11**). Only for AA24, C28 and C36, the Hill plots were single straight lines with α = 0.46, 0.35 and 0.35, respectively, indicating negative cooperativity. At low polymer concentrations of w/w ratio ≤ 25, the other polymers also expressed negative cooperativity with α values of 0.1–0.27 (**Table 4.2**). This is due to the structure of the PBAEs: the amine density (*AD*) is much lower than for PEIs, the backbones and side chains contain electronegative groups (–O–CO– and OH) and the side chains are bound to the nitrogen atoms of the backbone, causing steric hindrance in binding to DNA. As a consequence, to complex DNA fully, much higher N/P ratios are needed for the PBAEs than for PEIs and polypeptides. Typically, high concentrations of about w/w = 40–90[IV, 9] are needed for efficient transfection with PBAEs compared with the N/P = 5–15 used for high-molecular weight PEIs and PLL[I, 18, 31, 33, 55, 63, 65, 66, 69, 70, 71, 100, 103–105]. At high polymer concentrations (w/w ≥ 25), the α values varied from 0.7–1.5, indicating a change in the binding mechanism to nearly independent binding. The turning points of the binding isotherms are close to w/w = 20. Thus, it is possible that, at this N/P ratio, all the DNA is fully bound and the core polyplex has been formed. If this is the case, further binding with a nearly independent mechanism describes the binding of the extra polymer forming the shell around the polyplex core. It was not possible to observe this phase with PEIs and PLL since all the ETI escapes from the DNA during the core formation. However, due to the negative cooperativity during the core formation for PBAEs, some of the ETI molecules stay intercalated into the DNA. Some of these entrapped ETI molecules then escape from the polyplex during the shell formation.

The binding constants determined with the cooperative binding method are listed in **Table 4.2**. As generally is the case for systems with negative cooperativity, the overall cooperative binding constants were lower than the average cooperative binding constants per amine.

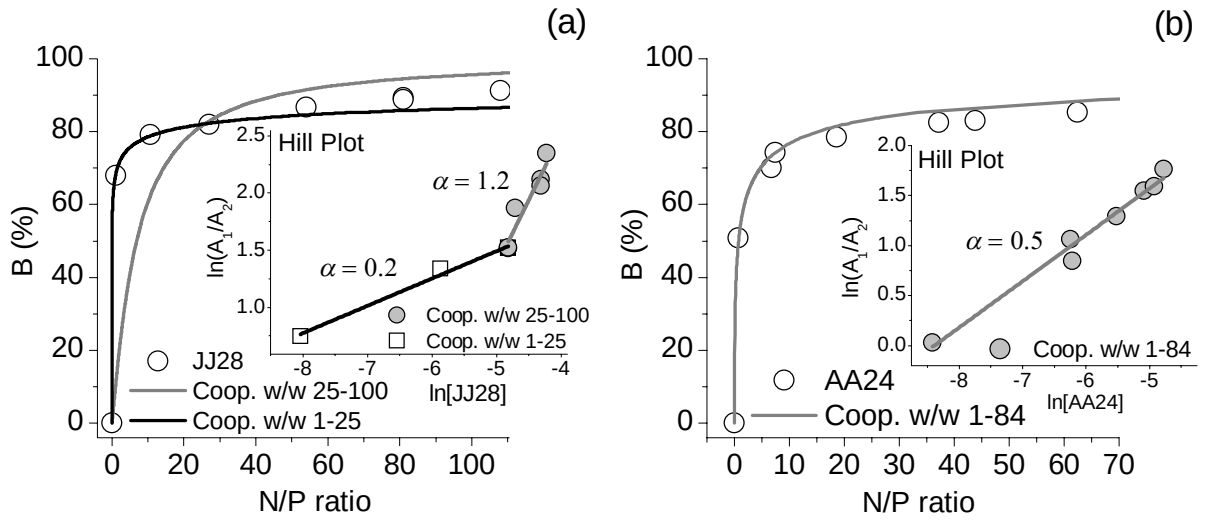

Figure 4.11 Binding isotherms for PBAEs series 1 polymers, JJ28 (a) and AA24 (b): (○) measured points and (——) calculated by the cooperative binding model (eq. 2.2.3.**1**). Inserts: Hill plots for PBAEs series 1 polymers, JJ28 (a) and AA24 (b).

Table 4.2 Cooperative binding constants of PBAEs without end caps. Hill's cooperativity coefficients, α, overall cooperative binding constant, $(K_{co})^{\alpha}$, and average cooperative binding constants per amine, K_{co}.

Polymer	w/w Range	N/P Range	α	$(K_{co})^{\alpha}$	K_{co} (M^{-1})
JJ28	1–25	1.1–27.0	0.24	14.7	7.54×10^4
	25–100	27.0–108.0	1.16	1.27×10^3	4.82×10^2
C32	1–25	1.1–27.0	0.21	9.48	3.54×10^4
	25–100	27.0–108.0	0.82	1.69×10^2	5.36×10^2
AA28	1–25	0.7–18.7	0.10	3.54	2.34×10^5
	25–100	18.7–74.7	0.86	2.55×10^2	6.11×10^2
AA24	1–84	0.7–62.5	0.46	48.7	4.40×10^3
C28	1–100	1.1–113.2	0.35	32.9	1.94×10^4
U28	1–25	0.8–20.2	0.27	13.0	1.13×10^4
	25–100	20.2–80.7	1.35	3.26×10^3	4.05×10^2
E28	1–25	1.0–25.8	0.27	16.7	2.89×10^4
	25–100	25.8–103.2	0.96	4.20×10^2	5.57×10^2
D24	1–25	0.6–15.8	0.29	12.6	6.28×10^3
	25–100	15.8–63.1	1.46	5.26×10^3	3.61×10^2
C36	1–100	1.0–103.2	0.35	13.1	1.55×10^3
F28	1–25	1.1–27.0	0.17	3.06	8.48×10^2
	25–100	27.0–108.0	0.73	49.1	2.07×10^2

As discussed, earlier the time-resolved fluorescence method used in this thesis to determine the binding isotherms and binding constants describes mostly the very first step in the gene delivery process, i.e., the formation of the polyplex core. Thus, no correlation between the binding constants and the transfection efficiencies was expected. The saturation levels obtained from the binding isotherms describe the efficiency of the polyplex formation. However, the differences between the polymers are not very clear. Thus, to estimate the relative efficiency of polyplex formation by the PBAEs without end caps, the maximum amplitudes $a_{i,max}$ at each N/P ratio were used. The relative

efficiency was estimated as the difference in the ratio of the maximum amplitudes of the two fluorescence components $a_{i,max}$ at each w/w ratio, according to eq. 4.2.1.**1** (Relative Efficiency of Polyplex Formation[III]).

$$Relative\ efficiency = \frac{\left(\frac{a_{1,max}}{a_{2,max}}\right)_{w/w} - R_{min}}{R_{max} - R_{min}}, \qquad (4.2.1.\mathbf{1})$$

where $$R_{max} = \left[\left(\frac{a_{1,max}}{a_{2,max}}\right)_{100}\right]_{max} \qquad (4.2.1.\mathbf{2})$$

and $$R_{min} = \left[\left(\frac{a_{1,max}}{a_{2,max}}\right)_{1}\right]_{min} \qquad (4.2.1.\mathbf{3})$$

For PBAEs without end caps R_{max} is the maximum amplitude ratio at w/w = 100, and R_{min} is the minimum amplitude ratio at w/w = 1. The relative nanoparticle formation efficiency was considered to be 0% at a w/w ratio of 1, at which there is minimal interaction between the polymer and the DNA. For 100% relative nanoparticle formation efficiency, a w/w ratio of 100 was used since, at this w/w, no further changes in the fluorescence signal were observed, and it is clearly higher than the useful w/w ratio for transfection (about 50[49]).

The nanoparticle formation efficiency was calculated with a w/w ratio of 50. The obtained relative efficiencies are presented in paper III, **Figure 5**, and they are compared in paper III, **Figure 6** with the relative transfection efficacy of the polymers that was reported earlier[49]. The increased relative nanoparticle formation efficiency is positively correlated with the increased transfection efficacy for most of the polymers. The *B* values and the relative nanoparticle formation efficiencies[III] support each other and, thus, some correlation between the *B* values, and the *in vitro* transfection efficacy is also observed.

Two groups with systematic change in the polymer structure can be separated from the ten PBAEs studied in paper III. In the first group, all the polymers contained amine monomer 28 with varying diacrylate monomers. From the saturation levels of these polymers presented in **Figure 4.12a** it is evident that the polymers with linear backbones (JJ, C, E and U) are more efficient than those with substituents between the acrylate moieties (AA and F) and that a shorter linear backbone with less carbon is slightly better than longer backbones. Concerning the $(K_{co})^{\alpha}$ values at low N/P ratios (**Figure 4.12b**, **Table 4.2**) the highest overall binding constant is obtained for C28, the other linear diacrylate monomers polymers have intermediate values and the polymers with branched diacrylate monomers (F28 and AA28) have very low values. For the other series, the backbone monomer was C and the side chain monomer increased in length from 4 to 6 carbons (C28, C32 and C36, respectively) between the amine and hydroxyl groups. For this series also, the saturation level decreases with increasing chain length (**Figure 4.12c**), and C28, with the shortest chain, again has the highest $(K_{co})^{\alpha}$ values (**Figure 4.12d**). Generally, a linear structure with high amine density seems to be most efficient structure, and the results for transfection efficacy mostly support these findings.

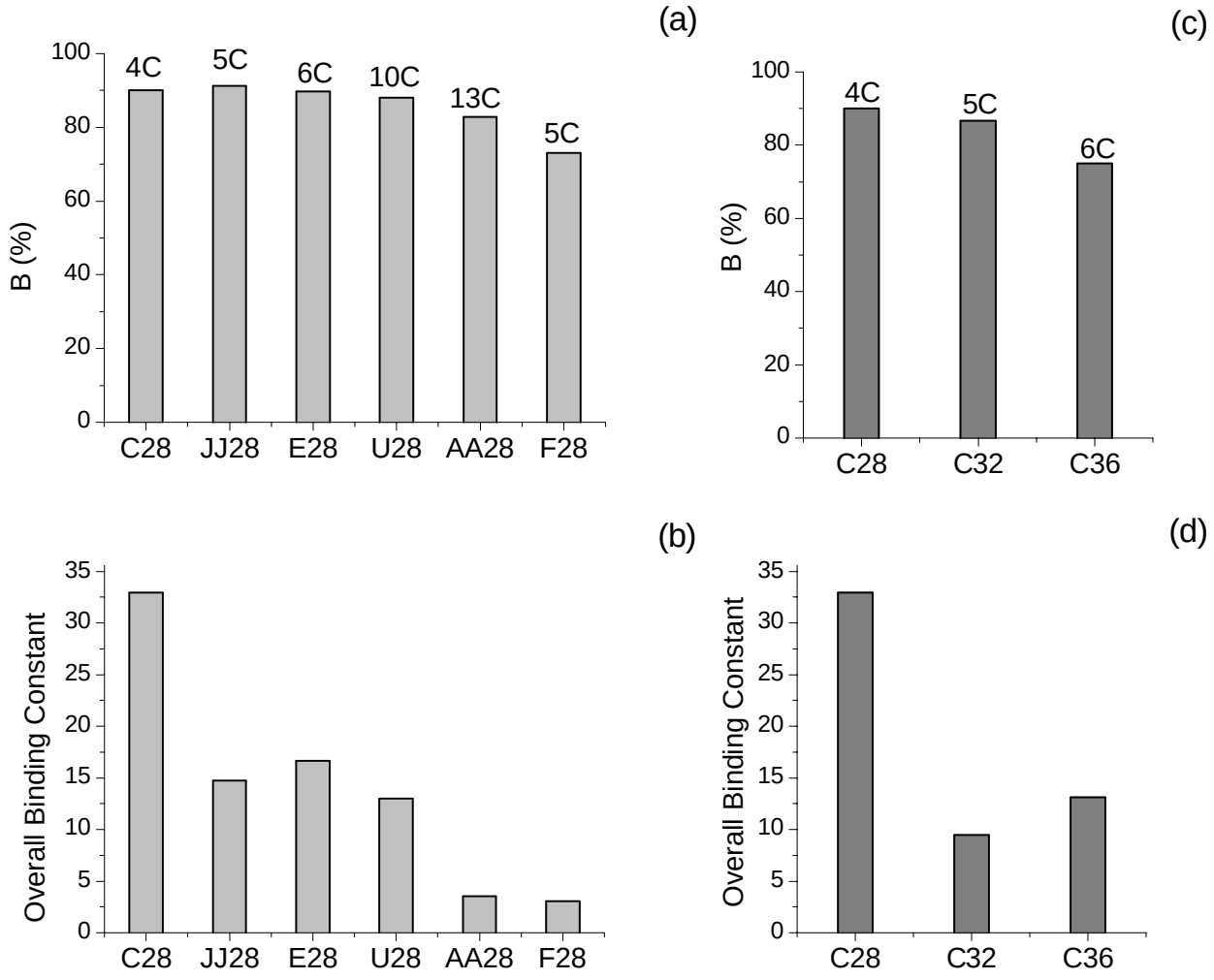

Figure 4.12 Saturation (*B* value) and overall binding constant differences between PBAEs without end caps compared with different backbones with side chain 28 (a, b) and different side chains with backbone C (c, d).

4.2.2 PBAEs with End Caps[IV]

The second series of fractionated PBAEs with end-cap groups (**Figure 3.2** and **Table 3.3**) were used to investigate polymer–DNA binding by varying (1) the polymer molecular weight by adding single carbons to (2) the backbone and to (3) the side chain of the monomers that constitute the polymers and by varying (4) the type of polymer end-cap group (shown in **Table 4.3**).

The effects of the changes in the polymer structure were characterised by the binding equilibrium using the cooperative binding model. The polyplex diameters and zeta potentials were measured at 60 w/w (polymer weight to DNA weight ratio). The transfection efficacy and cytotoxicity *in vitro* with two different cell lines (MDA-MB-231 human breast and GBM319 brain cancer cells) were measured at 30, 60 and 90 w/w. These weight ratios correspond to N/P ratios 34–40, 68–81 and 102–121, respectively. The polyplexes were prepared in 25 mM NaAc buffer at pH 5.2, regularly used for PBAEs in transfection and cytotoxicity studies[IV, 13, 48–50].

Table 4.3 Differences between studied PBAEs with end caps.

Molecular Weight	**Polymer Name**	**447L**	**447M**	**447H**		
M_w of polymer	M_w[a]	10.3 kDa	14.7 kDa	91.6 kDa		
	AD[b]	$(253\ Da)^{-1}$	$(262\ Da)^{-1}$	$(283\ Da)^{-1}$		
	N_N[c]	41	56	324		
Backbone	**Polymer Name**	**346**	**446**	**546**	**646**	
Number of C in back bone	N_C[d]	3	4	5	6	
	AD[b]	$(254\ Da)^{-1}$	$(267\ Da)^{-1}$	$(272\ Da)^{-1}$	$(288\ Da)^{-1}$	
	N_N[c]	44	44	33	37	
	M_w[a]	11.2 kDa	11.8 kDa	9.1 kDa	10.5 kDa	
Side Chain	**Polymer Name**	**437**	**447M**	**457**	**467**	
Number of C in side chain	N_C[d]	3	4	5	6	
	AD[b]	$(242\ Da)^{-1}$	$(262\ Da)^{-1}$	$(271\ Da)^{-1}$	$(282\ Da)^{-1}$	
	N_N[c]	43	56	49	47	
	M_w[a]	10.3 kDa	14.7 kDa	13.1 kDa	13.2 kDa	
End Cap	**Polymer Name**	**44**	**442**	**444**	**446**	**447L**
Type of the end cap	Added Amines	-	2NH, $2NH_2$	2NH, $2NH_2$	4NH, 2OH	2NH, 4N
	AD[b]	$(287\ Da)^{-1}$	$(264\ Da)^{-1}$	$(264\ Da)^{-1}$	$(267\ Da)^{-1}$	$(253\ Da)^{-1}$
	N_N[c]	40	40	39	44	41
	M_w[a]	11.6 kDa	10.4 kDa	10.3 kDa	11.8 kDa	10.3 kDa

[a]weight average molecular weights (M_w), [b]amine densities (AD), [c]number of amines per polymer (N_N), [d]number of carbons in polymer backbone or side chain (N_C)

The particle sizes and zeta potentials of PBAEs with end caps were measured at N/P = 60, where all the polymers had reached the saturation level. Hence, the net charges of the polyplexes were positive (IV, **Figure S7**). The mean diameters of the polyplexes ranged from 122 to 227 nm (III, **Figure S4**). The only trend in particle sizes was observed in the backbone group: the particle sizes decreased with increasing backbone length, i.e., with decreasing amine density and increasing hydrophobicity. The smallest particle size was observed for polymer 346, 122 nm, and the highest for polymer 646, 227 nm.

Figures 4.13–4.16 present the binding isotherms and Hill plots for PBAEs with end caps. For this series of polymers, the proportion of bound DNA increased with increasing N/P ratios until it reached a saturation limit of 64–96% at N/P ratios from 8 to 40 depending on the polymer. The B values of most of the PBAEs saturated close to 80% at an N/P ratio of about 20, and the turning points in the curves were near a B value of 70% at an N/P ratio ≤ 10 (i.e., **Figure 4.13**). The turning point for high-molecular weight PEIs and PLL was observed at N/P = 2[I], at the same N/P ratio where the charge of the polyplexes changes from negative to positive[15, 58, 67, 69, 98]. However, for PBAEs with end caps, the polyplexes were reported to be neutral still at an N/P ratio of 44[10]. At the turning point, most of the ETI has come out of the polyplexes into the bulk solution. The rest of the ETI stays intercalated to DNA even though the N/P ratio is increased. Whether this indicates that the polymer has bound only 64–96% of the DNA or that the remaining intercalated ETI has been trapped in the polyplex cannot be determined by this method.

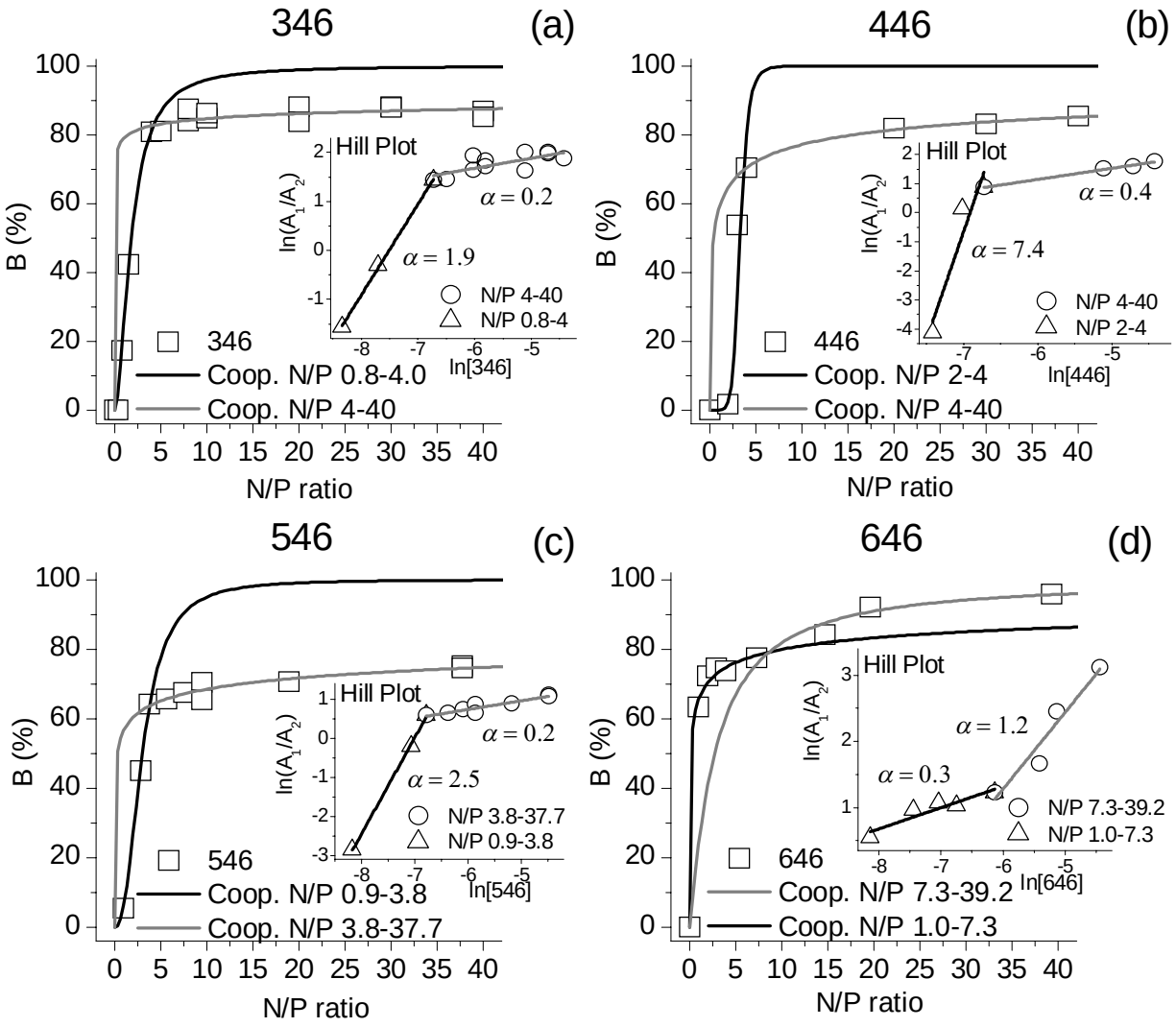

Figure 4.13 Binding isotherms for the backbone group for polymers 346 (a), 446 (b), 546 (c) and 646 (d): (□) measured points and (——) calculated by the cooperative binding model (eq. 2.2.3.**1**). Inserts: Hill plots for 346 (a), 446 (b), 546 (c) and 646 (d).

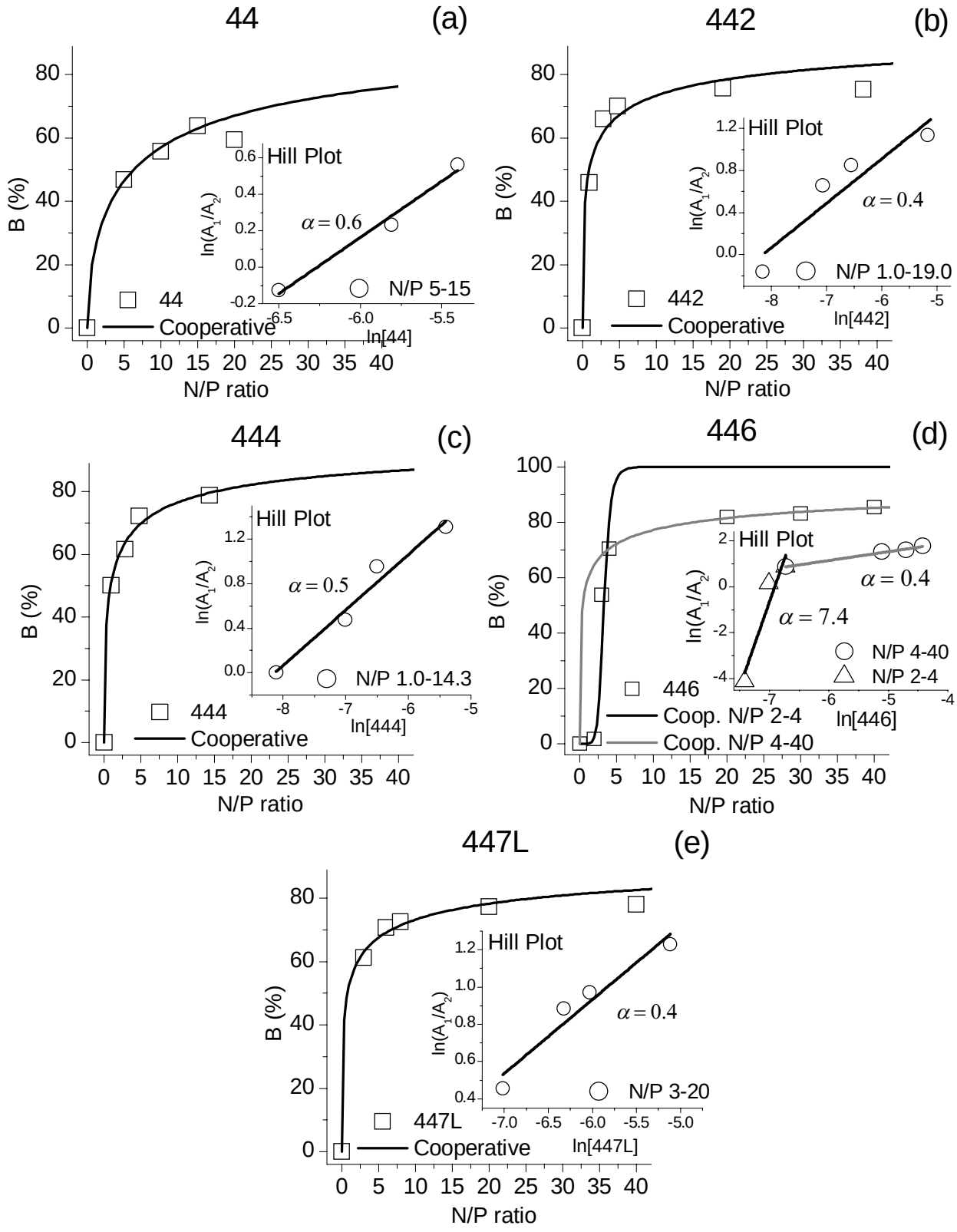

Figure 4.14 Binding isotherms for the end cap group for polymers 44 (a), 442 (b), 444 (c), 446 (d) and 447L (e): (□) measured points and (—) calculated by the cooperative binding model (eq. 2.2.3.**1**). Inserts: Hill plots for 44 (a), 442 (b), 444 (c), 446 (d) and 447L (e).

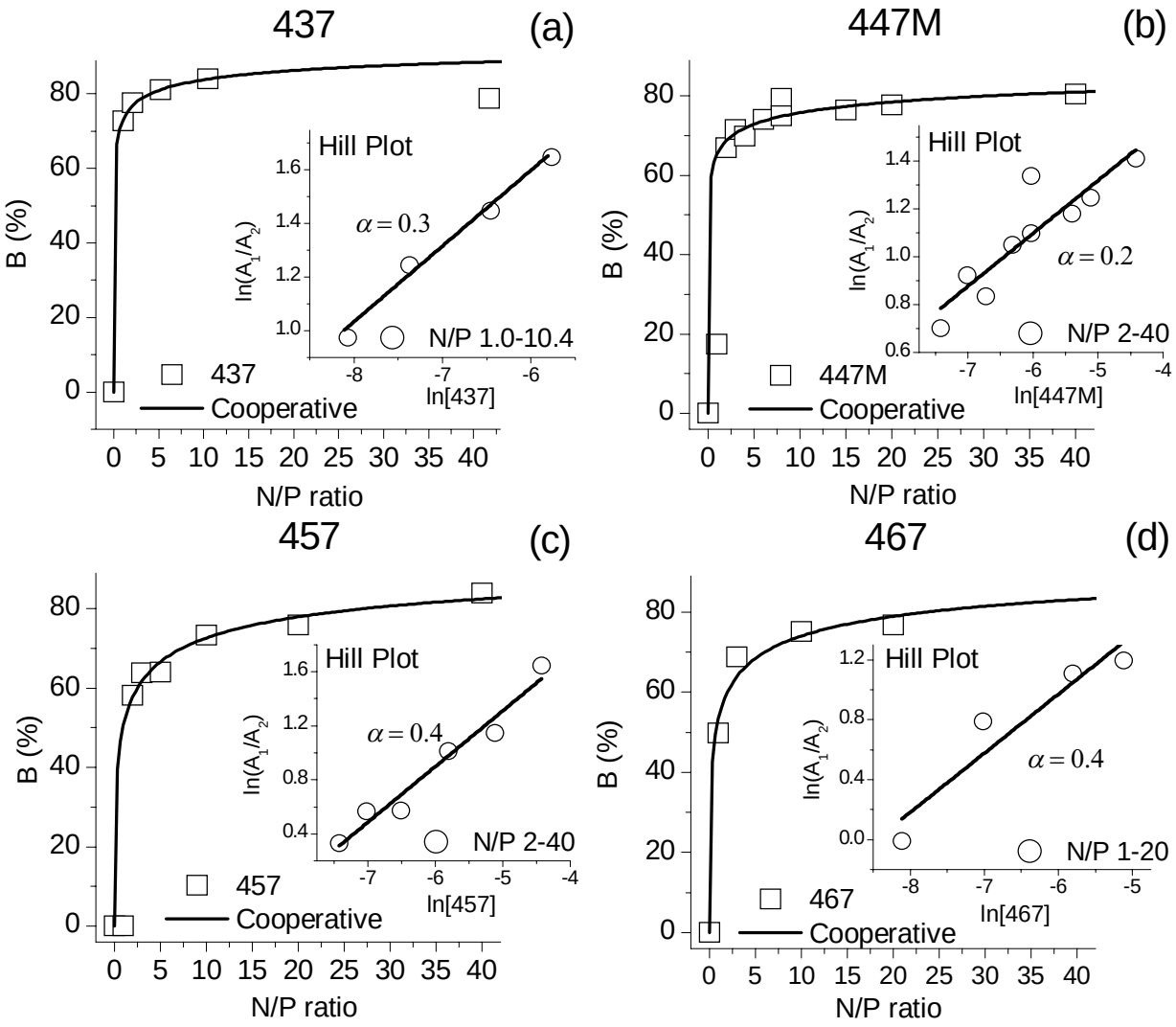

Figure 4.15 Binding isotherms for the side chain group for polymers 437 (a), 447M (b), 457 (c) and 467 (d): (□) measured points and (—) calculated by the cooperative binding model (eq. 2.2.3.**1**). Inserts: Hill plots for 437 (a), 447M (b), 457 (c) and 467 (d).

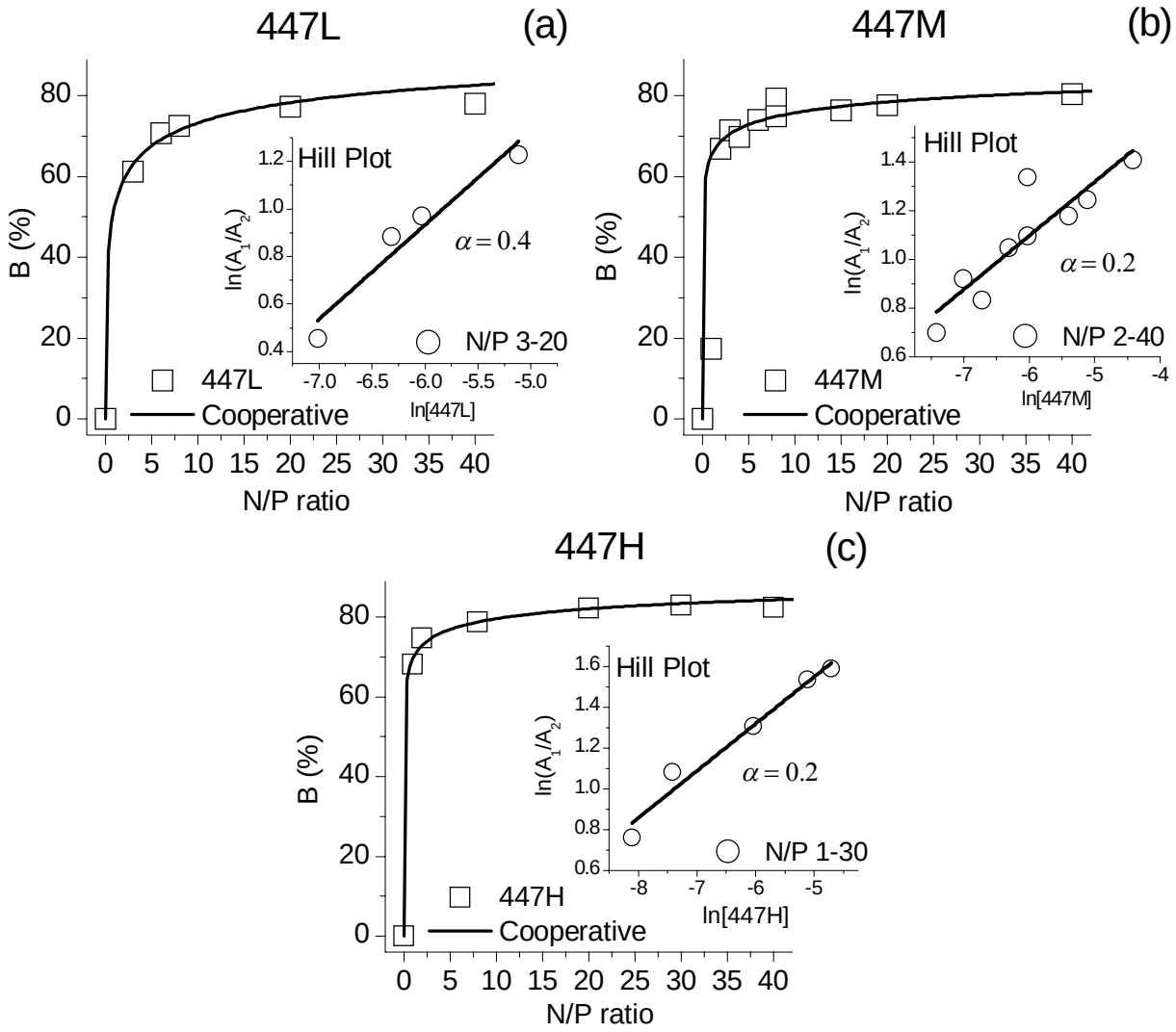

Figure 4.16 Binding isotherms for the molecular weight group for polymers 447L (a), 447M (b) and 447H (c): (□) measured points and (——) calculated by the cooperative binding model (eq. 2.2.3.**1**). Inserts: Hill plots for 447L (a), 447M (b) and 447H (c).

For the most of these PBAEs, the Hill plots are single straight lines, with $\alpha \leq 1$ indicating negative cooperativity (**Table 4.4**). As discussed in section 2.2.3, polymers with negative cooperativity typically have saturation levels under 100%, whereas polymers with positive cooperativity saturate near 100 %. In addition, the increase of *B* at low polymer concentrations is very strong for negative cooperativity. This is observed for these PBAEs to such an extent that it is difficult to obtain measuring points for $B < 50\%$.

The parameters calculated from the Hill plots shown in **Figures 4.13–4.16** are listed in **Table 4.4** for each group of structural variation. The Hill plots can be analysed as single straight lines with negative cooperativity ($\alpha < 1$) except for the backbone series (**Figure 4.13**), i.e., 346, 446, 546 and 646, for which the Hill plots are a composite of two lines with different slopes. For 346, 446 and 546, positive cooperativity at small N/P ratios followed by negative cooperativity at high N/P ratios was observed, whereas 646 showed negative cooperativity at low N/P ratios and positive cooperativity at high N/P ratios.

Table 4.4 Cooperative binding constants of PBAEs with end caps in 25 mM NaAc buffer (plasmid-enhanced green fluorescent protein (pEGFP-N1) DNA (Clontech)). Hill's cooperativity coefficients, α, overall cooperative binding constant, $(K_{co})^{\alpha}$, average cooperative binding constants per amine, K_{co}, and error of average cooperative binding constants per amine, ΔK_{co}.

Varying	Polymer	N/P Range	α	$(K_{co})^{\alpha}$	K_{co} (M^{-1})	ΔK_{co} (%)
Molecular Weight	447L	3.0–20.0	0.40	27.4 ± 3.5	4.2×10^3	0.279
	447M	2.0–40.0	0.22	11.3 ± 1.2	5.7×10^4	0.003
	447H	1.0–30.0	0.23	14.9 ± 2.2	1.2×10^5	0.008
Backbone	346	0.8–4.0	1.86	$(1.14 \pm 0.04) \times 10^6$	1.8×10^3	1.261
		4.0–40.0	0.17	14.6 ± 1.8	8.9×10^6	0.001
	446	2.0–4.0	7.4	$(1.7 \pm 0.5) \times 10^{22}$	1.0×10^3	85.27
		4.0–40.0	0.38	31.1 ± 1.0	8.0×10^3	0.013
	546	0.9–3.8	2.46	$(3.1 \pm 0.1) \times 10^6$	1.1×10^3	1.673
		3.8–37.7	0.22	7.91 ± 1.44	1.1×10^4	0.031
	646	1.0–7.3	0.32	25.8 ± 3.8	2.4×10^4	0.144
		7.3–39.2	1.16	$(3.8 \pm 0.5) \times 10^3$	1.2×10^3	5.647
Side Chain	437	1.0–10.4	0.28	26.7 ± 1.2	1.1×10^5	0.001
	447M	2.0–40.0	0.22	11.3 ± 1.2	5.7×10^4	0.003
	457	2.0–40.0	0.41	29.3 ± 2.2	3.5×10^3	0.098
	467	1.0–20.0	0.39	28.2 ± 5.1	4.7×10^3	0.868
End Cap	44	5.0–15.0	0.62	47.4 ± 5.8	5.3×10^2	1.428
	442	1.0–19.0	0.42	32.0 ± 6.8	3.7×10^3	2.032
	444	1.0–14.3	0.50	59.1 ± 6.2	3.6×10^3	0.358
	446	2.0–4.0	7.4	$(1.7 \pm 0.5) \times 10^{22}$	1.0×10^3	85.27
		4.0–40.0	0.38	31.1 ± 1.0	8.0×10^3	0.013
	447L	3.0–20.0	0.40	27.4 ± 3.5	4.2×10^3	0.279

Backbone Group. Increasing the number of carbons in the backbone monomers increases the distance between the backbone amine groups, thus decreasing the amine density. It also increases the hydrophobicity of the polymer. The Hill plots (**Figure 4.13**) for this group are a composite of two lines with different slopes. For 346, 446 and 546, positive cooperativity is observed at small N/P ratios of up to 4. The α values vary a lot, and no clear dependence is observed. More data points would be needed for reliable analysis, but unfortunately, not enough of the polymers were available for more measurements. At N/P ≥ 4, negative cooperativity was observed. 646 showed different behaviour: negative cooperativity at low N/P ratios and slightly positive at high N/P ratios. This resembles the behaviour of E28, the base polymer for 646 without end caps. The $(K_{co})^{\alpha}$ values of this group vary in a wide range following the degree of cooperativity. At N/P ≤ 4, the highest overall binding constant is obtained for 446, whereas at N/P > 4, polymer 646 has the highest overall binding constant. Thus, it seems that the intermediate backbone length, i.e., 4–5 carbon units, is optimal for the formation of the polyplex core. This could be due to steric hindrance for shorter and longer backbones. No clear correlation between the binding constant and transfection or cytotoxicity is observed in either of the cell lines used.

End Cap Group. The base polymer 44 was end-capped with monomers E2, E4, E6 and E7 (**Table 4.4** and **Figure 4.16**). This added one secondary amine group and either one primary amine group

(442 and 444) or another secondary amine group plus a hydroxyl group (446) or two tertiary amine groups (447L) to both ends of the polymer. At pH 5.2, the primary and secondary amines of the end caps are ~100% protonated, whereas the tertiary amines of the polymer backbone are about 50% protonated. In addition, after the end-capping, the amine density of the polymers were slightly higher than for the parent polymer. The order of amine densities is 447L > 442 > 444 > 446 > 44. However, the amine densities changed only a little, but the solubility of the polymers in the buffer increased considerably. All the end-capped polymers had higher K_{co} values than the base polymer 44, which is partly due to the lower solubility of 44 in NaAc buffer. No clear correlation with the other studied parameters and the K_{co} were observed. The cytotoxicity of the polymers increased in the following order: 442, 444 > 447 > 446. Thus, from the end-capped polymers, the polymers with secondary amine groups were less toxic and the polymers with primary amine groups were the most toxic.

Side Chain Group. Increasing the number of carbons in the side chain monomers does not change the distance between the backbone amine groups, but it nevertheless decreases the amine density. It also increases the hydrophobicity of the polymer. All four polymers of this group have Hill plots of single straight lines and negative cooperativity (inserts in **Figure 4.15**). The binding constant decreases with increasing side chain length. No correlation between the binding constant and transfection is observed for the MDA cell line, but for the GBM cell line, the transfection is more efficient for PBAEs with high binding constants. The cytotoxicity increases with decreasing K_{co} for both cell lines. For this series, the decrease in the K_{co} with increasing side chain length is more likely due to steric hindrance caused by the increasing side chain length than the decrease in the amine density since the physical distance between the amine groups does not change. The increasing cytotoxicity with the increasing length of the side chain is again probably due to the increased hydrophobicity of the polymers and thus to the reduced biodegradability.

Molecular Weight Group. The binding isotherms and Hill plots for 447L (10.3 kDa), 447M (14.7 kDa) and 447H (91.6 kDa) are shown in **Figure 4.16**. The degree of cooperativity is lower for 447M and 447H than for 447L. In addition to the Hill plot, this is also observed in the binding isotherms as a sharper turning point and a decreasing turning point N/P ratio with increasing molecular weight. The increasing polymer molecular weight leads to increasing polymer−DNA interactions[9] and higher K_{co} values but also to higher cytotoxicity. For the GBM cell line, the transfection efficiency mostly followed the cytotoxicity, and the best results were obtained for 447M at a high N/P ratio and for 447L at a low N/P ratio. For the MDA cell line, at low N/P ratios, the transfection efficiency increased with increasing molecular weight, but at high N/P ratios, 447M gave the best results.

4.2.3 Summary of Poly(β-amino ester)–DNA Polyplexes[III, IV]

In the first series of PBAEs, i.e., PBAEs without end caps, the branching versus the linear structure of the backbone was compared, and the linear structure proved to be better. The highest binding isotherm saturation levels and overall binding constants were observed for the polymers with shortest linear backbone and side chain.[III]

The end-capping of PBAEs increases the amine density, increases the efficiency of polyplex formation and thus increases the saturation levels of the binding isotherms. Type of end cap has an effect on the binding mechanism of the PBAEs. With the E6 end cap, the Hill plots are composites of two lines with different slopes, whereas for the other end caps, the Hill plots are a single straight line. In addition, the polymers with the E6 end cap reach the highest binding isotherm saturation levels.[IV]

The length of the backbone and the side chain of PBAEs were observed to be important to the complex formation via amine density, hydrophobicity and steric hindrances. Changing the length of the backbone has an effect on the binding mechanism: the intermediate chain lengths had the highest degree of cooperativity, and the longest chain length reached the highest binding isotherm saturation level of all PBAEs. The binding constant decreases with increasing side chain length (single phase cooperativity).[IV]

The molecular weights of the PBAEs (with end caps) were also observed to have an effect on complex formation. High-molecular weight PBAEs form polyplexes more effectively and reach higher binding isotherm saturation levels than smaller-molecular weight polymers.[IV]

5 Conclusion

The method for studying the mechanism of polymer–DNA polyplex formation based in time-resolved fluorescence measurements was successfully utilised with different types of polymers. Analysing the results with the cooperative binding model for multivalent ligand binding to a multi-subunit substrate gave quantitative information on the polyplex formation. The mechanism of polyplex formation varies from positive cooperativity to independent binding and, further, to negative cooperativity. For many polymers, the mechanism changes with increasing N/P ratios and changing environmental conditions, such as pH and ionic strength. In addition, small changes in the polymer structure can induce different binding mechanisms.

Important aspects to consider for efficient polyplex formation are the nature of the amine groups of the polymer and especially the degree of protonation of the amine groups in polyplex formation conditions. Generally, increasing molecular weight increases the efficiency of polyplex formation. For this property, a compromise should be found since increasing molecular weight increases the number of protonated amine groups and thus cytotoxicity. High amine density seems to induce positive cooperativity.

The method for studying the mechanism of polymer–DNA polyplex formation utilised in this thesis gives information mainly on the formation polyplex core since, after that, all the ETI has been freed to the bulk solution. For polymers, such as many PBAEs, that exhibit strongly negative cooperativity, both the formation core and the shell of the polyplex can be observed.

After the polyplex formation in a test tube, many other steps need to be overcome before the DNA reaches its destination. Thus, no correlation between the binding constants and the transfection efficiency can be expected. If such a correlation is observed, it is due to factors that affect both the polyplex formation and the overall gene delivery process similarly. For instance, for PBAEs with different amine side chain lengths, the longer side chain reduces polyplex formation due to steric hindrance. At the same time, it increases cytotoxicity since it makes the polymer more hydrophobic.

During the polyplex core formation, since most of the ETI is freed to the bulk solution, this method cannot be used for studying the role of excess polymer in the gene delivery process. For such studies, covalently labelled DNA and polymers are needed. However, the method developed and used in this thesis gives valuable information for understanding the packing of the polymer–DNA complexes into the field of gene-delivery.

6 References

[1.] Nielsen, L. L.; Maneval, D. C. P53 tumor suppressor gene therapy for cancer. *Cancer Gene Ther.* **1998**, *5*, 52–63.

[2.] Ziady, A. G.; Kelley, T. J.; Milliken, E.; Ferkol, T.; Davis, P. B. Functional Evidence of CFTR Gene Transfer in Nasal Epithelium of Cystic Fibrosis Mice *in Vivo* Following Luminal Application of DNA Complexes Targeted to the Serpin-Enzyme Complex Receptor. *Mol. Ther.* **2002**, *5*, 413–419.

[3.] Zuber, G.; Scherman, D. *Supramolecular Complexes of DNA. Nanoscience.* **2009**, Part 1, 101–128, DOI: 10.1007/978–3–540–88633–4_3.

[4.] Leong, K. W. *Polymer Design for Nonviral Gene Delivery*. *BioMEMS and Biomedical Nanotechnology*. **2006**, 239–263. DOI: 10.1007/978–0–387–25842–3_9.

[5.] Thomas, M.; Klibanov, A. M. Non-Viral Gene Therapy: Polycation-Mediated DNA Delivery. *Appl. Microbiol. Biotechnol.* **2003**, *62*, 27–34.

[6.] Sunshine, J. C.; Bishop, C. J.; Green, J. J. Advances in Polymeric and Inorganic Vectors for Nonviral Nucleic Acid Delivery. *Ther. Delivery* **2011**, *2*, 493–521.

[7.] Green, J. J. 2011 Rita Schaffer lecture: nanoparticles for intracellular nucleic acid delivery. *Ann. Biomed. Eng.* **2012**, 40, 1408–1418.

[8.] Merdan, T.; Kunath, K.; Fischer, D.; Kopecek, J.; Kissel, T. Intracellular Processing of Poly(Ethylene Imine)/Ribozyme Complexes Can Be Observed in Living Cells by Using Confocal Laser Scanning Microscopy and Inhibitor Experiments. *Pharm. Res.* **2002**, *19*, 140–146.

[9.] Green, J. J.; Langer, R.; Anderson, D. G. A combinatorial polymer library approach yields insight into nonviral gene delivery. *Acc. Chem. Res.* **2008**, *41*, 749–759.

[10.] Eltoukhy, A. A.; Siegwart, D. J.; Alabi, C. A.; Rajan, J. S.; Langer, R.; Anderson, D. G. Effect of Molecular Weight of Amine End-Modified Poly(β-amino ester)s on Gene Delivery Efficiency and Toxicity. *Biomaterials* **2012**, *33*, 3594–3603.

[11.] Wang, J.; Gao, S. J.; Zhang, P. C.; Wang, S.; Mao, M. Q.; Leong, K. W. Polyphosphoramidate gene carriers: effect of charge group on gene transfer efficiency. *Gene Ther.* **2004**, *11*, 1001–1010.

[12.] Zelikin, A. N.; Trukhanova, E. S.; Putnam, D.; Izumrudov, V. A.; Litmanovich, A. A. Competitive Reactions in Solutions of Poly-l-histidine, Calf Thymus DNA, and Synthetic Polyanions: Determining the Binding Constants of Polyelectrolytes. *J. Am. Chem. Soc.* **2003**, *125*, 13693–13699.

[13.] Sunshine, J. C.; Akanda, M. I.; Li, D.; Kozielski, K. L.; Green, J. J. Effects of Base Polymer Hydrophobicity and End-Group Modification on Polymeric Gene Delivery. *Biomacromolecules* **2011**, *12*, 3592–3600.

[14.] Merdan, T.; Kopeček, J.; Kissel, T. Prospects for cationic polymers in gene and oligonucleotide therapy against cancer. *Adv. Drug Deliv. Rev.* **2002**, *54*, 715–758.

[15.] Tang, M. X.; Szoka, F.C. The Influence of Polymer Structure on the Interactions of Cationic Polymers with DNA and Morphology of the Resulting Complexes. *Gene Ther.* **1997**, *4*, 823–832.

[16.] Wagner, E.; Cotten, M.; Foisner, R.; Birnstiel, M. L. Transferrin-Polycation-DNA Complexes: The effect of Polycations on the Structure of the Complex and DNA Delivery to Cells. *Proc. Natl. Acad. Sci. U. S. A.* **1991**, *88*, 4255–4259.

[17.] Vuorimaa, E.; Urtti, A.; Seppänen, R.; Lemmetyinen, H.; Yliperttula, M. Time-Resolved Fluorescence Spectroscopy Reveals Functional Differences of Cationic Polymer–DNA Complexes. *J. Am. Chem. Soc.* **2008**, *130*, 11695–11700.

[18.] Boussif, O.; Lezoualc'h, F.; Zanta, M. A.; Mergny, M. D.; Scherman, D.; Demeneix, B.; Behr, J.-P. A Versatile Vector for Gene and Oligonucleotide Transfer into Cells in Culture and in Vivo: Polyethylenimine. *Proc. Natl. Acad. Sci. U. S. A.* **1995**, *92*, 7297–7301.

[19.] Mao, H. Q; Roy, K.; Troung-Le, V. L.; Janes, K. A.; Lin, K. Y.; Wang, Y.; August, J. T.; Leong, K. W. Chitosan–DNA Nanoparticles as Gene Carriers: Synthesis, Characterization and Transfection Efficiency. *J. Control. Release* **2001**, *70*, 399–421.

[20.] Pun, S. H.; Davis, M. E. Development of a Nonviral Gene Delivery Vehicle for Systemic Application. *Bioconjug. Chem.* **2002**, *13*, 630–639.

[21.] Gabrielson, N. P.; Lu, H.; Yin, L.; Li, D.; Wang, F.; Cheng, J. A Reactive and Bioactive Cationic α-Helical Polypeptide Template for Nonviral Gene Delivery. *Angew. Chem. Int. Ed. Engl.* **2012**, *51*, 1143–1147.

[22.] Blessing, T.; Kursa, M.; Holzhauser, R.; Kircheis, R.; Wagner, E. Different Strategies for Formation of PEGylated EGF-Conjugated PEI/DNA Complexes for Targeted Gene Delivery. *Bioconjugate Chem.* **2001**, *12*, 529–537.

[23.] Brownlie, A.; Uchegbu, I. F.; Schatzlein, A. G. PEI-Based Vesicle-Polymer Hybrid Gene Delivery System with Improved Biocompatibility. *Int. J. Pharm.* **2004**, *274*, 41–52.

[24.] Gautam, A.; Waldrep, J. C.; Orson, F. M.; Kinsey, B. M.; Xu, B.; Densmore, C. L. Topical Gene Therapy for Pulmonary Diseases with PEI–DNA Aerosol Complexes. *Methods Mol. Med.* **2003**, *75*, 561–572.

[25.] Kunath, K.; von Harpe, A.; Fischer, D.; Kissel, T. Galactose-PEI–DNA Complexes for Targeted Gene Delivery: Degree of Substitution Affects Complex Size and Transfection Efficiency. *J. Control Rel.* **2003**, *88*, 159–172.

[26.] Lampela, P.; Soininen, P.; Urtti, A.; Männistö, P. T.; Raasmaja, A. Synergism in Gene Delivery by Small PEIs and Three Different Nonviral Vectors. *Int. J. Pharm.* **2004**, *270*, 175–184.

[27.] Green, J. J.; Shi, J.; Chiu, E.; Leshchiner, E. S.; Langer, R.; Anderson, D. G. Biodegradable Polymeric Vectors for Gene Delivery to Human Endothelial Cells. *Bioconjug. Chem.* **2006**, *17*, 1162–1169.

[28.] Mahato, R. I. Water Insoluble and Soluble Lipids for Gene Delivery. *Adv.Drug Deliv. Rev.* **2005**, *57*, 699–712.

[29.] Pelisek, J.; Gaedtke, L.; DeRouchey, J.; Walker, G. F.; Nikol, S.; Wagner, E. Optimized Lipopolyplex Formulations for Gene Transfer to Human Colon Carcinoma Cells under in Vitro Conditions. *J. Gene Med*. **2006**, *8*, 186–197.

[30.] Hashimoto, T.; Yamaoka, T. *Polymeric Gene Carriers*. *Non-Viral Gene Therapy*. **2005**, 1., 35–50. DOI: 10.1007/4–431–27879–6_4.

[31.] Boeckle, S.; von Gersdorff, K.; van der Piepen, S.; Culmsee, C.; Wagner, E.; Ogris, M. Purification of Polyethylenimine Polyplexes Highlights the Role of Free Polycations in Gene Transfer. *J. Gene Med.* **2004**, *6*, 1102–1111.

[32.] Wagner, E.; Kloeckner, J. Gene *Delivery Using Polymer Therapeutics. Polymer Therapeutics I: Advances in Polymer Science*. **2006**, Volume 192/2006, 135–173, DOI: 10.1007/12_023.

[33.] Kichler, A.; Leborgne, C.; Coeytaux, E.; Danos, O. Polyethylenimine-Mediated Gene Delivery: A Mechanistic Study. *J. Gene Med*. **2001**, *3*, 135–144.

[34.] Abdallah, B.; Hassan, A.; Benoist, C.; Goula, D.; Behr, J.-P.; Demeneix, B.A. A Powerful Nonviral Vector for in Vivo Gene Transfer Into the Adult Mammalian Brain: Polyethylenimine. *Hum. Gene Ther*. **1996**, *7*, 1947–1954.

[35.] Boletta, A.; Benigni, A.; Lutz, J.; Remuzzi, G.; Soria, M. R.; Monaco, L. Nonviral Gene Delivery to the Rat Kidney with Polyethylenimine. *Hum. Gene Ther*. **1997**, *8*, 1243–1251.

[36.] Kren, B. T.; Bandyopadhyay, P.; Steer, C. J. In Vivo Site-Directed Mutagenesis of the Factor IX Gene by Chimeric RNA/DNA Oligonucleotides. *Nat. Med.* **1998**, *4*, 285–290.

[37.] Bandyopadhyay, P.; Ma, X.; Linehan-Stieers, C.; Kren, B. T.; Steer, C. J. Nucleotide Exchange in Genomic DNA of Rathepatocytes Using RNA/DNA Oligonucleotides. Targeted Delivery of Liposomes and Polyethyleneimine to the Asialoglycoprotein Receptor. *J. Biol. Chem.* **1999**, *274*, 10163–10172.

[38.] Remy, J. S.; Behr, J.-P. Gene Transfer with Multivalent Synthetic Vectors. *J. Liposome Res.* **1996**, *6*, 535–544. .

[39.] Boussif, O.; Zanta, M. A.; Behr, J.-P. Optimized Galenics Improve in Vitro Gene Transfer with Cationic Molecules Up to 1000-Fold. *Gene Ther.* **1996**, *3*, 1074–1080.

[40.] von Harpe, A.; Petersen, H.; Li, Y.; Kissel, T. Characterization of Commercially Available and Synthesized Polyethylenimines for Gene Delivery. *J. Control. Release* **2000**, *69*, 309–322.

[41.] Turunen, M. P.; Hiltunen, M. O.; Ruponen, M.; Virkamäki, L.; Szoka, J. F. C.; Urtti, A.; Ylä-Herttuala, S. Efficient Adventitial Gene Delivery to Rabbit Carotid Artery with Cationic Polymer–Plasmid Complexes. *Gene Ther.* **1999**, *6*, 6–11.

[42.] Godbey, W. T.; Wu, K. K.; Mikos, A. G. Size Matters: Molecular Weight Affects the Efficiency of Poly(ethylenimine) as a Gene Delivery Vehicle. *J. Biomed. Mater. Res.* **1999**, *45*, 268–275.

[43.] Morille, M.; Passirani, C.; Vonarbourg, A.; Clavreul, A.; Benoit, J.-P. Progress in Developing Cationic Vectors for Non-Viral Systemic Gene Therapy Against Cancer. *Biomaterials*, **2008**, *29*, 3477–3496.

[44.] Kwoh, D. Y.; Coffin, C. C.; Lollo, C. P.; Jovenal, J.; Banaszczyk, M. G.; Mullen, P.; Phillips, A.; Amini, A.; Fabrycki, J.; Bartholomew, R. M.; Brostoff, S. W.; Carlo, D. J. Stabilization of Poly-L-lysine/DNA Polyplexes for in Vivo Gene Delivery to the Liver. *Biochim. Biophys. Acta* **1999**, *1444*, 171–190.

[45.] Wagner, E.; Ogris, M.; Zauner, W. Polylysine-Based Transfection Systems Utilizing Receptor-Mediated Delivery. *Adv. Drug Deliv. Rev.* **1998**, *30*, 97–113.

[46.] Lynn, D.M.; Langer, R. Degradable Poly(β-amino esters): Synthesis, Characterization, and Self-Assembly with Plasmid DNA. *J. Am. Chem. Soc.* **2000**, 122, 10761–10768.

[47.] Lynn, D.M.; Anderson, D.G.; Putnam, D.; Langer, R. Accelerated Discovery of Synthetic Transfection Vectors: Parallel Synthesis and Screening of a Degradable Polymer Library. *J. Am. Chem. Soc.* **2001**, *123*, 8155–8156.

[48.] Akinc, A.; Lynn, D.M.; Anderson, D.G.; Langer, R. Parallel Synthesis and Biophysical Characterization of a Degradable Polymer Library for Gene Delivery. *J. Am. Chem. Soc.* **2003**, *125*, 5316–5323.

[49.] Anderson, D. G.; Lynn, D. M.; Langer, R. Semi-Automated Synthesis and Screening of a Large Library of Degradable Cationic Polymers for Gene Delivery. *Angew. Chem. Int. Ed. Engl.* **2003,** *42*, 3153–3158.

[50.] Akinc, A.; Anderson, D. G.; Lynn, D. M.; Langer, R. Synthesis of Poly(beta-amino ester)s Optimized for Highly Effective Gene Delivery. *Bioconjug. Chem.* **2003**, *14*, 979–988.

[51.] van de Wetering, P.; Moret, E.E.; Schuurmans-Nieuwenbroek, N. M.; van Steenbergen, M. J.; Hennink, W.E. Structure-Activity Relationships of Water-Soluble Cationic Methacrylate/Methacrylamide Polymers for Non-Viral Gene Delivery. *Bioconjug. Chem.* **1999**, *10*, 589–597.

[52.] Ziebarth, J. D.; Wang, Y. Understanding the Protonation Behavior of Linear Polyethylenimine in Solutions Through Monte Carlo Simulations. *Biomacromolecules* **2010**, *11*, 29–38.

[53.] Zuidam et al. 2000: Zuidam, N. J.; Posthuma, G.; de Vries, E. T.; Crommelin, D. J.; Hennink, W. E.; Storm, G. Effects of Physicochemical Characteristics of Poly(2-(dimethylamino)ethyl methacrylate)-Based Polyplexes on Cellular Association and Internalization. *J. Drug Target* **2000**, *8*, 51–66.

[54.] Harada, A.; Kawamura, M.; Matsuo, T.; Takahashi, T.; Kono, K. Synthesis and Characterization of a Head-Tail Type Polycation Block Copolymer as a Nonviral Gene Vector. *Bioconjugate Chem.* **2006**, *17*, 3−5.

[55.] Fukushima, S.; Miyata, K.; Nishiyama, N.; Kanayama, N.; Yamasaki, Y.; Kataoka, K. PEGylated Polyplex Micelles from Triblock Catiomers with Spatially Ordered Layering of Condensed pDNA and Buffering Units for Enhanced Intracellular Gene Delivery. *J. Am. Chem. Soc.* **2005**, *127*, 2810–2811.

[56.] Stobiecka, M.; Hepel, M. Double-Shell Gold Nanoparticle-Based DNA-Carriers with Poly-L-lysine Binding Surface. *Biomaterials* **2011**, *32*, 3312–3321.

[57.] Guo, Y.; Xia, F.; Xu, L.; Li, J.; Yang, W.; Jiang, L. Switchable Wettability on Cooperative Dual-Responsive Poly-L-lysine Surface. *Langmuir* **2010**, *26*, 1024–1028.

[58.] Choosakoonkriang, S.; Lobo, B. A.; Koe, G. S.; Koe, J. G.; Middaugh, C. R. Biophysical Characterization of PEI/DNA Complexes. *J. Pharm. Sci.* **2003**, *92*, 1710–1722.

[59.] Clamme, J. P.; Azoulay, J.; Mély, Y. Monitoring of the Formation and Dissociation of Polyethylenimine/DNA Complexes by Two Photon Fluorescence Correlation Spectroscopy. *Biophys. J.* **2003**, *84*, 1960–1968.

[60.] Wang, Y.; Chen, P.; Shen, J. The Development and Characterization of a Glutathione-Sensitive Cross-Linked Polyethylenimine Gene Vector. *Biomaterials* **2006**, *27*, 5292−5298.

[61.] Kwan, K.; Lee, J. W.; Choi, J.-Y.; Shin, K. S. pH Effect on Surface Potential of Polyelectrolytes-Capped Gold Nanoparticles Probed by Surface-Enhanced Raman Scattering. *Langmuir* **2010**, *26*, 19163−19169.

[62.] Sonawane, N. D.; Szoka Jr., F. C.; Verkman, A. S. Chloride Accumulation and Swelling in Endosomes Enhances DNA Transfer by Polyamine–DNA Polyplexes. *J. Biol. Chem.* **2003**, *278*, 44826–44831.

[63.] Benjaminsen, R. V.; Mattebjerg, M. A.; Henriksen, J. R.; Moghimi, S. M.; Andresen, T. L. The Possible "Proton Sponge" Effect of Polyethylenimine (PEI) Does Not Include Change in Lysosomal pH. *Molecular Therapy* **2013**, *21*, 149–157.

[64.] Liang, W.; Lam, J. K. W. Dr. Ceresa, B. (Ed.). *Endosomal Escape Pathways for Non-Viral Nucleic Acid Delivery Systems. Molecular Regulation of Endocytosis.* **2012**, 429–456. ISBN: 978–953–51–0662–3, InTech, DOI: 10.5772/46006.

[65.] Hanzlíková, M.; Ruponen, M.; Galli, E.; Raasmaja, A.; Aseyev, V.; Tenhu, H.; Urtti, A.; Yliperttula, M. Mechanisms of Polyethylenimine-Mediated DNA Delivery: Free Carrier Helps to Overcome the Barrier of Cell-Surface Glycosaminoglycans. *J. Gene Med*. **2011**, *13*, 402–409.

[66.] Dai, Z.; Gjetting, T.; Mattebjerg, M. A.; Wu, C.; Andresen, T. L. Elucidating the Interplay Between DNA-Condensing and Free Polycations in Gene Transfection Through a Mechanistic Study of Linear and Branched PEI. *Biomaterials* **2011**, *32*, 8626–8634.

[67.] Ikonen, M.; Murtomäki, L.; Kontturi, K. Controlled Complexation of Plasmid DNA with Cationic Polymers: Effect of Surfactant on the Complexation and Stability of the Complexes. *Colloids Surf. B Biointerfaces* **2008**, *66*, 77–83.

[68.] Sitharman, B. (Ed.). *Nanobiomaterials Handbook*. CRC Press **2011**, Print ISBN: 978–1–4200–9466–4, eBook ISBN: 978–1–4200–9467–1, DOI: 10.1201/b10970–23.

[69.] Zou, S.-M.; Erbacher, P.; Remy, J.-S.; Behr, J.-P. Systemic Linear Polyethylenimine (L-PEI)-Mediated Gene Delivery in the Mouse. *J. Gene Med.* **2000**, *2*, 128–134.

[70.] Wightman, L.; Kircheis, R.; Rössler, V.; Carotta, S.; Ruzicka, R.; Kursa, M.; Wagner, E. Different Behavior of Branched and Linear Polyethylenimine for Gene Delivery *in Vitro* and *in Vivo*. *J. Gene Med.* **2001**, *3*, 362–372.

[71.] Ogris, M.; Steinlein, P.; Kursa, M.; Mechtler, K.; Kircheis, R.; Wagner, E. The Size of DNA/Transferrin-PEI Complexes is an Important Factor for Gene Expression in Cultured Cells. *Gene Ther.* **1998**, *5*, 1425–1433.

[72.] Ruponen, M.; Honkakoski, P.; Tammi, M.; Urtti, A. Cell-Surface Glycosaminoglycans Inhibit Cation-Mediated Gene Transfer. *J. Gene Med.* **2004**, *6*, 405–414.

[73.] Fischer, D.; Bieber, T.; Li, Y. *et al*. A Novel Non-Viral Vector for DNA Delivery Based on Low Molecular Weight, Branched Polyethylenimine: Effect of Molecular Weight on Transfection Efficiency and Cytotoxicity. *Pharm. Res.* **1999**, *16*, 1273–1279.

[74.] Connors, K. A. Binding Constants: The Measurements of Molecular Complex Stability. John Wiley & Sons, New York, **1987**.

[75.] Tinoco, I., Jr.; Sauer, K.; Wang, J.C.; Pauglisi, J.D. Challice, J. (Ed.). *Physical Chemistry: Principles and Applications in Biological Sciences*. 4th Edition. **2002** Prentice Hall, Inc. Upper Saddle River, New Jersy 07458. ISBN: 0–13–095943–X.

[76.] Gelamo, E. L.; Tabak, M. Spectroscopic Studies on the Interaction of Bovine (BSA) and Human (HSA) Serum Albumins with Ionic Surfactants. *Spectrochim. Acta, Part A* **2000**, 56, 2255–2271.

[77.] Gelamo, E.L.; Silva, C.H.T.P.; Imasato, H.; Tabak, M. Ineraction of Bovine (BSA) and Human (HSA) Serum Albumins with Ionic Surfactants: Spectroscopy and Modeling. *Biochim. Biophys. Acta* **2002**, *1594*, 84–99.

[78.] Nanduri, V.; Sorokulova I. B.; Samoylov A. M.; Simonian, A. L.; Petrenko, V. A.; Vodyanoy, V. Phage as a Molecular Recognition Element in Biosensors Immobilized by Physical Adsorption. *Biosens. Bioelectron.* **2007**, *22*, 986–992.

[79.] Michel, D. Cooperative Equilibrium Curves Generated by Ordered Ligand Binding to Multi-Site Molecules. *Biophys. Chem.* **2007**, *129*, 284–288.

[80.] Ryou, C.; Prusiner, S. B.; Legname, G. Cooperative Binding of Dominant-Negative Prion Protein to Kringle Domains. *J. Mol. Biol.* **2003**, *329*, 323–333.

[81.] Dam, T. K.; Roy, R.; Page, D.; Brewer, F. Negative Cooperativity Associated with Binding of Multivalent Carbohydrates to Lectins. Thermodynamic Analysis of the "Multivalency Effect". *Biochemistry*, **2002**, *41*, 1351–1358.

[82.] Dam, T. K.; Gerken, T. A.; Brewer, C. F. Thermodynamics of Multivalent Carbohydrate-Lectin Cross-Linking Interactions: Importance of Entropy in the Bind and Jump Mechanism. *Biochemistry* **2009,** *48*, 3822–3827.

[83.] Byrne, C. D.; de Mello, A. J. Photophysics of Ethidium Bromide Complexed to ct-DNA: a Maximum Entropy Study. *Biophys. Chem.* **1998**, *70*, 173–184.

[84.] Le Pecq J.-B.; Paoletti C. A New Fluorometric Method for RNA and DNA Determination. *Anal. Biochem.* **1996**, *17*, 100–107.

[85.] Hovhannisyan**,** V. A.; Avanessian, L. A. Fluorescence Study of DNA–Dye Complexes Using One-Photon and Two-Photon Picosecond Excitation. *Journal of Fluorescence* **1998**, *8*, 179–183.

[86.] Minasyan, S. H.; Tavadyan, L. A.; Antonyan, A. P.; Davtyan, H. G.; Parsadanyan, M. A.; Vardevanyan, P. O. Differential Pulse Voltammetric Studies of Ethidium Bromide Binding to DNA. *Bioelectrochemistry* **2006**, *68*, 48–55.

[87.] Olmsted III**,** J.; Kearns, D. R. Mechanism of Ethidium Bromide Fluorescence Enhancement on Binding to Nucleic Acids. *Biochemistry* **1977**, *16*, 3647–3654.

[88.] Pohl, F. M.; Jovin, T. M.; Baehr, W.; Holbrook, J. J. Ethidium Bromide as a Cooperative Effector of a DNA Structure. *Proc. Nat. Acad. Sci. U. S. A.* **1972**, *69*, 3805–3809.

[89.] Luedtke, N. W.; Liu, Q.; Tor, Y. On the Electronic Structure of Ethidium. *Chem. Eur. J.* **2005**, *11*, 495–508.

[90.] Saucier, J. M.; Festy, B.; LePecq, J.-B. The Change of the Torsion of the DNA Helix Caused by Intercalation: II-Measurement of the Relative Change of Torsion Induced by Various Intercalating Drugs. *Biochimie* **1971**, *53*, 973–980.

[91.] Borisova, O. F.; Shchiolkina, A. K.; Karapetian, A. T.; Surovaya, A. N. The Heterogeneity of Strong Binding Site of Ethidium Bromide on DNA. Fluorescent and Non-Fluorescent Complexes. *Mol. Biol. (Rus)* **1998**, *32*, 855–862.

[92.] Zhou, Y.-L; Li, Y.-Z. The Interaction of Poly(ethylenimine) with Nucleic Acids and Its Use in Determination of Nucleic Acids Based on Light Scattering. *Spectrochim. Acta A* **2004**, *60*, 377–384.

[93.] Sarkar, R.; Pal, S. K. Interaction of Hoechst 33258 and Ethidium with Histone1–DNA Condensates. *Biomacromolecules* **2007,** *8*, 3332–3339.

[94.] Xu, Y.; Hui, S.-W.; Frederik, P.; Szoka, F. C., Jr. Physicochemical Characterization and Purification of Cationic Lipoplexes. *Biophys. J.* **1999**, 77, 341–53.

[95.] Plank, C.; Tang, M. X.; Wolfe, A. R.; Szoka, F. C., Jr. Branched Cationic Peptides for Gene Delivery: Role of Type and Number of Cationic Residues in Formation and *in Vitro* Activity of DNA Polyplexes. *Hum. Gene Ther.* **1999**, *10*, 319–332.

[96.] Tkachenko, N. V. *Optical Spectroscopy: Methods and Instrumentations*. Elsevier, Amsterdam, **2006**. ISBN–13: 978–0–444–52126–2, ISBN–10: 0–444–52126–7.

[97.] *Zetasizer APS User Manual*. MAN0425 Issue 1.0. December **2008**.

[98.] Erbacher, P.; Bettinger, T.; Belguise-Valladier, P.; Zou, S.; Coll, J.-L.; Behr, J.-P.; Remy, J.-S. Transfection and Physical Properties of Various Saccharide, Poly(ethylene glycol), and Antibody Derivatized Polyethylenimines (PEI). *J. Gene Med.* **1999**; *1*: 210–222.

[99.] Jääskeläinen, I.; Mönkkönen, J.; Urtti, A. Oligonucleotide-Cationic Liposome Interactions. A Physicochemical Study. *Biochim. Biophys. Acta* **1994**, *1195*, 115–123.

[100.] Duan, X.; Xiao, J.; Yin, Q.; Zhang, Z.; Mao, S.; Li, Y. Amphiphilic Graft Copolymer Based on Poly(styrene-co-maleic anhydride) with Low Molecular Weight Polyethylenimine for Efficient Gene Delivery. *Int. J. Nanomedicine* **2012**, *7*, 4961–4972.

[101.] Ruponen, M.; Ylä-Herttuala, S.; Urtti, A. Interactions of Polymeric and Liposomal Gene Delivery Systems with Extracellular Glycosaminoglycans: Physicochemical and Transfection Studies. *Biochim. Biophys. Acta, Biomembr.* **1999**, *1415*, 331–341.

[102.] Ruponen, M.; Rönkkö, S.; Honkakoski, P.; Pelkonen, J.; Tammi, M.; Urtti A. Extracellular Glycosaminoglycans Modify Cellular Trafficking of Lipoplexes and Polyplexes. *J. Biol. Chem.* **2001**, *36*, 33875–33880.

[103.] Sharma, V. K.; Thomas, M.; Klibanov, A. M. Mechanistic Studies on Aggregation of Polyethylenimine–DNA Complexes and Its Prevention. *Biotechnol. Bioeng.* **2005**, *90*, 614–620.

[104.] Reul, R.; Nguyen, J.; Biela, A.; Marxer, E.; Bakowsky, U.; Klebe, G.; Kissel, T. Biophysical and Biological Investigation of DNA Nano-Complexes with a Non-Toxic, Biodegradable Amine-Modified Hyperbranched Polyester. *Int. J. Pharm.* **2012**, *436*, 97–105.

[105.] Männistö, M.; Reinisalo, M.; Ruponen, M.; Honkakoski, P.; Tammi, M.; Urtti, A. Polyplex-Mediated Gene Transfer and Cell Cycle: Effect of Carrier on Cellular Uptake and Intracellular Kinetics, and Significance of Glycosaminoglycans. *J. Gene Med.* **2007**, *9*, 479–487.

Publication I

Independent versus Cooperative Binding in Polyethylenimine–DNA and Poly(L-lysine)–DNA Polyplexes

Tiia-Maaria Ketola, Martina Hanzlíková, Linda Leppänen, Manuela Raviña, Corey J. Bishop, Jordan J. Green, Arto Urtti, Helge Lemmetyinen, Marjo Yliperttula and Elina Vuorimaa-Laukkanen, *J. Phys. Chem. B* 2013, *117*, 10405–10413.

Reprinted with permission from *The Journal of Physical Chemistry B* **2013**, *117*, 10405–10413.

THE JOURNAL OF PHYSICAL CHEMISTRY B

Article

pubs.acs.org/JPCB

Independent versus Cooperative Binding in Polyethylenimine–DNA and Poly(L-lysine)–DNA Polyplexes

Tiia-Maaria Ketola,[†] Martina Hanzlíková,[‡] Linda Leppänen,[‡] Manuela Raviña,[§] Corey J. Bishop,[∥] Jordan J. Green,[∥] Arto Urtti,[§] Helge Lemmetyinen,[†] Marjo Yliperttula,[‡] and Elina Vuorimaa-Laukkanen*[,†]

[†]Department of Chemistry and Bioengineering, Tampere University of Technology, Korkeakoulunkatu 10, 33720 Tampere, Finland

[‡]Division of Biopharmaceutics and Pharmacokinetics, [§]Centre for Drug Research, Faculty of Pharmacy, University of Helsinki, Viikinkaari 5, 00790 Helsinki, Finland

[∥]Department of Biomedical Engineering, the Wilmer Eye Institute, the Institute for Nanobiotechnology, and the Translational Tissue Engineering Center, Johns Hopkins University School of Medicine, 400 North Broadway, Baltimore, Maryland 21231, United States

Supporting Information

ABSTRACT: The mechanism of polyethylenimine–DNA and poly(L-lysine)–DNA complex formation at pH 5.2 and 7.4 was studied by a time-resolved spectroscopic method. The formation of a polyplex core was observed to be complete at approximately N/P = 2, at which point nearly all DNA phosphate groups were bound by polymer amine groups. The data were analyzed further both by an independent binding model and by a cooperative model for multivalent ligand binding to multisubunit substrate. At pH 5.2, the polyplex formation was cooperative at all N/P ratios, whereas for pH 7.4 at N/P < 0.6 the polyplex formation followed independent binding changing to cooperative binding at higher N/Ps.

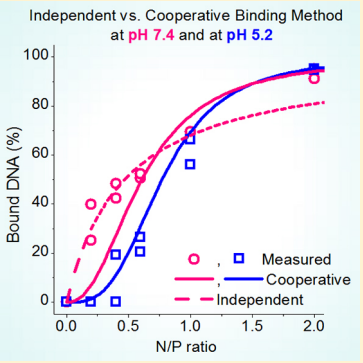

INTRODUCTION

The development of safe and effective nonviral vectors for gene medicines (DNA, siRNA, miRNA) is an important biomedical challenge.[1] Viral vectors are more effective than nonviral systems, but the latter have advantages of easier up-scaling and better safety. Polyethylenimine (PEI) is a cationic polymer that is able to complex DNA and it is widely used for DNA transfection in vitro.[2−5] PEI constitutes a high concentration of positively charged amine groups (primary, secondary, tertiary) which enable effective electrostatic binding and condensation of negatively charged DNA.[6] Similarly, poly(L-lysine) (PLL), a polycation with primary amines only, has been used to condense DNA into nanoparticles. However, in the presence of a competing polyelectrolyte, such as heparin sulfate, a glycosaminoglycan, PEI and PLL respond differently; PEI–DNA complexes dissociate, whereas PLL–DNA complexes do not dissociate as readily.[7−9] These different responses to a competing polyelectrolyte may in part explain the 100-fold higher transfection efficacy for branched PEI compared to PLL polyplexes as DNA must release from the polyplexes prior to its transcription and translation.[9,10]

Linear and branched PEI have been used to construct polyplex systems that have been applied in gene delivery and transfection studies.[2,5,11] Linear PEI (LPEI) is composed almost exclusively of secondary amines while branched PEI (BPEI) is composed of primary, secondary and tertiary amines (Figure 1). The chemical structure of PLL constitutes primary amines in the side chains which take part on binding DNA. At the physiological pH range (5.0–7.4), primary amines are in the protonated state, whereas the secondary and tertiary amines are only partially ionized.[12] Due to its secondary and tertiary amines, PEI shows buffering capacity and polymer swelling at the acidic pH of the endosomes.[12] PLL does not have these features that augment gene transfection at the cellular level.[12] Although the differences in the chemical structures account for the transfection efficiency and toxicity, differences in structure–activity relationship are not well understood.[5] Elucidating these structure–activity relationships is critical for controlling the functionality of novel biomaterials to be used for gene therapy.

Recently, we compared the DNA-complexation behavior of various PEI species (small, linear, and branched). Using time-resolved fluorescence spectroscopy, the binding constants for polyplex formation were determined using an independent binding model.[13] The independent binding model, in contrast to the cooperative binding model, does not take into account the simultaneous or subsequent binding of other amine ligands at unoccupied phosphate sites on DNA. Based on this analysis, we found that for both linear and branched PEI the complexation process was biphasic, suggesting the mechanism of polyplex formation varies as a function of amine

Received: May 16, 2013
Revised: August 13, 2013
Published: August 13, 2013

dx.doi.org/10.1021/jp404812a | J. Phys. Chem. B 2013, 117, 10405−10413

concentration. In the present study, we continue investigate the mechanism of polyplex formation by comparing the DNA-complexation behavior of branched and linear PEI and PLL at two different pH values in the pH range of endocytic vesicles. The binding equilibrium was analyzed using the independent[13] and cooperative[14] binding models.

EXPERIMENTAL METHODS

Materials. The plasmid pCMVβ (7164 bp) encoding for the beta-galactosidase enzyme as a reporter gene was purified using a QIAfilter Plasmid Giga Kit (QIAGEN) according to the manufacturer's instructions. Branched polyethylenimine (BPEI; Figure 1) with a mean weight-average molecular weight of 25 kDa was purchased from Sigma-Aldrich, titrated to pH 7, and used as a 1 mg/mL aqueous solution.

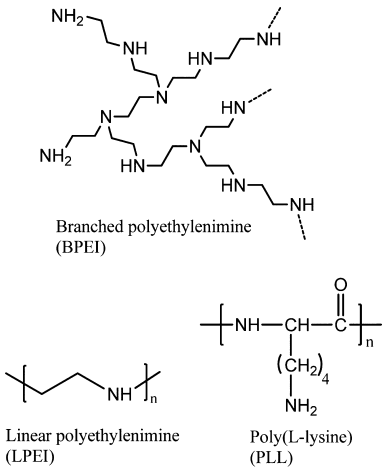

Figure 1. Molecular structures of BPEI, LPEI, and PLL.

Linear polyethylenimine (LPEI; Figure 1), ExGen 500, with a mean molecular weight of 22 kDa was obtained from Fermentas. Poly(L-lysine) (PLL; Figure 1), with a mean molecular weight of 200 kDa (Sigma-Aldrich), was chosen for this study, since at physiological levels of salt the polyplexes formed with 20 kDa PLL are less soluble due to aggregation.[11,15] For PLL, the backbone amines are part of the peptide bonds. Thus, only the side chain amines bind DNA and only they were taken into account when calculating the N/P ratios (the molar ratio of polymer nitrogen to DNA phosphate). Thus, for PLL only primary, for LPEI only secondary, and for BPEI all primary, secondary, and tertiary amines are participating to the formation of nanoparticles. Ethidium bromide (ETI) used as a fluorescent probe was purchased from Sigma-Aldrich.

Sample Preparation. All solutions were prepared in a buffer containing 50 mM MES, 50 mM HEPES, and 75 mM NaCl (adjusted to a pH of 5.2 and 7.4 using 5 M NaOH). The final nucleotide concentration of DNA used was 300 μM; the molar ETI/nucleotide ratio was 1:15. The polyplexes were prepared by a stepwise method: Independent of the final N/P ratio between the cationic polymer and DNA, an initial solution with N/P ratio 0.2 was prepared by vigorous mixing of equal volumes of ETI–DNA solution and cationic polymer solution. The complexation was followed by measuring the fluorescence spectrum of this initial solution. After the measurement, the next N/P ratio was adjusted by addition of the appropriate amount of polymer solution. The measured N/P range was from 0.2 to 8 in each polymer at pH 5.2 and at pH 7.4.

Fluorescence Measurements. The time-resolved fluorescence was measured by a time-correlated single photon counting (TCSPC) system as described earlier.[13] The decays were collected using a constant accumulation time with wavelengths of 560–670 nm with steps of 10 nm. The instrumental response function was measured separately, and the fluorescence decays were deconvoluted and analyzed by iterative least-squares method by simultaneously fitting to the sum of exponents in the equation

$$I(t, \lambda) = a_1(\lambda)\, e^{-t/\tau_1} + a_2(\lambda)\, e^{-t/\tau_2} \quad (1)$$

where τ_i is the global lifetime and $a_i(\lambda)$ is the local amplitude (pre-exponential factor) at a particular wavelength. The quality of the fit was judged in terms of the weighted mean-square deviation χ^2 for the individual curves and for the global fit (for acceptable fit $\chi^2 < 1.1$) and by visual inspection of the weighted residuals and their autocorrelation function. The amplitudes $a_i(\lambda)$ represent the decay associated spectra (DAS). In the case of a mixture of multiple noninteracting fluorescing species, the DAS corresponds to the individual spectra of the species. The local amplitudes ($a_i(\lambda)$) were corrected depending on the sensitivity of the detector at different wavelengths and the corrected spectral areas were calculated as $A_i = \int a_i(\lambda)\, d\lambda$. The relative quantum yield of ETI free in the solution versus ETI bound by the DNA, ϕ_{rel}, was determined from steady state absorption (UV–vis spectrophotometer Shimadzu UV-3600) and fluorescence (Fluorolog Yobin Yvon-SPEX λ_{exc} = 483 nm) measurements according to

$$\phi_{rel} = \frac{\phi_{ETI}}{\phi_{ED}} = \frac{I_{ETI}}{I_{ED}} \frac{A_{ED}}{A_{ETI}} \quad (2)$$

In eq 2, ϕ_{ETI} is the quantum yield of free ETI, ϕ_{ED} is the quantum yield of ETI–DNA complex, I_i is area of the fluorescence spectra with excitation wavelength of 483 nm, and A_i is the absorbance at wavelength of 483 nm. The ϕ_{rel} values of 0.130 and 0.136 were obtained at pH 5.2 and 7.4, respectively. The quantum yield corrected spectral area of the short-living component can be calculated as $A_{1,QY} = A_1/\phi_{rel}$. The proportion of the short-living decay component, B, corresponding to ETI free in the solution, was calculated from the spectral areas of the components as follows:

$$B = \frac{A_{1,QY}}{A_{1,QY} + A_2} \times 100\% \quad (3)$$

where A_2 is the spectral area of the long-living component (ETI:DNA complex).

We used ETI as a fluorescent probe for monitoring the equilibrium between DNA and the polymers (P). We chose the amount of ETI in the system so that in the beginning all ETI is intercalated in the DNA. When the polyplex is formed ETI is freed to the bulk solution:

$$\text{ETI:DNA} + \text{P} \rightleftharpoons \text{P:DNA} + \text{ETI} \quad (4)$$

Simultaneously the fluorescence lifetime of ETI decreases from 24 ns for ETI–DNA complex to 1.8 ns for free ETI. Thus, in the presence of polymer, a two-exponential decay curve is observed. As the relative amount of free ETI in the solution, B (eq 3), is directly proportional to the amount of formed polyplexes, the formation of polyplexes can be monitored by plotting B as a function of N/P ratio.

dx.doi.org/10.1021/jp404812a | J. Phys. Chem. B 2013, 117, 10405–10413

Binding Constants: Independent Binding Model. In the independent binding model reported in our previous studies,[13,16,17] binding of a ligand (polymer carrier) to a site on a macromolecule (DNA) has no impact on simultaneous or subsequent binding to other unoccupied sites and the reaction can be written as

$$\mathrm{P} + \mathrm{DNA} \rightleftharpoons \mathrm{P{:}DNA} \tag{5}$$

Thus, the proportion of DNA bound by the polymer, B, can be correlated to the binding constant of the polyplex formation, K_I, by

$$B = \frac{[\mathrm{P{:}DNA}]}{[\mathrm{DNA}] + [\mathrm{P{:}DNA}]} = \frac{K_I[\mathrm{P}][\mathrm{DNA}]}{[\mathrm{DNA}] + K_I[\mathrm{P}][\mathrm{DNA}]} = \frac{K_I[\mathrm{P}]}{1 + K_I[\mathrm{P}]} \tag{6}$$

From the fluorescence measurements, we get $B = A_{1,QY}/(A_{1,QY} + A_2)$. Combining this with eq 6 and taking reciprocal of the resulting equation, we obtain:

$$\frac{A_2}{A_{1,Qy}} = \frac{1}{K_I[\mathrm{P}]} \tag{7}$$

where K_I is the independent binding constant of the overall equilibrium and [P] is the concentration of the polymer amine groups (mol N-groups dm^{-3}). In eqs 6 and 7, [P] should be the free N-group concentration, but in our analysis it was approximated by the total N-group concentration. According to eq 7, plotting the ratio $A_2/A_{2,QY}$ as a function of the inverse polymer concentration, we should obtain a linear dependence with the binding constant equal to the inverse of the slope.

Binding Constants: Cooperative Binding Model. In cooperative binding the binding of a ligand to a site on a target molecule can influence the binding of other ligands to other unoccupied sites on the same target. For positive cooperativity the binding of first ligand makes it easier for the next one to be bound. In a plot of B as a function of free ligand concentration a characteristic sigmoidal shape is observed.[18] The Hill plot model for multivalent ligand binding to multisubunit substrate[19−22] was used to estimate the cooperativity of our systems through eq 8 (derivation presented in the Supporting Information).

$$\ln\left(\frac{A_{1,QY}}{A_2}\right) = \alpha \ln[\mathrm{P}] + \ln(K_{CO})^{\alpha} \tag{8}$$

where $(K_{CO})^{\alpha}$ is the overall cooperative binding constant for the reaction DNA + NP $\rightleftharpoons$ DNA:P_N, K_{CO} is the average cooperative binding constant for the binding of one functional amine group according to the reaction DNA:P_{x-1} + P $\rightleftharpoons$ DNA:P_x (x = 1, 2, ..., N), and α is the experimental Hill's coefficient. The values for the calculated curve of cooperative binding in Figures 6 and Supporting Information Figure S4 were obtained from

$$B = \frac{[\mathrm{P}]^{\alpha}(K_{CO})^{\alpha}}{1 + [\mathrm{P}]^{\alpha}(K_{CO})^{\alpha}} \tag{9}$$

Particle Size. Samples for the polyplex size measurements were prepared at both pHs with N/P ratios ranging from 0.4 to 8. The mean hydrodynamic diameters were measured by dynamic light scattering technique (Malvern Zetasizer Auto Plate Sampler, APS; medium refractive index of water = 1.33 and scattering angle of 90°) in triplicate from two different samples. Thus, each N/P-ratio was measured six times. The ages of the samples at different N/P-ratios differed from each other at the time of measuring. From the initial time of forming the first N/P polyplex formulation, the 0.4, 0.6, 1, 2, 4, and 8 N/P formulations were measured at 1.25, 2.5, 3.5, 4.75, 6.25, and 7.75 h, respectively.

Transfection. CHO cells (Chinese hamster ovary cell line) and CV1-P cells (monkey kidney fibroblasts) were grown in DMEM supplemented with 10% heat-inactivated fetal bovine serum, 2 mM L-glutamine, and antibiotics. ARPE-19 cells (human retinal pigment epithelial cell line) were cultured in DMEM/F-12 supplemented with 10% heat-inactivated fetal bovine serum, 2 mM L-glutamine, and antibiotics. Cells were maintained at 37 °C in a humidified atmosphere containing 7% CO_2 (CHO and ARPE-19) or 5% CO_2 (CV1-P) and subcultured twice a week. All cell culture media and reagents were purchased from Invitrogen.

Polyplexes were prepared in 50 mM MES-HEPES buffer (pH 7.2) by adding polymer solution to DNA solution (in equal volumes) at an N/P ratio of 8 (PEIs) and 4 (PLL). The complexes were allowed to incubate for 20 min at room temperature. DNA concentration in the resulting solution was 20 μg/mL of complex.

CHO (48 000 cells/well), CV1−P (32 000 cells/well), and ARPE-19 (50 00 cells/well) cells were seeded into 48-well plates 24 h prior to experiment to reach 80% confluency on the day of transfection. Immediately before transfection, cell culture medium was replaced with fresh DMEM without serum and 50 μL of polyplex solutions (corresponding to 1 μg DNA/well) was added dropwise per well. After 5 h incubation, polyplexes were aspirated, cells were washed twice with PBS and incubated in cell culture media for an additional 43 h at 37 °C in a 7% CO_2 humidified air atmosphere. Thereafter, cells were washed twice with PBS and lysed with 150 μL of lysis buffer (250 mM Tris-HCl buffer (pH 8.0), 0.1% Triton X-100) overnight at −70 °C. The β-galactosidase activity was determined by ONPG assay as described previously[7] and normalized to the protein content of each sample using a Bio-Rad protein assay kit (Bio-Rad) according to the manufacturer's microtiter plate protocol.

RESULTS

Formation of Polymer−DNA Polyplexes. Formation of polyplex can be monitored by plotting B as a function of N/P ratio. These plots are presented in Figure 2 for all polymers in both pHs. In all cases, B reaches close to 100% values at N/P = 2. This indicates that nearly all ETI is free in the solution (eq 3). The behavior of all polymers at a given pH is similar, but the pH has a clear effect. The sigmoidal shape of the curves observed at pH 5.2 is absent at pH 7.4.

The results of the particle size measurements are shown in Figure 3. At low N/P ratios, the particle sizes were 300−400 nm at pH 5.2 and 400−500 nm at pH 7.4. At N/P = 2, the particle size increases to values over 2000 nm with a simultaneous increase in the polydispersity index (PDI) of the sample reflecting a wider particle size distribution. At higher N/P ratios, the particle sizes of BPEI and PLL decrease again to values lower than 300 nm and PDI decreases to values < 0.2, indicating a fairly narrow size distribution. For LPEI, some decrease is observed at pH 5.2, but at pH 7.4 no decrease in particle size or PDI takes place up to N/P = 8. During the

dx.doi.org/10.1021/jp404812a | J. Phys. Chem. B 2013, 117, 10405−10413

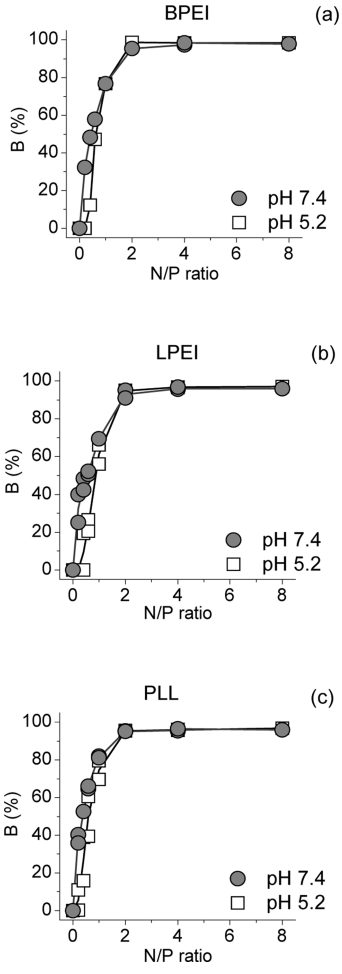

Figure 2. Proportion of the short-living component (B) versus N/P ratio at pH 5.2 and 7.4 for BPEI (a), LPEI (b), and PLL (c).

particle size measurements, the ages of the samples increased with increasing N/P ratio (see Experimental Methods). The particle sizes of LPEI and BPEI polyplexes have been observed to grow as a function of time in salt containing buffers.[23−27] Without salt in the buffer, the particle sizes are smaller and their sizes remain constant over time.[23,27] The particle sizes obtained in the present study are in agreement with these studies. The large particle sizes measured at N/P = 2 coincide with a visual change in the samples: at this N/P ratio, large particles can be seen by the naked eye. This effect was stronger at pH 7.4 than at pH 5.2. Similar effect has been observed for 50−60 kDa PEI by light scattering measurements.[28] According to the zeta potential measurements,[12,25,29] the appearance of very large particle sizes coincides with the change from negative to positive potential and takes place close to N/P ratio 2. Thus, the large particle sizes are probably due to aggregation of the nanoparticles when they are at nearly charge neutral state. The same phenomenon has been seen with cationic liposome−DNA complexes.[30] The particle sizes for all polymers are higher at pH 7.4 than at pH 5.2 which is likely due to the more positively charged environment at pH 5.2.

The differences between the polymers are also observed in the changes of the fluorescence lifetimes with increasing N/P ratio (Supporting Information Figure S1). For PLL at both pHs the changes in the fluorescence lifetimes are relatively small for both components and take place only at $N/P < 2$ (Figure S1a and b). For PEIs at $N/P < 2$, where the polyplexes still have some negative charges, the lifetime of the short-living component corresponding to free ETI varies from 0.6 to 1.9 ns (Figure S1c and e) and the lifetime of the long-living component corresponding to ETI−DNA complex decreases from 24 to 18.5 ns (Figure S1d and f). The fluorescence lifetime of ETI decreases in the presence of positive charges.[31] Thus, it is possible that at low N/P ratios, when the polyplex is still negatively charged, the ETI freed in the solution during polyplex formation does not all escape to the bulk solution, but part of it stays close to DNA. At $N/P \geq 2$, the polyplexes are

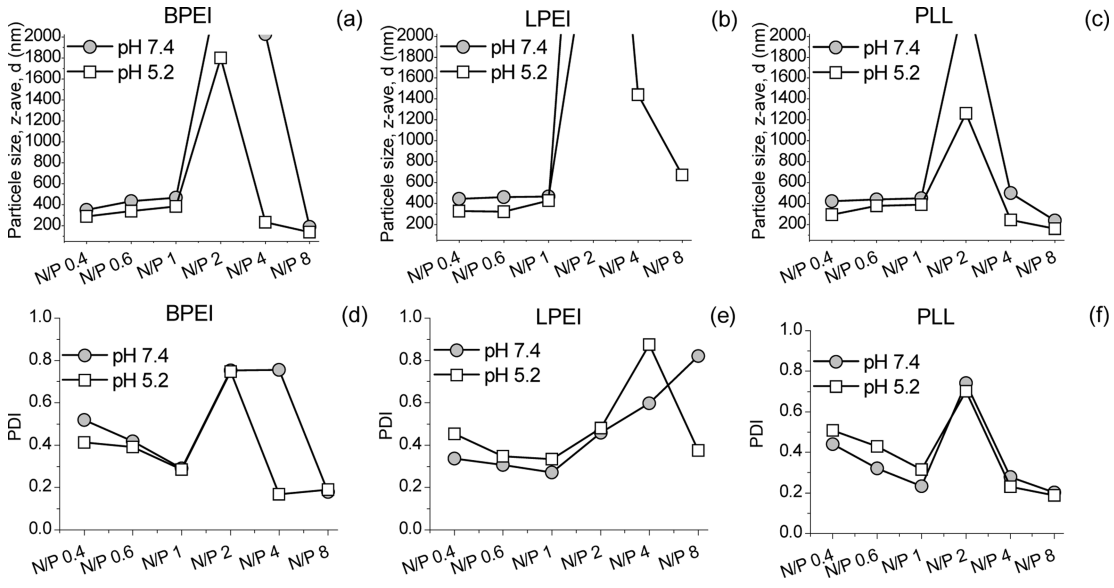

Figure 3. Mean hydrodynamic diameters and PDI values at different N/P ratios for BPEI (a, d), LPEI (b, e), and PLL (c, f) at pH 5.2 and 7.4. The upper limit of the device for the hydrodynamic diameter is 2000 nm, and thus, values higer than this are not shown in the figures. The errors in BPEI and PLL particles sizes were 1−7% for PDI < 0.6 and 21−47% for PDI > 0.6. For LPEI large errors were obtained between N/P 1 and 4 at pH 5.2 and N/P 2 and 8 at pH 7.4.

dx.doi.org/10.1021/jp404812a | J. Phys. Chem. B 2013, 117, 10405−10413

positively charged, ETI escapes to the bulk solution, and its lifetime is equal to that of free ETI in the absence of DNA. The changes in the fluorescence lifetimes observed for PEIs are smaller at pH 5.2 than at pH 7.4. Since the environment at pH 5.2 is positively charged, the addition of cationic polymers does not change the lifetimes as much as at pH 7.4.

According to the present studies, the largest particle sizes, coinciding with the change from negatively charged polyplexes to positively charged polyplexes, are observed at N/P = 2 (Figure 3). According to the fluorescence measurements, at this point all ETI has been freed into the solution (Figure 2) and reaction 4 has gone to completion. At higher N/P ratios, excess polymer is bound to the polyplex, causing the size of the polyplex to decrease again.[12,25,27,32−36]

Independent Binding Model. In Figure 4, the ratio $A_2/A_{1,QY}$ (eq 7) is plotted as a function of the inverse amine

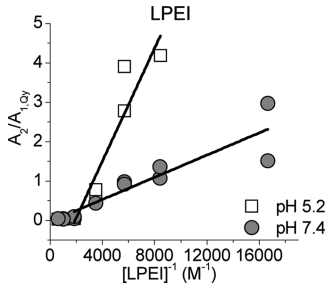

Figure 4. Ratio $A_2/A_{1,QY}$ as a function of the inverse polymer concentration for LPEI at pHs 5.2 and 7.4.

concentration for LPEI. At low polymer concentrations corresponding to N/P ratios from 0.2 to 2, $A_2/A_{1,QY}$ decreases linearly with increasing concentration. At higher concentrations, that is, N/P ≥ 2, $A_2/A_{1,QY}$ stays nearly constant with increasing concentration. This behavior corresponds to that observed in Figure 2: at low concentrations, the polyplex formation is observed, and at higher N/Ps the reaction (eq 4) has reached completion. At pH 5.2, the slope at low N/P ratios is clearly greater than at pH 7.4. Similar behavior is observed also for the BPEI and PLL (Supporting Information Figure S2). The binding constants K_I calculated from the slopes at N/P ≤ 2 are listed in Table 1. For all polymers, the binding constants using the independent binding model are smaller at pH 5.2 than at pH 7.4. For PEIs, the binding constants are nearly equal at each pH, but 1.3−2.0 times larger binding constants are observed for PLL.

Cooperative Binding Model. For the present systems, the Hill plot (eq 8) did not appear as single straight line but a composite of two (at pH 5.2) or three (at pH 7.4) lines with different slopes (Figure 5 and Supporting Information Figure S3). For pH 7.4 at low polymer concentrations (N/P ≤ 0.6), the α-values were 0.76−1.01, that is, close to 1 (Table 1). This implies that interaction between the polymers and DNA represents independent binding without cooperativity or, in the case of LPEI, slightly negative cooperativity. For pH 5.2, this was not the case and positive cooperativity was observed (α = 2.63−3.78). At very high polymer concentrations (N/P ≥ 2), the bound fraction reaches a maximum and additional binding does not take place.

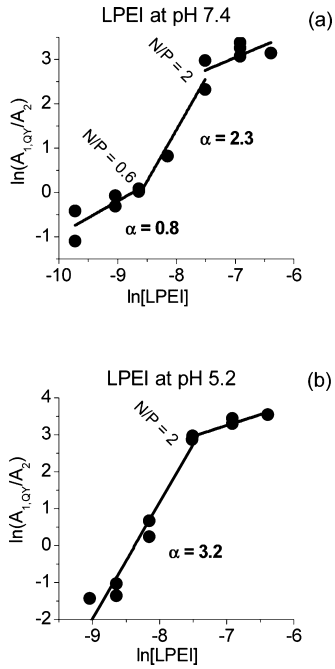

Figure 5. Hill plots (eq 8) for LPEI at pH 7.4 (a) and at pH 5.2 (b).

The α-values obtained at intermediate N/Ps for pH 7.4 and at N/P ≤ 2 for pH 5.2 (Table 1) indicate positive cooperativity of binding. The degree of cooperativity is higher at pH 5.2 for all polymers. Also, the overall cooperative binding constant

Table 1. Independent Binding Constants per amine (K_I), Hill's cooperativity coefficients (α), overall cooperative binding constant $(K_{CO})^{\alpha}$ and average cooperative binding constants per amine K_{CO} for PEIs and PLL at pH 5.2 and 7.4

		independent model	cooperative model			
polymer	pH	K_I (M^{-1})	N/P range	α	$(K_{CO})^{\alpha}$	K_{CO} (M^{-1})
BPEI	5.2	$(9.5 \pm 3.2) \times 10^2$	0.4−2.0	3.78	$(1.0 \pm 0.1) \times 10^{14}$	$(5.1 \pm 0.1) \times 10^3$
	7.4	$(7.3 \pm 0.4) \times 10^3$	0.6−2.0	2.31	$(5.4 \pm 0.6) \times 10^8$	$(6.1 \pm 0.2) \times 10^3$
			0.2−0.6	0.97	$(5.7 \pm 0.2) \times 10^3$	$(7.7 \pm 0.2) \times 10^3$
LPEI	5.2	$(1.4 \pm 0.2) \times 10^3$	0.4−2.0	3.16	$(3.0 \pm 0.3) \times 10^{11}$	$(4.3 \pm 0.2) \times 10^3$
	7.4	$(7.1 \pm 1.2) \times 10^3$	0.6−2.0	2.32	$(4.8 \pm 0.5) \times 10^8$	$(5.5 \pm 0.2) \times 10^3$
			0.2−0.6	0.76	$(7.5 \pm 2.4) \times 10^2$	$(6.3 \pm 1.4) \times 10^3$
PLL	5.2	$(1.9 \pm 0.7) \times 10^3$	0.4−2.0	2.63	$(6.8 \pm 0.7) \times 10^9$	$(5.5 \pm 0.2) \times 10^3$
	7.4	$(9.4 \pm 0.5) \times 10^3$	0.6−2.0	2.06	$(9.7 \pm 0.4) \times 10^7$	$(7.4 \pm 1.5) \times 10^3$
			0.2−0.6	1.01	$(1.1 \pm 0.1) \times 10^4$	$(1.01 \pm 0.09) \times 10^4$

dx.doi.org/10.1021/jp404812a | J. Phys. Chem. B 2013, 117, 10405−10413

$(K_{CO})^{\alpha}$ increases with decreasing pH (Table 1). For PEIs, the amount of protonated amine groups increases as the pH decreases, and thus, both the degree of cooperativity and the overall binding constant correlate with the amount of active amine groups present in the system. For PLL, all the active amine groups are protonated at the pH range studied and the effect of pH is smaller than that for PEIs. However, both α and $(K_{CO})^{\alpha}$ increase with decreasing pH also for PLL. This could be due to increased activity of the amine groups at lower pH.

The independent and cooperative binding models are compared in Figure 6 where the curves calculated from the parameters listed in Table 1 and the corresponding eqs 6 and 9 are shown together with the measured points for LPEI at both pHs. At pH 5.2, the cooperative model fits better to the measured points. At pH 7.4, the measured points follow the independent model up to N/P ≈ 0.6. Thus, at these N/P ratios, the B values are higher than those for pH 5.2. This gives an impression that the formation of the nanoparticles at low N/Ps would be more efficient at pH 7.4, although the real reason for the higher B values is the difference in the mechanism of polyplex formation. At higher N/Ps, the cooperative model gives more accurate results also for pH 7.4. Thus, it seems that pH has a clear influence on the mechanism of polyplex formation. The same behavior is observed also for BPEI and PLL (Supporting Information Figure S4).

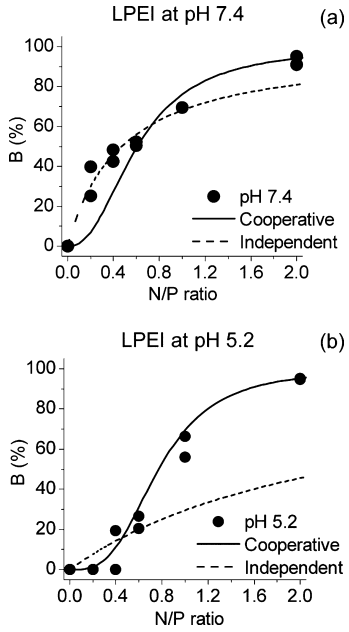

Figure 6. Proportion of DNA bound by the polymer, B, as a function of polymer amine group concentration for LPEI at pH 7.4 (a) and at pH 5.2 (b). (●) Measured points, calculated by (solid line) independent binding model and (dashed line) cooperative binding model.

With the independent binding model at pH 5.2, very small K_I values are obtained. Since at this pH the system follows cooperative binding model, these values are not relevant. For pH 7.4, the values from independent model are nearly equal to those obtained with the cooperative model at low N/Ps were the cooperativity degree indicates independent binding.

The transfection experiments are done at high N/Ps (N/P = 8 for PEIs and N/P = 4 for PLL). At intermediate N/P ratios (0.6–2.0), PEIs have both high overall cooperative binding constants (Supporting Information Figure S5) and transfection efficiencies compared with those of PLL. According to our data, 22 kDa LPEI is not quite as effective as 25 kDa BPEI to form nanoparticles with DNA, but the transfection experiments have proved that at these conditions and with these cell lines the most effective carrier is 22 kDa LPEI (Figure S5b). The binding constants reflect only the formation of the polyplexes according to reaction 4, which has gone to completion at N/P = 2. At higher N/Ps, extra polymer is bound to the nearly neutral core polyplexes. LPEI and BPEI are both functioning DNA carriers, but only LPEI still forms large agglomerates at N/P = 8 in salt containing buffers which seem to be important for in vitro and in vivo transfection.[23,37]

DISCUSSION

Very few binding constants for PEI and PLL polyplex formation have been reported in the literature.[25,28,29,38−40] The reported values have been mainly obtained by isothermal titration calorimeter (ITC) measurements. However, the heat exchange during ligand binding is often small and it cannot be separated

Table 2. Independent Binding Constants Per Molecule K_I' from the Present Study and Literature for BPEI and PLL

polymer	binding constant (M^{-1})	solution	pH	method	ref
BPEI 25 kDa	4.3×10^6	50 mM Mes, 50 mM Hepes, 75 mM NaCl	7.4	TCSPC with ETI, independent method	present study
	5.5×10^5		5.2		
BPEI 50−60 kDa	1.2×10^5	Tris-HCl buffer, ionic strength 0.03	7	luminescence (with ETI)	28
BPEI 750 kDa	$(2.3 \pm 1.8) \times 10^6$	5% glucose	[a]	ITC (25 °C)	25
BPEI 600 Da	2×10^5	0.1 mM NaCl	6	ITC, SSIS model	38
BPEI 600 Da	1.8×10^4	0.1 mM NaCl	7	ITC, SSIS model	
BPEI 600 Da	1.0×10^4	0.1 mM NaCl	8	ITC, SSIS model	
BPEI 600 Da	1×10^6	Mes or Hepes	7	ITC	
	1×10^5	H_2O	7	ITC	
BPEI 25 kDa	$(5.98 \pm 1.79) \times 10^6$	20 mM phosphate buffer	7.4	ITC (25 °C)	39
PLL 200 kDa	1.5×10^7	50 mM Mes, 50 mM Hepes, 75 mM NaCl	7.4	TCSPC with ETI, independent method	present study
	3.0×10^6		5.2		
PLL[b]	9.08×10^7	[c]	4.8	ITC	40
PLL[b]	1.97×10^5	[d]	6.8		

[a]Not specified. [b]Size of PLL not reported. [c]10 mM sodium cacodylate-acetic acid, 200 mM sodium chloride, and 20 mM magnesium chloride. [d]10 mM sodium cacodylate-cacodylic acid, 200 mM sodium chloride, and 20 mM magnesium chloride.

from the heat associated with conformational changes during polyplex formation. For instance, Choosakoonkriang et al.[29] did not report binding constants for PEIs (2−750 kDa BPEIs and 25 kDa LPEI at pH range 6.0 − 9.0). Ikonen et al.[25] did not report a binding constant for 750 kDa PLL, although they did obtain a value for 750 kDa BPEI. The values reported in the literature correspond to the K_I values obtained in the present study, but they were reported per polymer molecule. The K_I values per N-group listed in Table 1 can be converted to the binding constant per molecule, K_I', by multiplying with the average number of amine groups per polymer molecule. In Table 2, the binding constants obtained for BPEI and PLL in the present study are compared with the values reported in the literature. Taking into account the differences in molecular weights of the polymers and properties of the solutions, the values are in agreement.

Effect of pH. pH has a clear effect on the mechanism of polyplex formation for all polymers. At pH 7.4, the independent binding mechanism changes to a cooperative mechanism at N/P ratios close to 0.6, whereas for pH 5.2 the mechanism is cooperative for all N/P ratios. This change is also reflected in the degree of cooperativity and the overall cooperative binding constants which both are higher at pH 5.2 than at pH 7.4. Thus, once one amine is bound to the DNA, it induces the subsequent binding of other amine groups more efficiently at pH 5.2 than at pH 7.4. The pK_a values for PLL vary between 9 and 11.[41−44] Thus, at pH ≪ 9, all the primary amine groups taking part in the binding of DNA are positively charged and changing the pH from 7.4 to 5.2 has only relatively small effect on the α and$(K_{CO})^{\alpha}$ values. For LPEI, the pK_a = 7.4−8.5.[29,45] Thus, at pH 7.4, about 50% of the LPEI amine groups are protonated and decreasing the pH to 5.2 increases the degree of protonation. This is observed as a clear increase in $(K_{CO})^{\alpha}$ values with decreasing pH. The average pK_a for BPEI is equal to that of LPEI, that is, 7.4−8.5.[29,45,46] However, BPEI contains primary (100% protonated at pH ≪ 9), secondary (50% protonated at pH 7.4), and tertiary amine groups (pK_a = 6−7, less than 50% protonated at pH 7.4).[33,47] Thus, the effect of pH on $(K_{CO})^{\alpha}$ values is even larger than that for LPEI. The opposite is observed for the average cooperative binding constant per amine, K_{CO}: the values are higher at pH 7.4 than at pH 5.2. This is due to the lower cooperativity at pH 7.4 which in turn is due to the smaller amount of other positive species at pH 7.4 compared with pH 5.2. Thus, the competition from the negative phosphate groups is lower at pH 7.4 compared with pH 5.2.

Effect of Polymer. The α-values obtained for both PEIs are nearly equal at both pHs and clearly higher than those obtained for PLL. Also the $(K_{CO})^{\alpha}$ values were higher for PEIs than for PLL at both pHs. This is likely due to the different molecular structures of the polymers: for PEIs, there are only two carbon atoms between the amines, whereas in PLL there are 12. Since the active amine groups of PLL are at the ends of the flexible side chains, the difference in the average distance between the amine groups is actually not very large. However, the large hydrocarbon skeleton of PLL can cause steric hindrance and thus reduce the degree of cooperativity. At pH 7.4 the differences in α and $(K_{CO})^{\alpha}$ values are much smaller, since the higher degree of amine group protonation of PLL can partly compensate the structural differences. On the other hand, the K_{CO} values are always somewhat (1.1−1.6 times) higher for PLL than for PEIs (Table 1). Thus, the primary amine groups of PLL seem to bind DNA more strongly than the secondary amine groups of LPEI and the combined affinity between the primary, secondary, and tertiary amine groups of BPEI. This is in line with the observations indicating that the PEI−DNA complexes are more easily disrupted than PLL−DNA complexes in the presence of competing polyanions.[7,8]

Comparing the $(K_{CO})^{\alpha}$ values and transfection efficiencies (Supporting Information Figure S5), there is a similarity in the behavior of PLL. However, despite the lower overall binding constant, PLL forms nanoparticles with DNA and these nanoparticles do enter the cells.[7,9] The low transfection efficiency of PLL is a sum of many factors. One factor is the high pK_a values for PLL causing all its amine groups to be totally protonated at the pH of the transfection studies. Thus, PLL has little buffering capacity and has a minor effect on the pH of its environment. The amine groups of PEIs are not fully protonated at pH 7.4 and can buffer the pH of their environment to some extent, causing the proton sponge effect.[33,45,47−50] Also the average binding constant per amine group is higher for PLL than PEIs. This can make the release of DNA from the PLL-polyplexes more difficult than from PEI-polyplexes. It has been shown that the extracellular and cellular glycosoaminoglycans (GAGs) do not affect the release of DNA from PLL-carrier but they do affect the release of DNA from the BPEI-carrier.[7,9] The $(K_{CO})^{\alpha}$ values of 25 kDa BPEI are somewhat larger (1.1−333 times) than those of 22 kDa LPEI. However, the transfection efficiency of 22 kDa LPEI is higher than that of 25 kDa BPEI. The $(K_{CO})^{\alpha}$ values describe only the formation of the nanoparticle core, that is, until all the phosphate groups of the DNA are bound at about N/P = 2. After this, excess polymer binds to the nanoparticle core forming a protective shell around it.[33] This excess polymer has been shown to be a crucial factor in getting DNA to its destination, into the nucleus of the cell.[13,36,51]

■ CONCLUSIONS

Our studies explore the complexation of DNA with polyethylenimine and poly(L-lysine) by a spectroscopic method. Applying the cooperative binding model for multivalent ligand binding to multisubunit substrate showed that at pH 7.4 the mechanism of polyplex formation changes from independent binding to cooperative binding at N/P close to 0.6, whereas at pH 5.2 the polyplex formation is cooperative at all N/P values. The overall cooperative binding constants were higher at pH 5.2 than at 7.4, reflecting the higher degree of amine group protonation at lower pH. Thus, especially for polymer containing secondary and tertiary amine groups, it can be beneficial to prepare the nanoparticles at lower pH although the transfection is performed at biological pH. Both the amine density and overall cooperative binding constants are higher for PEIs than for PLL. However, the average binding constants per amine group were higher for PLL which contains only primary amine groups. For the present polymers, formation of the polyplex core is complete at approximately N/P = 2, at which point nearly all DNA phosphate groups are bound by polymer amine groups and all ETI has been freed to the solution. Thus, with the present fluorescence measurements, we cannot observe what happens to the polyplex at higher N/Ps using this TCSPC spectroscopic method. More studies involving fluorescently labeled polymers are needed to unravel this.

■ ASSOCIATED CONTENT

Supporting Information

Theory of Hill plot model for multivalent ligand binding to multisubunit substrate and the following figures: Figure S1, fluorescence lifetimes of PLL, LPEI, BPEI, free ETI, and ETI:DNA complex at both pH-values; Figure S2, for PLL and BPEI ratio $A_2/A_{1,QY}$ as a function of the inverse polymer concentration; Figure S3, Hill Plots of BPEI and PLL at both pH-values; Figure S4, independent vs cooperative models for BPEI, PLL, and LPEI at both pH-values; Figure S5, overall cooperative binding constants at pH 7.4 and transfection efficiencies in different cell lines at pH 7.4 for BPEI, LPEI, and PLL. This material is available free of charge via the Internet at http://pubs.acs.org.

■ AUTHOR INFORMATION

Corresponding Author

*E-mail: elina.vuorimaa@tut.fi.

Author Contributions

The manuscript was written through contributions of all authors. All authors have given approval to the final version of the manuscript.

Notes

The authors declare no competing financial interest.

■ ACKNOWLEDGMENTS

A Natural Science Foundation Graduate Research Fellowship and Nordic Research Opportunity Grant DGE-0707427 to C.J.B. are acknowledged. This work was supported in part by the National Institutes of Health (R21CA152473), Tekes PrinCell II 40050/09 Finland, and the Academy of Finland. The authors thank the Microscopy and Imaging Core Module of the Wilmer Core Grant (EY001765).

■ REFERENCES

(1) Mintzer, M. A.; Simanek, E. E. Nonviral Vectors for Gene Delivery. *Chem. Rev.* **2009**, *109*, 259−302.

(2) Boussif, O.; Lezoualc'h, F.; Zanta, M. A.; Mergny, M. D.; Scherman, D.; Demeneix, B.; Behr, J.-P. A Versatile Vector for Gene and Oligonucleotide Transfer into Cells in Culture and in Vivo: Polyethylenimine. *Proc. Natl. Acad. Sci. U.S.A.* **1995**, *92*, 7297−7301.

(3) Lungwitz, U.; Breunig, M.; Blunk, T.; Göpferich, A. Polyethylenimine-Based Non-Viral Gene Delivery Systems. *Eur. J. Pharm. Biopharm.* **2005**, *60*, 247−266.

(4) Neu, M.; Fischer, D.; Kissel, T. Recent Advances in Rational Gene Transfer Vector Design Based on Poly(ethyleneimine) and Its Derivatives. *J. Gene Med.* **2005**, *7*, 992−1009.

(5) Parhamifar, L.; Larsen, A. K.; Hunter, A. C.; Andresen, T. L.; Moghimi, S. M. Polycation Cytotoxicity: a Delicate Matter for Nucleic Acid Therapy − Focus on Polyethylenimine. *Soft Matter.* **2010**, *6*, 4001−4009.

(6) Dunlap, D. D.; Maggi, A.; Soria, M. R.; Monaco, L. Nanoscopic Structure of DNA Condensed for Gene Delivery. *Nucleic Acids Res.* **1997**, *25*, 3095−3101.

(7) Ruponen, M.; Ylä-Herttuala, S.; Urtti, A. Interactions of Polymeric and Liposomal Gene Delivery Systems with Extracellular Glycosaminoglycans: Physicochemical and Transfection Studies. *Biochim. Biophys. Acta, Biomembr.* **1999**, *1415*, 331−341.

(8) Ruponen, M.; Rönkkö, S.; Honkakoski, P.; Pelkonen, J.; Tammi, M.; Urtti, A. Extracellular Glycosaminoglycans Modify Cellular Trafficking of Lipoplexes and Polyplexes. *J. Biol. Chem.* **2001**, *36*, 33875−33880.

(9) Männistö, M.; Reinisalo, M.; Ruponen, M.; Honkakoski, P.; Tammi, M.; Urtti, A. Polyplex-Mediated Gene Transfer and Cell Cycle: Effect of Carrier on Cellular Uptake and Intracellular Kinetics, and Significance of Glycosaminoglycans. *J. Gene Med.* **2007**, *9*, 479−487.

(10) Matsumoto, Y.; Itaka, K.; Yamasoba, T.; Kataoka, K. Intranuclear Fluorescence Resonance Energy Transfer Analysis of Plasmid DNA Decondensation from Nonviral Gene Carriers. *J. Gene Med.* **2009**, *11*, 615−623.

(11) Morille, M.; Passirani, C.; Vonarbourg, A.; Clavreul, A.; Benoit, J.-P. Progress in Developing Cationic Vectors for Non-Viral Systemic Gene Therapy Against Cancer. *Biomaterials* **2008**, *29*, 3477−3496.

(12) Tang, M. X.; Szoka, F. C. The Influence of Polymer Structure on the Interactions of Cationic Polymers with DNA and Morphology of the Resulting Complexes. *Gene Ther.* **1997**, *4*, 823−832.

(13) Ketola, T.-M.; Hanzlikova, M.; Urtti, A.; Lemmetyinen, H.; Yliperttula, M.; Vuorimaa, E. Role of Polyplex Intermediate Species on Gene Transfer Efficiency: Polyethylenimine−DNA Complexes and Time-Resolved Fluorescence Spectroscopy. *J. Phys. Chem. B* **2011**, *115*, 1895−1902.

(14) Bishop, C.; Ketola, T.-M.; Tzeng, S. Y.; Sunshine, J. C.; Urtti, A.; Lemmetyinen, H.; Vuorimaa-Laukkanen, E.; Yliperttula, M.; Green, J. J. The Effect and Role of Carbon Atoms in Poly(β-amino ester)s for DNA Binding and Gene Delivery. *J. Am. Chem. Soc.* **2013**, *135*, 6951−6957..

(15) Ward, C. M.; Ward, M. L.; Seymour, L. W. Systemic Circulation of Poly(L-lysine)/DNA Vectors is Influenced by Polycation Molecular Weight and Type of DNA: Differential Circulation in Mice and Rats and the Implications for Human Gene Therapy. *Blood* **2001**, *97*, 2221−2229.

(16) Vuorimaa, E.; Urtti, A.; Seppänen, R.; Lemmetyinen, H.; Yliperttula, M. Time-Resolved Fluorescence Spectroscopy Reveals Functional Differences of Cationic Polymer-DNA Complexes. *J. Am. Chem. Soc.* **2008**, *130*, 11695−11700.

(17) Vuorimaa, E.; Ketola, T.-M.; Green, J. J.; Hanzlíková, M.; Lemmetyinen, H.; Langer, R.; Anderson, D. G.; Urtti, A.; Yliperttula, M. Poly(β-amino ester)-DNA Complexes: Time-Resolved Fluorescence and Cellular Transfection Studies. *J. Controlled Release* **2011**, *154*, 171−176.

(18) Connors, K. A. *Binding Constants: The Measurements of Molecular Complex Stability*; John Wiley & Sons: New York, 1987.

(19) Gelamo, E. L.; Tabak, M. Spectroscopic Studies on the Interaction of Bovine (BSA) and Human (HSA) Serum Albumins with Ionic Surfactants. *Spectrochim. Acta, Part A* **2000**, *56*, 2255−2271.

(20) Gelamo, E. L.; Silva, C. H. T. P.; Imasato, H.; Tabak, M. Ineraction of Bovine (BSA) and Human (HSA) Serum Albumins with Ionic Surfactants: Spectroscopy and Modeling. *Biochim. Biophys. Acta* **2002**, *1594*, 84−99.

(21) Nanduri, V.; Sorokulova, I. B.; Samoylov, A. M.; Simonian, A. L.; Petrenko, V. A.; Vodyanoy, V. Phage as a Molecular Recognition Element in Biosensors Immobilized by Physical Adsorption. *Biosens. Bioelectron.* **2007**, *22*, 986−992.

(22) Michel, D. Cooperative Equilibrium Curves Generated by Ordered Ligand Binding to Multi-Site Molecules. *Biophys. Chem.* **2007**, *129*, 284−288.

(23) Wightman, L.; Kircheis, R.; Rössler, V.; Carotta, S.; Ruzicka, R.; Kursa, M.; Wagner, E. Different Behavior of Branched and Linear Polyethylenimine for Gene Delivery in Vitro and in Vivo. *J. Gene Med.* **2001**, *3*, 362−372.

(24) Sharma, V. K.; Thomas, M.; Klibanov, A. M. Mechanistic Studies on Aggregation of Polyethylenimine-DNA Complexes and Its Prevention. *Biotechnol. Bioeng.* **2005**, *90*, 614−620.

(25) Ikonen, M.; Murtomäki, L.; Kontturi, K. Controlled Complexation of Plasmid DNA with Cationic Polymers: Effect of Surfactant on the Complexation and Stability of the Complexes. *Colloids Surf., B* **2008**, *66*, 77−83.

(26) Pelisek, J.; Gaedtke, L.; DeRouchey, J.; Walker, G. F.; Nikol, S.; Wagner, E. Optimized Lipopolyplex Formulations for Gene Transfer to Human Colon Carcinoma Cells under in Vitro Conditions. *J. Gene Med.* **2006**, *8*, 186−197.

(27) Ogris, M.; Steinlein, P.; Kursa, M.; Mechtler, K.; Kircheis, R.; Wagner, E. The Size of DNA/Transferrin-PEI Complexes is an

Important Factor for Gene Expression in Cultured Cells. *Gene Ther.* **1998**, *5*, 1425−1433.
(28) Zhou, Y.-L; Li, Y.-Z. The Interaction of Poly(ethylenimine) with Nucleic Acids and Its Use in Determination of Nucleic Acids Based on Light Scattering. *Spectrochim. Acta, Part A* **2004**, *60*, 377−384.
(29) Choosakoonkriang, S.; Lobo, B. A.; Koe, G. S.; Koe, J. G.; Middaugh, C. R. Biophysical Characterization of PEI/DNA Complexes. *J. Pharm. Sci.* **2003**, *92*, 1710−1722.
(30) Jääskeläinen, I.; Mönkkönen, J.; Urtti, A. Oligonucleotide-Cationic Liposome Interactions. A Physicochemical Study. *Biochim. Biophys. Acta* **1994**, *1195*, 115−123.
(31) Byrne, C. D.; de Mello, A. J. Photophysics of Ethidium Bromide Complexed to ct-DNA: a Maximum Entropy Study. *Biophys. Chem.* **1998**, *70*, 173−184.
(32) Duan, X.; Xiao, J.; Yin, Q.; Zhang, Z.; Mao, S.; Li, Y. Amphiphilic Graft Copolymer Based on Poly(styrene-co-maleic anhydride) with Low Molecular Weight Polyethylenimine for Efficient Gene Delivery. *Int. J. Nanomed.* **2012**, *7*, 4961−4972.
(33) Wang, Y.; Chen, P.; Shen, J. The Development and Characterization of a Glutathione-Sensitive Cross-Linked Polyethylenimine Gene Vector. *Biomaterials* **2006**, *27*, 5292−5298.
(34) Yu, J.-H.; Quan, J.-S.; Huang, J.; Nah, J.-W.; Cho, C.-S. Degradable Poly(amino ester) Based on Poly(ethylene glycol) Dimethacrylate and Polyethylenimine as a Gene Carrier: Molecular Weight of PEI Affects Transfection Efficiency. *J. Mater. Sci.: Mater. Med.* **2009**, *20*, 2501−2510.
(35) Rungsardthong, U.; Ehtezazi, T.; Bailey, L.; Armes, S. P.; Garnett, M. C.; Stolnik, S. Effect of Polymer Ionization on the Interaction with DNA in Nonviral Gene Delivery Systems. *Biomacromolecules* **2003**, *4*, 683−690.
(36) Dai, Z.; Gjetting, T.; Mattebjerg, M. A.; Wu, C.; Andresen, T. L. Elucidating the Interplay Between DNA-Condensing and Free Polycations in Gene Transfection Through a Mechanistic Study of Linear and Branched PEI. *Biomaterials* **2011**, *32*, 8626−8634.
(37) Blessing, T.; Kursa, M.; Holzhauser, R.; Kircheis, R.; Wagner, E. Different Strategies for Formation of PEGylated EGF-Conjugated PEI/DNA Complexes for Targeted Gene Delivery. *Bioconjugate Chem.* **2001**, *12*, 529−537.
(38) Utsuno, K.; Uludag, H. Thermodynamics of Polyethylenimine-DNA Binding and DNA Condensation. *Biophys. J.* **2010**, *99*, 201−207.
(39) Reul, R.; Nguyen, J.; Biela, A.; Marxer, E.; Bakowsky, U.; Klebe, G.; Kissel, T. Biophysical and Biological Investigation of DNA Nano-Complexes with a Non-Toxic, Biodegradable Amine-Modified Hyperbranched Polyester. *Int. J. Pharm.* **2012**, *436*, 97−105.
(40) Torigoe, H.; Akaike, T.; Maruyama, A. Promotion Mechanism of Triplex DNA Formation by Comb-Type Polycations: Thermodynamic Analyses of Sequence Specificity and Ionic Strength Dependence. *Nucleic Acids Symp. Ser.* **1999**, *42*, 137−138.
(41) Harada, A.; Kawamura, M.; Matsuo, T.; Takahashi, T.; Kono, K. Synthesis and Characterization of a Head-Tail Type Polycation Block Copolymer as a Nonviral Gene Vector. *Bioconjugate Chem.* **2006**, *17*, 3−5.
(42) Fukushima, S.; Miyata, K.; Nishiyama, N.; Kanayama, N.; Yamasaki, Y.; Kataoka, K. PEGylated Polyplex Micelles from Triblock Catiomers with Spatially Ordered Layering of Condensed pDNA and Buffering Units for Enhanced Intracellular Gene Delivery. *J. Am. Chem. Soc.* **2005**, *127*, 2810−2811.
(43) Stobiecka, M.; Hepel, M. Double-Shell Gold Nanoparticle-Based DNA-Carriers with Poly-L-lysine Binding Surface. *Biomaterials* **2011**, *32*, 3312−3321.
(44) Guo, Y.; Xia, F.; Xu, L.; Li, J.; Yang, W.; Jiang, L. Switchable Wettability on Cooperative Dual-Responsive Poly-L-lysine Surface. *Langmuir* **2010**, *26*, 1024−1028.
(45) Ziebarth, J. D.; Wang, Y. Understanding the Protonation Behavior of Linear Polyethylenimine in Solutions Through Monte Carlo Simulations. *Biomacromolecules* **2010**, *11*, 29−38.
(46) Clamme, J. P.; Azoulay, J.; Mély, Y. Monitoring of the Formation and Dissociation of Polyethylenimine/DNA Complexes by Two Photon Fluorescence Correlation Spectroscopy. *Biophys. J.* **2003**, *84*, 1960−1968.
(47) Kwan, K.; Lee, J. W.; Choi, J.-Y.; Shin, K. S. pH Effect on Surface Potential of Polyelectrolytes-Capped Gold Nanoparticles Probed by Surface-Enhanced Raman Scattering. *Langmuir* **2010**, *26*, 19163−19169.
(48) Kichler, A.; Leborgne, C.; Coeytaux, E.; Danos, O. Polyethylenimine-Mediated Gene Delivery: A Mechanistic Study. *J. Gene Med.* **2001**, *3*, 135−144.
(49) Midoux, P.; Pichon, C.; Yaouanc, J.-J.; Jaffrès, P.-A. Chemical Vectors for Gene Delivery: A Current Review on Polymers, Peptides and Lipids Containing Histidine or Imidazole as Nucleic Acids Carriers. *Br. J. Pharmacol.* **2009**, *157*, 166−178.
(50) Godbey, W. T.; Wu, K. K.; Mikos, A. G. Size Matters: Molecular Weight Affects the Efficiency of Poly(ethylenimine) as a Gene Delivery Vehicle. *J. Biomed. Mater. Res.* **1999**, *45*, 268−275.
(51) Hanzlíková, M.; Ruponen, M.; Galli, E.; Raasmaja, A.; Aseyev, V.; Tenhu, H.; Urtti, A.; Yliperttula, M. Mechanisms of Polyethylenimine-Mediated DNA Delivery: Free Carrier Helps to Overcome the Barrier of Cell-Surface Glycosaminoglycans. *J. Gene Med.* **2011**, *13*, 402−409.

Independent vs. cooperative binding in polyethylenimine-DNA and poly(L-lysine)-DNA polyplexes

*Tiia-Maaria Ketola [†], Martina Hanzlíková [‡], Linda Leppänen [‡], Manuela Raviña [ξ], Corey J. Bishop [§], Jordan J. Green [§], Arto Urtti [ξ], Helge Lemmetyinen [†], Marjo Yliperttula [‡] and Elina Vuorimaa-Laukkanen *,[†]*

[†] Department of Chemistry and Bioengineering, Tampere University of Technology, Korkeakoulunkatu 10, 33720 Tampere, Finland;

[‡] Division of Biopharmaceutics and Pharmacokinetics, [ξ] Centre for Drug Research, Faculty of Pharmacy, University of Helsinki, Viikinkaari 5, 00790 Helsinki, Finland;

[§] Department of Biomedical Engineering, the Wilmer Eye Institute, the Institute for Nanobiotechnology, and the Translational Tissue Engineering Center. Johns Hopkins University School of Medicine 400 North Broadway, Baltimore,MD 21231, United States.

Supporting Information

Hill plot model for multivalent ligand binding to multi-subunit substrate. Binding of a multivalent ligand such as cationic polymer to a multisubunit substrate such as DNA can be described by following binding equilibria:

	Binding constant
$DNA + P \rightleftharpoons DNA{:}P$	K_1
$DNA{:}P + P \rightleftharpoons DNA{:}P_2$	K_2
⋮	
$DNA{:}P_{N-1} + P \rightleftharpoons DNA{:}P_N$	K_N

where P is one binding group of the ligand i.e. an active amine group of the polymer. The binding constant for the overall reaction $DNA + NP \rightleftharpoons DNA{:}P_N$ is

$$K_{tot} = K_1 \times K_2 \times \ldots \times K_N = \frac{[\mathrm{DNA{:}\,P_N}]}{[DNA][P]^N}$$

The binding constants $K_1, K_2, \ldots, K_N$ will be unequal since the binding of an amine group to the DNA influences the binding off subsequent amine groups on the same DNA molecule, i.e. the binding is cooperative. If all phosphate groups of DNA are either unoccupied or all are occupied and no other situation is possible, the system is fully cooperative and *N* corresponds to the number of phosphate groups on the DNA. In practice the degree of cooperativity is less extreme and *N* is replaced with Hill coefficient *α:*

$$K_{tot} = \frac{[\mathrm{DNA{:}\,P_N}]}{[DNA][P]^{\alpha}}$$

The proportion of DNA bound by the polymer, B, is

$$B = \frac{[\mathrm{DNA{:}\,P_N}]}{[DNA] + [\mathrm{DNA{:}\,P_N}]}$$

and the proportion of free DNA is

$$1 - B = \frac{[DNA]}{[DNA] + [\mathrm{DNA{:}\,P_N}]}$$

Taking a ratio of these leads to

$$\frac{B}{1-B} = \frac{[\mathrm{DNA{:}\,P_N}]}{[DNA]}$$

Combining this with the equation for K_{tot} :

$$\frac{B}{1-B} = K_{tot}[P]^{\alpha} = (K_{CO})^{\alpha}[P]^{\alpha}$$

where K_{CO} is the average of the individual binding constants $K_1, K_2, \ldots, K_N$. Taking the logarithm of both sides we obtain the Hill equation for multivalent ligand binding to multi-subunit substrate:

$$\ln\left(\frac{B}{1-B}\right) = \alpha \ln[P] + \ln(K_{CO})^{\alpha}$$

Since $\frac{B}{1-B} = \frac{A_{1,QY}}{A_2}$, we get

$$\ln\left(\frac{A_{1,QY}}{A_2}\right) = \alpha \ln[P] + \ln(K_{CO})^{\alpha}$$

which was used to determine the degree of cooperativity and binding constant for the present systems.

The values for the calculated curve of cooperative binding in **Figures 6** and **S4**, were obtained from

$$B = \frac{[P]^{\alpha}(K_{CO})^{\alpha}}{1 + [P]^{\alpha}(K_{CO})^{\alpha}}$$

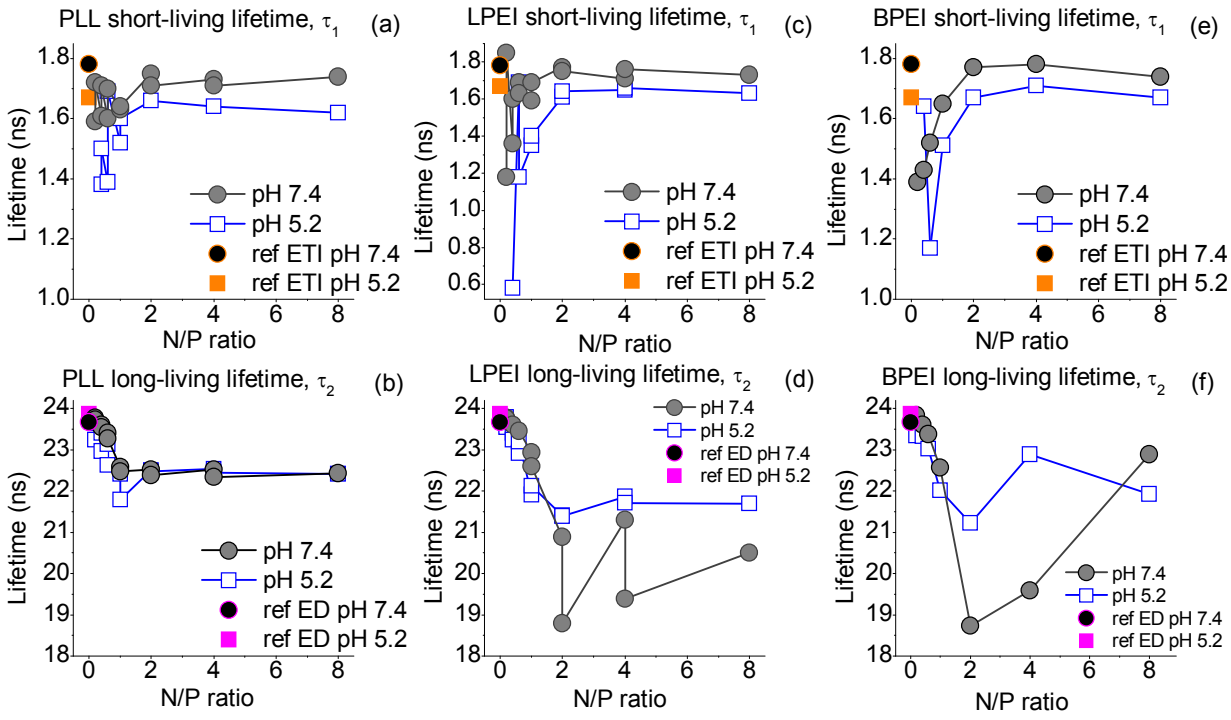

Figure S1. Fluorescence lifetimes of PLL (a, b), LPEI (c, d) and BPEI (e, f) at different pH-values. (ref ETI = free ETI in buffer at pH 7.4 (○) and at pH 5.2 (□), ref ED = ETI:DNA complex in buffer at pH 7.4 (○) and at pH 5.2 (□).) Short-living components (a, c, e) and long-living components (b, d, f).

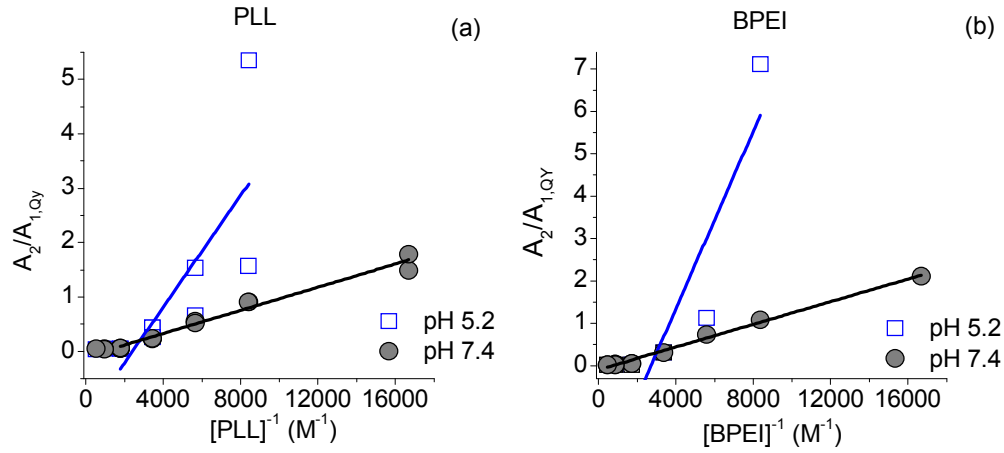

Figure S2. Ratio $A_2 / A_{1,QY}$ as a function of the inverse polymer concentration that the binding constant (as dm^{-3} mol) is equal to the inverse of the slope.

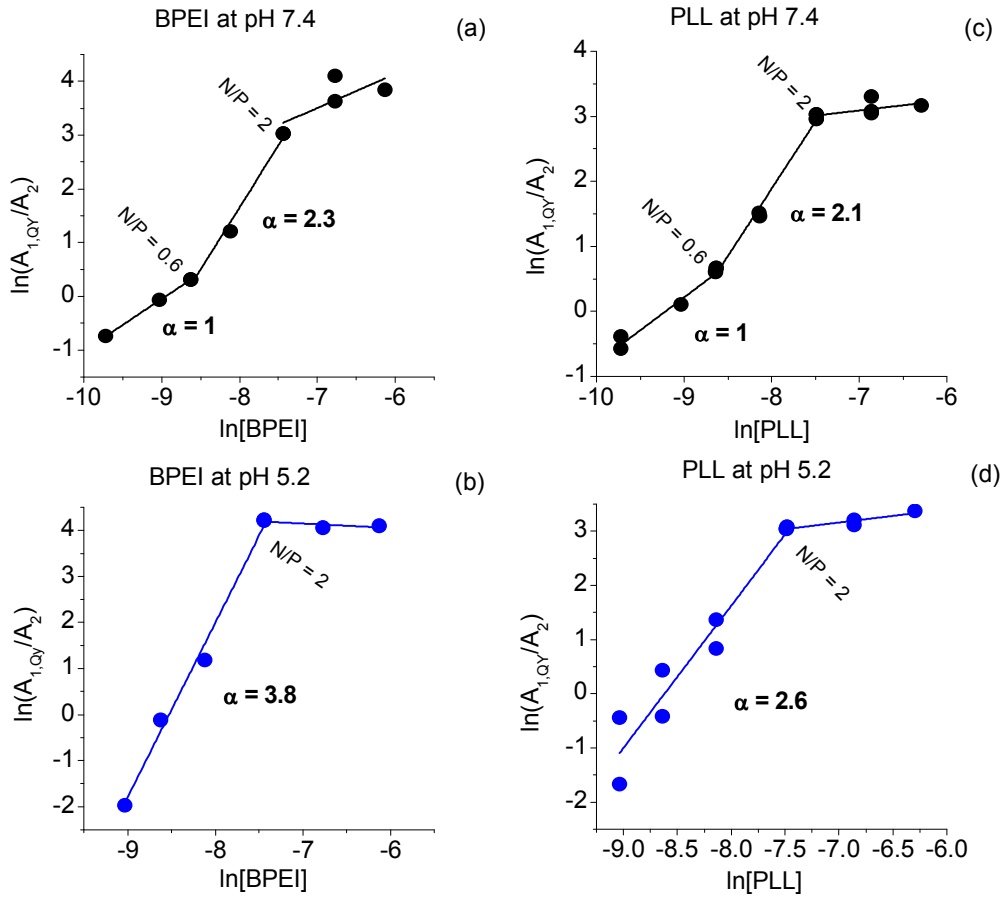

Figure S3. Hill Plots of BPEI (a, b) and PLL (c, d) at pH 7.4 (a, c) and at pH 5.2 (b, d).

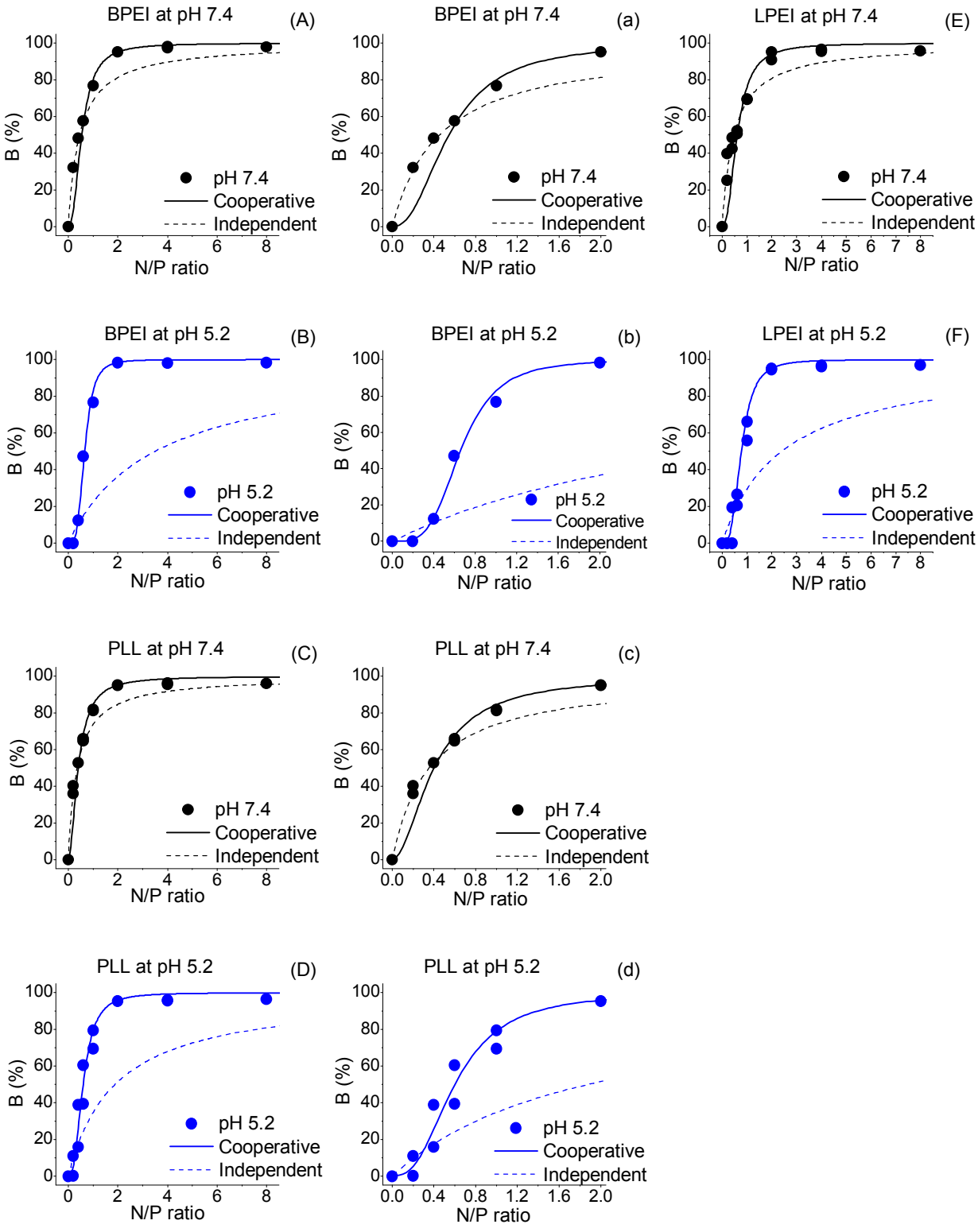

Figure S4. Independent vs. cooperative models for BPEI (A, a, B, b), PLL (C, c, D, d) and LPEI (E, F) at pH 7.4 (A, a, C, c, E) and at pH 5.2 (B, b, D, d, F).

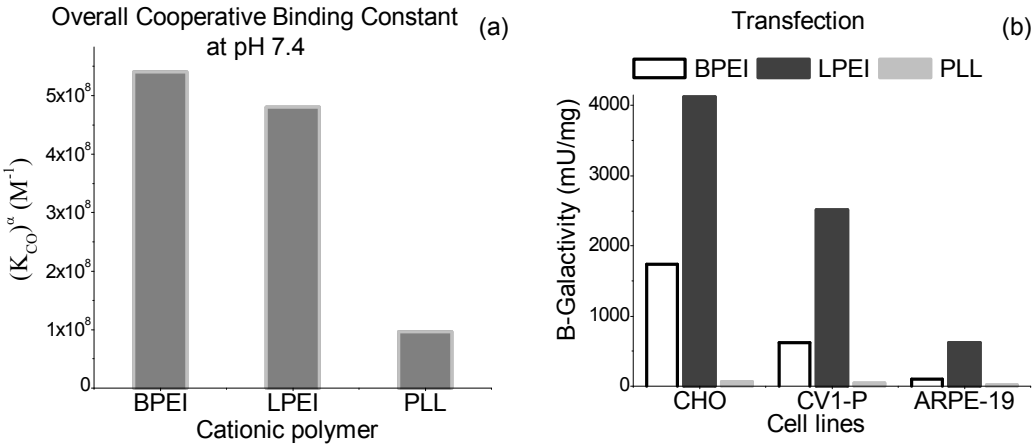

Figure S5. Overall cooperative binding constants at pH 7.4 (a) and transfection efficiencies in different cell lines at pH 7.2 (MES-HEPES-NaCl buffer) (b) for BPEI, LPEI and PLL.

Publication II

Role of Polyplex Intermediate Species on Gene Transfer Efficiency: Polyethylenimine–DNA Complexes and Time-Resolved Fluorescence Spectroscopy

Tiia-Maaria Ketola, Martina Hanzlíková, Arto Urtti, Helge Lemmetyinen, Marjo Yliperttula and Elina Vuorimaa, *J. Phys. Chem. B* **2011**, *115*, 1895–1902.

THE JOURNAL OF PHYSICAL CHEMISTRY B

ARTICLE

pubs.acs.org/JPCB

Role of Polyplex Intermediate Species on Gene Transfer Efficiency: Polyethylenimine−DNA Complexes and Time-Resolved Fluorescence Spectroscopy

Tiia-Maaria Ketola,[†] Martina Hanzlíková,[§,⊥] Arto Urtti,[‡] Helge Lemmetyinen,[†] Marjo Yliperttula,[⊥,*] and Elina Vuorimaa[†]

[†]Department of Chemistry and Bioengineering, Tampere University of Technology, Tampere, Finland;

[‡]Centre for Drug Research, University of Helsinki, Helsinki, Finland;

[§]Division of Pharmacology and Toxicology, University of Helsinki, Finland;

[⊥]Division of Biopharmaceutics and Pharmacokinetics, University of Helsinki, Helsinki, Finland

Supporting Information

ABSTRACT: Polyethylenimine (PEI) is a cationic DNA condensing polymer that facilitates gene transfer into the mammalian cells. The highest gene transfer with branched PEI is obtained at high nitrogen/phosphate (N/P) ratios with free PEI present. The small molecular weight PEI alone is not able to mediate DNA transfection. Here, we used recently developed time-resolved fluorescence spectroscopic method to study the mechanism of PEI−DNA complex formation and to investigate how free PEI, mean molecular weight, and branching of PEI affect the complexes. Analysis of fluorescence lifetimes and time-resolved spectra revealed that for both linear and branched high-molecular-weight PEI the complexation takes place in two steps, but the small-molecular-weight branched PEI complexed DNA at a single step. According to the binding constants obtained from time-resolved spectroscopic measurements, the affinity of N/P complexation per nitrogen atom is highest for LPEI and weakest for BPEI, whereas SPEI−DNA complexation showed intermediate values. Thus, the binding constant alone does not give adequate measure for transfection efficiency. On the other hand, the presence of intermediate states during the polyplex formation seems to be favorable for the gene transfection. Free PEI had no impact on the physical state of PEI−DNA complexes, even though it was essential for gene transfection in the cell culture. In conclusion, the molecular size and topology of PEI have direct influence on the DNA complexation but the free PEI does not. Free PEI must facilitate transfection at the cellular level and not via indirect effects on the PEI−DNA complexes.

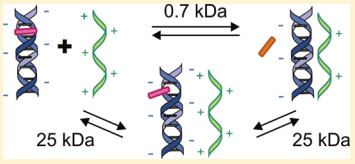

INTRODUCTION

During the postgenomic era, any DNA sequence from the human genome can, in principle, be transferred into the cells for gene therapy and associated protein expression. The gene transfer process is not, however, properly understood, and the current DNA delivery methods tend to be problematic. Many drawbacks and safety concerns[1] of otherwise efficient viral gene delivery vectors draw close attention to the investigation of alternative nonviral delivery systems, such as DNA polymeric nanoparticles. Efficacy of nonviral gene transfer systems has not matched the viral vectors yet.

The DNA nanoparticle systems are based on the complexation of the plasmid DNA with cationic polymers, liposomes, micelles, or peptides.[2] DNA must be delivered into the target cells by endocytosis and, thereafter, successfully transferred to the cytosol and nucleus.[3] Because only released DNA can be transcribed to mRNA and further translated to protein, it is evident that the DNA release upon disassembly of the complexes is a critical step in the gene delivery process.[4] The disassembly of the DNA−polycation complexes is assumed to take place via electrostatic competition with the extracellular and cellular polyanions.[5] The DNA release is dependent on the polymer structure, but the structure−property relationships and principles of DNA complexation are not well-known.

Polyethyleneimine (PEI) is widely used cationic polymer that is able to complex DNA and mediate efficient DNA transfection in the cell culture.[6] Previous studies have shown functional differences between branched polyethylenimine (BPEI) and poly-L-lysine (PLL).[5,7] Both polymers can pack and condense DNA into small nanoparticles (less than 100 nm in diameter) but upon challenge by polyanionic glycosaminoglycans, like heparan sulfate, BPEI−DNA complexes may be relaxed and even disintegrated, whereas PLL−DNA complexes retain DNA in a tightly bound complex.[5] In cellular studies, BPEI has shown more efficient transfections than PLL. This difference is not due to the increased cell uptake or nuclear entry, because the amount of DNA delivered into the cell nuclei was similar for both PLL−DNA and BPEI−DNA complexes.[4] Because DNA release or substantial relaxation from the DNA complexes is required for the transcription,[8] this may explain the 100-fold higher transfection activity of BPEI complexes compared to the PLL complexes.[4]

Received: October 18, 2010
Revised: December 28, 2010
Published: February 3, 2011

Recently, we introduced a new spectroscopic method to analyze DNA−polycation interactions in the complexes. Steady-state and time-resolved fluorescence experiments at different +/− charge ratios (carrier/DNA) suggest that the conformation of the BPEI−DNA is not locked: at least two states of DNA are present in the BPEI−DNA complexes, whereas the PLL−DNA particles include only one locked conformation of DNA.[9] Presumably, the less ordered and possibly mobile structure of BPEI−DNA complexes may turn these complexes more susceptible to the polyanion-triggered DNA release in the cells. Furthermore, the small PEI species (molecular weight 1800 and below) have been shown to exert negligible activity, but in combination with other complexing agents it improves gene transfection in the cells.[10]

An efficient PEI-mediated gene delivery in the cells requires the excess of free PEI in the solution.[11] The optimal N/P ratio (PEI nitrogen/DNA phosphate) of the complexes is usually 4−10, whereas the DNA−polycation binding becomes saturated at an N/P ratio of about 2.5. Although Ernst Wagner and co-workers demonstrated that the removal of free PEI from the complexes abolished their gene transfection ability,[12] the exact mechanism of improved transfection by free PEI is still unknown. Free PEI might change the structure of the PEI−DNA nanoparticles or alternatively have some independent role at the cellular level.

In this study, we compared the DNA-complexation behavior of different PEI species (small, linear, and branched). Time-resolved fluorescence spectroscopy and wide N/P-range, from 0.2 to 8, were used to reveal differences in the complexation mechanism and to determine the binding constants for the studied PEIs. The role of free PEI on the PEI−DNA nanoparticle formation and structure was also studied and the results were compared with in vitro transfection studies.

MATERIALS AND METHODS

Materials. The plasmid pCMVβ that encodes beta-galactosidase enzyme as a reporter gene was purified by QIAfilter Plasmid Giga Kit (QIAGEN) according to the manufacturer's instructions. Branched polyethylenimines with a mean molecular weight of 25 kDa (BPEI) and 700 Da (small PEI, SPEI) were purchased from Sigma-Aldrich and used as 1 mg/mL aqueous stock solutions titrated to pH 7. ExGen 500, a 22 kDa linear polyethylenimine (LPEI), was obtained from Fermentas. Heparan sulfate was purchased from Sigma-Aldrich. All cell culture reagents were obtained from Gibco-Invitrogen.

Sample Preparation. All solutions were prepared in 50 mM MES-HEPES buffer (pH 7.4). The final DNA concentration was adjusted to 300 μM per nucleotide and the molar ethidium bromide (ETI)/nucleotide ratio was 1:15. The polyplexes were prepared by a stepwise and direct method. In the stepwise method, independent of the final charge ratio between the cationic polymer and DNA, an initial solution with a molar ratio of PEI nitrogen to DNA phosphate (N/P ratio) 1:5 or 2:5 was prepared by vigorous mixing of equal volumes of ETI−DNA solution and cationic polymer solution. We followed the complexation by measuring the fluorescence spectrum. After the measurement, the final charge ratio was adjusted by addition of the appropriate amount of polymer solution. In the direct method, the final charge ratio was reached with the single addition of PEI to ETI−DNA solution; at volume ratio of 1:1.

Purification of BPEI−DNA Complexes. The BPEI−DNA complexes were prepared in HBG buffer (5% glucose, 20 mM Hepes, pH 7.4) by mixing equal volumes of BPEI and DNA solutions at the N/P ratio of 6. The final DNA concentration of the resulting BPEI−DNA solution was 200 μg/mL. The BPEI−DNA complexes were purified by size exclusion chromatography as described previously.[12] For the spiking of purified BPEI−DNA complexes, BPEI solution was added to the purified complexes to restore the original N/P ratio of 6. The spiked complexes were incubated for at least 20 min at room temperature prior to further analysis.

Fluorescence Measurements. The time-resolved fluorescence was measured by a time-correlated single photon counting (TCSPC) system (PicoQuant GmBH) consisting of a PicoHarp 300 controller and a PDL 800-B driver. The samples were excited with the pulsed diode laser head LDH-P-C-485 at 483 nm at a time resolution of 130 ps. The signals were detected with a microchannel plate photomultiplier tube (Hamamatsu R2809U). To diminish the influence of the scattered excitation, a cutoff filter was used in front of the monitoring monochromator. To study the time-resolved spectra, the decays were collected with a constant accumulation time in the 560−670 nm wavelength range with steps of 10 nm. The decays were simultaneously fitted to the sum of exponents in the equation

$$I(t,\lambda) = \sum a_i(\lambda)e^{-t/\tau_i} \quad (1)$$

where τ_i is the global lifetime and $a_i(\lambda)$ is the local pre-exponential factor at a particular wavelength. The factors $a_i(\lambda)$ represent the decay-associated spectra (DAS), which in the case of a mixture of different noninteracting fluorescing species corresponds to the individual spectra of the species. The amplitudes were corrected depending on the sensitivity of the detector at different wavelengths. The spectral areas (A_i) of the components can be calculated by integrating the pre-exponential factors over the measured wavelength range as indicated in the following equation:

$$A_i = \int a_i(\lambda)\mathrm{d}\lambda \quad (2)$$

The proportions of the decay components can be calculated from the spectral areas of the components as follows:

$$x_i = \frac{A_i}{A_1 + A_2} \times 100\% \quad (3)$$

Transfection. Chinese hamster ovary cells (CHO), monkey kidney fibroblasts (CV1−P), and rabbit aortic smooth muscle cells (SMC) were grown in DMEM supplemented with 10% heat-inactivated fetal bovine serum and 1% penicillin−streptomycin. The cells were passaged twice a week. CHO (10 000 cells/well), CV1−P (20 000 cells/well), and SMC (20 000 cells/well) cells were seeded into 96 well plates in 100 μL of growth medium 24 h prior to the transfection. Purified, nonpurified, and spiked complexes were diluted in HBG buffer to achieve a final concentration of 0.8 μg of DNA per well. Transfection complexes were incubated with the cells in a serum-free medium for 5 h, after which time the cells were washed with PBS, and a growth medium was added. The beta-galactosidase activity was measured 48 h after the transfection by ONPG assay as described previously.[5]

RESULTS

PEI−DNA Nanoparticle Formation. The degree of DNA condensation was determined as a function of the N/P ratio by a fluorescence method using ethidium bromide (ETI). It is well-known that the fluorescence intensity and the lifetime of ETI decrease with increasing the N/P ratio due to the displacement of the ETI molecules intercalated in the DNA double helix by

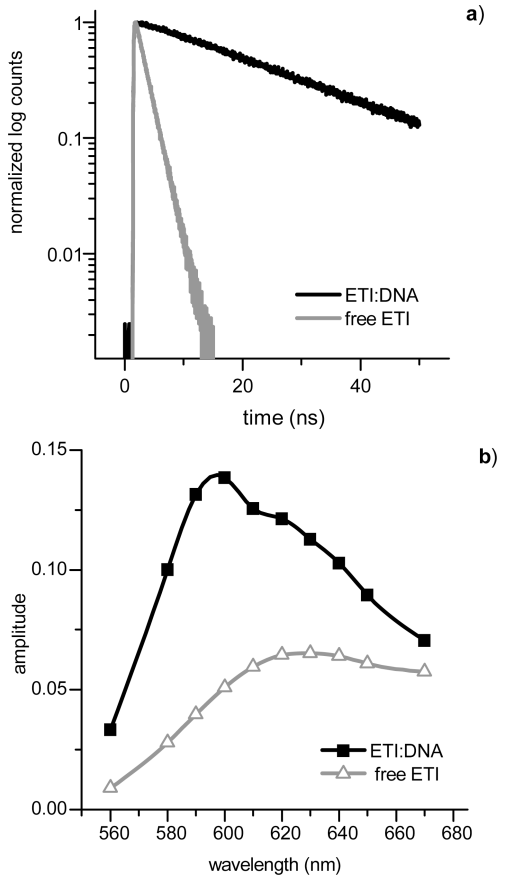

Figure 1. a) Normalized fluorescence decays at 610 nm and b) the steady-state fluorescence spectra for ETI−DNA complex and free ETI in buffer (pH 7.4). The curves are obtained by plotting the amplitudes from global fittings of the one-exponential decay curves as a function of the monitoring wavelength.

interaction with polycations.[13,14] The fluorescence decays at 610 nm, fluorescence spectra of ETI−DNA complex, and free ETI in buffer (pH 7.4) are shown in Figure 1. The increase in fluorescence intensity is accompanied with a hypsochromic shift in the fluorescence maximum from 630 nm in the absence, to 600 nm in the presence of DNA. Because of the complexation with DNA, the fluorescence lifetime of ETI increases from 1.87 ± 0.01 ns in buffer to 23.48 ± 0.11 ns in the presence of DNA. At the ETI−DNA molar ratio used in this study, ETI is fully bound by DNA, as evidenced by the one-exponential fluorescence decay in the presence of DNA (Figure 1).

BPEI Complexes Prepared by the Stepwise Method. The fluorescence decay of ETI in the presence of PEI was always two exponential (Figure 2). The lifetime of the longer-living fluorescence component, 22.78 ns, obtained in the presence of BPEI, is similar to the values obtained for ETI−DNA complex in the absence of PEI. The proportion of the long-living component (eq 3) decreases with the increasing BPEI concentration (S1). At low charge ratios (0.2−1.0), the lifetime of the short-living component is 3.13 ns. This finding is in agreement with our previous studies: at these molar ratios ETI does not totally detach from DNA during polyplex formation but it is still loosely bound to it. At higher charge ratios the obtained lifetime 1.85 ns is nearly equal to free ETI in the absence of DNA. Consequently, it seems that at very low N/P ratios, BPEI forms a loosely bound polyplex with DNA (Scheme 1). Upon addition of more BPEI to the system, a tightly bound polyplex is formed. The

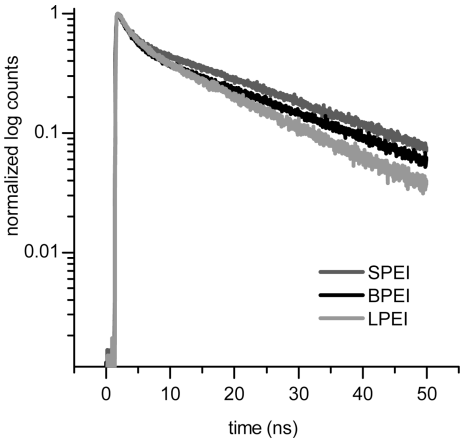

Figure 2. Normalized fluorescence decays at 610 nm for small PEI (SPEI), linear PEI (LPEI), and branched PEI (BPEI) complexes with N/P = 4.0 prepared by the stepwise method.

Scheme 1. Formation of DNA Nanoparticles in the Presence of BPEI and the Fluorescence Properties of ETI at Different Steps

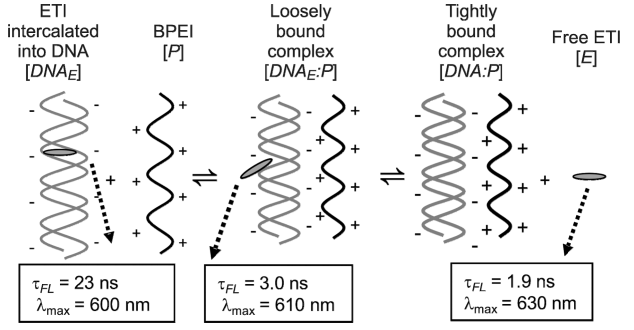

loosely bound complex acts as an intermediate in the overall equilibrium. Its amount remains constant but minimal at all N/P ratios and thus its presence cannot be observed at high N/P ratios.

The decay-associated spectra (DAS) for BPEI at the N/P ratio of 0.4 and 4.0 are shown in parts b and e of Figure 3. The shape of the shorter-living component closely resembles the shape of free ETI (Figure 1) independent of the N/P ratio. The shape of the long-living component is broader than for the ETI−DNA complex in the absence of PEI, and the maximum is slightly red-shifted. The normalized time-resolved spectra for BPEI at the N/P ratios of 0.4 and 4.0 are shown in parts b and e of Figure 4. At low N/P ratios up to 1.0, only a small shift in time can be detected, whereas at N/P ratios 2.0 and higher a clear shift in time from 615 to 605 nm can be observed. At low N/P ratios, the main component present in the system is the ETI−DNA complex. Small amounts of the loosely bound DNA_E−BPEI with ETI still attached to the polyplex are also present. The spectrum of this complex is not known, but its effect can be clearly observed as the round shape and slight red shift of the spectrum 0.6 ns after excitation. At higher N/P ratios, tight BPEI−DNA complexes are formed and ETI is released into the solution. This pattern can be observed as the characteristic red-shifted spectrum at 0.6 ns after excitation. As the fluorescence of free ETI decays, the spectrum becomes blue-shifted as the remaining fluorescence of ETI−DNA complex begins to dominate the signal.

dx.doi.org/10.1021/jp109984c |J. Phys. Chem. B 2011, 115, 1895–1902

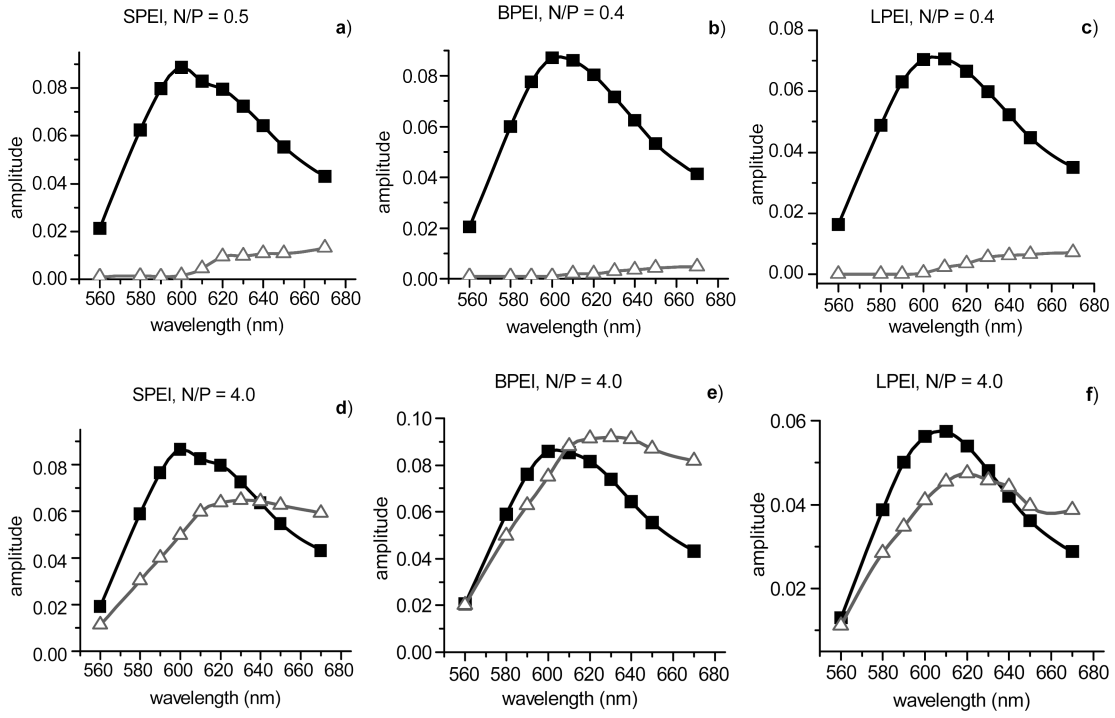

Figure 3. DAS for SPEI, BPEI, and LPEI complexes prepared by the stepwise method: (△) short-living and (■) long-living decay component.

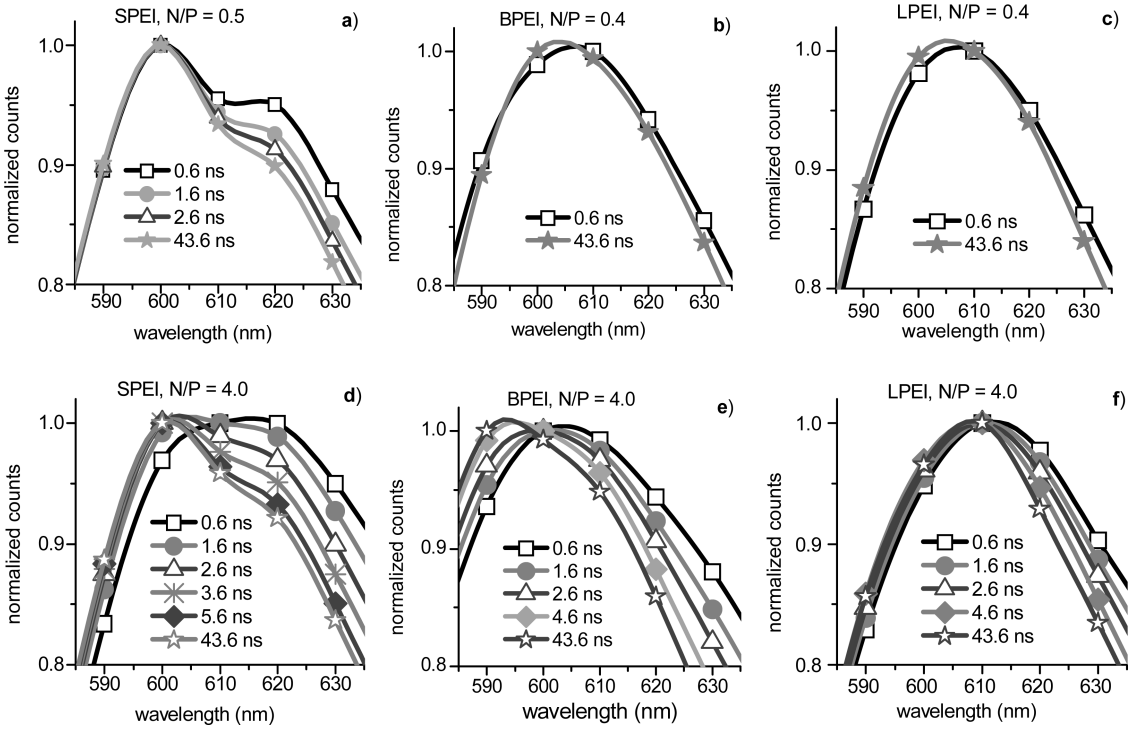

Figure 4. Normalized time-resolved spectra at different times after excitation for SPEI, BPEI, and LPEI complexes prepared by the stepwise method.

According to Scheme 1, the polyplex formation is a two-step reaction that can be simplified to the scheme:

$$\mathrm{DNA_E} + \mathrm{P} \rightleftharpoons \mathrm{DNA_E{-}P} \rightleftharpoons \mathrm{DNA{-}P} + \mathrm{E} \qquad (4)$$

where $\mathrm{DNA_E}$ is the ETI−DNA complex, P is BPEI, $\mathrm{DNA_E}$−P the loosely bound polyplex, DNA−P the tightly bound polyplex, and E the free ETI. At high N/P ratios the amount of loosely bound $\mathrm{DNA_E}$−P complex is negligible and the proportion of DNA bound by the polymer, B, is given by the equation[9]

$$B = \frac{[\mathrm{DNA{-}P}]}{[\mathrm{DNA_E}] + [\mathrm{DNA{-}P}]} = \frac{K_{\mathrm{tot}}[P]}{1 + K_{\mathrm{tot}}[P]} \qquad (5)$$

dx.doi.org/10.1021/jp109984c |J. Phys. Chem. B 2011, 115, 1895–1902

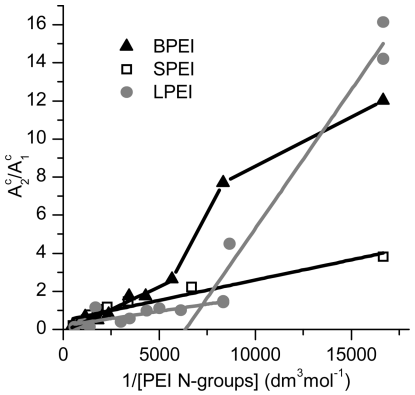

Figure 5. A_2^c/A_1^c as a function of 1/[PEI N-groups] for SPEI, LPEI, and BPEI prepared by the stepwise method.

where K_{tot} is the binding constant of the overall equilibrium (eq 4). On the other hand, at low N/P ratios the second step is negligible and the B can be written as:

$$B = \frac{[\mathrm{DNA_E{-}P}]}{[\mathrm{DNA_E}] + [\mathrm{DNA_E{-}P}]} = \frac{K_1[\mathrm{P}]}{1 + K_1[\mathrm{P}]} \qquad (6)$$

where K_1 is the binding constant of the first step in the equilibrium (eq 4). Eqs 5 and 6 can be presented in a linear form as $1/B = 1 + 1/K_i[\mathrm{P}]$. To correlate the factor B with the time-resolved fluorescence measurements, the spectral areas of the components, A_i, were corrected according to the relative fluorescence quantum yield of the components.[15] The corrected values A_1^c obtained for the short-living component correspond [$\mathrm{DNA_E{-}P}$] at low [P] and to [DNA−P] at high [P] and the values A_2^c obtained for the long-living component correspond to [$\mathrm{DNA_E}$] (eq 4). Thus, the ratio B can be expressed as $B = A_1^c/(A_2^c + A_1^c) \propto A_1^c/A_2^c$, which can be presented in a linear form as:

$$\frac{A_2^c}{A_1^c} = C + \frac{1}{K_i[\mathrm{P}]} \qquad (7)$$

where C is a proportionality factor correcting the difference between the spectroscopic data and the actual concentration. Thus, plotting the ratio A_2^c/A_1^c as a function of the inverse PEI concentration (as mol N-groups dm^{-3}) we should obtain a linear dependence with the binding constant equal to the inverse of the slope. In the plot obtained for BPEI shown in Figure 5, two phases are visible: (1) at low N/P ratios up to 0.6 the A_2^c/A_1^c ratio decreases strongly and (2) at N/P ratio higher than 0.6 the decrease of A_2^c/A_1^c is much smaller. At low N/P ratios, the slope is about four times larger than at high N/P ratios indicating that the binding constant of the first step in the equilibrium (eq 4), 500 mol N-groups dm^{-3}, is about four times lower than the binding constant of the second equilibrium, 2100 mol N-groups dm^{-3}. Thus, the first step in the equilibrium is the rate-determining step for the overall reaction and its presence can only be detected at very low N/P ratios. At N/P ratios 0.6 and higher, there is sufficient amount of BPEI for efficient formation of the tightly bound polyplex, and the number of loosely bound polyplex in the reaction mixture remains very small.

Effect of Molecular Weight. The effect of the polymer molecular weight on the polyplex formation was studied by comparing the results of 25 kDa BPEI and 700 Da SPEI. The lifetime of the longer-living component, 23.22 ns, obtained in the presence of SPEI agreed again well with that obtained for the free ETI−DNA complex. The proportion of the short-living component increased with the increasing SPEI concentration (S1), but its lifetime was shorter than that for free ETI for all N/P ratios. On the DAS (parts a and d of Figure 3), the shape of the shorter-living component resembles closely to that of free ETI and the shape of the longer-living component was nearly equal to that of ETI−DNA complex in the absence of PEI. In the time-resolved spectrum (parts a and d of Figure 4), clearly two bands were present at all charge ratios: the band at 620 nm resembling the free ETI spectrum was present directly after excitation, leaving only the longer-living band, resembling that of ETI−DNA present at longer measuring times. Thus, no evidence of the loosely bound polyplex could be observed for SPEI: only the presence of ETI−DNA complex at 600 nm and free ETI at 620 nm could be observed. Plotting the A_2^c/A_1^c ratio as a function of inverse SPEI concentration (Figure 5) yielded a linear dependence at all N/P ratios. This finding is in line with the other data: for SPEI the loosely bound $\mathrm{DNA_E}$−P complex does not exist and the polyplex formation proceeds with a simple one-step equilibrium:

$$\mathrm{DNA_E} + \mathrm{P} \rightleftharpoons \mathrm{DNA{-}P} + \mathrm{E} \qquad (8)$$

The binding constant obtained from the slope, 4700 mol N-groups dm^{-3}, was clearly higher than that obtained for BPEI (Table 1).

Effect of Polymer Topology. The effect of the PEI branching on the polyplex formation was studied by comparing the results obtained with BPEI and LPEI. The proportion of the short-living component (S1) was higher for LPEI at all N/P ratios. At very low charge ratios (0.2−0.4) the lifetime of the short-living component for LPEI is 2.10 ns. This is somewhat smaller than 3.13 ns obtained for BPEI. At higher N/P ratios, the obtained lifetime 1.87 ns is again in good agreement with free ETI in the absence of DNA. The lifetime of the long-living component at N/P ratios 0.2−3.0, 21.3 ns, is slightly smaller than 23.5 ns obtained for ETI−DNA complex in the absence of PEI. At higher N/P ratios, the LPEI solutions were very cloudy and the lifetime of the long-living component decreased even further. On DAS (parts c and f of Figure 3), the shapes of the component spectra for LPEI resemble closely those observed for BPEI, except no changes in the shape of the long-living component were observed at high N/P ratios. Also, the time-resolved spectra (parts c and f of Figure 4) resemble closely to those obtained for BPEI at N/P ratios 0.2−1.0, but at higher N/P ratios only a small time dependence is observed. It seems that at high N/P ratios the LPEI polyplexes form larger aggregates causing the cloudiness in the solutions and gathering also unbound ETI−DNA to the structures. This leads to the decrease in the ETI−DNA lifetimes and the red-shifted fluorescence also at high N/P ratios observed in DAS and time-resolved spectra.

Plotting the A_2^c/A_1^c ratio as a function of 1/[LPEI] (Figure 5) reveals a similar behavior as observed for BPEI. The binding constant of 680 mol N-groups dm^{-3} for loosely bound polyplex is very close to 500 mol N-groups dm^{-3} obtained for BPEI but the binding constant of 6600 mol N-groups dm^{-3} for the overall equilibrium is three times higher than 2100 mol N-groups dm^{-3} obtained for BPEI.

Effect of Preparation Method. The BPEI−DNA complexes were prepared by two different methods: the stepwise and direct (Materials and Methods for details). At high N/P ratios, the proportion of the short-living component is clearly higher for the direct method (S2), but no great differences in the fluorescence lifetimes between the two methods were observed (S1). In DAS (S3), the shapes of the short-living components are nearly equal, but the spectrum of the longer-living component is further red-shifted when the direct complexation method is used. Furthermore, the

Table 1. Binding Constants Determined from eq 7 as Mol N-groups per dm^3 for BPEI, SPEI, and LPEI Prepared by the Stepwise Method and for BPEI Prepared by the Direct Method (BPEI-D)[a]

PEI	K_1 (mol_N dm^{-3})[b]	K_{tot} :(mol_N dm^{-3})[b]	K_1' (mol_{PEI} dm^{-3})[c]	K_{tot}' (mol_{PEI} dm^{-3})[c]
BPEI	500	2100	2.9×10^5	1.2×10^6
SPEI		4700		7.6×10^4
LPEI	680	6600	3.5×10^5	3.4×10^6
BPEI-D	460	3000	2.7×10^5	1.7×10^6

[a] These binding constants were converted to the binding constants per molecule by K_i' = (average molecular weight of the polymer/molecular weight per N-group) × K_i. [b] mol N-groups per dm^3. [c] mol PEI molecules per dm^3.

change in the shape of the long-living component with increasing N/P ratio is seen only in the case of the stepwise method, but not for the direct method. Similar differences are observed also in the time-resolved spectra (S3). Plotting the A_2^c/A_1^c ratio as a function of 1/[BPEI] yields nearly equal dependence with the stepwise method (S4). However, the second phase is slightly steeper for the direct method and thus the A_2^c/A_1^c ratio at the second turning point is lower than for the stepwise method. This leads to a slightly smaller binding constant, 460 mol N-groups dm^{-3}, for the first step of the direct method and to a higher binding constant, 3000 mol N-groups dm^{-3}, for the overall equilibrium (Table 1). Thus, it seems that with the direct method, the amount of the loosely bound polyplex stays even smaller than for the stepwise method. Apart from this, the preparation method does not have a significant effect on the overall formation of the polyplex.

Stability. The stability of the polyplexes was studied by measuring the fluorescence decays at different times. The lifetime of the short-living component stayed constant but the lifetime and proportion of the long-living component decreased with time at least up to 6 h (S5 and S6). After the measurement, the samples were stored at +4 °C for 18 h. Then the samples were allowed to warm up to the room temperature and were measured again. No more changes in the sample properties could be observed.

Effect of Purification. To study the role of the excess BPEI on the complex properties, the extra BPEI was removed by size exclusion chromatography. The initial sample N/P ratio of 6.0 decreased close to 3.0 during purification. ETI was added to the complexes after the purification. The purified samples were spiked with BPEI to restore the original N/P ratio of 6.0. The fluorescence decays for the BPEI complexes at an N/P ratio of 3.0 prepared by adding ETI before and after BPEI are shown in Figure 6, and the lifetimes and the proportions of the long-living component x_2 are listed in Table 2. The proportion of the short-living component is clearly higher for the samples were ETI has been added after BPEI. At an N/P ratio of 3.0, most of the DNA is in the polyplexes and the positive charges of BPEI are hindering the interaction between ETI and DNA when ETI has been added to the system after BPEI. However, because the presence of the long-living component can be observed, part of ETI is able to bind on DNA. Although the results cannot be compared with those reported above, we can use ETI to show if any differences occur on the polyplexes during spiking. Only very small changes can be observed in the decays (Table 1; DAS and time-resolved spectra S7 and S8) of the purified, spiked and the nonpurified samples where ETI was added after the complexation. Therefore, it seems that the properties of the nanoparticles do not change during purification and spiking, but retain the structure formed at the original N/P ratio.

The transfection studies with three different cell lines showed that the removal of excess BPEI from the polyplexes resulted in approximately 80−90% decrease in transgene expression (Figure 7). The expression levels were restored to the original level by spiking the purified complexes with BPEI.

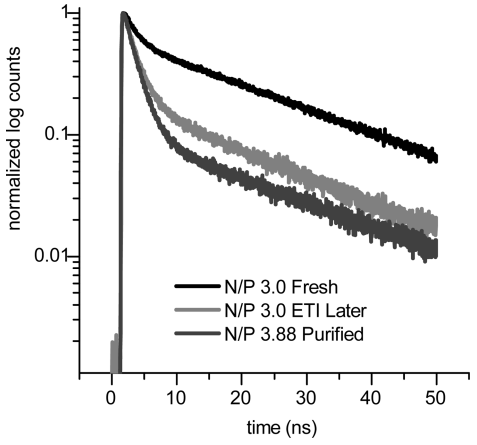

Figure 6. Fluorescence decays at 610 nm for N/P = 3.0 prepared using the direct method, prepared by adding ETI after polyplex formation, and purified from N/P = 6.0 to N/P = 3.88 for the sample.

Table 2. Fluorescence Lifetimes, τ_i, and the Proportion of the Longer-Living Component A_2 of the Purified, Spiked, and Different Control Samples

	N/P	τ_1(ns)	τ_2(ns)	x_2(%)
Reference samples:				
ETI added before BPEI	3.0	1.85 ± 0.06	22.11 ± 0.10	49
BPEI added before ETI	3.0	1.78 ± 0.04	19.12 ± 0.26	15
Purified sample:				
before purification[a]	6.0	1.78 ± 0.03	20.74 ± 0.40	11
purified [a]	3.88	1.77 ± 0.02	21.39 ± 0.32	8
spiked[b]	6.0	1.80 ± 0.03	21.77 ± 0.39	12

[a] Measured 24 h after preparation, ETI added 10 min before measurements. [b] After the measurements, the appropriate amount of BPEI was added to the purified sample.

DISCUSSION

We have used time-resolved fluorescence spectroscopy to investigate how the excess of polymer, its topology, and mean molecular weight influence the complexation with DNA. According to the binding constants obtained from time-resolved spectroscopic measurements, the affinity of N/P complexation per nitrogen atom is highest for LPEI and weakest for BPEI, whereas SPEI−DNA complexation showed intermediate values. This is probably due to pK_a values of different amino groups in PEI molecules and steric factors during complexation. Compared to

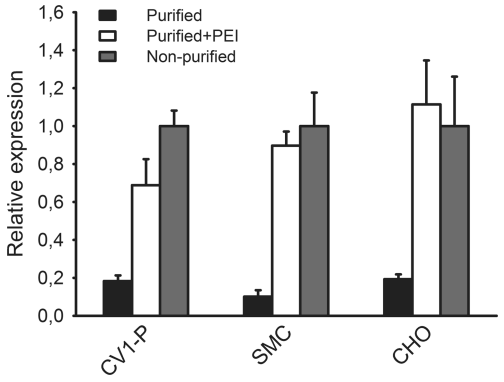

Figure 7. Relative gene expression levels after PEI complex mediated transfections. Normalized beta-galactosidase transfection of CHO, SMC, and CV1−P cells by purified and spiked (purified+PEI) complexes in comparison to nonpurified control. The results are expressed as mean ± SEM (n = 1−5).

branched BPEI, the charges of linear LPEI and small SPEI may reach the phosphates of the DNA double helix more effectively. Furthermore, SPEI is slightly more basic than LPEI and BPEI.[16]

SPEI is much less efficient than BPEI and LPEI in gene transfection.[10,17] Still the binding constant is even higher than the K_{tot} observed for BPEI and no loosely bound complex is present for SPEI. It seems that, as in the case of PLL, the release of DNA from the complex rather than the efficient formation of the complex is the crucial step for efficient gene transfection. To compare the release kinetics for the studied PEIs, the binding constants per PEI molecule (K_{tot}') were calculated. At the level of entire PEI molecules, BPEI and LPEI with high numbers of amino groups show 16 and 44 times higher binding constants than SPEI, respectively. SPEI molecules may have too weak overall binding per molecule to the DNA and, therefore, it may form too labile complexes for efficient DNA transfection.[18,19] Therefore, the high N to P binding constant and single stable state of DNA in the polyplex may not indicate efficient gene delivery. Rather, a combination of high molecular binding constant per polycation molecule and existence of a loosely bound DNA state in the complex seem to be preferred properties for DNA transfection. High overall binding constant (K_{tot}') provides adequate stability in the extracellular space, and the loosely bound intermediate state in the complex may provide DNA release in the cells, a prerequisite for DNA transcription.

The first equilibrium step does not affect the cell uptake of the polyplexes because the PEI−DNA complexes are usually prepared at higher N/P ratios to achieve optimal transfection. Presumably, the DNA release from BPEI and LPEI takes place also in two-step process: from tightly bound state to the loose state before the final DNA dissociation from the complex. This feature may influence the intracellular release kinetics of DNA but more studies are needed to understand the impact of loosely bound DNA state on the cellular gene delivery.

Despite its negligible efficacy as transfection agent as such SPEI has been shown to improve DNA transfection as a component in cationic copolymers[20,21] and in complexes with multiple DNA binding cations.[22,23] For example, DNA transfection by cationic lipids (DOTAP, Lipofectamine, DOSPER) and polyamidoamine dendrimers was improved when SPEI was included as an additional component in the complexes.[22] Stability of these DNA complexes is dependent both on SPEI and other components, like cationic lipids. Improved efficacy of transfection may be mediated by other factors instead of DNA binding properties. For example, proton sponge effect, prevention of endosomal acidification, endosomal swelling, and their resulting fragility are expected facilitate DNA entry to the cytosol and DNA transfection.[24]

The presence of free PEI was essential for the transfection efficacy in this study (Figure 7) and in the literature.[12] After the removal of the excess of PEI, BPEI−DNA complexes lost most of their transfection activity. In analogous experiment, Xu et al.[25] showed that purification of the excess cationic lipid (DOTAP) from the lipid−DNA complexes reduced the cellular toxicity of the transfection, but the efficacy of gene transfer was maintained at least at the same level. Therefore, it seems that excess of DOTAP is not beneficial for transfection, but free BPEI is important. In our study, the time-resolved fluorescence measurements prove that the excess of free BPEI had no influence on the physical state of BPEI−DNA complexes. Therefore, it is obvious that the free BPEI must have an effect of its own on the cellular level. Its effect may be related to the endosomal buffering[6,19] or interactions of the polycation with the cellular glycosaminoglycans,[26] but the exact mechanism is not known and requires further research. The excess of free BPEI is easy to use in the cell culture transfection studies but when applied in vivo, free BPEI may cause toxicity. Controlling the free PEI concentration in vivo is difficult at the target tissue. Exploration of the mechanisms of DNA complexation increases the understanding in the field and may pave way to the development of improved nonviral gene delivery systems.

CONCLUSIONS

Our studies explore the complexation of DNA with polyethyleneimine by spectroscopic method. Two important issues are highlighted by the present study. First, the two-step complexation equilibrium, which includes a loosely bound DNA−PEI intermediate complex, is seen with efficient gene delivery systems LPEI and BPEI. Small molecular weight PEI does not form loose intermediate complex; it forms complexes with DNA at high affinity per N−P pair, but the overall binding constant per small molecular weight PEI molecule is low compared to larger branched and linear PEI molecules. The high overall binding constant may provide adequate stability in the extracellular space, whereas the loosely bound intermediate complex state may facilitate DNA release in the cells, a prerequisite for DNA transcription. The second discovery of the present study demonstrates that the presence of free PEI does not have impact on the PEI−DNA complexes. Thus, the positive effects of free PEI on transfection must be mediated by independent mechanisms at cellular level.

ASSOCIATED CONTENT

Supporting Information. Fluorescence lifetimes and proportions of the components for the PEI−DNA complexes and other spectroscopic data for BPEI complexes prepared by the direct method, stability studies, purified and spiked samples. This material is available free of charge via the Internet at http://pubs.acs.org.

AUTHOR INFORMATION

Corresponding Author

*E-mail: marjo.yliperttula@helsinki.fi.

■ ACKNOWLEDGMENT

This study was supported by the Academy of Finland.

■ REFERENCES

(1) Nayak, S.; Herzog, R. W. *Gene Ther.* **2010**, *17*, 295–304.
(2) Midoux, P.; Pichon, C.; Yaouanc, J.-J.; Jaffrès, P.-A. *Br. J. Pharmacol.* **2009**, *157*, 166–178.
(3) Zabner, J.; Fasbender, A. J.; Moninger, T.; Poellinger, K. A.; Welsh, M. J. *J. Biol. Chem.* **1995**, *270*, 18997–9007.
(4) Männistö, M.; Reinisalo, M.; Ruponen, M.; Honkakoski, P.; Tammi, M.; Urtti, A. *J. Gene Med.* **2007**, *9*, 479–487.
(5) Ruponen, M.; Ylä−Herttuala, S.; Urtti, A. *Biochim. Biophys. Acta, Biomembr.* **1999**, *1415*, 331–341.
(6) Boussif, O.; Lezoualc'h, F.; Zanta, M. A.; Mergny, M. D.; Scherman, D.; Demeneix, B.; Behr, J.-P. *Proc. Natl. Acad. Sci. U.S.A.* **1995**, *92*, 7297–7301.
(7) Xu, Y.; Szoka, F. C., Jr. *Biochemistry* **1996**, *35*, 5616–5623.
(8) Matsumoto, Y.; Itaka, K.; Yamasoba, T.; Kataoka, K. *J. Gene Med.* **2009**, *11*, 615–623.
(9) Vuorimaa, E.; Urtti, A.; Seppänen, R.; Lemmetyinen, H.; Yliperttula, M. J. *Am. Chem. Soc.* **2008**, *130*, 11695–11700.
(10) Godbey, W. T.; Wu, K. K.; Mikos, A. G. *J. Biomed. Mater. Res.* **1999**, *45*, 268–275.
(11) Clamme, J. P.; Azoulay, J.; Mély, Y. *Biophys. J.* **2003**, *84*, 1960–1968.
(12) Boeckle, S.; von Gersdorff, K.; van der Piepen, S.; Culmsee, C.; Wagner, E.; Ogris, M. *J. Gene Med.* **2004**, *6*, 1102–1111.
(13) Sarkar, R.; Pal, S. K. *Biomacromolecules* **2007**, *8*, 3332–3339.
(14) Olmsted, J.; Kearns, D. R. *Biochemistry* **1977**, *16*, 3647–3654.
(15) At excitation at 485 nm the relative fluorescence quantum yield of free ETI Φ_{ETI}^{rel} = 0.273 when $\Phi_{ETI-DNA}^{rel}$ for the ETI−DNA complex is set to 1.
(16) Choosakoonkriang, S.; Lobo, B. A.; Koe, G. S.; Koe, J. G.; Middaugh, C. R. *J. Pharm. Sci.* **2003**, *92*, 1710–1722.
(17) Neu, M.; Fischer, D.; Kissel, T. *J. Gene Med.* **2005**, *7*, 992–1009.
(18) Papisov, I. M.; Litmanovich, A. A. *Adv. Polym. Sci.* **1988**, *90*, 139–179.
(19) Godbey, W. T.; Wu, K. K.; Mikos, A. G. *J. Controlled Release* **1999**, *60*, 149–160.
(20) Zhong, Z.; Feijen, J.; Lok, M. C.; Hennink, W. E.; Christensen, L. V.; Yockman, J. W.; Kim, Y. H.; Kim, S. W. *Biomacromolecules* **2005**, *6*, 3440–3448.
(21) Park, M. R.; Kim, H. W.; Hwang, C. S.; Han, K. O.; Choi, Y. J.; Song, S. C.; Cho, M. H.; Cho, C. S. *J. Gene Med.* **2008**, *10*, 198–207.
(22) Lampela, P.; Soininen, P.; Urtti, A.; Männistö, P. T.; Raasmaja, A. *Int. J. Pharm.* **2004**, *270*, 175–184.
(23) Lampela, P.; Räisänen, J.; Männistö, P. T.; Ylä-Herttuala, S.; Raasmaja, A. *J. Gene Med.* **2002**, *4*, 205–214.
(24) Sonawane, N. D.; Szoka, F. C., Jr.; Verkman, A. S. *J. Biol. Chem.* **2003**, *278*, 44826–31.
(25) Xu, Y.; Hui, S.-W.; Frederik, P.; Szoka, F. C., Jr. *Biophys. J.* **1999**, *77*, 341–53.
(26) Ruponen, M.; Honkakoski, P.; Tammi, M.; Urtti, A. *J. Gene Med.* **2004**, *6*, 405–414.

Role of Polyplex Intermediate Species on Gene Transfer Efficiency: Polyethylenimine–DNA Complexes and Time-Resolved Fluorescence Spectroscopy

Tiia-Maaria Ketola,[a] Arto Urtti,[b] Martina Hanzlíková,[c,d] Helge Lemmetyinen,[a] Marjo Yliperttula,[d] and Elina Vuorimaa [a]*

[a] Department of Chemistry and Bioengineering, Tampere University of Technology, Tampere, Finland; [b] Centre for Drug Research, University of Helsinki, Helsinki, Finland; [c] Division of Pharmacology and Toxicology, University of Helsinki, Finland; [d] Division of Biopharmaceutics and Pharmacokinetics, University of Helsinki, Helsinki, Finland

*Correspondance: marjo.yliperttula@helsinki.fi

Supporting information: Fluorescence lifetimes and proportions of the components for the DNA:PEI complexes and other spectroscopic data for BPEI complexes prepared by the direct method, stability studies, purified and spiked samples.

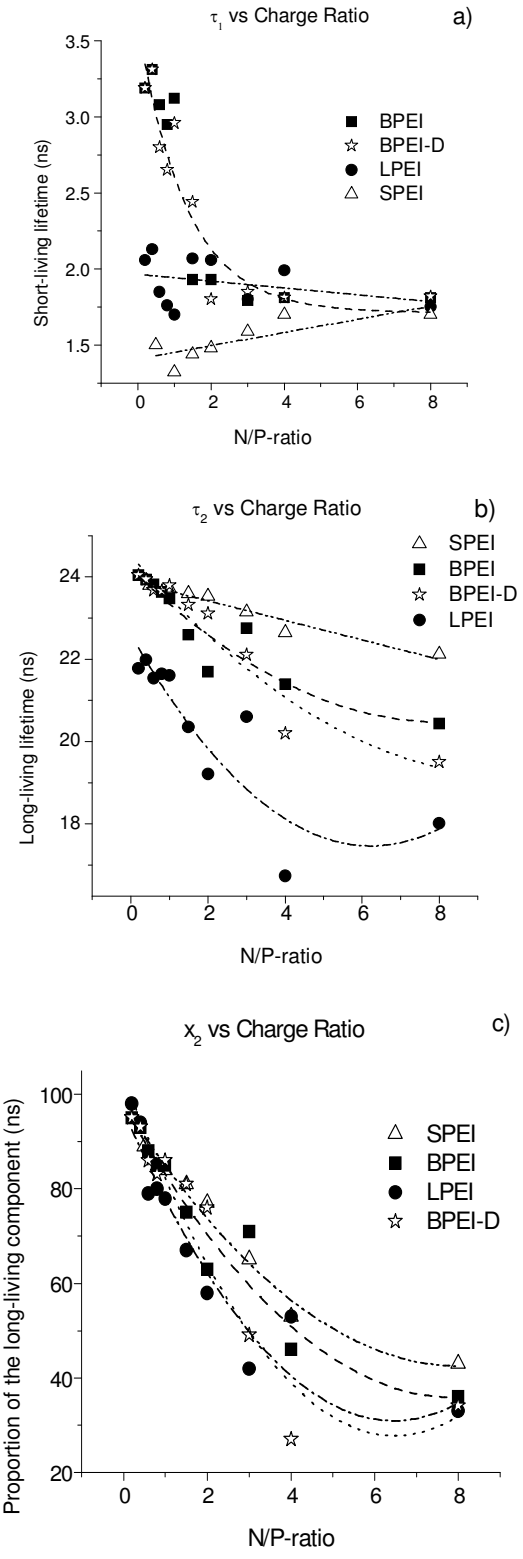

S1. Fluorescence lifetimes for a) the short-living component τ_1, b) the long-living component τ_2 and c) the proportion of the longer-living component x_2 (eq 3) at different N/P ratios for SPEI, BPEI and LPEI prepared using the stepwise method and BPEI-D prepared using the direct method.

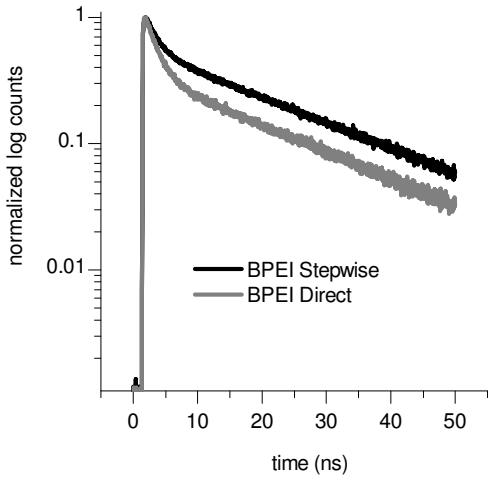

S2. Normalized fluorescence decays at 610 nm for BPEI polyplexes with N/P = 4.0 prepared by stepwise and direct method.

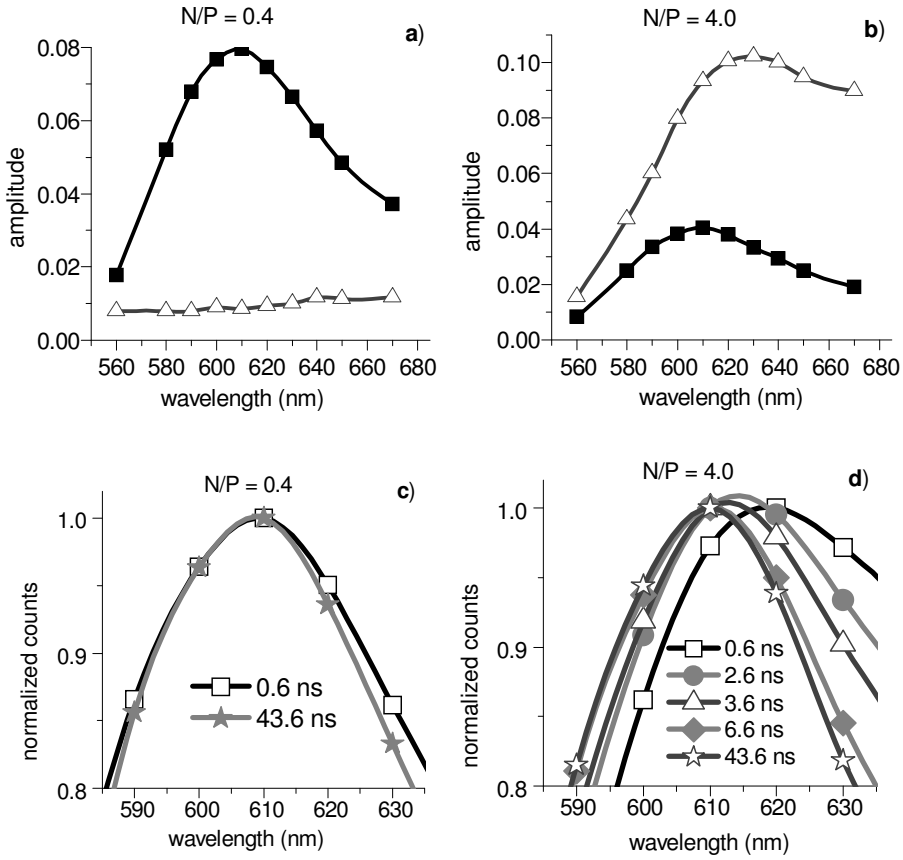

S3. DAS for BPEI prepared by direct method with a) N/P = 0.5 and b) N/P = 4.0, (Δ) short-living and (■) long-living decay component. Normalized time-resolved spectra at different times after excitation for BPEI prepared by direct method with c) N/P = 0.5 and d) N/P = 4.0.

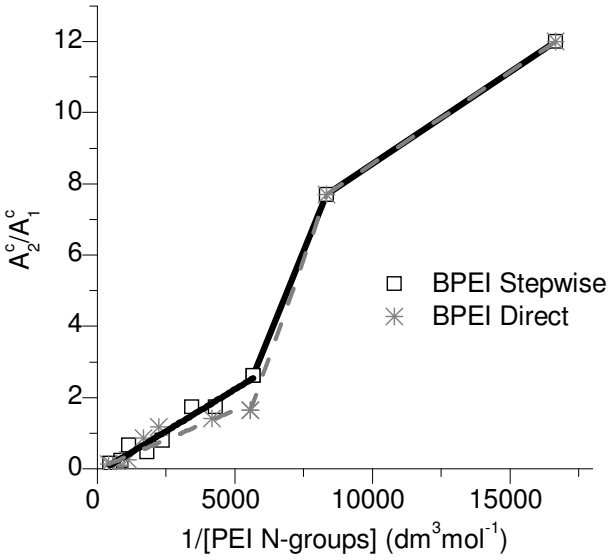

S4. A_2^c / A_1^c as a function of 1/[PEI N-groups] for SPEI, LPEI and BPEI prepared by the stepwise method.

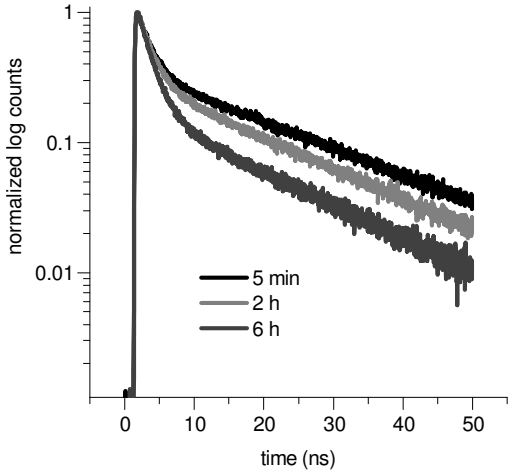

S5. Normalized fluorescence decays at 610 nm measured at different times after preparation for BPEI polyplexes with N/P = 6.0 prepared with direct method.

S6. Fluorescence lifetimes, τ_i, and the proportion of the longer living component A_2 for N/P = 6.0 prepared by direct method at different times after preparation.

Time after preparation	τ_1 (ns)	τ_2 (ns)	A_2 (%)
5 min	1.87 ± 0.05	20.28 ± 0.20	27
2 h	1.86 ± 0.03	18.33 ± 0.13	23
6 h	1.88 ± 0.03	17.01 ± 0.21	14

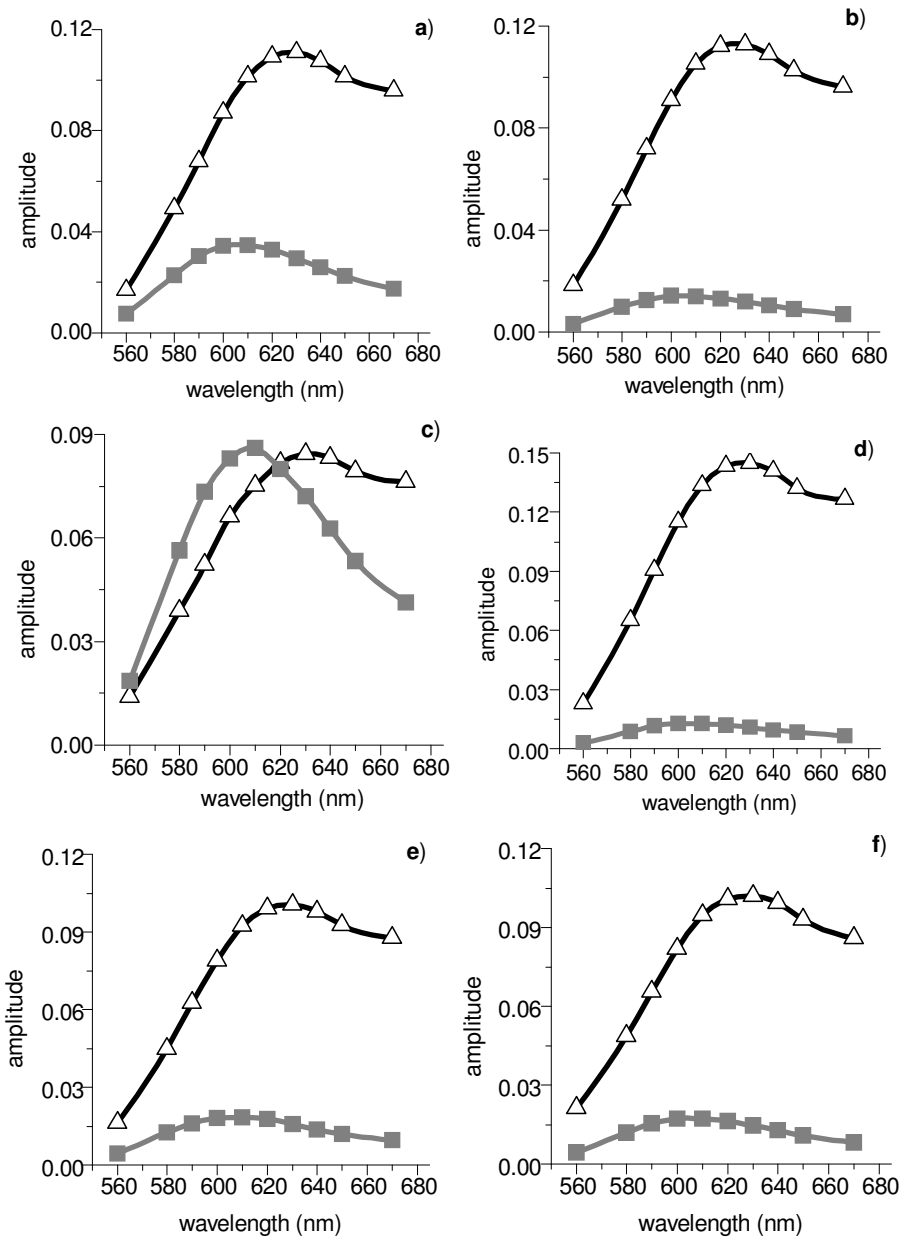

S7. DAS for purified, spiked and different control samples: a) N/P = 6.0 fresh, b) N/P = 6.0 after 24 h c) N/P = 3.0 fresh, d) purified N/P = 3.9 after 24 h, e) N/P = 3.0 ETI later, fresh and f) N/P = 6.0 spiked. (Δ) short-living and (■) long-living decay component.

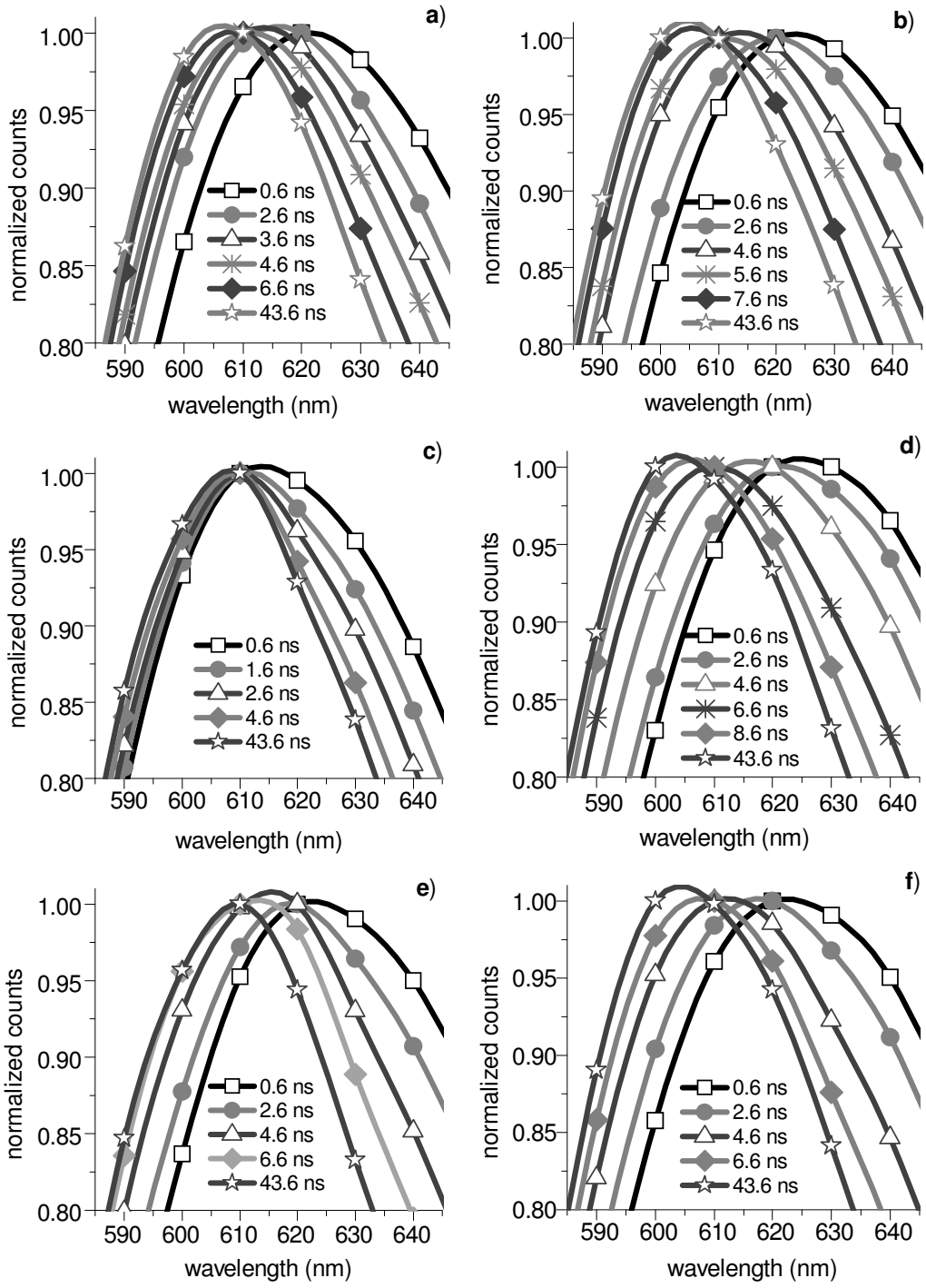

S8. Time-resolved fluorescence spectra for purified, spiked and different control samples: a) N/P = 6.0 fresh, b) N/P = 6.0 after 24 h c) N/P = 3.0 fresh, d) purified N/P = 3.9 after 24 h, e) N/P = 3.0 ETI later, fresh and f) N/P = 6.0 spiked.

Publication III

Poly(*β*-amino ester)–DNA Complexes: Time-Resolved Fluorescence and Cellular Transfection Studies

Elina Vuorimaa, Tiia-Maaria Ketola, Jordan J. Green, Martina Hanzlíková, Helge Lemmetyinen, Robert Langer, Daniel G. Anderson, Arto Urtti and Marjo Yliperttula, *J. Control. Release* **2011**, *154*, 171–176.

Reprinted with permission from *Journal of Controlled Release* **2011**, *154*, 171–176.

Journal of Controlled Release 154 (2011) 171–176

Poly(β-amino ester)-DNA complexes: time-resolved fluorescence and cellular transfection studies

Elina Vuorimaa [a], Tiia-Maaria Ketola [a], Jordan J. Green [b], Martina Hanzlíková [c], Helge Lemmetyinen [a], Robert Langer [d], Daniel G. Anderson [d], Arto Urtti [e], and Marjo Yliperttula [c,*]

[a] Department of Chemistry and Bioengineering, Tampere University of Technology, P.O. Box 541, FIN-33101 Tampere, Finland
[b] Biomedical Engineering and the Institute for Nanobiotechnology, The Johns Hopkins University School of Medicine, 400 N Broadway, Smith Building 5017, Baltimore, MD 21231, USA
[c] Division of Biopharmaceutics and Pharmacokinetics, Faculty of Pharmacy, P. O. Box 56, FI-00014 University of Helsinki, Finland
[d] The David H. Koch Institute for Integrative Cancer Research, Massachusetts Institute of Technology, 77 Massachusetts Avenue , Cambridge, MA 02139, USA
[e] Centre for Drug Research, Faculty of Pharmacy, P. O. Box 56, FI-00014 University of Helsinki, Finland

***** Corresponding author: Marjo Yliperttula, Division of Biopharmaceutics and Pharmacokinetics, Faculty of Pharmacy, P. O. Box 56, FI-00014 University of Helsinki, Finland, tel: +358-9-440935566, fax: +358-9-191 59580, e-mail: marjo.yliperttula@helsinki.fi.

Abstract

A large number of different polymers have been developed and studied for application as DNA carriers for non-viral gene delivery, but the DNA binding properties are not understood. This study describes the efficiency of nanoparticle formation by time-resolved fluorescence measurements for poly(β-amino esters), cationic biodegradable polymers with DNA complexation and transfection capability. From the large library of poly(β-amino esters) ten polymers with different transfection efficacies were chosen for this study. The binding constants for nanoparticle formation were determined and compared to polyethylene imines with the same method. Although the DNA binding efficiency of the amine groups are similar for both types of polymers, the overall binding constants are an order of magnitude smaller for poly(β-amino esters) than for 25 kDa polyethylenimines, but yet poly(β-amino esters) show comparable DNA transfection efficacy with polyethyleneimines. Within this series of polymers the transfection efficacy showed increasing trend in association with relative efficiency of nanoparticle formation.

Keywords: gene delivery; poly(β-amino esters); DNA complexation; DNA binding; time-resolved fluorescence spectroscopy

1. Introduction

The viruses are able to transfer their genetic cargo to the host cells. Although most of current gene therapy research relies on viral vectors, safety problems (incl. deaths in clinical trials) have slowed down the progress of this approach [1-3]. Non-viral (chemical) vectors, based on nanoparticles, are potential alternatives to the viral vectors. They offer advantages that are difficult to achieve with viral vectors: versatility, lack of immunogenicity, easy large-scale production, unrestricted DNA size, and possibility to incorporate several different DNA species to the same particle [4]. However, the chemical vectors show poor transfection efficacy [5]. Typical non-viral DNA delivery systems involve polycationic species, like cationic polymers, cationic

liposomes or micelles, that complex and condense plasmid DNA in solution forming nanoparticles of 40–500 nm in diameter [6-9]. Nanoparticle mediated gene transfection involves several phases: DNA complexation, binding to the cell surface, endocytic uptake, endosomal escape to the cytosol, nuclear entry, transcription and translation. Importantly, DNA must be released from the nanoparticles before transcription.

Poly(*β*-amino esters) (PBAEs) [10-13] are promising agents for non-viral gene delivery due to their (1) large potential for structural diversity, (2) ability to condense DNA into small and stable nanoparticles, (3) ability to buffer the endosome and facilitate endosomal escape, (4) biodegradability via hydrolytic cleavage of ester groups, (5) low cytotoxicity compared with some other cationic polymers, and (6) relatively high efficacy *in vitro* and *in vivo*. The best PBAEs are linear, synthesized at an amine/acrylate ratio of 1.2:1, and have a molecular weight of ~10 kDa [13,14].

Steady state fluorescence measurements of ethidium bromide are widely used to characterize DNA binding by cationic polymers and lipids. Due to the overlapping and broad spectra of free and DNA bound ethidium bromide, this method cannot be used in quantitative manner to resolve the binding constants of DNA and cationic polymers. Previously [15] we demonstrated that the nanoparticle formation and DNA-polymer binding constants and possible multiple states of binding can be determined with time-resolved fluorescence using ethidium bromide (ETI) as the fluorescent probe. Because fluorescence lifetimes and their proportions instead of intensity are used to analyze the state of the system, the method is not hampered by scattering and thus allowing more quantitative analysis than steady state measurements. The method revealed DNA complexation differences between an efficient transfection agent (polyethylenimine; PEI) and poor transfection agent (poly-L-lysine; PLL). For these polymers both the nature and the density of the amine groups taking part in the complexation of DNA are different: PEI contains primary, seconday and tertiary amines, whereas PLL includes only primary amines.

The purpose of this study was to extend the detailed DNA binding constant analyses to polymers with only tertiary amines. From a large library of PBAEs [13] ten polymers with different transfection efficacies were chosen for this purpose. We determined the DNA–complexation behaviour of different PBAEs over a wide amine to phosphate (N/P) range, from 1 to 100, to reveal the complexation efficiency and mechanism, and to determine the binding constants for the studied PBAEs. In addition, we investigated a possible correlation between fluorescence parameters and transfection efficacy of PBAEs.

2. Materials and methods

2.1. Materials

Plasmid DNA (pCMVβ) that encodes β-galactosidase reporter gene was produced in *E. coli*, and isolated and purified using a Qiagen Plasmid Giga kit (Qiagen, Germany). Ten different poly(*β*-amino esters) (PBAEs) (**Table 1**) with average molecular weights ranging from 8 to 28 kDa were synthesized by the conjugate addition of amine monomers (numbers) to diacrylate monomers (letters) solvent free at 95°C or in DMSO at 60°C [12]. The reaction proceeds in one step without the production of any byproducts. The PBAEs were then dissolved in DMSO to 100 mg ml^{-1} concentration and were further diluted into 50 mM MES-HEPES buffer (pH 7.4) to a final concentration of 6 mg ml^{-1}.

2.2. Sample preparation

All solutions were prepared in 50 mM MES-HEPES buffer (pH 7.4). In preparing the Polymer/DNA complexes, the molar ratio of PEI nitrogen to DNA phosphate (N/P ratio) was used. The final DNA concentration was adjusted to 0.0975 mg ml^{-1}, i.e. 300 μM per nucleotide and the ethidium bromide (ETI) : nucleotide ratio was 1:15. With the DNA:ETI molar ratio used ETI is fully bound by DNA, which is observed as one-exponential decay in the presence of DNA. The polyplexes

were prepared by mixing the (DNA) : (ETI) solution and the cationic polymer solution at volume ratio of 1:1. Solutions were mixed rigorously to ensure effective complexation between DNA and the polymer.

Table 1 Structures of the diacrylate and amine monomers of the studied PBAEs, their average molecular weights (MW) and amine:acrylate ratios (Am:Ac).

Polymer MW (Da) Am/Ac	Diacrylate monomer	Amine monomer
F28 16100 1.025	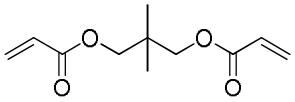	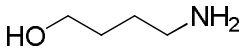
C36 21200 1.2	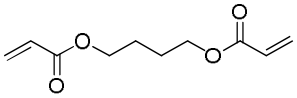	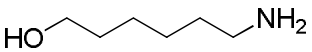
D24 9542 1.05	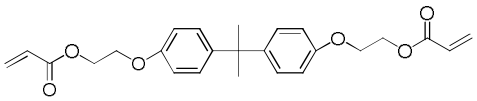	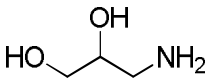
E28 14300 1.1	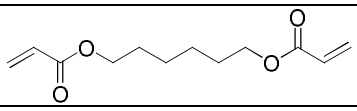	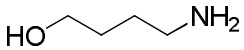
U28 15600 1.1	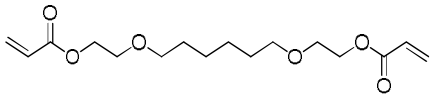	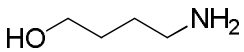
C28 27900 1.05	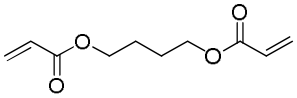	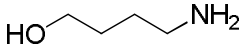
AA24 8058 1.3	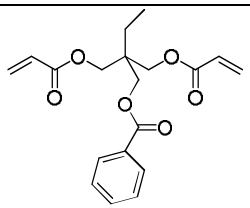	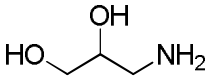
AA28 20900 1.1	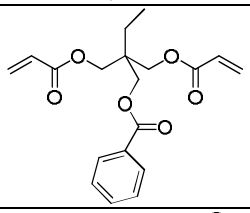	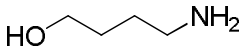
C32 18100 1.2	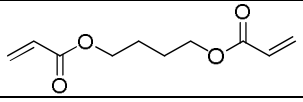	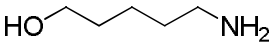
JJ28 16800 1.1	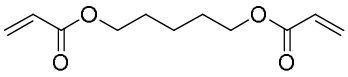	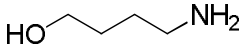
Synthesis of PBAEs	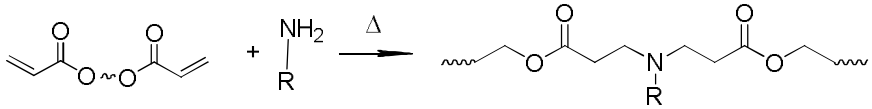	
Diacrylate monomer + Amine monomer → PBAEs		

2.3. *Fluorescence measurements*

The time-resolved fluorescence was measured using a time-correlated single photon counting (TCSPC) system (PicoQuant GmBH) consisting of PicoHarp 300 controller and PDL 800-B driver. The samples were excited with the pulsed diode laser head LDH-P-C-485 at 483 nm and the time resolution was about 130 ps. The signals were detected with a microchannel plate photomultiplier tube (Hamamatsu R2809U). To diminish the influence of the scattered excitation, a cutoff filter was used in front of the monitoring monochromator. To study the time-resolved spectra the decays were collected with a constant accumulation time (300 s) in the 560–670 nm wavelength range with steps of 10 nm. The decays were simultaneously fitted to the sum of exponents in the equation $I(t,\lambda) = \sum a_i(\lambda) e^{-t/\tau_i}$, where τ_i is the global the lifetime and $a_i(\lambda)$ is the local the pre-exponential factor at a particular wavelength. The factors $a_i(\lambda)$ represent the decay-associated spectra (DAS), which in the case of a mixture of different non-interacting fluorescing species correspond to the individual spectra of the species. The amplitudes were corrected according to the sensitivity of the detector at different wavelengths and the relative fluorescence quantum yields of the components. The relative fluorescence quantum yield of free ETI $\Phi_{ETI}^{rel} = 0.273$ when $\Phi_{ETI:DNA}^{rel}$ for the ETI:DNA complex is set to 1. The spectral areas (A_i) of the components were calculated by integrating the corrected pre-exponential factors over the measured wavelength range. The proportions of the decay components can be calculated from the spectral areas of the components as $x_2 = [A_i/(A_1 + A_2)] \times 100\%$.

3. Results

The degree of DNA condensation was determined as a function of the polymer/DNA N/P ratio by a time-resolved fluorescence method using ethidium bromide (ETI). ETI shows significant enhancement of fluorescence intensity and lifetime upon intercalation with DNA (23 ns) compared to that in bulk buffer (1.9 ns) [16-18]. During the nanoparticle formation the ETI molecules intercalated in the DNA double helix are displaced by interaction with polycations and ETI is freed into the bulk solution. The two lifetime values are so distinct that their relative contribution can be used to estimate the extent of nanoparticle formation [15,19].

Table 2 The average fluorescence lifetimes, $<\tau_i>$, for the studied PBAEs.

Polymer	$<\tau_1>$ (ns)	$<\tau_2>$ (ns)
F28	1.63 ± 0.16	22.53 ± 0.12
C36	1.75 ± 0.20	22.56 ± 0.14
D24	1.89 ± 0.16	22.35 ± 0.13
E28	1.75 ± 0.11	22.26 ± 0.14
U28	1.76 ± 0.13	22.32 ± 0.13
C28	1.84 ± 0.10	22.41 ± 0.15
AA24	1.79 ± 0.14	22.44 ± 0.14
AA28	1.73 ± 0.15	22.39 ± 0.14
C32	1.95 ± 0.12	23.18 ± 0.14
JJ28	1.86 ± 0.10	22.30 ± 0.15

The fluorescence decays in the presence of all the PBAEs studied here are clearly two exponential. As an example, the decays observed at 610 nm for C32 at different N/P ratios are shown in **Fig. 1**. The fluorescence lifetimes stay constant irrespective of the N/P ratio and the average lifetimes for each polymer are listed in **Table 2**.

The lifetimes of the long-living component obtained in the presence of PBAEs are similar to the values obtained for ETI:DNA complex in the absence of PBAEs. The lifetimes of the short-living component are nearly equal to free ETI in the absence of DNA. The proportion of the short-living decay component, x_1, increases with increasing N/P ratio for all polymers (**Fig. 2**). Very small differences between the

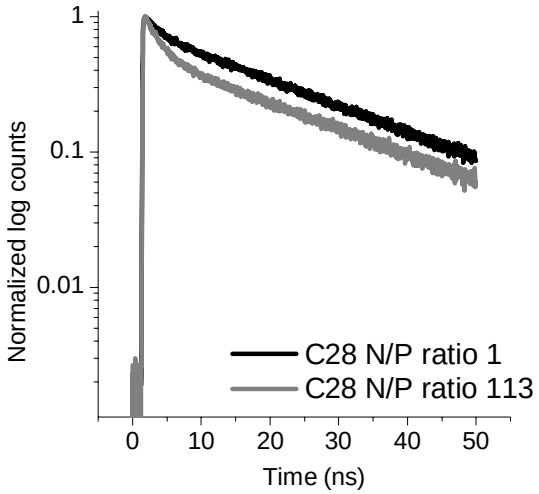

Fig. 1. Normalized fluorescence decays at 610 nm for C28 with N/P ratio 1 and 113.

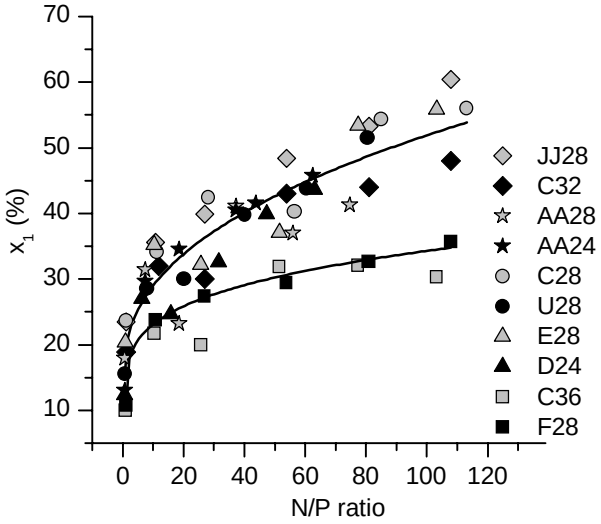

Fig. 2. Proportion of the short-living decay component, x_1, as a function of N/P-ratio for the studied PBAEs.

polymers are observed although for C36 and F28 the increase is less than for the others. The increase in the proportion of the short-living component is also clearly observed in **Fig. 3**, where the decay associated spectra for C36 and C28 at N/P ratios 25 and 100 are presented. The shape of the shorter-living component resembles closely to that of free ETI for all cases. The shape of the longer-living component is broader than for ETI:DNA complex in the absence of the polymers and the maximum is red shifted from 600 to 610 nm. These changes are usually observed during nanoparticle formation: the proportion of free ETI in the system corresponds to the formation of tightly bound polymer:DNA complexes and the changes observed in the longer-living component correspond to the changes in the environment of the DNA that is not yet tightly bound by the polymer [18].

3.1. Binding constants

In a previous study [15,18] on the polyplex formation between polyethylenimine (PEI) and DNA, we used the time-resolved fluorescence data to determine the binding constants. To compare the behavior of the present PBAEs with PEIs, the binding constants for PBAEs were determined in the same way. The corrected spectral areas A_1^c obtained for the short-living component correspond to the amount of polyplex and the values A_2^c obtained for the long-living component correspond to the amount of unbound DNA. The ratio A_2^c/A_1^c can be expressed as [18]:

$$\frac{A_2^c}{A_1^c} = C + \frac{1}{K[P]} \qquad (1)$$

where K is the binding constant of the overall equilibrium, [P] is the concentration of the polymer and C is a proportionality factor correcting the difference between the spectroscopic data and the actual concentration. Plotting the ratio A_2^c/A_1^c as a function of the inverse PBAE concentration (as mol N-groups dm^{-3}) a linear dependence was observed for all PBAEs at least up to N/P ratio 50. At this N/P ratio, the complexation seems to have reached equilibrium and the A_2^c/A_1^c ratio remained nearly constant with increasing [P]. For some polymers, further decrease in the A_2^c/A_1^c ratio was observed (**Fig. 4**) indicating that the formed polyplexes start to aggregate at higher N/P ratios. Examples of both types of behavior are shown in **Fig. 6**. The binding constants per N-group calculated

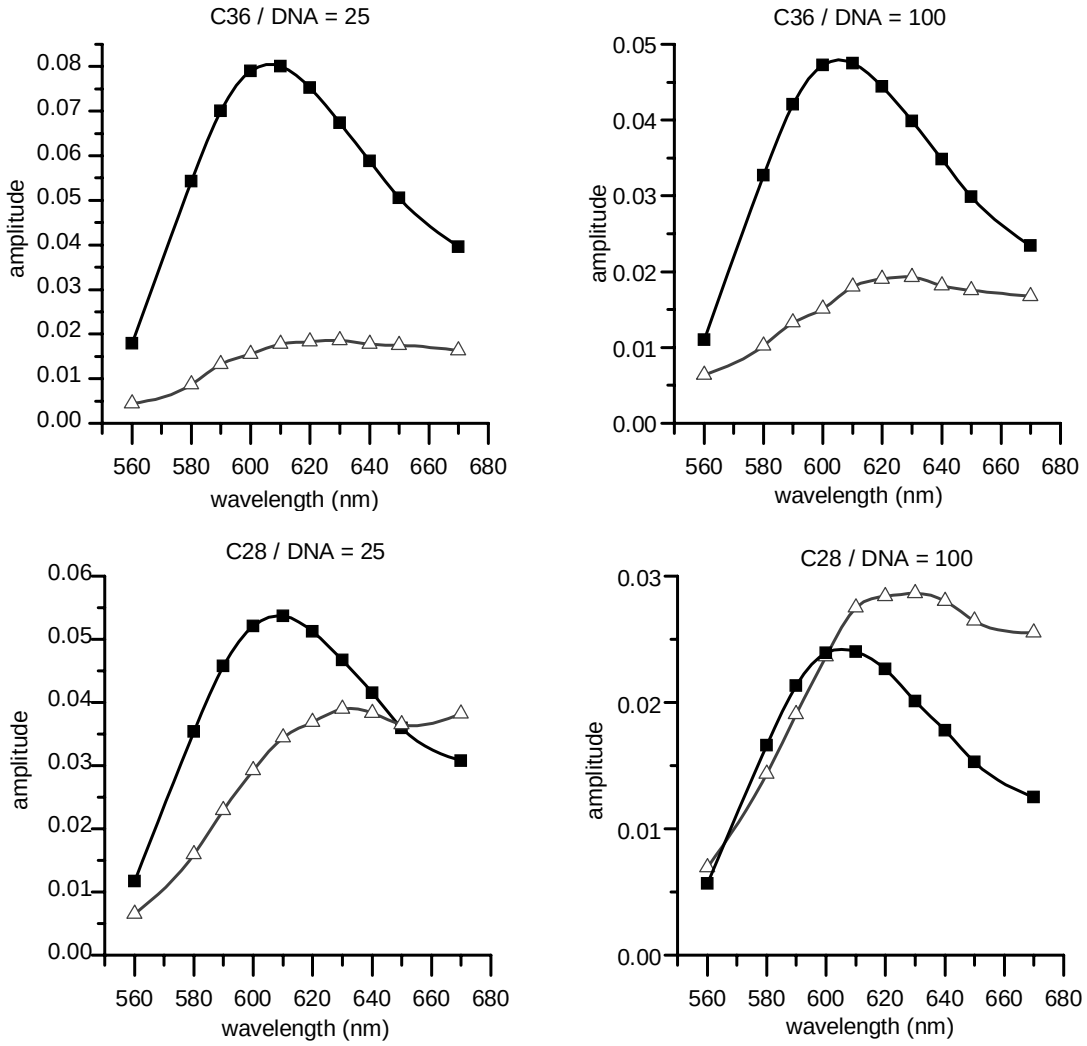

Fig. 3. Decay associated spectra for C36 and C28 at N/P ratios 25 and 100. (Δ) short-living and (■) long-living decay component.

from the slopes were between 2000 and 6300 dm^3 mol^{-1} N-groups for all PBAEs (**Table 3**). These values are similar to those obtained for PEIs (2100–6600 dm^3 mol^{-1} N-groups).

3.2 Efficiency of nanoparticle formation

The spectral areas of each component, A_i, represent the amount of the component in the system. The differences of the spectral areas of the components in the decay associated spectra (**Fig. 3**) are however relatively small and thus prone to experimental errors. To obtain more reliable tool for estimating the relative efficiency of polyplex formation by the studied PBAEs, the maximum amplitudes $a_{i,max}$ at each N/P ratio were used. The relative efficiency was estimated as the difference in the ratio of the maximum amplitudes of the two fluorescence components $a_{i,max}$ at each N/P ratio according to Eq. (3):

$$\text{Relative efficiency} = \frac{\left(\frac{a_{1,max}}{a_{2,max}}\right)_{N/P} - R_{min}}{R_{max} - R_{min}} \qquad (2)$$

where $R_{max} = \left[\left(\frac{a_{1,max}}{a_{2,max}}\right)_{100}\right]_{max}$ is the maximum amplitude ratio at N/P =100 and $R_{min} = \left[\left(\frac{a_{1,max}}{a_{2,max}}\right)_{1}\right]_{min}$ is the minimum amplitude ratio at N/P = 1 obtained for this series of polymers. The relative nanoparticle formation efficiency was considered to be 0 % at N/P ratio 1 at which

there is minimal interaction between polymer and DNA. For 100 % relative nanoparticle formation efficiency N/P ratio 100 was used, since at this N/P no further changes in the fluorescence signal was observed and it is clearly higher than the useful N/P ratio for transfection (about 50 [14]). Thus, we calculated the nanoparticle formation efficiency for this N/P ratio 50. The obtained relative efficiencies are presented in **Fig. 5**, and they are compared in **Fig. 6** with the relative transfection efficacy of the polymers that was reported earlier [14]. The increased relative nanoparticle formation efficiency is positively correlated with the increased transfection efficacy for most of the polymers.

Table 3 Molecular weights and binding constants determined as mol N-groups per dm^3 for the studied PBAEs. These binding constants were converted to the binding constants per molecule by $K_i' = (\text{average molecular weight of the polymer/molecular weight per N-group}) \times K_i$. The values for PEIs are from reference [18].

PBAE	M_{av} (kDa)	K_{tot} ($dm^3\ mol_N^{-1}$)[b]	K_{tot}' ($dm^3\ mol_{polymer}^{-1}$)[c]
F28	16.1	3870	2.1×10^5
C36	21.2	2090	1.4×10^5
D24	9.5	4020	7.5×10^4
E28	14.3	4550	2.1×10^5
U28	15.6	3950	1.5×10^5
C28	27.9	6220	6.0×10^5
AA24	8.1	2690	5.0×10^4
AA28	20.9	4700	2.3×10^5
C32	18.1	4440	2.7×10^5
JJ28	16.8	6100	3.4×10^5
linear PEI	22.0	6600	3.4×10^6
branched PEI	25.0	2100	1.2×10^6
branched PEI	0.7	4700	7.6×10^4

[a] dm^3 per mol N-groups
[b] dm^3 per mol polymer molecules

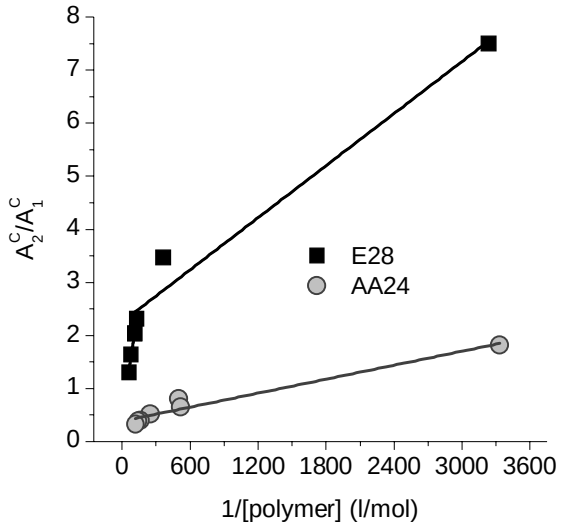

Fig. 4. A_2^c / A_1^c as a function of 1/[polymer N-groups] for AA24 and E28.

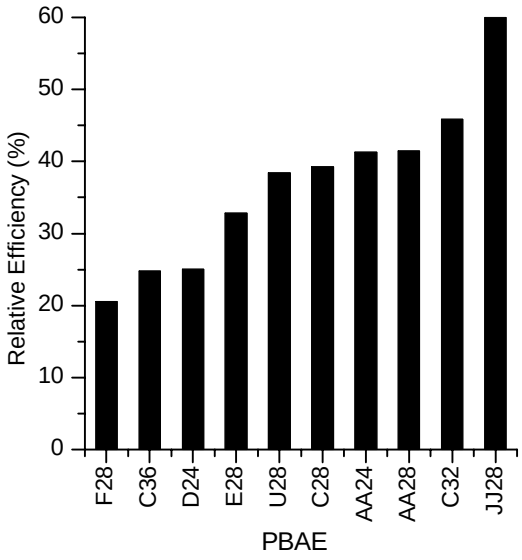

Fig. 5. Relative efficiencies of the nanoparticle formation for the studied PBAEs determined by the fluorescence method. The relative error of the efficiencies is ±2%.

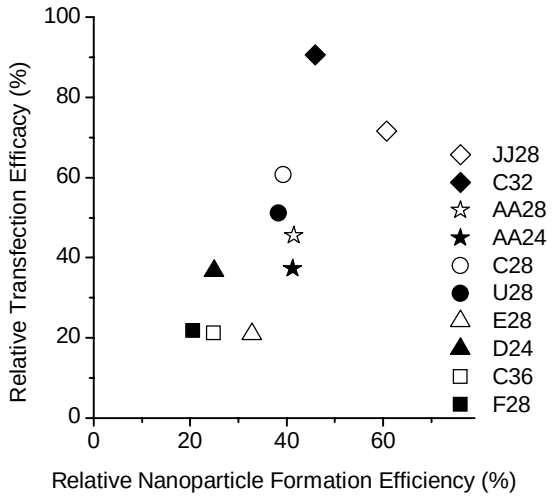

Fig. 6. Correlation between the relative nanoparticle formation efficiency and the in vitro transfection efficacy.

4. Discussion

Previously we demonstrated differences between DNA nanoparticle formation with PEI and PLL. In general PEI shows higher transfection activity than PLL. Unlike PLL, that has only primary amines, the branched PEI includes primary, secondary and tertiary and high charge density. PEI has a high density of groups with pK_a values close to 7. These groups are able to buffer the acidic environment of the endosome and facilitate endosomal escape through the "proton sponge" mechanism [20-22]. According to our previous studies both branched and linear 22 kDa PEI condense DNA into nanoparticles via a two step equilibrium: first of loosely bound DNA:PEI intermediate complex is formed followed by the formation of the tightly bound DNA:PEI nanoparticle. The rate of formation for the tightly bound nanoparticle is much higher than for the loosely bound complex. Thus, the amount of the loosely bound complex remains very small during the polyplex formation. This deviates from the single step nanoparticle formation with PLL.

In this study, we investigated DNA complex formation with PBAEs that have previously shown to have good transfection activity. Like in the case of PEI, the tertiary amines of PBAEs are able to buffer the endosomes and facilitate cytoplasmic delivery of DNA. However, the PBAE mediated DNA complexation took place in one step. Although the binding constants per nitrogen atom are similar in PBAEs and PEI, the binding constants per polymer molecule are 2 - 68 times smaller lower for PBAEs than for high molecular weight PEIs. This is due to the structure of the PBAEs: the density of N-groups in the polymer chain is much lower than for PEIs. The distance between the N-groups is so long that the co-operativity of binding to DNA is lower than for PEIs. The PBAEs also have lower ratio of primary and secondary amines to tertiary amines compared to PEI. As a consequence, the PBAEs require more N-groups than PEI in order to fully complex DNA. Typically, high N/P ratios of about 50:1 are needed for efficient transfection compared with about 6:1 as used for high molecular weight PEIs [13]. To further modify the function of PBAEs, the end groups of the diacrylate-terminated polymers have been substituted with primary amines [24-26]. This increases the cationic charge of the polymers, improves DNA binding affinity and condensation of DNA into nanoparticles. Such derivative (C32) was highly effective in transfection [24]. In fact, PBAE polymer mediated transfection seems to improve with increasing nanoparticle formation. This may be related to the overall weak DNA binding levels. On the contrary, for tight DNA binders further increase in binding affinity is expected to decrease transfection due to the impaired DNA release in the cells.

One of the crucial steps for efficient gene delivery is the release of DNA from the nanoparticle to the cytosol. Because this process is the reverse reaction of the nanoparticle formation, for PEIs this takes place in two steps. The present results suggest that with PBAEs, this process takes place in one step, but the low DNA binding constants of PBAEs are expected to facilitate DNA release. This process involves exchange reaction in which polycation will bind to the cellular polyanions thereby rendering pDNA free [23]. On longer time scales the degradation of PBAEs in the cells may provide another mechanism for DNA release.

DNA binding affinity and nanoparticle formation efficiency are important parameters for effective non-viral polymeric gene delivery and these parameters can be designed by tuning polymer structure.

5. Conclusions

Recently introduced time-resolved fluorescence assay was applied to estimate the relative efficiency of DNA complexation by poly(β-amino ester)s. The binding constants per amine were in the same order of magnitude for PBAEs and branched 25 kDa PEI, but the overall binding constants per PBAE molecule were ~10 times smaller. This explains why the N/P ratios needed for the formation of DNA:PBAE nanoparticles are ~10 times higher. In contrast with PEI, PBAEs complex DNA in one step, but still they are able to release DNA effectively.

Acknowledgements

This work was supported by the Academy of Finland and by NIH grants CA132091 and CA115527.

References

[1] C.E. Thomas, A. Ehrhardt, M.A. Kay. Progress and problems with the use of viral vectors for gene therapy, Nature Reviews Genetics. 4 (2003) 346-358.

[2] E. Check. Gene therapy put on hold as third child develops cancer, Nature. 433 (2005) 561.

[3] S. Nayak, R.W. Herzog. Progress and prospects: immune responses to viral vectors, Gene Ther. 17 (2010) 295-304.

[4] S. Li, L. Huang. Non-viral is superior to viral gene delivery, J. Control. Rel. 123 (2007) 181-183.

[5] D.W. Pack, A.S. Hoffman, S. Pun, P.S. Stayton. Design and development of polymers for gene delivery, Nat. Rev. Drug Discov.. 4 (2005) 581-593.

[6] O. Boussif, F. LezoualC'H, M.A. Zanta, M.D. Mergny, D. Scherman, B. Demeneix, et al. A versatile vector for gene and oligonucleotide transfer into cells in culture and in vivo: Polyethylenimine, Proc.Natl.Acad.Sci.U.S.A. 92 (1995) 7297-7301.

[7] R.I. Mahato. Water insoluble and soluble lipids for gene delivery, Adv.Drug Deliv.Rev. 57 (2005) 699-712.

[8] J. Pelisek, L. Gaedtke, J. DeRouchey, G.F. Walker, S. Nikol, E. Wagner. Optimized lipopolyplex formulations for gene transfer to human colon carcinoma cells under in vitro conditions, J.Gene Med. 8 (2006) 186-197.

[9] T. Merdan, J. Kopeček, T. Kissel. Prospects for cationic polymers in gene and oligonucleotide therapy against cancer, Adv.Drug Deliv.Rev. 54 (2002) 715-758.

[10] D.M. Lynn, R. Langer. Degradable poly(b-amino esters): Synthesis, characterization, and self-assembly with plasmid DNA, J.Am.Chem.Soc. 122 (2000) 10761-10768.

[11] D.M. Lynn, D.G. Anderson, D. Putnam, R. Langer. Accelerated discovery of synthetic transfection vectors: Parallel synthesis and screening of a degradable polymer library, J.Am.Chem.Soc. 123 (2001) 8155-8156.

[12] A. Akinc, D.M. Lynn, D.G. Anderson, R. Langer. Parallel synthesis and biophysical characterization of a degradable polymer library for gene delivery, J.Am.Chem.Soc. 125 (2003) 5316-5323.

[13] J.J. Green, R. Langer, D.G. Anderson. A combinatorial polymer library approach yields insight into nonviral gene delivery, Acc.Chem.Res. 41 (2008) 749-759.

[14] D.G. Anderson, D.M. Lynn, R. Langer. Semi-automated synthesis and screening of a large library of degradable cationic polymers for gene delivery, Angewandte Chemie - International Edition. 42 (2003) 3153-3158.

[15] E. Vuorimaa, A. Urtti, R. Seppänen, H. Lemmetyinen, M. Yliperttula. Time-resolved fluorescence spectroscopy reveals functional differences of cationic polymer-DNA complexes, J.Am.Chem.Soc. 130 (2008) 11695-11700.

[16] J. Olmsted, D.R. Kearns. Mechanism of ethidium bromide fluorescence enhancement on binding to nucleic acids, Biochemistry (N.Y.). 16 (1977) 3647-3654.

[17] R. Sarkar, S.K. Pal. Interaction of hoechst 33258 and ethidium with histone1 - DNA condensates, Biomacromolecules. 8 (2007) 3332-3339.

[18] T. Ketola, M. Hanzlikova, A. Urtti, H. Lemmetyinen, M. Yliperttula, E. Vuorimaa. Role of Polyplex Intermediate Species on Gene Transfer Efficiency: Polyethylenimine–DNA Complexes and Time-Resolved Fluorescence Spectroscopy, J. Phys. Chem. B 115 (2011) 1895-1902.

[19] J. Yang, P. Zhang, L. Tang, P. Sun, W. Liu, P. Sun, et al. Temperature-tuned DNA condensation and gene transfection by PEI-g-(PMEO2MA-b-PHEMA) copolymer-based nonviral vectors, Biomaterials. 31 (2010) 144-155.

[20] A. Kichler, C. Leborgne, E. Coeytaux, O. Danos. Polyethylenimine-mediated gene delivery: a mechanistic study, J Gene Med. 3 (2001) 135-44.

[21] A. Akinc, M. Thomas, A.M. Klibanov, R. Langer. Exploring polyethylenimine-mediated DNA transfection and the proton sponge hypothesis, J.Gene Med. 7 (2005) 657-663.

[22] N.D. Sonawane, F.C. Szoka Jr, A.S. Verkman. Chloride accumulation and swelling in endosomes enhances DNA transfer by polyamine-DNA polyplexes J.Biol.Chem. 278 (2003) 44826-44831.

[23] Y. Xu, F. Szoka, Jr. Mechanism of DNA Release from Cationic Liposome/DNA Complexes Used in Cell Transfection, Biochemistry 35 (1996) 5616-5623.

[24] J. Sunshine, J. J. Green, K. P. Mahon, F. Yang, A. A. Eltoukhy, D. N. Nguyen, R. Langer, D. G. Anderson. Small-Molecule End-Groups of Linear Polymer Determine Cell-Type Gene-Delivery Efficacy, Adv Mater. 21 (2009) 4947–4951.

[25] J.J. Green, G.T. Zugates, N.C. Tedford, Y.-. Huang, L.G. Griffith, D.A. Lauffenburger, et al. Combinatorial modification of degradable polymers enables transfection of human cells comparable to adenovirus, Adv Mater. 19 (2007) 2836-2842.

[26] G.T. Zugates, N.C. Tedford, A. Zumbuehl, S. Jhunjhunwala, C.S. Kang, L.G. Griffith, et al. Gene delivery properties of end-modified poly(b-amino ester)s, Bioconjug.Chem. 18 (2007) 1887-1896.

Publication IV

The Effect and Role of Carbon Atoms in Poly(β-amino ester)s for DNA Binding and Gene Delivery

Corey J. Bishop, Tiia-Maaria Ketola, Stephany Y. Tzeng, Joel C. Sunshine, Arto Urtti, Helge Lemmetyinen, Elina Vuorimaa-Laukkanen, Marjo Yliperttula and Jordan J. Green, *J. Am. Chem. Soc.* **2013**, *135*, 6951–6957.

Reprinted with permission from *Journal of the American Chemical Society* **2013**, *135*, 6951–6957.

JACS
JOURNAL OF THE AMERICAN CHEMICAL SOCIETY
Article
pubs.acs.org/JACS

The Effect and Role of Carbon Atoms in Poly(β-amino ester)s for DNA Binding and Gene Delivery

Corey J. Bishop,[†,∞] Tiia-Maaria Ketola,[‡] Stephany Y. Tzeng,[†,∞] Joel C. Sunshine,[†,∞] Arto Urtti,[§] Helge Lemmetyinen,[‡] Elina Vuorimaa-Laukkanen,[‡] Marjo Yliperttula,[∥] and Jordan J. Green*[,†,¶,∞,#]

[†]Department of Biomedical Engineering, the [#]Department of Ophthalmology, the [∞]Translational Tissue Engineering Center, and the [¶]Institute for Nanobiotechnology, Johns Hopkins University School of Medicine, 400 North Broadway, Baltimore, Maryland 21231, United States

[‡]Department of Chemistry and Bioengineering, Tampere University of Technology, P.O. Box 541, FI-33101 Tampere, Finland

[§]Division of Biopharmacy and Pharmacokinetics and [∥]Centre for Drug Research, Faculty of Pharmacy, University of Helsinki, Viikinkaari 5E, 00014 Helsinki, Finland

Supporting Information

ABSTRACT: Polymeric vectors for gene delivery are a promising alternative for clinical applications, as they are generally safer than viral counterparts. Our objective was to further our mechanistic understanding of polymer structure–function relationships to allow the rational design of new biomaterials. Utilizing poly(β-amino ester)s (PBAEs), we investigated polymer–DNA binding by systematically varying the polymer molecular weight, adding single carbons to the backbone and side chain of the monomers that constitute the polymers, and varying the type of polymer end group. We then sought to correlate how PBAE binding affects the polyplex diameter and ζ potential, the transfection efficacy, and its associated cytotoxicity in human breast and brain cancer cells in vitro. Among other trends, we observed in both cell lines that the PBAE–DNA binding constant is biphasic with the transfection efficacy and that the optimal values of the binding constant with respect to the transfection efficacy are in the range $(1–6) \times 10^4$ M^{-1}. A binding constant in this range is necessary but not sufficient for effective transfection.

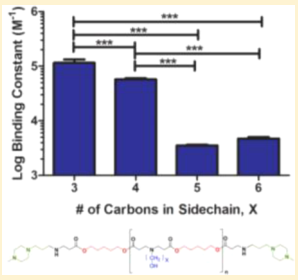

INTRODUCTION

Inheritable diseases and cancer can result from inactive genes (i.e., CFTR in cystic fibrosis or P53 as a tumor suppressor).[1,2] Delivering DNA and small hairpin RNA to encode and generate a functional copy or to inhibit mRNA expression of a nonfunctioning protein can potentially treat and cure many genetic diseases. Viruses have been used as delivery vectors because they are highly efficient in nucleic acid delivery, but they can cause insertional mutagenesis, immunogenic responses, and toxicity.[3] The safety and efficacy of the viral vectors depend on the viral vector type, route of administration, and therapeutic target. To date, only two gene therapy formulations have been approved, one by the State Food and Drug Administration of China (2003) and the other by the European Medicines Agency (2012); there are still no U.S. Food and Drug Administration-approved gene therapies.[4] Degradable cationic polymers are an attractive alternative to viruses, as they are generally safer, are easier to manufacture and mass produce, and have more functional capabilities than viruses.[5] Varying a polymer's structure and functional groups allows one to optimize the nucleic acid delivery properties while minimizing toxicity levels.[6] High-throughput analyses of combinatorial biomaterial libraries allow a vast number of polymers to be screened, but rational design of structure to control function would be more efficient.[7,8]

We are interested in evaluating polymer structure–function relationships to further our mechanistic understanding of polymeric materials for nonviral gene delivery and improve their performance (Scheme 1). We previously investigated poly(β-amino esters) (PBAEs) as biodegradable cationic polymers capable of promoting gene delivery to various types of cells.[9−11] These polymers are promising because of their ability to condense DNA into nanoparticles containing many

Scheme 1. Nanoparticle Formulation and Extracellular and Intracellular Barriers for Successful Gene Delivery

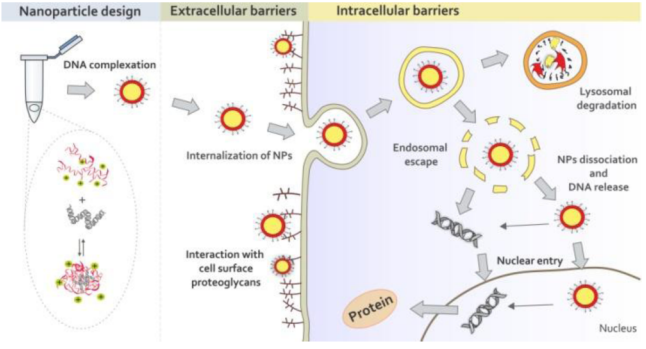

Received: January 9, 2013
Published: April 9, 2013

dx.doi.org/10.1021/ja4002376 | J. Am. Chem. Soc. 2013, 135, 6951−6957

plasmids per particle,[12] facilitate cellular uptake,[13] and mediate endosomal escape.[14,15] Certain PBAE nanoparticles have been shown to be effective for in vivo gene delivery in the eye[16] and to tumors.[17] Despite this progress, the efficiency of gene delivery using polymers remains lower than that for viral delivery. One challenge in evaluating and optimizing polymer structure is that synthetic polymers can be polydisperse, with variable extents of reaction and molecular weight heterogeneity.[18−20] Isolating precise polymer structures with uniform molecular weight is key for enabling the evaluation of polymer structure.

The interactions between a cationic polymer and DNA are critical for facilitating DNA protection, nanoparticle formation, cellular uptake, and subsequent DNA release.[21,22] Anionic phosphate groups on the DNA associate with and bind to positively charged amine groups on cationic polymers, resulting in nucleic acid condensation and protection. This is important because the degradation half-life of naked DNA in the presence of serum is on the order of minutes.[23] Binding with a cationic carrier (i.e., a polymer) can substantially increase the nucleic acid half-life.[24,25] An optimal DNA carrier system should bind, condense, and protect DNA in the extracellular space but release DNA effectively within cells. The design of such systems requires proper understanding of the binding between DNA and polycations.[26,27]

In this work, we used time-resolved fluorescence spectroscopy,[28,29] a new approach for probing polymer−DNA interactions and binding quantitatively. Here we report the results of our systematic investigation of binding properties of DNA and monodisperse, size-fractionated PBAEs with differential structures. In particular, we investigated series of polymers in which the following were varied: molecular weight; the number of carbons in the backbone, which varied the amine density and hydrophobicity; the number of carbons in the side chain, which varied the distance of a hydroxyl group from the backbone and its hydrophobicity; and the end-cap type [primary, secondary, or tertiary amine or no end cap (diacrylate-terminated)]. The effects of these small changes in the polymer structure were characterized by fluorescence spectroscopy and gene delivery efficacy in human brain cancer cells and human breast cancer cells in vitro.[30] The experimental procedures, including materials and methods and the naming convention for the polymers, can be found in the Supporting Information.

RESULTS AND DISCUSSION

Polymer Synthesis and Fractionation. In the 447 polymer series with varying molecular weight (447 Low M_w, 447 Med M_w, and 447 High M_w), the weight-average molecular weights (M_w) were 10.3, 14.7, and 91.6 kDa, respectively, and the polydispersity index (PDI) increased as M_w increased (PDI = 1.3, 1.4, and 2.9, respectively) (Table S1 in the Supporting Information). The average M_w's for the groups in which the backbone, side chain, and end caps were varied were 10 ± 1, 13 ± 2, and 10.9 ± 0.7 kDa, respectively, and the corresponding average PDIs were 1.3 ± 0.1, 1.3 ± 0.1, and 1.34 ± 0.09 (Table S1). The molecular weights of the polymers were determined by gel-permeation chromatography (GPC) (Figure 1). The molecular weights varied considerably for the 447 molecular weight series but were similar for the other polymers. The similarity of the M_w values and the narrow PDIs of the comparable polymers with small differences in the backbone, side chain, and end cap allowed comparisons between the groups and ensured that differences were due to the monomer type as opposed to M_w or size heterogeneity.

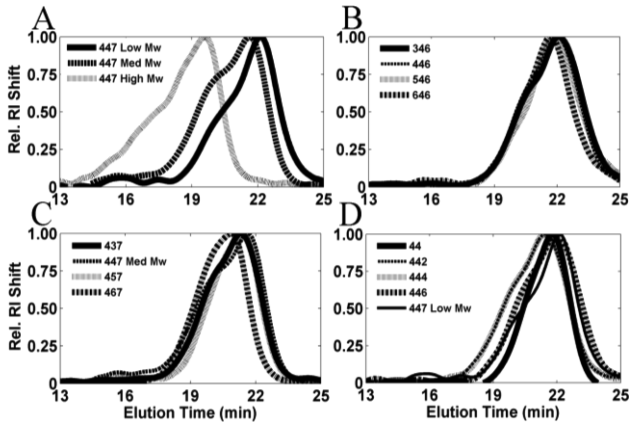

Figure 1. GPC curves of fractionated polymers [relative refractive index (RI) shift (mV/max mV) vs elution time (min)] for groups with varying (A) molecular weight (Low, Med, and High), (B) backbone, (C), side chain, and (D) end caps.

Representative ^{1}H NMR spectra of polymers 44, 442, 444, 446, and 447 can be found in Figure S1 in the Supporting Information.[6]

Binding Constants for Polyplex Formation. The polyplex formation can be monitored by plotting the proportion of bound DNA (B in eq 5 in the Supporting Information) against the concentration of amine. As an example, the plot for polymer 442 is shown in Figure 2. The

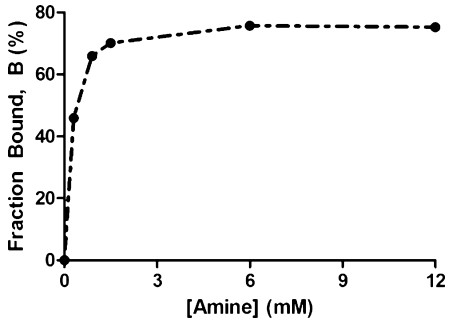

Figure 2. Fraction of bound DNA as a function of amine concentration for polymer 442.

proportion of bound DNA increased with increasing polymer concentration until it reached a saturation limit of approximately 76% at a polymer/DNA weight/weight (w/w) ratio of 24. Most of the PBAE polymers saturated close to 80%. The saturation limits for polymers 44 and 346 were 60% and 96%, respectively. Polymers with negative cooperativity typically have saturation less than 100%, whereas polymers with high positive cooperativity saturate near 100%.

The Hill plots for the 447 molecular weight series are shown in Figure 3A. Similar linear curves with negative cooperativity (Table S1 in the Supporting Information) were obtained for all of the polymers except polymer 646 (Figure 3B−D). The fact that the Hill plots for most of the polymers entailed negative cooperativity and the fact that the bound fraction for most of the polymers saturated close to 80% are in agreement.

While most of the polymers showed a single linear Hill plot, varying the polymer backbone structure (646) enabled a biphasic response (Figure 3B). Polymer 646's Hill plot is

dx.doi.org/10.1021/ja4002376 | J. Am. Chem. Soc. 2013, 135, 6951−6957

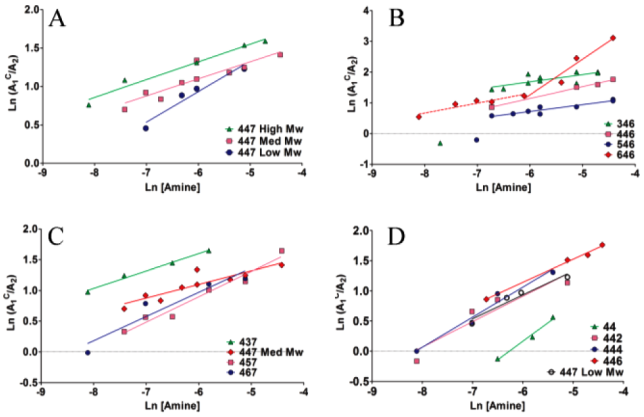

Figure 3. Hill plots for polymer series with varying (A) M_w, (B) backbone, (C) side chain, and (d) end caps.

associated with negative- and positive-cooperativity phases, which may explain why polymer 646 saturated at 96%.

This biphasic nature of binding suggests a change in the binding mechanism increasing amine/phosphate molar ratio (N/P). The analysis and discussion of polymer 646 will focus on the positive-cooperativity slope associated with higher N/P, as all of the other experiments (i.e., transfection, toxicity, diameters, etc.) were carried out at w/w ratios of 30, 60, or 90 (N/P > 35). Polymers 346 and 546 (Figure 3B) have a data point that may be either an outlier or associated with a biphasic binding mechanism similar to that for polymer 646. The fact that there were too few data points in these regions where there may be positive cooperativity for polymers 346 and 546 restricted further analysis. The multiphase cooperativity is an interesting aspect for future investigation.

As the molecular weight of 447 increased, the binding constant per amine (K) increased (Figure 4A). Thus, a larger polymer molecular weight led to increased polymer–DNA interactions and stronger binding. By utilizing this trend, one could potentially fractionate a polymer with a particular molecular weight corresponding to a desired binding constant.

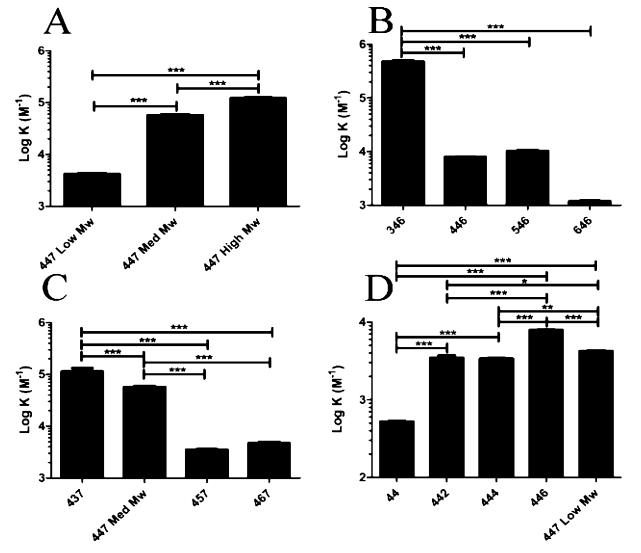

Figure 4. Binding constants (M^{-1}) for the series with varying (A) M_w, (B) backbone, (C) side chain, and (D) end caps. Statistical analysis was accomplished by a one-way ANOVA and a Tukey posthoc analysis: *, $P < 0.05$; **, $P < 0.01$; ***, $P < 0.001$.

When the effect of the number of carbons in the monomer backbone (n_B = 3, 4, 5, or 6) was evaluated, the binding constants decreased as n_B increased (Figure 4B). The binding affinity was reduced 400-fold when n_B increased from 3 to 6. The decrease in the binding constant is likely due to the decrease in amine density with increasing n_B.

The binding constants in the side-chain series (437, 447 Med M_w, 457, 467) decreased with increasing side-chain length n_S (Figure 4C). As the number of carbons in the side chain was increased from 3 to 6, the binding affinity was reduced 24-fold. Again, the decrease in the binding constant is likely due to the decrease in amine density as n_S increases.

The base polymer (polymer 44) had a smaller binding constant than any of the end-capped polymers (442, 444, 446, and 447 Low M_w). The binding constant increased by factors of 6.6 ± 0.1, 15.2, and 8.0 when the base polymer was end-capped using primary (442 and 444), secondary (446), and tertiary amines (447 Low M_w), respectively (Figure 4D). Considering the pK_a values of primary, secondary, and tertiary amines, one would suspect that there would be greater binding for primary versus tertiary amine end caps; however, these differences would be diminished as the buffer pH was 5.2. We observed a larger K value than expected for polymer 446. This larger K value is understandable when the molecular weight of the 446 polymer is considered: the molecular weight of the 446 polymer was 14% higher than the other molecular weights in the end-cap polymer series (Table S1 in the Supporting Information) and thus had 3–5 more amines per polymer strand than the other polymers in the group (the non-end-capped and primary, secondary, and tertiary amine-capped polymers had 40, 39, 44, and 41 amines per polymer strand, respectively).

Comparison of Binding Constant Calculation Methodology. The binding constant of the cationic peptide $(KK)_2KGGC$ was also evaluated to compare our time-resolved fluorescence spectroscopy binding assay to other binding assays found in the literature. The proportion of bound DNA (B in eq 5 in the Supporting Information) as a function of $(KK)_2KGGC$ concentration displayed a saturation level close to 90%. The Hill plot of the peptide presented in Figure S3 in the Supporting Information shows the presence of two phases, similar to the case for polymer 646. The kink point corresponds to a w/w ratio of 3.6. The peptide, perhaps because of the presence of positive cooperativity (at low w/w ratio), was associated with a higher saturation than most of the PBAEs, similar to what was observed with polymer 646. The Hill coefficients of the positive- and negative-cooperativity phases were 2.2 and 0.50, respectively, suggesting that further binding is hindered by the already-bound amines. The overall binding constant K^{α} obtained from the positive-cooperativity phase was $(1.2 \pm 0.2) \times 10^7$ M^{-1}. Plank et al.[21] obtained a value of 2.09×10^6 M^{-1} with this peptide, which is ~6 times smaller than obtained by our method.

Relationship Between Polyplex Diameter and Binding. The mean diameters of the polyplexes (nanoparticles) formed through binding and self-assembly of cationic polymers with anionic DNA ranged from 122 to 227 nm (Figures S4 and S5 in the Supporting Information). While a polymer with one of the smallest binding constants (646, 1.19×10^3 M^{-1}) formed polyplexes of the largest size (227 nm) and the polymer with the largest binding constant (346, 4.8×10^5 M^{-1}) formed polyplexes of the smallest size (122 nm), there was not an overall trend between the PBAE–DNA binding affinity and the

dx.doi.org/10.1021/ja4002376 | J. Am. Chem. Soc. 2013, 135, 6951–6957

polyplex size (Figure S4). For the case of polymer backbone length, there was an apparent decrease in the diameter as the binding constant increased (or as the backbone lengths decrease; Figure S4B). As the backbone length increase, the amine density decreases and the hydrophobicity increases as well.

While an increased binding constant appears to correlate with smaller polyplex diameter, the trend is not very strong, as a range of polymer binding constants and polymer structures can produce polyplexes of similar size (Figure S5A). Our data suggest that tighter binding (i.e., larger binding constant) may but does not necessarily result in smaller polymer/DNA polyplexes. The number of plasmids per polyplex, the number of polymer chains per polyplex, and the association of individual polyplexes with each other in ion-containing buffer solutions can all affect the polyplex size.

The polyplex/particle diameter did not appear to show any clear trend in transfection efficacy for either cell line (Figure S5B and S5C). This finding suggests that the diameter of the polymer/DNA polyplexes is not a key determining factor for this class of PBAE particles in these cell lines. As all of the nanoparticles studied were relatively small in diameter, they should be able to mediate successful endocytic cellular uptake.

Polyplexes were successfully formed at both pH values (5.2 and 7.4) and at various ionic strengths (Figure S6 in the Supporting Information). Under these conditions, the diameters of the polyplexes ranged from approximately 100 to 300 nm, and no significant aggregation was observed (Figure S6).

Relationship Between Polyplex ζ Potential and Binding. The polyplexes' ζ potentials (ZPs) (Figures S7 and S8 in the Supporting Information) ranged from +5 to +18 mV. There were no apparent trends between the binding constant and the ZP (Figures S7 and S8A). In contrast to our cationic ZPs, Eltoukhy et al.[18] found that their PBAEs were neutral in sodium acetate, which is likely explained by the use of different polymer structures as well as formulations with w/w ratios of 20−40, which use less polymer than what was tested in our experiments (w/w ratio = 60). Our nanoparticles were weakly positively charged, allowing interaction with a cell's anionic surface. Their charge was not excessive, and they did not cause high toxicity when added to cells. Comparison of the ZP measurements against transfection efficacies revealed no clear trends for either cell line (Figure S8B,C).

These findings suggest that the ZP of the polymer/DNA particles is not a key determining factor for transfection for this class of PBAE particles in these cell lines. As all of the nanoparticles studied were relatively weakly positive in ZP, they should be able to mediate successful cellular uptake.

The ZP of the polyplexes at both pH values (5.2 and 7.4) and at various ionic strengths ranged from approximately +6 to +25 mV (Figure S9 in the Supporting Information). The ZP appeared to be inversely proportional to pH. At pH 5.2, the ZP decreased as the salt content increased. At pH 7.4, the ZP did not appear to increase in all cases as the salt content decreased (Figure S9). The ZPs at 1:100 dilution were comparable to those for the undiluted case.

Effect of Binding Constant on Transfection Efficacy. Two human cancer cell lines (MDA-MB-231 and GBM319) were utilized in these experiments to evaluate the transfection efficacy. The former is derived from invasive triple-negative human breast cancer and the latter is from human glioblastoma multiforme (GBM). Generally speaking, we found both cell lines to be difficult to transfect, with MDA-MB-231 (Figure 5A,C,E,G) being more difficult to transfect than GBM319 (Figure 5B,D,F,H). The relative amount of enhanced green fluorescent protein (EGFP) per cell according to the normalized mean fluorescence was linearly correlated with the transfection efficacy as measured by percent of cells with EGFP (Figure S10 in the Supporting Information).

The optimal molecular weight of the 447 polymer that resulted in the highest transfection efficacy was polymer 447 Med M_w at a w/w ratio of 90 in both cell lines (Figure 5A,B).

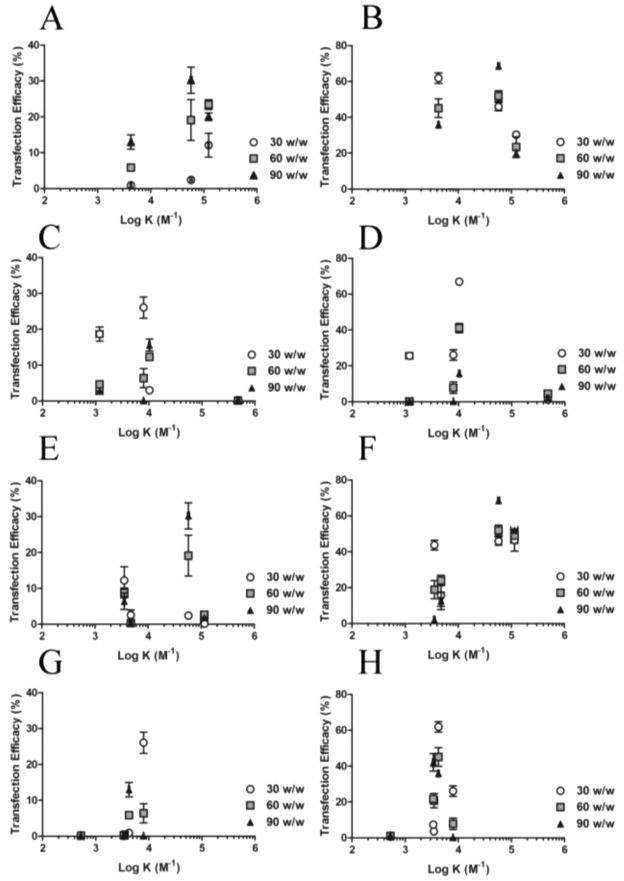

Figure 5. Effect of binding constant on transfection efficacy in (A, C, E, G) MDA-MB-231 cells and (B, D, F, H) GBM319 cells for the series with varying (A, B) M_w, (C, D) backbone, (E, F) side chain, and (G, H) end caps.

By flow cytometry, the 447 Med M_w polymer achieved 30 ± 4% and 69 ± 1% transfection in the MDA-MB-231 and GBM319 cell lines, respectively. In MDA-MB-231 cells, the PBAE nanoparticle formulation with the highest transfection efficacy achieved 74% of the transfection percentage achieved with Lipofectamine 2000, a highly effective positive control widely used in the nonviral gene delivery community; positive and negative controls can be found in Figure S11 in the Supporting Information. In GBM319 cells, the leading PBAE nanoparticles transfected 240% of the amount achieved with Lipofectamine 2000. Naked DNA (i.e., the same dose of plasmid DNA without added polymer) resulted in no transfection in either cell line.

When all of the binding constants were analyzed with the transfection efficacy, a biphasic trend was observed, with the peak transfection occurring at an intermediate binding affinity (Figure S12A,B in the Supporting Information). However, the

dx.doi.org/10.1021/ja4002376 | J. Am. Chem. Soc. 2013, 135, 6951−6957

correlation is not straightforward, as similar binding affinities can also lead to dramatically lower transfection. This is to be expected because binding constants alone are likely insufficient to predict whether a particular polymer will deliver DNA successfully, as there are many factors that affect gene delivery such as cellular uptake, endosomal escape, DNA release, and nuclear import (Scheme 1).[5]

I. Effect of M_w. In the MDA-MB-231 cells, a comparison of the 447 polymers with incremental molecular weight (Figure 5A) revealed a biphasic response, with the highest transfection efficacy occurring at intermediate polymer molecular weight (447 Med M_w) and intermediate binding affinity (58 000 M^{-1}). For the w/w ratio = 30 group, there was an increase in transfection efficacy for the MDA-MB-231 cell line as the molecular weight increased (Figure 5A), whereas there was a decrease for the GMB319 cell line (Figure 5B). Polymer 447 Med M_w with a binding constant of 58 000 M^{-1} was the most effective polymer evaluated in terms of transfection efficacy for the GBM319 cells (Figure 5B). This suggests that there is an optimal range: having a binding constant that is either too small or too large is unfavorable. Polymers with small binding constants may not be able to condense and protect the DNA sufficiently, and ones with excessively large binding constants likely do not release the DNA as efficiently.[22] As the molecular weight increased from 10.3 to 91.6 kDa, the transfection efficacy decreased from approximately 60% to 30% positive cells in the GBM319 cells.

II. Effect of Single Carbon Differences. When the molecular weight was held approximately constant and the backbone and side chain were varied, the optimal binding constant was near 58 000 M^{-1} (polymer 447 Med M_w) for MDA-MB-231 cells (Figure 5C,E), and the transfection was similarly high (~70%) for GBM319 cells for binding constants in the range (1−6) × 10^4 M^{-1} (Figure 5D,F). In cases where the binding constant is smaller than 10^4 M^{-1}, increasing the binding constant correlates with increased transfection efficacy for MDA-MB-231 cells. GBM319 cells are better transfected by polymers with smaller binding constants (10^3−10^4 M^{-1}) than the MDA-MB-231 cells are, and this is likely due to intrinsic differences in the gene delivery transport steps (Scheme 1) for these two cell types. For both cell types, when the binding constant increased further (>10^5 M^{-1}), even at constant molecular weight, transfection decreased.

Although it is common practice to use 10% fetal bovine serum for in vitro transfection experiments, higher media serum content may be more physiologically relevant. When 70% serum was used to assess the transfection efficacy and its correlation with the observed binding constants in the GBM319 cell line, the highest transfection achieved in the presence of high serum was similar to that observed with low serum, approximately 70% of human cells positively transfected. A biphasic trend similar to that under 10% serum conditions was also observed (Figure S13 in the Supporting Information), and a similar optimal range of binding constants, ~10^4 M^{-1}, was able to result in the highest transfection efficacy.

III. Effect of End Caps. The MDA-MB-231 and GBM319 cell lines had very low transfection for the non-end-capped, acrylate-terminated polymer (polymer 44). Furthermore, the primary-amine-capped polymers (polymers 442 and 444) were not able to transfect MDA-MB-231 cells effectively, whereas polymers capped with primary, secondary, and tertiary amines were able to transfect the GB319 cells.

Secondary or tertiary amine end caps, depending on the w/w ratio, were required for effective transfection of the MDA-MB-231 cell line with these polymers. The GBM319 cell line could be successfully transfected via PBAE polymers end-capped with primary amines (442 and 444) in addition to the polymers end-capped with secondary or tertiary amines. However, there did not appear to be a strong trend with the binding constant and transfection efficacy in the end-capped series (Figure 5G,H).

Effect of Binding Constant on Cytotoxicity. In general, the cytotoxicity increased with increasing polymer/DNA w/w ratio (Figure 6). In both cell lines tested, it appeared that there

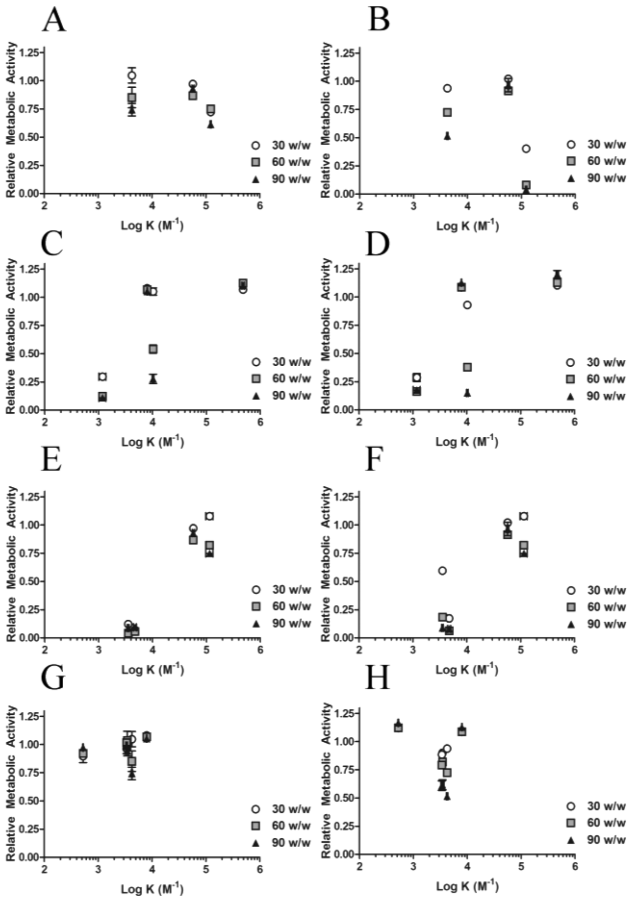

Figure 6. Effect of binding constant on relative metabolic activity in (A, C, E, G) MDA-MB-231 cells and (B, D, F, H) GBM319 cells for the series with varying (A, B) M_w, (C, D) backbone, (E, F) side chain, and (G, H) end caps.

was low cytotoxicity with polymers that had binding constants in the 10^4−10^5 M^{-1} range (Figure S12C,D in the Supporting Information).

I. Effect of M_w. Particle-induced cytotoxicity in both cell lines increased as the binding constant (and M_w) increased (Figure 6A,B). There was relatively less toxicity in the MDA-MB-231 cell line than in the GB319 cell line, especially for the 447 High M_w polymer.

II. Effect of Single Carbon Differences. The cytotoxicity in both cell lines increased as the number of carbons in the backbone or side chain increased. Thus, the cytotoxicity decreased (and the relative metabolic activity increased) as the binding constant increased (Figure 6C−F).

III. Effect of End Caps. There was no significant cytotoxicity in the MDA-MB-231 cell line with the 44, 442, 444, 446, and

dx.doi.org/10.1021/ja4002376 | J. Am. Chem. Soc. 2013, 135, 6951−6957

447 Low end-cap series, whereas there appeared to be some cytotoxicity in the GBM319 cell line with the primary and tertiary amine end caps. Secondary amine end caps may be particularly less cytotoxic in the GBM319 cell line (Figure 6G,H). There was not a clear trend in the relative metabolic activity when the type of end cap was varied.

Heparin Competition Release. The 44 polymer associated with the weakest binding constant (526 M^{-1}) released its DNA with the lowest amount of heparin (<2 μg/mL) (Figure S14 in the Supporting Information). Polymer 447 Low M_w was associated with a binding constant of 4.2×10^3 M^{-1} and released its DNA at a heparin concentration between 16 and 64 μg/mL (Figure S14). The 446 and 447 High M_w polymers were associated with binding constants of 7.97×10^3 and 1.23×10^5 M^{-1}, respectively, and both released their DNA at heparin concentrations between 128 and 256 μg/mL. The 446 polymer exhibited a faint supercoiled DNA band at 128 μg/mL, suggesting that this polymer likely releases its DNA at a lower heparin concentration than does 447 High M_w (Figure S14). The DNA release from the polyplexes appeared to be inversely proportional to the binding affinity between DNA and the polymers.

CONCLUSIONS

Evaluation of polymer−DNA binding constants using time-correlated single-photon counting and comparison of these values to transfection efficacies allowed us to observe that binding constants of $(1-6) \times 10^4$ M^{-1} were optimal for both human cancer cell lines tested. Our data reveal that the polymer−DNA binding affinity for PBAEs is biphasic with respect to transfection efficacy, with an intermediate binding affinity being optimal. A binding constant in the optimal range is necessary but not sufficient for effective transfection. This intermediate binding affinity can be independently tuned by adding single carbons to the backbone or side-chain structure, by varying the monomer ratio during synthesis and/or using GPC fractionation to tune the polymer molecular weight, and by modifying a small-molecule end group used to end-cap a linear polymer. Probing a specific gene delivery bottleneck with a class of polymers that were synthesized to have subtle structural differences has revealed new quantitative and mechanistic insights concerning how they function for gene delivery.

ASSOCIATED CONTENT

Supporting Information

Materials and methods; ^{1}H NMR spectra of polymers 44, 442, 444, 446, and 447 (Figure S1); decay-associated spectra (Figure S2); lists of M_n, M_w, PDI, degree of polymerization, Hill coefficient, K, diameter, and ZP for the studied polymers (Table S1); peptide Hill plot (Figure S3); plots of diameter versus binding constant for various polymer series (Figure S4); plots of diameter versus binding constant and transfection efficacy versus diameter (Figure S5); figure of polyplex diameters at various pHs and ionic strengths (Figure S6); plots of ZP versus binding constant for various polymer series (Figure S7); plots of ZP versus binding constant and of transfection efficacy versus ZP (Figure S8); figure of polyplex ZP at various pHs and ionic strengths (Figure S9); correlations between geometric and arithmetic mean fluorescences (FL1-A) and percent positive transfection efficacies in both cell lines (Figure S10); positive and negative controls for transfection and relative metabolic activity (Figure S11); plots of binding constants and relative metabolic activities versus transfection efficacy (Figure S12); plot of transfection efficacy versus binding constant in 70% serum for the GBM319 cell line (Figure S13); and heparin release competition assay via gel electrophoresis (Figure S14). This material is available free of charge via the Internet at http://pubs.acs.org.

AUTHOR INFORMATION

Corresponding Author

green@jhu.edu

Notes

The authors declare no competing financial interest.

ACKNOWLEDGMENTS

A Natural Science Foundation Graduate Research Fellowship and Nordic Research Opportunity Grant DGE-0707427 to C.J.B. are acknowledged. This work was supported in part by the National Institutes of Health (R01EB016721-01 and R21CA152473), Tekes PrinCell II 40050/09 Finland, and the Academy of Finland. The authors thank the Microscopy and Imaging Core Module of the Wilmer Core Grant (EY001765). We acknowledge Martina Hanzlikova for Scheme 1.

REFERENCES

(1) Nielsen, L. L.; Maneval, D. C. *Cancer Gene Ther.* **1998**, *5*, 52.
(2) Ziady, A. G.; Kelley, T. J.; Milliken, E.; Ferkol, T.; Davis, P. B. *Mol. Ther.* **2002**, *5*, 413.
(3) Thomas, M.; Klibanov, A. M. *Appl. Microbiol. Biotechnol.* **2003**, *62*, 27.
(4) Pearson, S.; Jia, H. P.; Kandachi, K. *Nat. Biotechnol.* **2004**, *22*, 3.
(5) Sunshine, J. C.; Bishop, C. J.; Green, J. J. *Ther. Delivery* **2011**, *2*, 493.
(6) Sunshine, J. C.; Akanda, M. I.; Li, D.; Kozielski, K. L.; Green, J. J. *Biomacromolecules* **2011**, *12*, 3592.
(7) Green, J. J. *Ann. Biomed. Eng.* **2012**, *40*, 1408.
(8) Green, J. J.; Langer, R.; Anderson, D. G. *Acc. Chem. Res.* **2008**, *41*, 749.
(9) Shmueli, R. B.; Sunshine, J. C.; Xu, Z. H.; Duh, E. J.; Green, J. J. *Nanomedicine (New York)* **2012**, *8*, 1200.
(10) Sunshine, J.; Green, J. J.; Mahon, K. P.; Yang, F.; Eltoukhy, A. A.; Nguyen, D. N.; Langer, R.; Anderson, D. G. *Adv. Mater.* **2009**, *21*, 4947.
(11) Tzeng, S. Y.; Guerrero-Cazares, H.; Martinez, E. E.; Sunshine, J. C.; Quinones-Hinojosa, A.; Green, J. J. *Biomaterials* **2011**, *32*, 5402.
(12) Bhise, N. S.; Shmueli, R. B.; Gonzalez, J.; Green, J. J. *Small* **2012**, *8*, 367; Corrigendum: **2012**, *8*, 1129.
(13) Akinc, A.; Lynn, D. M.; Anderson, D. G.; Langer, R. *J. Am. Chem. Soc.* **2003**, *125*, 5316.
(14) Akinc, A.; Langer, R. *Biotechnol. Bioeng.* **2002**, *78*, 503.
(15) Sunshine, J. C.; Peng, D. Y.; Green, J. J. *Mol. Pharmaceutics* **2012**, *9*, 3375.
(16) Sunshine, J. C.; Sunshine, S. B.; Bhutto, I.; Handa, J. T.; Green, J. J. *PloS One* **2012**, *7*, No. e37543.
(17) Huang, Y. H.; Zugates, G. T.; Peng, W.; Holtz, D.; Dunton, C.; Green, J. J.; Hossain, N.; Chernick, M. R.; Padera, R. F., Jr.; Langer, R.; Anderson, D. G.; Sawicki, J. A. *Cancer Res.* **2009**, *69*, 6184.
(18) Eltoukhy, A. A.; Siegwart, D. J.; Alabi, C. A.; Rajan, J. S.; Langer, R.; Anderson, D. G. *Biomaterials* **2012**, *33*, 3594.
(19) Wang, J.; Gao, S. J.; Zhang, P. C.; Wang, S.; Mao, M. Q.; Leong, K. W. *Gene Ther.* **2004**, *11*, 1001.
(20) Zelikin, A. N.; Trukhanova, E. S.; Putnam, D.; Izumrudov, V. A.; Litmanovich, A. A. *J. Am. Chem. Soc.* **2003**, *125*, 13693.
(21) Plank, C.; Tang, M. X.; Wolfe, A. R.; Szoka, F. C., Jr. *Hum. Gene Ther.* **1999**, *10*, 319.
(22) Schaffer, D. V.; Fidelman, N. A.; Dan, N.; Lauffenburger, D. A. *Biotechnol. Bioeng.* **2000**, *67*, 598.

(23) Leong, K. W.; Mao, H. Q.; Truong-Le, V. L.; Roy, K.; Walsh, S. M.; August, J. T. *J. Controlled Release* **1998**, *53*, 183.
(24) Tam, P.; Monck, M.; Lee, D.; Ludkovski, O.; Leng, E. C.; Clow, K.; Stark, H.; Scherrer, P.; Graham, R. W.; Cullis, P. R. *Gene Ther.* **2000**, *7*, 1867.
(25) Yu, R. Z.; Geary, R. S.; Leeds, J. M.; Watanabe, T.; Fitchett, J. R.; Matson, J. E.; Mehta, R.; Hardee, G. R.; Templin, M. V.; Huang, K.; Newman, M. S.; Quinn, Y.; Uster, P.; Zhu, G.; Working, P. K.; Horner, M.; Nelson, J.; Levin, A. A. *Pharm. Res.* **1999**, *16*, 1309.
(26) Green, J. J.; Zugates, G. T.; Tedford, N. C.; Huang, Y. H.; Griffith, L. G.; Lauffenburger, D. A.; Sawicki, J. A.; Langer, R.; Anderson, D. G. *Adv. Mater.* **2007**, *19*, 2836.
(27) van der Aa, M. A. E. M.; Huth, U. S.; Hafele, S. Y.; Schubert, R.; Oosting, R. S.; Mastrobattista, E.; Hennink, W. E.; Peschka-Suss, R.; Koning, G. A.; Crommelin, D. J. A. *Pharm. Res.* **2007**, *24*, 1590.
(28) Ketola, T. M.; Hanzlikova, M.; Urtti, A.; Lemmetyinen, H.; Yliperttula, M.; Vuorimaa, E. *J. Phys. Chem. B* **2011**, *115*, 1895.
(29) Vuorimaa, E.; Ketola, T. M.; Green, J. J.; Hanzlikova, M.; Lemmetyinen, H.; Langer, R.; Anderson, D. G.; Urtti, A.; Yliperttula, M. *J. Controlled Release* **2011**, *154*, 171.
(30) Vuorimaa, E.; Urtti, A.; Seppanen, R.; Lemmetyinen, H.; Yliperttula, M. *J. Am. Chem. Soc.* **2008**, *130*, 11695.

The Effect and Role of Carbon Atoms in Poly(beta-amino ester)s for DNA Binding and Gene Delivery

Corey J. Bishop, Tiia-Maaria Ketola, Stephany Y. Tzeng, Joel C. Sunshine, Arto Urtti, Helge Lemmetyinen, Elina Vuorimaa-Laukkanen, Marjo Yliperttula, Jordan J. Green

Experimental Procedure

I. Materials (*Reagents, assays, cells and instruments*)

The polymers were synthesized from commercially available monomers: 1,3-propanediol diacrylate (B3) (Monomer-Polymer and Dajac Laboratories Inc.), 1,4-butanediol diacrylate (B4) (Alfa Aesar), 1,5-pentanediol diacrylate (B5) (Monomer-Polymer and Dajac Laboratories Inc.), 1,6-hexanediol diacrylate (B6) (Alfa Aesar), 3-amino-1-propanol (S3), 4-amino-1-butanol (S4) (Alfa Aesar), 5-amino-1-pentanol (S5) (Alfa Aesar), 6-amino-1-hexanol (S6) (Sigma Aldrich), 2,2-dimethyl-1,3-propanediamine (E2) (Sigma Aldrich), 2-methyl-1,5-diaminopentane (E4) (TCI America), 2-(3-aminopropylamino)ethanol (E6) (Sigma Aldrich), 1-(3-aminopropyl)-4-methylpiperazine (E7) (Alfa Aesar). Other reagents include the following and were used as received: peptide $(KK)_2KGGC$ (Biomatik), tetrahydrofuran (THF) (Sigma Aldrich), dimethyl sulfoxide (DMSO), (Sigma Aldrich), ethidium bromide (ETB; Sigma Aldrich), Lipofectamine™ 2000 (Invitrogen, Carlsbad, CA), OptiMEM I (Invitrogen), plasmid enhanced green fluorescent protein (pEGFP-N1) DNA (Clontech), amplified and purified by Aldevron (Fargo, ND). The breast cancer cell line (MDA-MB-231; ATCC) is of human origin and was cultured using DMEM high glucose 1x media and supplemented with 10% heat inactivated fetal bovine serum (FBS) and 100 U/mL of penicillin and 100 μg/mL of streptomycin (Invitrogen). The glioblastoma multiforme (GBM) cell line (GBM319) was derived from brain tumor stem cells from a 79-year old patient, was cultured as previously described in DMEM:Ham's F12 (1:1) (Invitrogen) supplemented with 10% heat inactivated FBS and 1x Antibiotic-Antimycotic (Invitrogen).[1] All cells were cultured in a humid 37°C and 5% CO_2 atmosphere. Propidium iodide (PI) (Invitrogen), 25 mM sodium acetate buffer (NaAc, pH=5.2) (Sigma Aldrich), CellTiter® Aqueous One Solution Cell Proliferation Assay (Promega), Gel Permeation Chromatography (GPC) (Waters®, Breeze 2 software), a Bruker nuclear magnetic resonance (NMR) spectrometer, UV-Vis Spectrometer (Synergy2, BioTek®, Gen5 software), and a BD Accuri™ C6 flow cytometer equipped with HyperCyt® (Intellicyt Corp.) for high-throughput were used following manufacturer instructions. A Visi-Blue™ Transilluminator was used for imaging agarose gels. The single photon counting instrumentation consisted of a PicoQuant GmBH, PicoHarp 300 controller and a PDL 800-B driver.

II. Methods

Polymer Synthesis and Fractionation

Diacrylate monomers that form the polymer backbones (B3, B4, B5, B6) and amine monomers that form the polymer side chains (S3, S4, S5, S6) were mixed neat using 1.05:1, 1.2:1, or 1.4:1 mole ratios and endcapped as previously described with slight modification (E2, E4, E6, E7) (Scheme S1).[2] Briefly, the base polymer (diacrylate and side chain) reactions were carried out for 24 hours at 90°C, solvated in THF and endcapped for 1 hr using a 0.5 M amine monomer solution. Subsequently, the polymers were purified in anhydrous diethyl ether and vacuum dried for at least 24 hours and then fractionated by gel permeation chromatography (Waters Corp.,

Milford MA) using THF Styragel columns (3 7.8 x 300 mm in series). Two minute time fractions were collected at a 1 mL/min flow rate and again ether purified and vacuum dried for 48 hours. The polymers were then solvated in anhydrous DMSO to 100 mg/mL and stored at -20°C in small aliquots to minimize freeze-thaw cycles. GPC was used to assess molecular weight of the fractionated polymers. Synthetic PBAE polymers are referred to by the order of their constituent monomers: backbone acrylate monomer, side chain amine monomer, and end group amine monomer. For example, B4-S4-E7 is 447 as an abbreviation (Scheme S1).

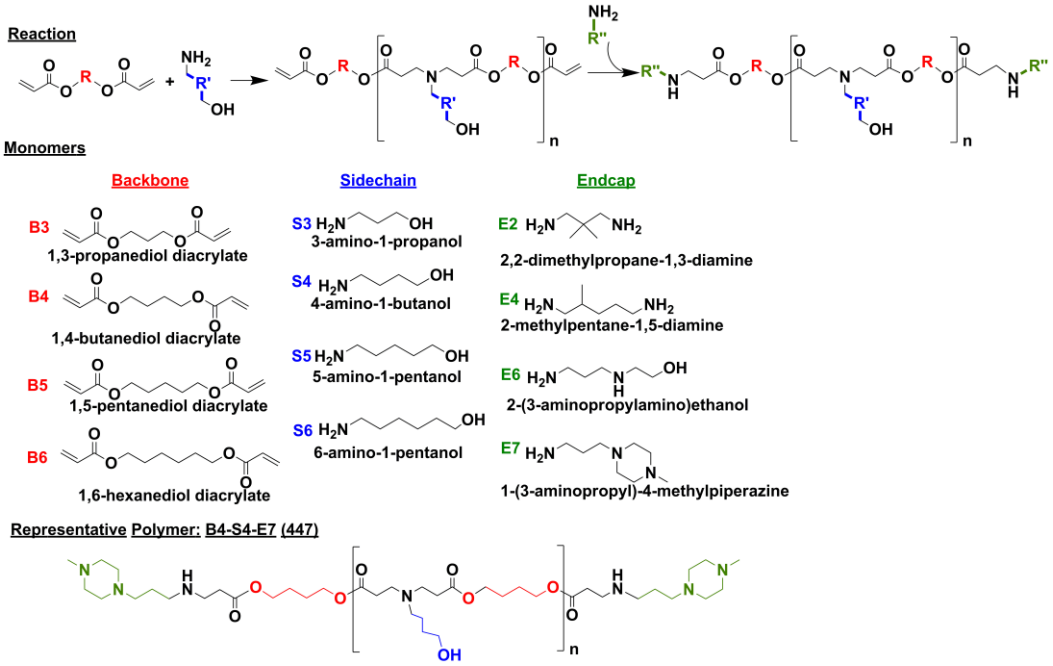

Scheme S1. Reaction of PBAE synthesis; backbone (B3-6), sidechain (s3-6) and various endcap (E2, E4, E6, E7) monomers used in the PBAE library. A representative polymer (447) is shown.

Nuclear Magnetic Resonance

Representative acrylate-terminated base polymers and amine-terminated end-capped polymers were analyzed via ^{1}H NMR. Polymers designated as "ether-purified" were synthesized in THF (or, in the case of 44 base polymer, dissolved in THF without reaction) and then precipitated into diethyl ether as described. After 48 hr drying under vacuum, polymers were dissolved in deuterated chloroform ($CDCl_3$) with 0.03% v/v tetramethylsilane (TMS) at 10-20 mg/mL. Other 44 base polymers were not purified after neat synthesis and were similarly dissolved in $CDCl_3$ with TMS. All spectra were obtained with Bruker instruments (400 MHz, Topspin 2.0 or 2.1 software) and analyzed with NMR Processor v.12 (ACD Labs, Toronto, Canada).[2]

Fluorescence Measurements

Plasmid DNA encoding enhanced green fluorescent protein (pEGFP) at 0.0975 mg/mL (300 µM of phosphate concentration) was added to ETB (20 µM) in a 15:1 mole ratio in 250 µL of 25 mM sodium acetate (NaAc, pH 5.2). The resulting intercalated DNA-ETB complex was a homogeneous pink color. Subsequently, 250 µL of each polymer was added to the resulting solution in polymer weight to DNA weight ratio (w/w) ranging from 1.2 to 47 w/w (N/P ratios ranging from 1 to 40) and was immediately mixed thoroughly. The polyplexes were allowed to stabilize for 10 minutes before beginning fluorescence measurements. The time-resolved fluorescence was measured by a time-correlated single photon counting (TCSPC) system (PicoQuant GmBH) consisting of a PicoHarp 300 controller and a PDL 800-B driver. The samples were excited with the pulsed diode laser head

LDH-P-C-485 at 483 nm with 130 ps time resolution. The signals were detected with a microchannel plate photomultiplier tube (Hamamatsu R2809U). To diminish the influence of the scattered excitation, a cut-off filter was used in front of the monitoring monochromator. To study the decay associated spectra (DAS), the decays were collected with a constant accumulation time in the 560–670 nm wavelength range with 10 nm increments. The decays were simultaneously fitted to the sum of two exponents in the equation (1):

$$I(t,\lambda) = a_1(\lambda)e^{-t/\tau_1} + a_2(\lambda)e^{-t/\tau_2} \quad (1)$$

where τ_i is the global lifetime and $a_i(\lambda)$ is the local amplitude at a particular wavelength. The factors $a_i(\lambda)$ represent the DAS (Figure S2), which in the case of a mixture of different non-interacting fluorescing species corresponds to the individual spectra of the species (ETB bound to DNA and ETB free in solution). The photomultiplier tube becomes increasingly less sensitive at higher wavelengths which was taken into account. The spectral areas (A_i) of the components can be calculated by integrating the pre-exponential factors over the measured wavelength range as indicated in the following equation:

$$A_i = \int a_i(\lambda)d\lambda \quad (2)$$

The short-living component, corresponding to free ETB in the bulk solution, has a lower fluorescence quantum yield than the long-living component corresponding to ETB bound to DNA. The relative fluorescence quantum yield of the short-living component, ϕ_{rel} = 0.112 (equation 3), was calculated from the steady state absorption (UV-VIS spectrophotometer Shimadzu UV-3600) and fluorescence (Fluorolog Yobin Yvon-SPEX, l_{ex} = 483 nm) spectra according to the following equation:

$$\phi_{rel} = \frac{\phi_{ETB}}{\phi_{DNA-ETB}} = \frac{I_{ETB}A_{DNA-ETB}}{I_{DNA-ETB}A_{ETB}} \quad (3)$$

where ϕ_{ETB} is the quantum yield of ETB free in solution, $\phi_{DNA\text{-}ETB}$ is the quantum yield of the DNA-ETB complex, I_i is the area of the fluorescence spectra with an excitation wavelength of 483 nm and A_i is the absorbance at a wavelength of 483 nm. The corrected spectral area (A_i^c) for the short living component is obtained by dividing A_i by ϕ_{rel}. As polymer (P) is added to the DNA-ETB complex, the polymer binds DNA and the ETB is freed into solution as follows:

$$\text{DNA-ETB} + \text{P} \rightleftharpoons \text{DNA-P} + \text{ETB} \quad (4)$$

The proportion of the short-living decay component of the total area of the DAS spectra, B, is the proportion or ratio of free ETB and is directly proportional to the amount of formed polyplexes (or the fraction of DNA bound to polymer). Thus, the bound fraction of DNA, B, can be assessed by monitoring the ratio of free ETB and can be calculated from the spectral areas of the components as follows:

$$B = \frac{A_1^c}{A_1^c + A_2} \quad (5)$$

The bound fraction of DNA as a function of amine concentration was assessed and the maximum was determined. All data points up to the maximum bound fraction were used to determine the binding constants. Of note, the initial concentration of ETB in the system is chosen such that without polymer there is no free ETB.

Binding Constant Calculation

The Hill plot equation for multivalent ligands binding to multi-subunit substrates was used to estimate the cooperativity and binding constants for the polyplex formation[3-6]:

$$\ln \frac{A_1^c}{A_2} = \alpha \ln [P] + \alpha \ln K \quad (6)$$

K^{α} is the overall binding constant for the reaction DNA + nP ⇌ DNA-P_n, K is the binding constant for the binding of one functional amine group according to the reaction DNA-P_{x-1} + P ⇌ DNA-P_x (X = 1, 2, …, n) and the slope of the Hill plot, α, is the experimental Hill´s coefficient (α = 1 for non-cooperative systems, α < 1 for negative cooperativity and α > 1 for positive cooperativity). The error in K is calculated from the standard error of the y-value in the linearly fitted Hill plots.

Particle Diameter and Zeta Potential

Particle diameter was determined by nanoparticle tracking analysis (NTA) using a NanoSight NS500 (Amesbury, UK, 532 nm laser), and zeta potential was determined using a Malvern Zetasizer Nano ZS (Malvern Instruments, UK, detection angle 173°, 633 nm laser) in triplicate. Polymer/DNA nanoparticles were made at a 60 w/w ratio in 25 mM sodium acetate buffer (pH = 5.2) at a DNA concentration of 0.005 mg/ml and diluted into 1x PBS, pH 7.4. Particles were diluted 100-fold into PBS before NTA measurement. Particles were diluted 5-fold into PBS when using the Zetasizer; average electrophoretic mobilities were measured at 25°C, and zeta potentials (ZP) were analyzed using the Smoluchowski model. Additional experiments of representative polyplexes were conducted at concentrations comparable to delivery conditions at various pHs (5 and 7.4) and various ionic strengths (150, 75, 38, 19 mM) using dynamic light scattering (Malvern Instruments, UK).

Transfection and Cytotoxicity (Relative Metabolic Activity)

MDA-MB-231 and GBM319 cells were seeded in 96-well plates at 15,000 cells per well and allowed to adhere overnight at 37°C and 5% CO_2. Polymers and DNA were diluted in 25 mM NaAc and mixed in a 1:1 v/v ratio at 30, 60, and 90 w/w. Particles were allowed to self-assemble for 10 minutes prior to *in vitro* delivery. Subsequently, 20 µL of particle solution was delivered to each well already containing 100 µL of media (10% or 70% serum) for a DNA dosage of 600 ng/well (5 µg/mL) in quadruplicate. Naked DNA at the same final concentration in 25 mM sodium acetate and an untreated group were used as negative controls. Lipofectamine 2000 was used as a positive control to deliver 100 and 200 ng of DNA per well using a 2.5:1 v/w ratio (Lipofectamine reagent:DNA) in quadruplicates (following manufacturer recommendations). After 4 hours of incubation, the wells were aspirated and replenished with fresh media. To assess relative metabolic activity as an indication of toxicity at 24 hours post-delivery, each of the wells were aspirated and incubated with 110 µL of a 10:1 mixture of culture media to CellTiter 96® Aqueous One Solution in quadruplicate according to the manufacturer's instructions. The absorbance at 490 nm was measured using the Synergy2 UV-Vis spectrometer.

Flow Cytometry

The transfection efficacy was assessed using flow cytometry at 48 hours post-delivery. The 96-well plates were aspirated, washed with PBS, and trypsinized. After quenching with 2% FBS (in PBS) with propidium iodide (PI) at 1:200 v/v, the contents were transferred to a round-bottom 96-well plate and centrifuged at 800 RPM for 5 minutes. After centrifuging, all but 30 µL of buffer was removed, and each cell pellet was triturated before loading on the Hypercyt high-throughput reader. FlowJo (v. 7.6) was used for gating and further analysis. Singlets were identified using FSC-H vs SSC-H; dying cells were identified with PI (a DNA intercalator which fluoresces with a

compromised cell membrane) using FSC-H vs FL3-H; FL1-H vs FL3-H was used to identify the GFP-positive population.

Geometric and arithmetic fluorescence means of the flow cytometer's FL1-A channel can be an indicator of the relative amount of EGFP present on a per cell basis. Normalized fluorescence means of the FL1-A channel were calculated by dividing the viable singlet population's FL1-A mean fluorescence by the untreated conditions' mean fluorescence.

Heparin Competition Release Assay

Gel electrophoresis was accomplished using 1% agarose gels containing 1 μg/mL of ETB in a 1x TAE buffer. The gels were loaded with 15 μL of polyplexes at 60 w/w (pEGFP-N1 of 0.01 mg/mL). The polyplexes were allowed to stabilize for 10 minutes. Just prior to the loading the polyplexes were added to glycerol (30% v/v). The gels were run for 1 hour using 100 volts and imaged using a Visi-Blue™ Transilluminator. Four representative polymers ranging from the weakest to the strongest binding constants were used for the release assay (44, 447 Low M_w, 446, 447 High M_w).

Statistics

All binding constants are reported as previously described; transfection and toxicity plots show the mean and standard error of the mean. All other physical characterizations and data plotted show the mean and standard deviation. One-way ANOVA tests were used with Tukey post-hoc analyses to assess significance between multiple groups. Differences were considered significant with p-values < 0.05 (* < 0.05, ** < 0.01, *** < 0.001).

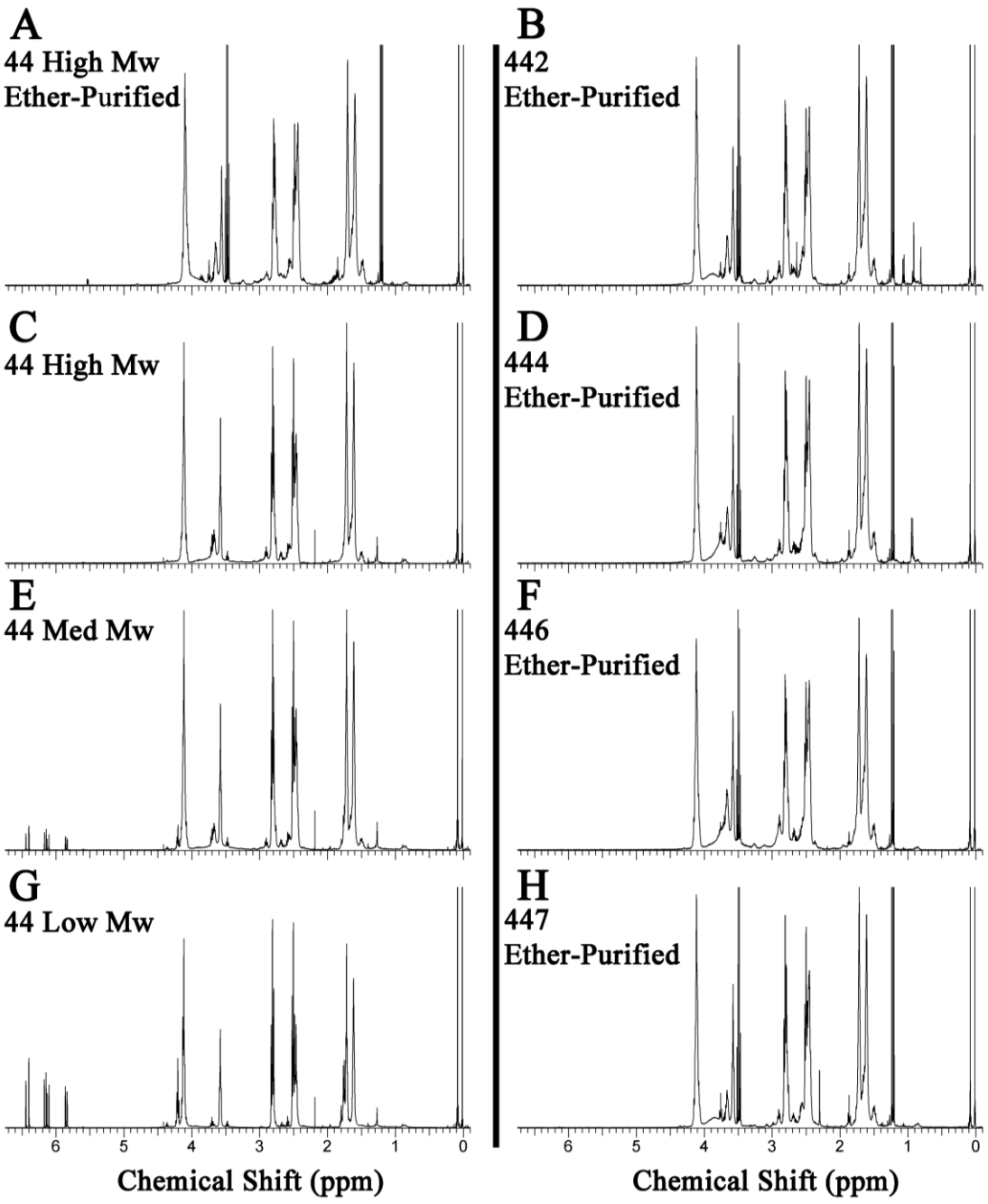

Figure S1. ^{1}H NMR spectra of polymers 44 High (A, C), Med (E), Low M_w (G), 442 (B), 444 (D), 446 (F), and 447 (H). These spectra are consistent with NMR analyses published previously (Sunshine, Akanda, et al.) along with spectra of the other polymers used in this study.[2] (See below for further peak analyses.)

Nuclear Magnetic Resonance Spectra

Some of the spectra above include the following sharp peaks corresponding to the solvent in which the polymer was synthesized (tetrahydrofuran, THF) or diethyl ether, used to precipitate the polymer:

THF: 1.85 ppm
Diethyl ether: 3.45-3.55 ppm (q, $CH_3C\boldsymbol{H_2}OC\boldsymbol{H_2}CH_3$)

Diethyl ether: 3.15-3.25 ppm (t, C***H***$_3$CH$_2$OCH$_2$C***H***$_3$)

Solvent peaks were not considered during analysis. Shown in the spectra below:

<u>44 (B4-S4) (all molecular weights)</u>
1.45-1.6 (m, NCH$_2$C***H***$_2$CH$_2$CH$_2$OH and NCH$_2$CH$_2$C***H***$_2$CH$_2$OH)
1.6-1.75 (t, COOCH$_2$C***H***$_2$C***H***$_2$CH$_2$OOC)
2.35-2.6 (t, COOC***H***$_2$CH$_2$NCH$_2$C***H***$_2$OOC and t, NC***H***$_2$CH$_2$CH$_2$CH$_2$OH)
2.7-2.85 (t, COOCH$_2$C***H***$_2$NC***H***$_2$CH$_2$OOC)
3.55-3.7 (t, NCH$_2$CH$_2$CH$_2$C***H***$_2$OH)
4.0-4.2 (t, COOC***H***$_2$CH$_2$CH$_2$C***H***$_2$OOC)
5.8-5.9 (d, CH$_2$OOCCH=C***H***H)
6.1-6.2 (dd, CH$_2$OOCC***H***=CHH)
6.35-6.5 (d, CH$_2$OOCCH=CH***H***)

<u>442 (B4-S4-E2)</u>
0.9-0.95 (s, NHCH$_2$C(CH$_3$)$_2$CH$_2$NH$_2$)
1.45-1.6 (m, NCH$_2$C***H***$_2$CH$_2$CH$_2$OH and NCH$_2$CH$_2$C***H***$_2$CH$_2$OH)
1.6-1.75 (t, COOCH$_2$C***H***$_2$C***H***$_2$CH$_2$OOC)
2.35-2.6 (t, COOC***H***$_2$CH$_2$NCH$_2$C***H***$_2$OOC and t, NC***H***$_2$CH$_2$CH$_2$CH$_2$OH and
t, NHC***H***$_2$C(CH$_3$)$_2$C***H***$_2$NH$_2$)
2.7-2.85 (t, COOCH$_2$C***H***$_2$NC***H***$_2$CH$_2$OOC)
3.55-3.7 (t, NCH$_2$CH$_2$CH$_2$C***H***$_2$OH)
4.0-4.2 (t, COOC***H***$_2$CH$_2$CH$_2$C***H***$_2$OOC)

<u>444 (B4-S4-E4)</u>
0.9-1.0 (m, NCH$_2$CH$_2$C***H***$_2$CH(C***H***$_3$)CH$_2$N)
1.45-1.6 (m, NCH$_2$C***H***$_2$CH$_2$CH$_2$OH and NCH$_2$CH$_2$C***H***$_2$CH$_2$OH and NCH$_2$C***H***$_2$CH$_2$C***H***(CH$_3$)CH$_2$N)
1.6-1.75 (t, COOCH$_2$C***H***$_2$C***H***$_2$CH$_2$OOC)
2.35-2.5 (t, COOC***H***$_2$CH$_2$NCH$_2$C***H***$_2$OOC and t, NC***H***$_2$CH$_2$CH$_2$CH$_2$OH and
m, NC***H***$_2$CH$_2$CH$_2$CH(CH$_3$)C***H***$_2$N)
2.7-2.85 (t, COOCH$_2$C***H***$_2$NC***H***$_2$CH$_2$OOC)
3.55-3.7 (t, NCH$_2$CH$_2$CH$_2$C***H***$_2$OH)
4.0-4.2 (t, COOC***H***$_2$CH$_2$CH$_2$C***H***$_2$OOC)

<u>446 (B4-S4-E6)</u>

1.45-1.6 (m, NCH$_2$C***H***$_2$CH$_2$CH$_2$OH and NCH$_2$CH$_2$C***H***$_2$CH$_2$OH)
1.6-1.75 (t, COOCH$_2$C***H***$_2$C***H***$_2$CH$_2$OOC and quin, NCH$_2$C***H***$_2$CH$_2$NHCH$_2$CH$_2$OH)
2.35-2.6 (t, COOC***H***$_2$CH$_2$NCH$_2$C***H***$_2$OOC and t, NC***H***$_2$CH$_2$CH$_2$CH$_2$OH and
m, NC***H***$_2$CH$_2$C***H***$_2$NHC***H***$_2$CH$_2$OH)
2.7-2.85 (t, COOCH$_2$C***H***$_2$NC***H***$_2$CH$_2$OOC)
3.55-3.7 (t, NCH$_2$CH$_2$CH$_2$C***H***$_2$OH and t, NCH$_2$CH$_2$CH$_2$NHCH$_2$C***H***$_2$OH)
4.0-4.2 (t, COOC***H***$_2$CH$_2$CH$_2$C***H***$_2$OOC)

447 (B4-S4-E7)

1.45-1.6 (m, $NCH_2C\boldsymbol{H_2}CH_2CH_2OH$ and $NCH_2CH_2C\boldsymbol{H_2}CH_2OH$ and
t, $NCH_2C\boldsymbol{H_2}CH_2N<(CH_2CH_2)_2>NCH_3$)

1.6-1.75 (t, $COOCH_2C\boldsymbol{H_2}C\boldsymbol{H_2}CH_2OOC$)

2.3 (s, $NCH_2CH_2CH_2N<(CH_2CH_2)_2>NC\boldsymbol{H_3}$)

2.35-2.6 (t, $COOC\boldsymbol{H_2}CH_2NCH_2C\boldsymbol{H_2}OOC$ and t, $NC\boldsymbol{H_2}CH_2CH_2CH_2OH$ and m, $NC\boldsymbol{H_2}CH_2C\boldsymbol{H_2}N<(C\boldsymbol{H_2}C\boldsymbol{H_2})_2>NCH_3$)

2.7-2.85 (t, $COOCH_2C\boldsymbol{H_2}NC\boldsymbol{H_2}CH_2OOC$)

3.55-3.7 (t, $NCH_2CH_2CH_2C\boldsymbol{H_2}OH$)

4.0-4.2 (t, $COOC\boldsymbol{H_2}CH_2CH_2C\boldsymbol{H_2}OOC$)

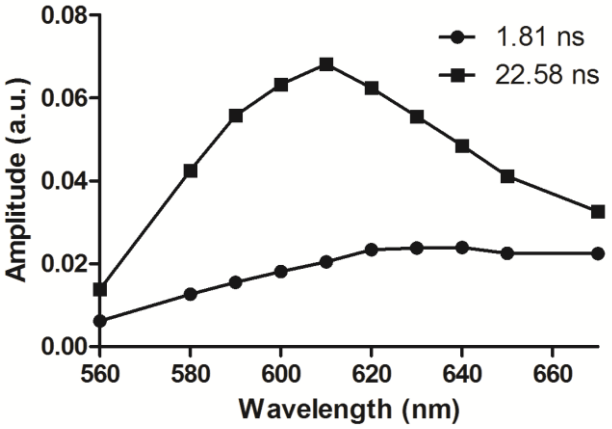

Figure S2. Decay-associated spectra. The fluorescence lifetimes of ethidium bromide bound to DNA and free in the solution are 22.58 and 1.81 ns, respectively, in this particular case.

Table S1. List of PBAE polymers and their number average molecular weights (M_n), weight average molecular weights (M_w), polydispersity indices (PDI), degree of polymerizations (DP), Hill coefficients (α), binding constants (*K*), diameters (nm), and zeta potentials (ZP; mV).

Varying	Polymer	M_n (kDa)	M_w (kDa)	PDI	DP	α	*K* (M^{-1})	Diameter (nm)	ZP (mV)
Molecular Weight	447 Low M_w	7.9	10.3	1.3	27	0.40	$4.2 \pm 0.1 \times 10^3$	180	14
	447 Med M_w	10.4	14.7	1.4	35	0.22	$5.8 \pm 0.3 \times 10^4$	135	6
	447 High M_w	32.0	91.6	2.9	110	0.23	$1.23 \pm 0.03 \times 10^5$	171	14
Backbone	346	7.5	11.2	1.5	27	0.24	$4.8 \pm 0.2 \times 10^5$	122	14
	446	8.3	11.8	1.4	28	0.38	$7.97 \pm 0.09 \times 10^3$	130	18
	546	7.0	9.1	1.3	23	0.22	$1.03 \pm 0.04 \times 10^4$	178	15
	646	8.1	10.0	1.2	24	1.16	$1.19 \pm 0.04 \times 10^3$	230	15
Sidechain	437	8.1	10.3	1.3	29	0.28	$1.15 \pm 0.01 \times 10^5$	170	9
	447 Med M_w	10.4	14.7	1.4	35	0.22	$5.8 \pm 0.3 \times 10^4$	134	6
	457	10.3	13.1	1.3	33	0.41	$3.5 \pm 0.1 Ex10^3$	160	9
	467	10.3	12.5	1.2	31	0.39	$4.7 \pm 0.3 \times 10^3$	165	8
Endcap	44	9.3	11.6	1.2	32	0.62	526 ± 9	180	11
	442	7.5	10.4	1.4	25	0.42	$3.5 \pm 0.2 \times 10^3$	200	12
	444	7.4	10.3	1.4	25	0.50	$3.4 \pm 0.1 \times 10^3$	190	13
	446	8.3	11.8	1.4	28	0.38	$7.97 \pm 0.09 \times 10^3$	130	18
	447 Low M_w	7.9	10.3	1.3	27	0.40	$4.2 \pm 0.1 \times 10^3$	180	14

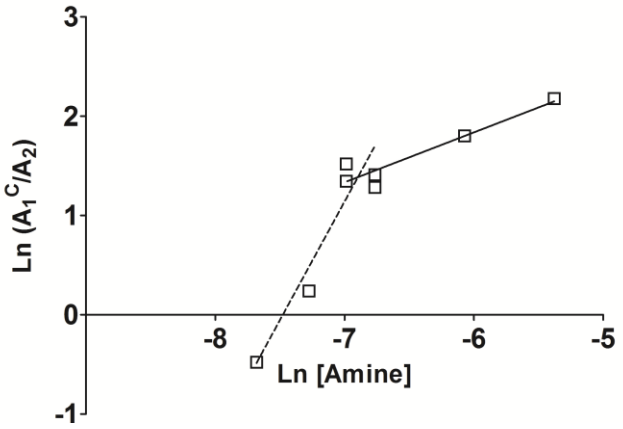

Figure S3. Hill plot of peptide $(KK)_2KGGC$.

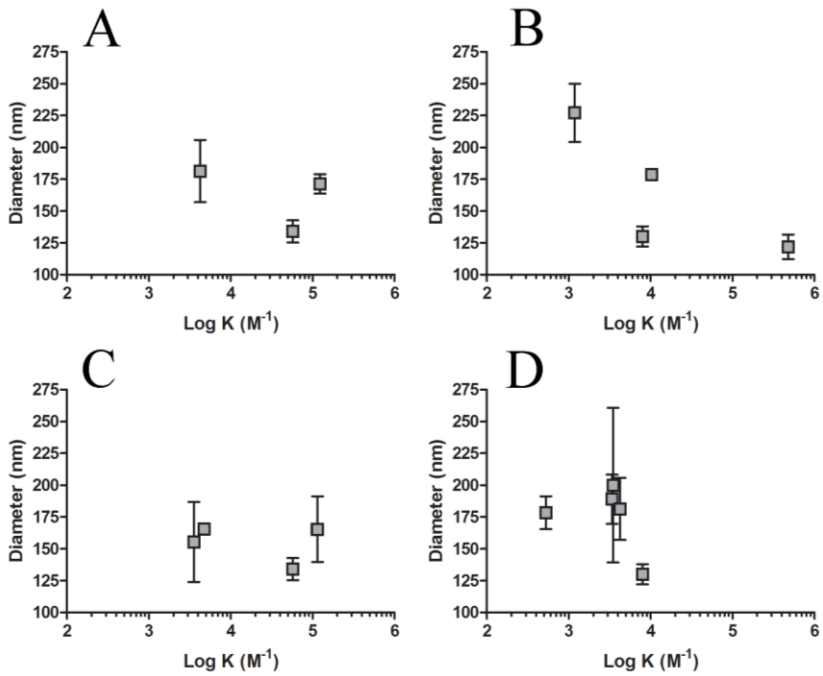

Figure S4. The relationship between polyplex diameter and the binding constant (M^{-1}) of each of the series comparing M_w (A), backbone (B), sidechain (C), and endcaps (D).

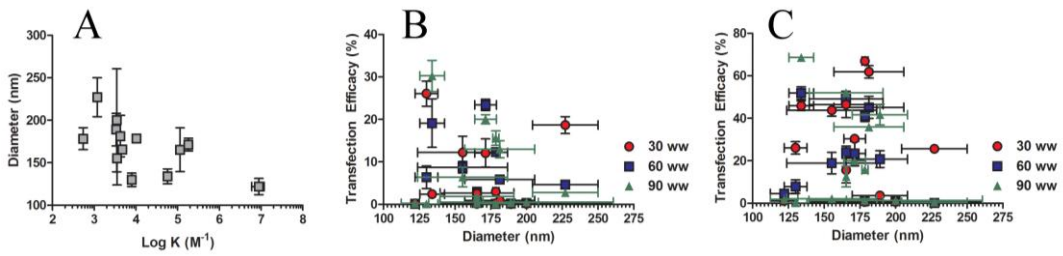

Figure S5. All diameters versus binding constants (A); dependence of transfection efficacy on polyplex diameters in MDA-MB-231 (B) and GBM319 cells (C).

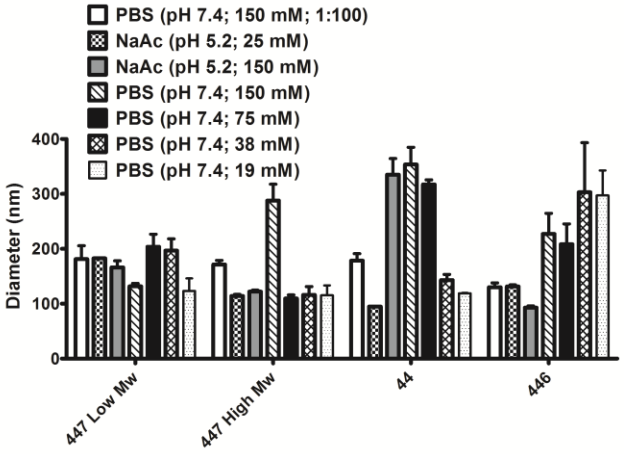

Figure S6. Diameter of four representative polymers at various pHs and ionic strengths. (White group was via NTA; remainder was via DLS.)

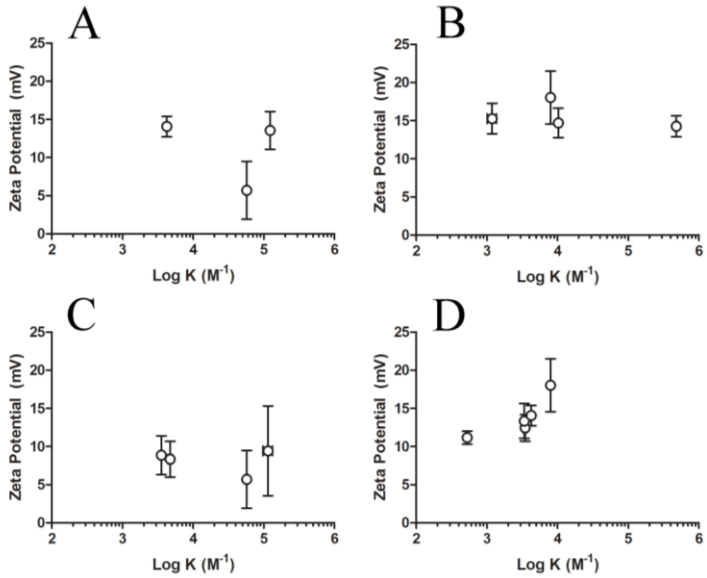

Figure S7. The relationship between zeta potential and the binding constant (M^{-1}) of each of the series comparing M_w (A), backbone (B), sidechain (C), and endcaps (E).

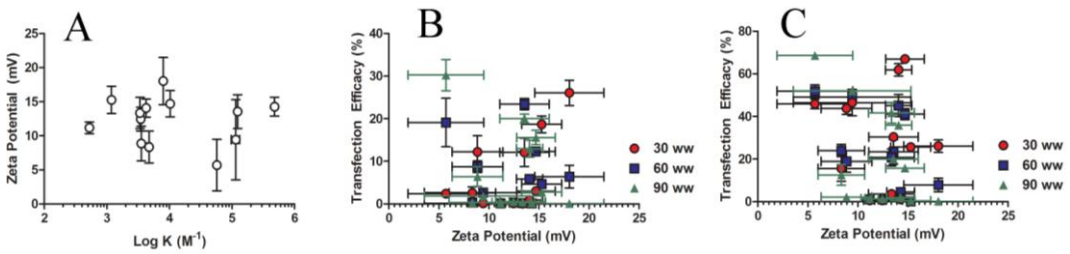

Figure S8. All ZP values irrespective of series versus binding constants (A); dependence of transfection efficacy on ZP in MDA-MB-231 (B) and GBM319 cells (C).

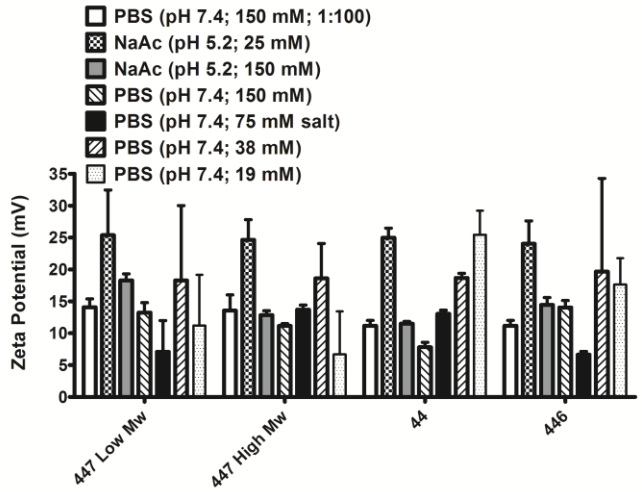

Figure S9. ZP of four representative polymers at various pHs and ionic strengths.

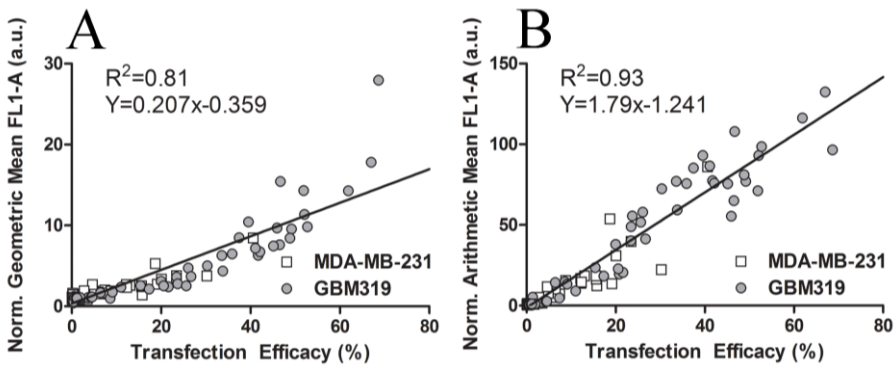

Figure S10. Normalized geometric (A) and arithmetic (B) means versus transfection efficacy in the MDA-MB-231 and GBM319 cell lines.

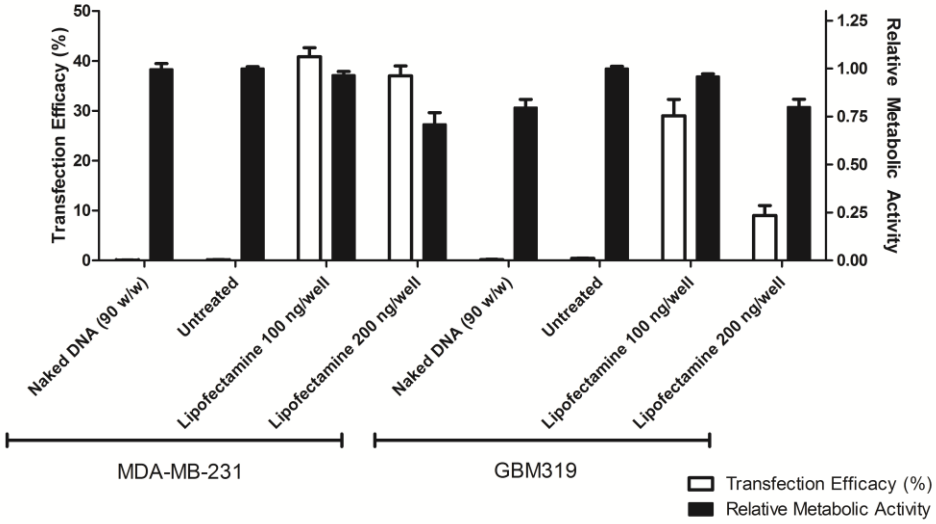

Figure S11. Positive (Lipofectamine 2000 at 100 and 200 ng/well) and negative controls (naked DNA and untreated) for transfection and relative metabolic activity in MDA-MB-231 and GBM319 cells.

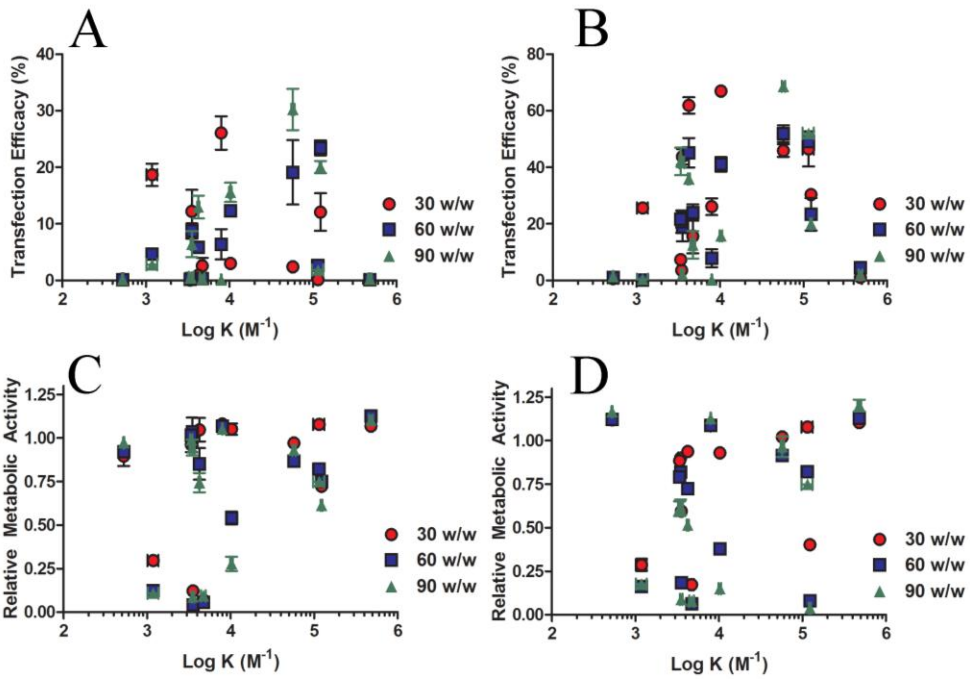

Figure S12. All binding constants for each of the series of comparison against transfection efficacy in MDA-MB-231 cells (A) and GBM319 cells (B), as well as cytotoxicity in MDA-MB-231 cells (C) and GBM319 cells (D).

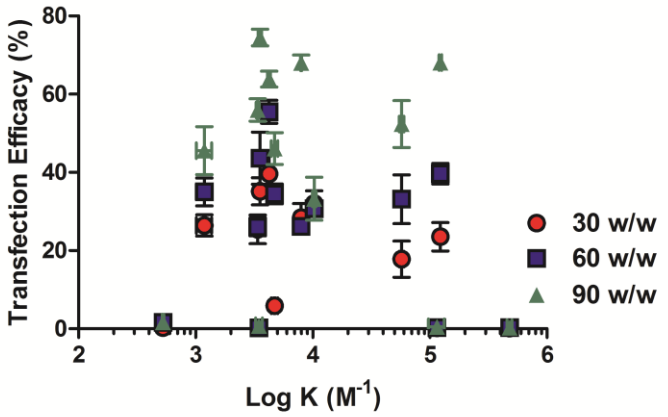

Figure S13. Binding constants compared to transfection efficacy using 70% serum in the GBM319 cell line.

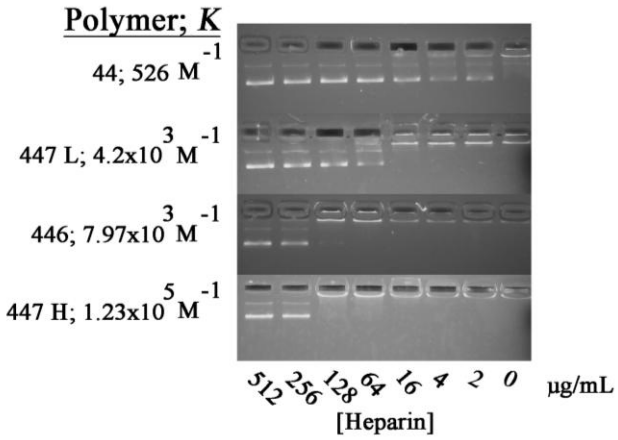

Figure S14. Heparin (ranging from 0 to 512 µg/mL) competition release assay of four representative polymers using gel electrophoresis; binding constants range from 526 (weakest *K* measured) to 1.23x10^5 M^{-1} (strongest *K* measured).

REFERENCES

1. Tzeng, S. Y.; Guerrero-Cazares, H.; Martinez, E. E.; Sunshine, J. C.; Quinones-Hinojosa, A.; Green, J. J., *Biomaterials* **2011,** *32*, 5402.
2. Sunshine, J. C.; Akanda, M. I.; Li, D.; Kozielski, K. L.; Green, J. J., *Biomacromolecules* **2011,** *12*, 3592.
3. Nanduri, V.; Sorokulova, I. B.; Samoylov, A. M.; Simonian, A. L.; Petrenko, V. A.; Vodyanoy, V., *Biosens. Bioelectron.* **2007,** *22*, 986.
4. Michel, D., *Biophys. Chem.* **2007,** *129*, 284.
5. Gelamo, E. L.; Tabak, M., *Spectrochim. Acta A* **2000,** *56*, 2255.
6. Gelamo, E. L.; Silva, C. H. T. P.; Imasato, H.; Tabak, M., *BBA-Protein Struct. M* **2002,** *1594*, 84.

Tampereen teknillinen yliopisto
PL 527
33101 Tampere

Tampere University of Technology
P.O.B. 527
FI-33101 Tampere, Finland

ISBN 978-952-15-3216-0
ISSN 1459-2045